**Universidade Federal do Rio Grande – FURG**

**Instituto de Oceanografia**

Programa de Pós-Graduação em Oceanologia

# O EFEITO DA MORFOLOGIA DOS MOLHES NO TRANSPORTE DE OVOS E LARVAS DA CORVINA *MICROPOGONIAS FURNIERI* NO ESTUÁRIO DA LAGOA DOS PATOS

MARIA HELENA PAULO ANTÓNIO

Tese apresentada a Coordenação do PPGO como requisito parcial para a obtenção do título de Doutor

Orientadora: *Profª. Drª.* ELISA HELENA FERNANDES
Co-orientador: *Prof°. Dr°.* JOSÉ HENRIQUE MUELBERT
Universidade Federal do Rio Grande (FURG), Brasil

Rio Grande, RS, Brasil
Setembro, 2020.

# O EFEITO DA MORFOLOGIA DOS MOLHES NO TRANSPORTE DE OVOS E LARVAS DA CORVINA *MICROPOGONIAS FURNIERI* NO ESTUÁRIO DA LAGOA DOS PATOS

Tese apresentada ao Programa de Pós-Graduação em Oceanologia, como parte dos requisitos para a obtenção do Título de Doutor.

por

MARIA HELENA PAULO ANTÓNIO

Rio Grande, RS, Brasil
Setembro, 2020.

ANTÓNIO, MARIA HELENA PAULO
O EFEITO DA MORFOLOGIA DOS MOLHES NO TRANSPORTE DE OVOS E LARVAS DA CORVINA *MICROPOGONIAS FURNIERI* NO ESTUÁRIO DA LAGOA DOS PATOS / Maria Helena Paulo António – Rio Grande: FURG, 2020.
Número de páginas 165p.
Tese (Doutorado) – Universidade Federal do Rio Grande. Doutorado em Oceanologia. Área de Concentração: Oceanografia Física.

1. Configuração dos Molhes. 2. Transporte de Ovos e Larvas. 3. Modelagem Numérica. I. Modelagem do Transporte de Ovos e Larvas da Corvina *Micropogonias Furnieri* no estuário da Lagoa dos Patos.

# Agradecimentos

*Agradecer em primeiro lugar a Deus pela saúde, força, fé e tudo vivido nesta caminhada. Agradecer aos meus orientadores a Profª. Elisa H. Fernandes e o Profº. José H. Muelbert pelo suporte, pela paciência e pelo conhecimento transmitido durante estes anos.*

*Ao Programa de Pós-graduação Ciência para o Desenvolvimento (PGCD) do Instituto Gulbenkian de Ciência e à Coordenação de Aperfeiçoamento de Pessoal de Nível Superior (CAPES) pelas bolsas concedidas. A Escola Superior de Ciências Marinhas e Costeiras (ESCMC), em particular ao Prof. António Hoguane, muito obrigada pelo suporte desde o meu ingresso na academia.*

*Um agradecimento especial à minha mãe (Maria Estrela A. Afonso) e ao meu pai (Emílio Beula), por torcerem sempre para que eu tenho êxitos na vida, me dando ânimo e força para me levantar e seguir em frente nos momentos complicados, rezando, comemorando e vivenciando cada etapa desta trajetória em especial. Estando disponíveis a ouvir, dar colo e conselho mesmo que distantes, me ajudando em tudo, sem ao certo entenderem grande parte do que estava sendo feito no doutorado, muito obrigada pelo imenso amor.*

*Agradecer de forma particular e especial a minha irmã (Maria Esperança Beula) e meu cunhado (Hedgar Dezembro) palavra nenhuma conseguirá expressar a gratidão por terem se tornando os pais do meu filho. Que Deus vos abençoe grandiosamente. O meu muito, muito, muito obrigada. De forma extensiva os meus agradecimentos vão ao Celso Matsinhe, a minhã irmã Edma M. Beula e todos meus irmãos, sobrinhos, familiares e amigos que se fizeram presentes ao longo deste tempo, em particular ao meus amigos Avelino, Joelma, Janett, Gisett, Caroline pela amizade, companheirismo e partilha de momentos que levarei para a vida.*

*Gratidão imensa vai para a minha família de coração os Cicatielo que me integrou como parte dela, sempre dado amor, carinho, aconchego, muita força, fizeram crescer a minha fé e esperança em mim e neste mundo. Partilhamos tudo da vida, desde os momentos de doença, dor, tristeza e luto, há momentos de alegria, festa e comemoração. A tia Pequena (Julieta), a Alaide, Vera e a irmã Maria, muita obrigada por tudo, estarem sempre no meu coração. Agradecer a família que a FURG me deu, ao pessoal do meu laboratório, em especial a Tati, Liliane (minha chuchu), Pablo, Roberto, Paulo Victor e a todos outros, foram ótimos os anos que juntos passamos partilhando momentos de ciência e da vida, obrigada pelos momentos além da FURG, pela amizade e momentos vividos. Sem me esquecer dos colegas do Doutorado, aos professores e demais com os quais interagi direta e indiretamente na FURG. Agardecimento extensivo ao suporte da CAPES ao PPG em Oceanologia, que permitiu recursos para o desenvolvimento da Tese.*

*E o mais importante da minha vida, o meu FILHO, a quem dedico este trabalho. Com lágrimas nos olhos eu tento encontrar palavras para te agradecer por tudo, pelo amor, pela maturidade e compreensão apesar da tenra idade. Agradecer a Deus por ter cuidado de você durante estes anos em que estivemos distantes fisicamente, mas sempre juntos. Te AMO mais que o tamanho de todos planetas juntos e tudo que existe no universo, palavras nossas. Tu és minha força, meu pilar, minha fortaleza, melhor aconchego, o meu tesouro.*

*Tem pessoas as quais tenho imensas e eternas saudades, pois partiram durante esta caminhada e as agradeço porque em vida acreditaram e destacaram sempre a capacidade e a realização desse desejo. Meu amado avó Paulo T. Afonso e a minha querida Teresinha Cicatielo que Deus vos dê um eterno descanso. Muito obrigada por verem a força e a garra que nem eu sabia que teria. Obrigada pelo exemplo de grandiosidade e pelas palavras de sabedoria dadas, as lembrarei sempre.*

# Índice

**Agradecimento**……...4
**Lista de Figuras da Tese**……...8
**Lista de Figuras do Manuscrito 1** ……..…9
**Lista de Figuras do Manuscrito 2** ……..…11
**Lista de Tabelas** ……....13
**Resumo**……..…14
**Abstract**……15
Organização tese……..…16
**Capítulo I:** Introdução……..……17
1.1. Infraestruturas costeiras e estuarinas ……..……....17
1.2. Sistema lagunar da Lagoa dos Patos ……..……20
1.3. Recrutamento de ictioplancton para estuarios..…….……..……...28
1.4. Corvina *Micropogonias Furnieri* ……..……..30
1.5. Dinâmica do transporte de ovos e larvas…….……..……33
**Capítulo II:** Hipótese……..35
**Capítulo III:** Objetivos…….....36
2.1. Objetivo Geral ……....36
2.2. Objetivos Específicos ……..36
**Capítulo IV:** Materiais e Métodos……36
4.1. Modelo hidrodinâmico TELEMAC-3D ……36
4.2. Domínio numérico e Malhas batimétricas……..…44
4.3. Condições iniciais e de contorno do modelo hidrodinâmico……45
4.4. Calibração e Validação do modelo ……..48
4.5. Modelagem lagrangeana do transporte de ovos e larvas……..…56
**Capítulo V:** Resultados e Discussão……**60**
**Manuscrito 1**
**Abstract**……....**61**
**1. Introduction**……**62**
**2. Numerical Model**……...**65**
2.1. Model description ……..……...65
2.2. Model grid ……..……...65
2.3. Initial and boundary conditions ……..……66
2.4. Calibration and Validation……..……68
2.5 Data analysis ……...……...73

**3. Results ……...73**
3.1. Hydrodynamics……..73
3.2. Alteration in saltwater distribution……..……..……77
3.3. Changes in salinity stratification at the mouth of the estuary ……...84
**4. Discussion ……90**
**5. Conclusions……...97**
**Acknowledgments**……....97
**Supplement A…**……....98
**Manuscrito 2**
**Abstract……...100**
1. **Introduction**……..……...101
1.1. Study area……...104
2. **Methodology……..105**
2.1. Hydrodynamic numerical model……..…..105
2.2. Particle Tracking model……..……..…..108
2.3. Model Experiments……..……..……...109
2.4. Data processing……..……110
**3. Results ……...**112
3.1. Saltwater distribution……..……....112
3.2. Transport and dispersion of larvae…….....115
3.3. Larvae travel distance…….....119
3.4. Larvae trajectories……..……....121
3.5. Spatiotemporal distribution of eggs and larvae……..……....123
3.6. Lateral stratification at the mouth of estuary……..…130
**4. Discussion……**135
**5. Conclusions and Remarks……...**140
**Acknowledgments……...**141
Supplement B……....142
**Capítulo VI:** Considerações Finais.....……....143
**Referências Bibliográficas**.....……..144

# Lista de Figuras da Tese

**Figura 1:** Área de estudo: a Lagoa dos Patos e seus principais tributários. Divisão da morfológica: (R-I) Estuário, (R-II) Estuário superior (lagoa central) e (R-III) Zona límnica (modificado de Vieira et al, 2010). Pontos indicando os locais de colecta de dados in situ: Região costeira (preto), Praticagem (vermelho), São Lourenço (amarelo), Arambaré (azul) e Ipanema (verde)……22
**Figure 2:** Localização do Porto Novo e Porto Velho no estuário da Lagoa dos Patos. Divisão morfológica: (R-I) Estuário, (R-II) Estuário superior (lagoa central) e (R-III) Zona límnica (modificado de Vieira et al, 2010)……23
**Figura 3:** Oscilação do nível do mar na Lagoa dos Patos em função dos ventos NE (A) e SO (B). A linha azul representa a elevação da superfície forçada pelo vento considerando a Lagoa dos Patos fechada nas duas extremidades. Os vetores representam o sentido das correntes (Castelão e Möller Jr, 2003)……..26

**Figura 4:** Corvina *Microponias Furnieri* (modificado da FAO, 2020)……31

**Figura 5:** Ciclo de vida da corvina *Micropogonias furnieri,* no estuário da Lagoa dos Patos. (1) desova realizada na zona costeira adjacente; (2) ovos e larvas sãoo advectadas para o estuário; (3) juvenis se desenvolvem nas zonas razas; (4) indivíduos maturos com cerca de 20-25 cm; (5) adultos aptos para desovar, deslocam-se para o mar ou desovam dentro do estuário. (Fonte: Oliveira e Bemvenuti, 2006)……..32

**Figura 6:** Malha tridimensional do Telemac-3D……..38

**Figura 7:** (A) Malha batimétrica da área de estudo, e a aplicação das condições iniciais e de contorno (B) Antiga e (C) Nova configuração dos Molhes da Barra de Rio Grande……..46
**Figura 8:** Campo inicial de (A) Salinidade e (B) Temperatura para todo o domínio em estudo……47
**Figura 9:** Séries temporais da descarga dos rios Guaíba, Camaquã e do Canal São Gonçalo para os períodos estudados de A) alta (2002-2003) e B) baixa (2011-2012) descarga continental……..48
**Figura 10:** Séries temporais de intensidade do vento para os períodos estudados na (A) alta (2002-2003) e (B) baixa (2011-2012) descarga continental……48
**Figura 11:** Exercício de calibração – Comparação entre velocidade da corrente modelada (linha vermelha) e medida (linha preta) na superfície (painel esquerdo) e no fundo (painel direito), para antiga (A e B) e nova (C e D) configuração dos Molhes da Barra……..53
**Figura 12:** Resultado da validação, comparação entre dados de velocidade de corrente, salinidade e elevação modelado (linha vermelha) e observado (linha preta) para a antiga e configuração dos Molhes da Barra. Velocidade (A) e salinidade (C) da superfície, velocidade (B) e salinidade (D) do fundo. (E - G) Dados da elevação da superfície nos pontos E1 (São Lourenço), E2 (Arambaré), e E3 (Ipanema)……..54
**Figura 13:** Resultado da validação, comparação entre dados de salinidade e elevação modelado (linha vermelha) e observado (linha preta) para a antiga e configuração dos Molhes. Salinidade da superfície(A) e salinidade do fundo (D). (C - E) Dados da

elevação da superfície nos pontos E1 (São Lourenço), E2 (Arambaré), e E3 (Ipanema) ……..
**Figura 14:** Séries temporais da intensidade do vento SO (A, B), S (C, D) e SE (E, F), para os períodos estudados em anos característicos de alta (painel esquerdo) e baixa (Painel direito) descargas continentais…….57

# Lista de Figuras do Manuscrito 1

**Figure 1.** The study site located in Southeast South America, depicting A) The Patos Lagoon and its main tributaries, where the three blue points (E1 – São Lourenço, E2 - Arambaré and E3 - Ipanema) indicate the position where the water level was obtained and one red point (N) where current velocity was obtained at the coastal region. Dotted line indicates the estuarine limit (Ponta da Feitoria). B) Patos Lagoon estuary, where eight black points (P1 – P8) show the location where the model results were extracted……..……..64
**Figure 2.** Southern Oscillation Index (SOI) and discharge anomaly for the 2002-2012 period (top and middle panels). Black rectangles represent periods of Patos Lagoon high discharge during El-Niño (bottom left) and low discharge during La-Niña (bottom right), the years that were simulated in this study…….67
**Figure 3:** A) The model domain and the finite element mesh highlighting the initial and boundary conditions applied to the old and new configuration of Molhes da Barra. The lower Patos Lagoon estuary in the (B) old, and (C) new jetty configuration……...68
**Figure 4:** Calibration exercise - comparison between modeled (red line) and measured (black line) current velocity at the surface (left panel) and bottom (right panel), in the old (A and B) and new (C and D) jetty configurations……..…..70
**Figure 5:** Validation results, comparison between modeled (red line) and measured (black line) current velocity, salinity and water elevation for the old jetty configuration. Surface velocity (A) and salinity (C) and bottom velocity (B) and salinity (D). (E-G) water elevation for points E1 (São Lourenço), E2 (Arambaré) and E3 (Ipanema)….71
**Figure 6:** Validation results, comparison between modeled (red line) and measured (black line) salinity and water elevation for new jetty configuration. Surface (A) and bottom (B) salinity data. (C-E) Water elevation for points E1 (São Lourenço), E2 (Arambaré) and E3 (Ipanema), respectively……72
**Figure 7.** Time series of river discharge and wind for the period between 04/2002 and 03/2003. South (North) winds are positive (negative) (A). Current velocity time series at surface (left) and bottom (right) at points P1 (B and C), P2 (D and E), P3 (F and G), P4 (H and I) and P5 (J and K) for old (black line) and new (red line) jetties configuration during 04/2002 and 03/2003. Positive (negative) values denote inflow (outflow). The blue line in all plots shows the difference between the old and new jetty configuration……75
**Figure 8.** Time series of river discharge and wind for the period between 08/2011 and 07/2012. South (North) winds are positive (negative) (A). Current velocity time series at surface (left) and bottom (right) at points P1 (B and C), P2 (D and E), P3 (F and G), P4 (H and I) and P5 (J and K) for old (black line) and new (red line) jetties configuration during 08/2011 and 07/2012. Positive (negative) values denote inflow

(outflow). The blue line in all plots shows the difference between the old and new jetties configuration……...76
**Figure 9.** Time series of river discharge and wind for the period between 04/2002 and 03/2003. South (North) winds are positive (negative) (A). Salinity time series at surface (left) and bottom (right) at points P1 (B and C), P2 (D and E), P3 (F and G), P4 (H and I) and P5 (J and K), for old (black) and new (red) jetties configuration during 2002-2003 (El Niño). The blue line in all plots shows the difference between the old and new jetties configuration……78
**Figure 10.** Spatial distribution of salinity during maximum flood (top panels) and maximum ebb (bottom panels) during the period of high discharge (2002-2003), considering the old (left) and new (center) scenarios and the calculated difference in salinity distribution (right). Results are presented for the surface (A, B, C, G, H, I) and for bottom (D, E, F, J, K, L)……..79
**Figure 11.** (A, D, G and J) Time series of salinity and (B, E, H and K) wavelet power spectrum of the time series for the estuary entrance (P1, top 2 panels) and near estuary limit (P4, bottom 2 panels), during the high discharge 2002-2003 period for the old (A, B, G and H) and for the new (D, E, J and K) jetties configuration. Thick contour line enclosed regions of greater than 95% confidence. Dash-dot regions indicate the cone of influence where edge effect becomes important. (C, F, I and L). The global wavelet power spectrum of the time series and the dotted red line indicate the 95% confidence level……80
**Figure 12.** Time series (top) of river discharge and wind for the period between 08/2011 and 07/2012. South (North) winds are positive (negative) (A). Salinity time series at surface (left) and bottom (right) at points P1 (B and C), P2 (D and E), P3 (F and G), P4 (H and I) and P5 (J and K), for the old (black) and new (red) jetties configuration during 2011-2012 (La Niña). The blue line in all plots shows the difference between the old and new jetties configuration. ……82
**Figure 13.** Spatial distribution of salinity during maximum flood (top panels) and maximum ebb (bottom panels) during the period of low discharge (2011-2012), considering the old (left) and new (center) scenarios, and the calculated difference in salinity distribution (right). Results are presented for the surface (A, B, C, G, H, I) and for the bottom (D, E, F, J, K, L)……..83
**Figure 14.** (A, D, G and J) Time series of salinity and (B, E, H and K) wavelet power spectrum of the time series for the estuary entrance (P1, top 2 panels) and estuary limit (P5, bottom 2 panels), during the low discharge 2011-2012 period for the old (A, B, G and H) and for the new (D, E, J and K) jetties configuration. Thick contour line enclosed regions of greater than 95% confidence. Dash-dot regions indicate the cone of influence where edge effect becomes important. (C, F, I and L). The global wavelet power spectrum of the time series and the dotted red line indicate the 95% confidence level……86
**Figure 15.** Spatial distribution of salinity at the mouth of the estuary depicting changes in intensity and the lateral stratification between the jetties during the high discharge period 2002-2003. Flood (top panels) and ebb (bottom panels), for the old (left) and new (center) scenarios, and the calculated difference in salinity distribution (right) at the surface (A, B, C, G, H, I) and bottom (D, E, F, J, K, L)……..87
**Figure 16.** Vertical cross-section distribution of salinity during ebb flow at the estuary entrance (P1) from west (left) to east (right) jetties, for the old (A) and new (B) jetties configuration, during high discharge period 2002-2003 (El Niño)……88

**Figure 17.** Current velocity time series from 3 points between the jetties (point P1) for the old (black line) and the new (colored lines) jetties configuration, during high discharge period of 2002-2003 (El Niño). The points are located at: first near the west jetty (top panel), second at the center of the channel (center panel) and the third near the east jetty (bottom panel), both for surface (left panel) and bottom (right panel). Positive (negative) values denote inflow (outflow)……..89
**Figure 18.** Frequency distribution of velocity and incidence angle at surface for points at the west (A and D), center (B and E) and east (C and F) jetties in the estuary entrance (P1), for the old (top) and new (bottom) jetties configurations, during the high discharge period 2002-2003 (El Niño). Northward (southward) velocities denote outflow (inflow)……91
**Figure 19.** Frequency distribution of velocity and incidence angle at bottom for points at the west (A and D), center (B and E) and east (C and F) jetties in the estuary entrance (P1), for the old (top) and new (bottom) jetties configurations, during the high discharge period 2002-2003 (El Niño). Northward (southward) velocities denote outflow (inflow)……..93

## Lista de Figuras do Manuscrito 2

**Figure 1:** The study site located in Southeast South America, depicting the Patos Lagoon (A) and the estuary (B). Dotted line indicates the estuarine limit (Ponta da Feitoria). Five rectangle areas (A1 – A5) show locations where modeled organism concentration results were extracted. The lower Patos Lagoon estuary in the (C) old, and (D) new jetty configuration. Black points indicate the position where M. furnieri eggs were released……106

**Figure 2:** Wind and discharge from 26/12/2002 to 5/01/2003 (left panel) and from 26/12/2011 to 5/01/2012 (right panel). (A and B) SW wind, (C and D) S wind and (E and F) SE wind. Black doted rectangles represent characteristic periods of Patos Lagoon high discharge (G) during El-Niño (left panel) and low discharge (H) during La-Niña (right panel) that were simulated in this study……..113

**Figure 3:** Spatial distribution of salinity excursion at the end of 5 days of simulation during the high continental discharge condition, considering SW (A and D), S (B and E) and SE (C and F) wind experiments (black arrows). Results are presented for the old (top panel) and for the new (bottom panel) jetty configurations. Black line indicates salinity reference of 5 psu……114

**Figure 4:** Spatial distribution of salinity excursion at the end of 5 days of simulation during the low continental discharge condition, considering SW (A and D), S (B and E) and SE (C and F) wind experiments (black arrows). Results are presented for the old (top panel) and for the new (bottom panel) jetty configurations. Black line indicates salinity reference of 5 psu……116

**Figure 5:** Spatial distribution pattern of excursion of *Micropogonias furnieri* larvae at the end of 5 days of transport, during the period of high continental discharge, considering the SW (A and D), S (B and E) and SE (C and F) wind experiments.

Results are presented for the old (top panel) and for the new (bottom panel) jetty configurations. Black arrows indicate the wind direction……..118

**Figure 6:** Spatial distribution pattern of excursion of *Micropogonias furnieri* larvae at the end of 5 days of transport, during the period of low continental discharge, considering the SW (A and D), S (B and E) and SE (C and F) wind experiments. Results are presented for the old (top panel) and for the new (bottom panel) jetty configurations. Black arrows indicate the wind direction……..……120

**Figure 7:** Distribution of the mean distance traveled by *Micropogonias furnieri* larvae sampled during the SW wind experiment at the end of each of the 5 days (day 1, day 2, day 3, day 4 and day 5), simulated during the period of high water discharge (A) and low water discharge (B), for the old (black) and the new (red) jetty configuration. ……122

**Figure 8:** Trajectory of *Micropogonias furnieri* eggs and larvae for the SW wind experiment at the end of each of the 5 days (1h, day 1, day 2, day 3, day 4 and day 5), during the period of high (top panel) and low (bottom panel) water discharge for the old (A,C) and new (B, D) jetty configuration. Particle tracking trajectory during the SW wind experiment, at the end of each of the 5 days of simulation (1h, 1 day, 2 days, 3 days, 4 days and 5 days, marked dots)……..124

**Figure 9:** Spatio-temporal distribution of the abundance of eggs and larvae of *Micropogonias furnieri* in the 5 areas (A1, A2, A3, A4 and A5) at the end of each of the 5 days of simulation (day 1, day 2, day 3, day 4 and day 5), for old (blue) and new (yellow) jetty configuration, during the period of high continental discharge. Considering the SW (Top panel), S (center panel) and SE (bottom panel) wind experiments……..128

**Figure 10:** Spatio-temporal distribution of the abundance of eggs and larvae of *Micropogonias furnieri* in the 5 areas (A1, A2, A3, A4 and A5) at the end of each of the 5 days of simulation (day 1, day 2, day 3, day 4 and day5), for old (black) and new (blue) jetty configuration, during the period of low continental discharge. Considering the SW (Top panel), S (center panel) and SE (bottom panel) wind experiments…….129

**Figure 11:** Spatial distribution of salinity in the estuarine mouth during low continental discharge at: 1h (A and D), 7h (B and E), 10h (C and F), considering the SW (A and D), S (B and E) and SE (C and F) wind experiments. Results are presented for the old (top panel) and for the new (bottom panel) jetty configurations. Black arrows indicate the wind direction…….133

**Figure 12:** Egg abundance of *Micropogonias furnieri* between the jetties during lateral stratification, considering the SW (A, D and G), S (B, E and H) and SE (C, F and I) wind experiments, at: jetties root (A, B, C), jetties center (D, E, F), an jetties mouth (G, H, I), during the period of low water discharge……134

**Figure 13:** Schematic diagram of the differences in the transport of eggs and larvae of *Micropogonias furnieri* from the coastal region to the Patos Lagoon estuary

induced by changes in the configuration of the jetties. Coastal circulation induced by SW (A), S (B) e SE (C) winds. Black lines and arrows indicate the current velocity. Green arrows indicate the wind direction. (D) Diagram of the resulted effects in the eggs and larvae transport……..139

# Lista de Tabelas

Tese

**Tabela 1:** Dados in situ coordenadas, local de colecta e o tipo de teste realizado…49

**Tabela 2:** Parâmetros que apresentaram melhores resultados na calibração do modelo…….51

**Tabela 3:** Escala da classificação do coeficiente do RMAE para o desempenho do modelo (Walstra *et al.,* 2001)……...52

**Tabela 4:**Resultados do Erro Absoluto Médio Relativo dos testes de validação do modelo hidrodinâmico nas duas configurações dos Molhes da Barra…….56

Artigo 1

**Table 1:** Relative Mean Absolute Error (RMAE) results for the hydrodynamic model validation.

Antigo 2

**Table 1:** Controlled simulations experiments.

**Table 2:** Total number and percentage of lavae of *Micropogonias furnieri* transported towards the estuary at the end of the 5 days of simulation, during south quadrant winds for the old and new configurations.

**Resumo**

Os Molhes da Barra do Rio Grande, na desembocadura do estuário da Lagoa dos Patos, sofreram recentemente modificações que aumentaram o seu comprimento, tornando-os simétricos, mais afunilados e convergentes. Estudos tem reportado que a construção ou modificação de infraestruturas costeiras afetam a dinâmica da região, que por conseguinte pode influenciar o transporte e distribuição de propriedades ou organismos no estuário. A corvina, *Micropogonias furnieri*, é um peixe com ovos e larvas planctônicos e ciclo de vida estuarino-dependente que têm importância econômica para a pesca regional. Nesta tese, eu estudo o efeito da mudança nos Molhes da Barra no transporte de ovos e larvas da corvina para o estuário da Lagoa dos Patos (ELP). O transporte foi simulado com o modelo hidrodinâmico TELEMAC-3D acoplado a um módulo de partículas passivas. Duas categorias de simulações foram feitas com características extremas de vazão e situações controladas de ventos. A primeira, meramente hidrodinâmica, considerou forçantes dinâmicas extremas de vazante características durante a ocorrência de eventos ENOS (El Niño Oscilação Sul), para análise das mudanças hidrodinâmicas ocorridas entre a antiga e a nova configuração dos Molhes da Barra. Posteriormente, foram realizadas simulações controladas com ventos SW, S e SE com 5 (cinco) dias de duração no mês de janeiro dos mesmos anos, acoplando partículas passivas à componente hidrodinâmica. Os resultados demonstraram que as modificações feitas nos Molhes da Barra reduziram a extensão da intrusão salina na nova configuração. De forma similar, mudanças na estrutura da estratificação lateral, bem como o seu tempo de ocorrência foi reduzido em cerca de um terço da antiga para a nova configuração dos Molhes da Barra. Um atraso no início da estratificação lateral foi observado em função do vento incidente, estabelecendo-se primeiro durante os ventos SW, seguido dos ventos S e posteriormente o vento SE. Este atraso foi sempre maior na nova configuração para os 3 ventos. Pequenas mudanças no ângulo de incidência bem como redução em cerca de 20% da intensidade das velocidades de corrente, tanto de enchente como de vazante, foram constatados, assim como uma centralização parcial do fluxo ao longo do canal de navegação. As mudanças hidrodinâmicas ocorridas refletiram sobre o transporte de ovos e larvas, constatando-se uma redução da abundância e extensão da incursão para o interior do estuário com a nova configuração dos Molhes da Barra. A redução também foi percebida na distância média percorrida pelas larvas ao final de cada dia de simulação. Os resultados do estudo são os primeiros a reportar as mudanças ocorridas no transporte de ovos e larvas da corvina após as recentes obras de modernização e servem de base para estudos posteriores associados a aspetos do ciclo de vida da espécie. Associados a outros estudos já feitos na região, estes resultados servem de base para a compreensão e tomada de medidas de gestão para contornar o cenário de declínio dos estoques pesqueiros no estuário e região costeira adjacente à Lagoa dos Patos.

***Palavras-chave:*** Estruturas Costeiras, Lagoa dos Patos, ENSO, Modelagem Numérica, TELEMAC-3D, Ovos e larvas de corvina.

**Abstract**

The Molhes da Barra jetties, at the mouth of Patos Lagoon estuary, have recently undergone modifications that have increased their length, making them symmetrical, more tapered and convergent. Studies have reported that construction or modification of coastal structures affects the dynamics of regional circulation, which can therefore influence the transport and distribution of properties and organisms in the estuary. The croaker, *Micropogonias furnieri*, is an estuarine dependent fish with planktonic eggs and larvae, which has economic importance for regional fisheries. In this thesis, I study the influence of the changes in the Molhes da Barra jetties on the transport of croaker eggs and larvae to the Patos Lagoon estuary (PLE). Transport was simulated using the TELEMAC-3D hydrodynamic model coupled to a passive particle module. Two categories of simulations were performed with extreme flow characteristics and controlled wind situations. The first, purely hydrodynamic, considered extreme run-off conditions characteristic of periods of ENSO events, to analyze the differences between the old and the new configuration of the Molhes da Barra jetties. Subsequently, controlled simulations with SW, S and SE winds lasting 5 (five) days in January of the same years were carried out, coupling passive particles to the hydrodynamic component. Results showed that the modifications made to the Molhes da Barra jetties reduced the extent of saline intrusion in the new configuration. Similarly, changes in the structure of the lateral stratification, as well as on its time of occurrence, were reduced by about one third in the new configuration of the jetties. A delay in the beginning of lateral stratification was observed due to the incident wind, establishing itself first during the SW winds, followed by the S winds and then the SE wind. This delay was more evident in the new configuration. Slight changes in the angle of incidence as well as a reduction of about 20% in the intensity of the current speeds of both flood and ebb flows and a partial centralization of the flow along the navigation channel were observed. The hydrodynamic changes influenced the transport of eggs and larvae, with a reduction in the abundance and extension of the incursion into the estuary with the new configuration of the jetties. The reduction was also noticeable in the average distance traveled by the larvae at the end of each day. Results of this study are the first to report the changes in the transport of eggs and larvae of the croaker after the recent modernization works and serve as a basis for further studies associated with respect to the species' life cycle. Associated with other regional studies, these results can be used as a basis for understanding and taking management measures to circumvent the scenario of declining fishing stocks in the estuary and coastal region adjacent to Patos Lagoon.

***Keywords**:* Coastal structures, Patos Lagoon, ENSO, numerical modelling, TELEMAC-3D, croaker eggs and larvae.

**Organização da Tese**

O Capítulo I apresenta a introdução ao trabalho, destacando a importância associada a dinâmica das regiões costeiras e estuarinas, tendo em conta a ação antrópica na construção de infraestruturas costeiras e modificação da geomorfologia, seus efeitos e consequências para a dinâmica dos ecossistemas marinhos. O Capítulo destaca a caracterização da área de estudo pelas modificações feitas no ponto de vista físico, geomorfológico e sua relação com a dinâmica comportamental característica da espécie em estudo. Também destaca a aplicação da técnica de modelagem numérica aplicada como forma de obter melhor abrangência da área de estudo e compreensão do processo do transporte de ovos e larvas desde a região costeira adjacente até ao interior do estuário da Lagoa dos Patos. A hipótese do estudo é apresentada no Capítulo II. Os objetivos gerais e específicos são apresentados no Capítulo III. O Capítulo IV apresenta a metodologia utilizada no desenvolvimento do trabalho, descrevendo o modelo numérico utilizado, a construção das malhas numéricas, tipo e as fontes de dados observacionais utilizados nos exercícios de calibração e validação do modelo. O domínio computacional, as condições iniciais e de contorno utilizado, e os testes de calibração e validação do modelo numérico, bem como a configuração básica do modelo hidrodinâmico e do modelo de partículas passivas acoplado ao modelo hidrodinâmico aplicado baseando-se na espécie em estudo, também são apresentados neste capítulo. O Capítulo V apresenta os resultados obtidos em forma de 2 artigos científicos. O primeiro trata do efeito das mudanças na configuração dos Molhes da Barra na hidrodinâmica da Lagoa dos Patos e o segundo do efeito das mudanças da configuração na desembocadura do estuário da Lagoa dos Patos no transporte e dispersão de ovos e larvas de corvina *Micropogonias furnieri*. O Capítulo VI apresenta as conclusões do estudo e sugestões para trabalhos futuros e finalmente, são apresentadas as Referências Bibliográficas citadas nos Capítulos anteriores.

# Capítulo I:
# Introdução

## 1. INTRODUÇÃO

### 1.1. Infraestruturas costeiras e estuarinas

Os estuários são ambientes ecológicos chave que conectam os ecossistemas terrestres e marinhos, fornecendo habitats e berçário para peixes de estuários e regiões costeiras (Hoguane et al. 2020), tornando-os assim de extrema importância tanto no aspecto ambiental como econômico (Seiler et al., 2015). A dinâmica da circulação destes ambientes é controlada por fatores que variam na escala temporal desde diurnas a semi-diurnas (marés) até a anual e mais longos, sendo controlados pela diferença de densidade, aquecimento superficial dos oceanos, maré astronômica e ventos (Schmidt e Luther, 2002; Wong et al., 2003a).

Os padrões de salinidade e qualidade de água em um estuário resultam da dinâmica do fluxo de entrada ou de saída de sal no estuário, que é conduzido pela descarga da água doce, pelos ventos, pelos efeitos de maré e outros processos hidrodinâmicos de mistura (Pritchard, 1956; Fernandes et al., 2002; Odebrecht et al., 2005; Ji et al., 2011; Gong et al., 2018). Todavia, a entrada de água doce nos estuários apresenta variabilidades na escala temporal que podem aumentar ou diminuir o fluxo de entrada ou saída nos estuários devido a precipitação, fatores esses que variam desde padrões sazonaais, padrões meteorológicos sinóticos e de larga escala, bem como variação interanual e climática produzidas pelos ciclos El Niño Southern Oscilation (ENSO) (Möller Jr et al., 2001; Schmidt e Luther, 2002; Fernandes et al., 2002; Seiler et al., 2015; Távora et al., 2019).

Ao longo da história, os estuários e regiões costeiras têm sido usados como centros de assentamento e comércio humano, levando ao desenvolvimento de grandes cidades costeiras em todo o mundo, uma tendência que se mantém até os dias atuais (Seeliger e Costa, 2010; Dugan et al., 2011; Du et al., 2016). Desta forma, impactos humanos na evolução morfológica de estuários, deltas e regiões costeiras têm sido progressivamente intensificados, como resposta ao rápido crescimento da população, expansão da urbanização e desenvolvimento da terra

que estão se intensificando e aumentando a pressão sobre os ecossistemas costeiros (Cunha e Calliari, 2009; Seeliger e Costa, 2010; Azarmsa et al., 2009; Seiler et al., 2015; Lisboa e Fernandes, 2015). Fatos esses associados a forma que o ser humano tenta garantir a rápida e eficaz exploração dos recursos costeiros implementando projetos de infraestruturas de pequena e larga escala (Cunha e Calliari, 2009; Du et al., 2016). Entretanto, a costa é um lugar onde uma grande abundância de vida é nutrida (Clark, 1997; Dugan et al., 2011).

As modificações ambientais decorrentes da demanda de infraestruturas expansivas para o desenvolvimento urbano, industrial e agrícola, vão desde a conversão da terra, modificação da linha da costa, dragagem no mar e canais de navegação, poluição da água, construção de infraestruturas costeiras como molhes, diques, paredões, barragens, expansão de portos e de marinas, entre outros (Cunha e Calliari, 2009; Ghasemizadeh e Tajziehchi, 2013; Du et al., 2016). Estas alterações geralmente afetam a interação entre a região costeira e oceânica e resultam em mudanças que ocorrem devido ao desequilíbrio dos fatores ambientais naturais ao redor do ambiente criado durante anos (Clark, 1997; Seeliger e Costa, 2010; Möller Jr e Fernandes, 2010; Kriauciuniene et al., 2013; Lisboa e Fernandes, 2015; Du et al., 2016; Prumm e Iglesias, 2016). Variações morfológicas estão entre as respostas mais perceptíveis, potencialmente causando mudança estrutural do canal de navegação, erosão ao redor dos canais e fundações estruturais ou sedimentação nos portos (Azarmsa et al., 2009; Seeliger e Costa, 2010; Calliari et al., 2010; Silva et al., 2015; Prumm e Iglesias, 2016).

As consequências da construção de infraestruturas associadas à urbanização e intervenções humanas nos processos costeiros incluem entre outros a transformação direta ou indireta da geomorfologia, hidrodinâmica e a dinâmica dos ecossistemas costeiros e estuarinos, problema de crescente intensidade e preocupação, que na maioria das vezes está associado a políticas deficientes de defesa costeira (Clark, 1997; Cunha e Calliari, 2009; An et al., 2009; Möller Jr e Fernandes, 2010; Dugan et al., 2011; Du et al., 2016). Importante salientar que a gestão sustentável dos ecossistemas aquáticos demanda um profundo entendimento e habilidade para prever o comportamento do ambiente marinho e os impactos a eles associados em virtude de qualquer mudança (Azarmsa et al., 2009;

Seiler et al., 2015; Prumm e Iglesias, 2016). Muitas decisões regulatórias e de gestão que impactam nas regiões costeiras e estuarinas são baseadas no padrão de circulação e são essenciais para o entendimento e expansão do conhecimento da dinâmica destas regiões (Schmidt e Luther, 2002).

Apesar do uso de infraestruturas de cunho antrópico nas regiões costeiras e estuarinas ao redor do mundo já ocorrerem há milhares de anos, existe um debate muito ativo sobre os impactos geomórficos dessas estruturas nas costas abertas e abrigadas, com ênfase nos efeitos ecológicos que têm sido pouco estudados e mal compreendidos (Yuk e Aoki, 2007; An et al., 2009; Dugan et al., 2011). Uma revisão recente, focada em regiões costeiras protegidas, mostrou que pouco se sabe sobre os efeitos das estruturas de defesa costeira nos habitats costeiros nativos e em suas comunidades, nem sobre como eles alteram as funções e serviços do ecossistema fornecido por ecossistemas naturais ou introduzidos (NRC, 2007).

Deve ser salientado que, historicamente, qualquer modificação antrópica resultante de estruturas projetadas e colocadas em ambientes costeiros alterará a hidrodinâmica e a dinâmica das demais regiões no estuário e regiões adjacentes, podendo modificar o fluxo de água, regime de ondas, o balanço entre as correntes de vazante e enchente, a dinâmica de sedimentos, o tamanho de grão e processos de erosão e deposição (Cunha e Calliari, 2009; Calliari et al., 2010; Dugan et al., 2011; Lisboa e Fernandes, 2015; Silva et al., 2015; Du et al., 2016). Outras implicações passam pela modificação nas características da circulação das zonas costeiras, pelas mudanças na propagação de maré e no tempo de residência em sistemas lagunares (Malhadas et al., 2009). Pois, modificações batimétricas tanto de cunho natural ou antrópicas podem alterar as correntes e o prisma de maré, que por sua vez implica em alterações nos canais principais e nas trocas entre os sistemas estuarino e oceânico, alterando as características da água (Picado et al., 2010).

Estudos vem reportando os efeitos da ação antrópica em regiões costeiras e estuarinas. Sherwood et al. (1990) verificaram diferenças e diminuição na intrusão de águas mais salinas no estuário de rio Columbia (USA), nos anos a posterior das intervenções de dragagem que promoveram aumento nas velocidades de vazante. Yuk e Aoki (2007) constataram que após a construção de molhes na entrada do Lago Hamana (Japão), as correntes no interior do lago tornaram-se fortes

acelerando a mistura vertical, afetando a entrada da água salgada e as enchentes no estreito canal, resultando em mudanças na topografia e batimetria. Azarmsa et al. (2009) perceberam uma redução significativa na altura das ondas após a construção de Molhes na entrada da lagoa Kiashahr (Irão), presumindo que a atenuação da energia da onda pode impactar na saúde do ecossistema. Ghasemizadeh e Tajziehchi (2013) observaram que após a construção do longo molhe na costa leste de Bandar Abbas (Irão), ocorreram mudanças que definiram locais de ocorrência da sedimentação e da erosão, estando a direção do transporte de sedimentos consistente com a direção das ondas dominantes. Prum e Iglesias (2016) constataram que após a expansão do porto de Ribadeo (Espanha), houve um aumento da sedimentação na margem leste, assoreando o canal de navegação vital para a operacionalidade de outro porto e dos estaleiros próximos ao local. Cunha e Calliari (2009) concluíram que a construção dos Molhes da Barra na desembocadura do estuário da Lagoa dos Patos moveu a dinâmica do canal de navegação para o lado leste, alterando também o volume de sedimentos em suspensão exportado. Todavia, Lisboa e Fernandes (2015) e Silva et al. (2015) constataram que modificações recentes feitas no comprimento e no formato dos mesmos Molhes reduziram as correntes ao longo do canal de navegação bem como alteraram as regiões de erosão e deposição de sedimentos no estuário.

### 1.2. Sistema lagunar da Lagoa dos Patos

A Lagoa dos Patos (Figura 1) está localizada no extremo sul do Brasil, entre 30º a 32º Sul e 50º a 52º Oeste e é formada por uma suave linha de costa, longas praias de areia e lagoas costeiras. Segundo Kjerfve (1986) a Lagoa dos Patos é a maior lagoa costeira do tipo estrangulado do mundo. Possui um comprimento de cerca de 250 km e 40 km de largura média, cobrindo uma área total de 10,360 $km^2$. É classificada como do tipo pouco profunda, com uma profundidade média de cerca de 5 m, sendo a parte central do canal do estuário a mais profunda (Möller Jr et al., 2001). O sistema lagunar conecta-se com o oceano Atlântico por um único e estreito canal de 700 m de largura, e cerca de 16-18 m de profundidade ao longo do canal de acesso (Kjerfve, 1986; Möller Jr et al., 2001; Martins et al., 2007; Marques et al., 2009; Lisboa e Fernandes, 2015).

Os ambientes transicionais entre os rios e oceanos, como o caso de lagoas costeiras são de extrema importância ambiental e econômica (Seiler et al., 2015). O fluxo lento das águas da Lagoa dos Patos em direção ao oceano Atlântico favorecem a deposição de grandes quantidades de sedimentos, o que historicamente vem interferindo na navegação, exigindo constantes atividades de dragagem que desde 1830 vem sendo realizadas ao longo do canal de navegação (Cunha e Calliari, 2009). De forma a mitigar o problema, ampliar as atividades econômicas com a entrada de navios com grandes calados para o Porto do Rio Grande, bem como a instalação do polo de construção naval no estuário, foi dado o início em 1910 e concluída 1917 a construção dos Molhes da Barra do Rio Grande (Möller Jr e Fernandes, 2010; Seeliger e Costa, 2010; Cunha e Calliari, 2009). E em 2010 foram terminadas as recente obras de modificação dos Molhes (Fernandes et al., 2012). Os Molhes da Barra são considerados o maior trabalho de engenharia costeira já realizado no Brasil (Cunha e Calliari, 2009) e a modificação antrópica mais significativa no estuário (Calliari et al. 2010). Com formato convergente e afunilado das suas bordas, os molhes iniciais apresentavam orientação sul-leste e atingiram no período de sua conclusão a isóbata de 10 m, com o molhe oeste menor que o leste, ambos com 4,012 m e 4,250 m respectivamente de base (Cunha e Calliari, 2009; Seeliger e Costa, 2010).

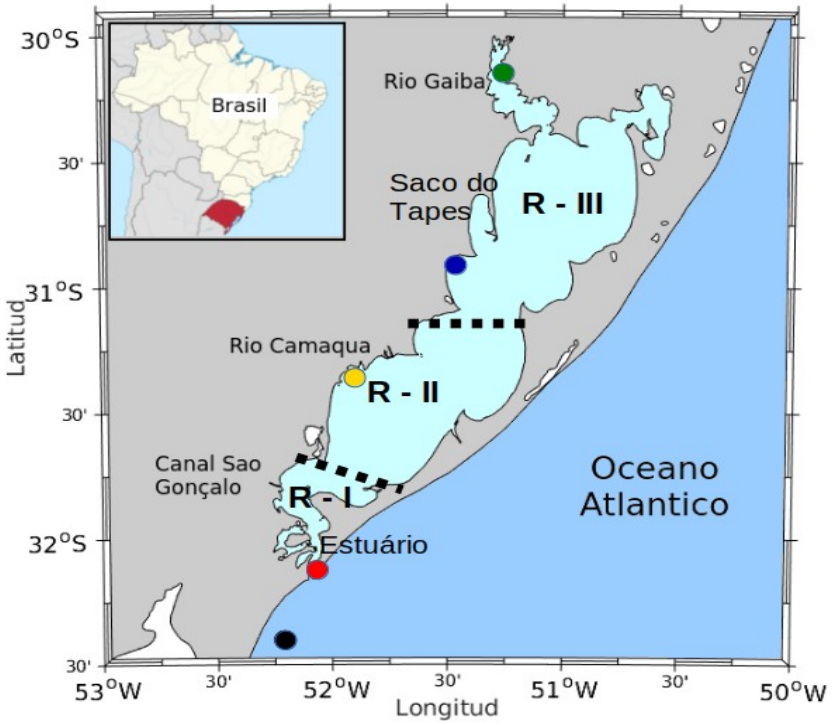


Figura 1: Área de estudo: a Lagoa dos Patos e seus principais tributários. Divisão da morfológica: (R-I) Estuário, (R-II) Estuário superior (lagoa central) e (R-III) Zona límnica (modificado de Vieira et al, 2010). Pontos indicando os locais de colecta de dados in situ: Região costeira (preto), Praticagem (vermelho), São Lourenço (amarelo), Arambaré (azul) e Ipanema (verde).

Outra modificação antrópica corrida no estuário foi a abertura da Bacia do Porto Novo e do Canal de ligação com o Porto Velho (Figura 2) sobre o Baixio do Ladino, com o objetivo de aumentar a área portuária e reduzir a distância e o tempo de navegação ao estuário (Calliari et al. 2010). As mudanças ocorridas com o estabelecimento do Porto Novo, resultaram no aumento da profundidade do Porto Velho, e aliado a construção dos Molhes da Barra causaram alterações no fluxo de vazante e enchente, bem como nas características hidráulicas e sedimentares naturais (Calliari et al. 2010). Desta forma, mesmo com a construção dos Molhes com o intuito de reduzir as atividades de dragagem, esse propósito não foi alcançado de forma satisfatória, levando a continuidade das atividades de dragagem para remoção de sedimentos finos nas últimas décadas, nos diferentes canais no

estuário (Calliari et al. 2010; Lisboa e Fernandes, 2015) de modo a garantir segurança da navegação.

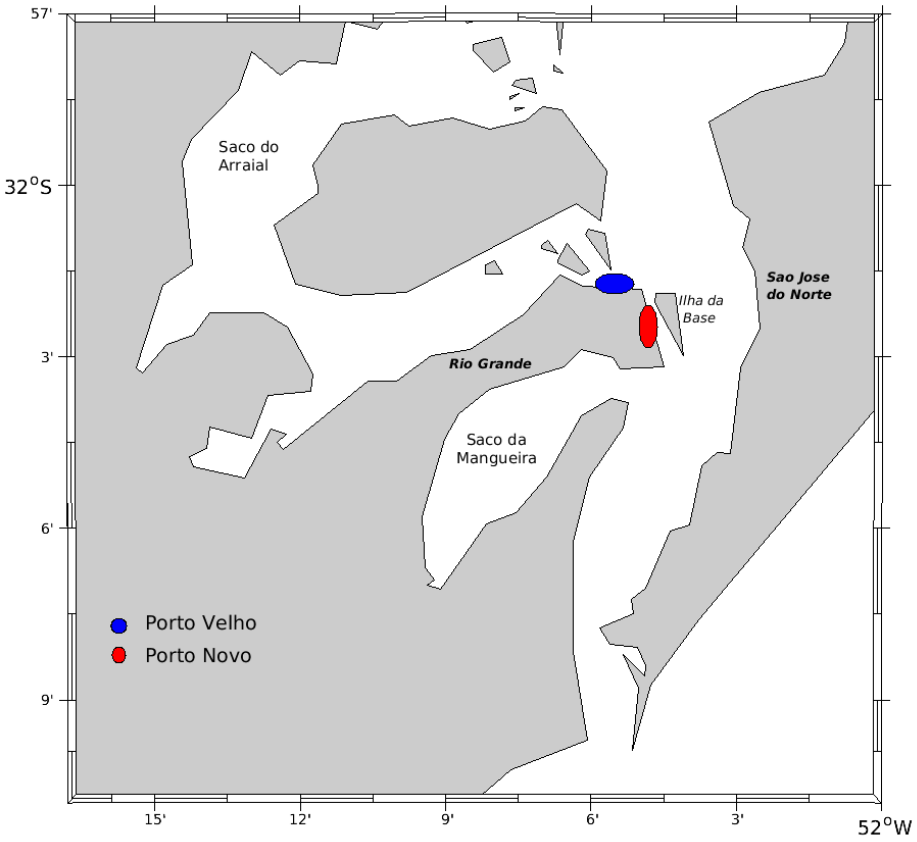


Figura 2: Localização do Porto Novo e do Porto Velho no estuário da Lagoa dos Patos

### 1.2.1. Morfologia da Lagoa dos Patos

Möller Jr et al. (2001) e Vieira et al. (2010) assumem que morfologicamente, a Lagoa dos Patos é dividida em 3 principais regiões: a região norte ou Zona Limnítica (R-III, confluência com os rios Jacuí e Taquari), a lagoa central ou estuário superior (R-II), que juntas representam cerca de 90% da área da total da lagoa, e o estuário na região sul (R-I), que representa cerca de 10% da área total (Figura 1). A zona estuarina da Lagoa dos Patos situa-se entre os Molhes da Barra (ao sul) e a Ponta da Feitoria (ao norte), que é o limite mais frequente do alcance da intrusão salina, sendo que a sua secção transversal aumenta exponencialmente para o interior da lagoa (Möller Jr et al., 2001; Cunha e Calliari, 2009). As mudanças geomorfológicas

do estuário são resultado da ação dos fatores hidrodinâmicos associados as características meteorológicas da região.

A região do Rio Grande do Sul apresenta uma margem continental do tipo passivo, com baixo relevo e o desenvolvimento de uma ampla planície costeira (Calliari et al., 2009). Geomorfologicamente, o estuário da Lagoa dos Patos é predominantemente composto por grandes bancos de areia pouco profundos (1-5 m) e esporões arenosos recurvados (Calliari et al., 2010). Baseado em elementos batimétricos e sedimentológicos, o relevo submerso do corpo da lagoa é subdividido em duas grandes unidades morfológicas: a primeira predominantemente arenosa, que abrange a área entre as regiões rasas dos bancos, as margens até isóbata de 5 m, e a segunda abrange as partes mais profundas da lagoa, os canais profundos e as enseadas rasas, dominadas por sedimentos lamacentos argilo-siltosos (Toldo, 1991; Martins, 1971, citado por Calliari et al., 2010).

Longitudinalmente, a taxa de sedimentação no fundo da Lagoa dos Patos decresce de norte para o sul, apresentando uma correlação direta com a precipitação, e as maiores taxas de sedimentação são registradas em anos de ocorrência de El-Niño (Ivanoff et al., 2020). A Lagoa dos Patos é uma fonte significativa de sedimentos finos para a região costeira adjacente e a plataforma continental interna da região do Atlântico Sul, sedimentos esses oriundos da bacia de drenagem da Lagoa de Patos e dos efeitos antrópicos associados a atividades de dragagem e desmatamento seculares relacionados a assentamentos e culturas agrícolas (Calliari et al., 2009). Segundo Tavora et al. (2019), a concentração de sedimentos em suspensão na Lagoa dos Patos é dependente da descarga dos rios, e o seu transporte é controlado pelo vento NE e pelo vento SO.

### 1.2.2. Hidrodinâmica da Lagoa dos Patos

O estuário da Lagoa dos Patos recebe as descargas provenientes da parte norte das planícies costeiras do Rio Grande do Sul e dos afluentes do sistema da Lagoa dos Patos-Mirim, e promove a interação com as águas salgadas do oceano Atlântico Sul, formando um ambiente com características particulares em relação à

hidrodinâmica, dinâmica dos sedimentos, qualidade da água, condições físico-químicas, e dinâmica dos organismos no geral (Seeliger, 2010).

A hidrodinâmica da Lagoa dos Patos é dominada pelos ventos associados a descargas continentais (Möller Jr et al. 2001; Fernandes et al. 2002; Möller Jr e Fernandes, 2010), com pouca interferência da variabilidade das marés, um comportamento típico de lagoas costeiras (Kjerfve, 1986). A ação das marés restringem-se ao canal de acesso da Lagoa, pois este funciona como um filtro dinâmico atenuando a amplitude dos constituintes da maré durante a sua propagação estuário adentro, removendo cerca de 80% da energia da maré por fricção (Möller Jr et al, 2001; Fernandes et al., 2004; Möller Jr e Fernandes, 2010). As marés no estuário são do tipo mistas com dominância diurna, apresentando uma média de 0,3 m (Kjerfve, 1986; Möller Jr e Fernandes, 2010). As marés têm ação moduladora contribuindo para a mistura da coluna de água e transporte da água mais para o norte da lagoa, durante períodos de menor intensidade dos ventos (Möller Jr et al, 2001; Fernandes et al., 2002; Marques et al. 2009).

A ação dos ventos na dinâmica da lagoa tem a influência das componentes local e não-local do vento, assim como pela combinação dos dois (Möller Jr et al., 2001). O efeito local ocorre através da transferência direta de momento pela tensão de cisalhamento superficial sobre o corpo hídrico, gerando correntes e oscilações de curto período (~ 24 h) e desníveis entre suas extremidades (Möller Jr et al., 1996; Möller Jr et al., 2001; Fernandes et al. 2001; 2002). O efeito não-local ocorre pelo Transporte de Ekman na região costeira adjacente, onde ventos paralelos à costa com direções de NE causam diminuição e os ventos de SO causam aumento do nível do mar nesta região, tendo como consequência fluxos de vazante e enchente no estuário, respectivamente (Möller Jr et al., 2001; Fernandes et al., 2005; Möller Jr e Fernandes, 2010).

A ação dos ventos remotos causa gradientes de pressão barotrópica entre a lagoa, seu estuário e a região costeira adjacente. Durante períodos de vento NE (Figura 3A), ocorre diminuição do nível da água no norte da lagoa e um acúmulo de água na Feitoria, observando-se um empilhando ao sul junto a desembocadura da lagoa. O efeito não-local impulsionado pelo Transporte Ekman (atuando 90º à esquerda do vento) diminui o nível da água próximo à desembocadura, causando

em gradiente de pressão para fora da lagoa. O oposto ocorre durante períodos de ventos SO (Figura 3B), quando o efeito local aumenta o nível da água no norte da lagoa e diminui na Feitoria. O efeito não-local impulsionado pelo transporte de Ekman inverte e acumula água perto da desembocadura. A combinação dos dois efeitos gera um gradiente de pressão barotrópica em direção à Feitoria, o que favorece a penetração da água da região costeira adjacente na lagoa (Castelão e Möller Jr, 2003; Fernandes et al., 2005).

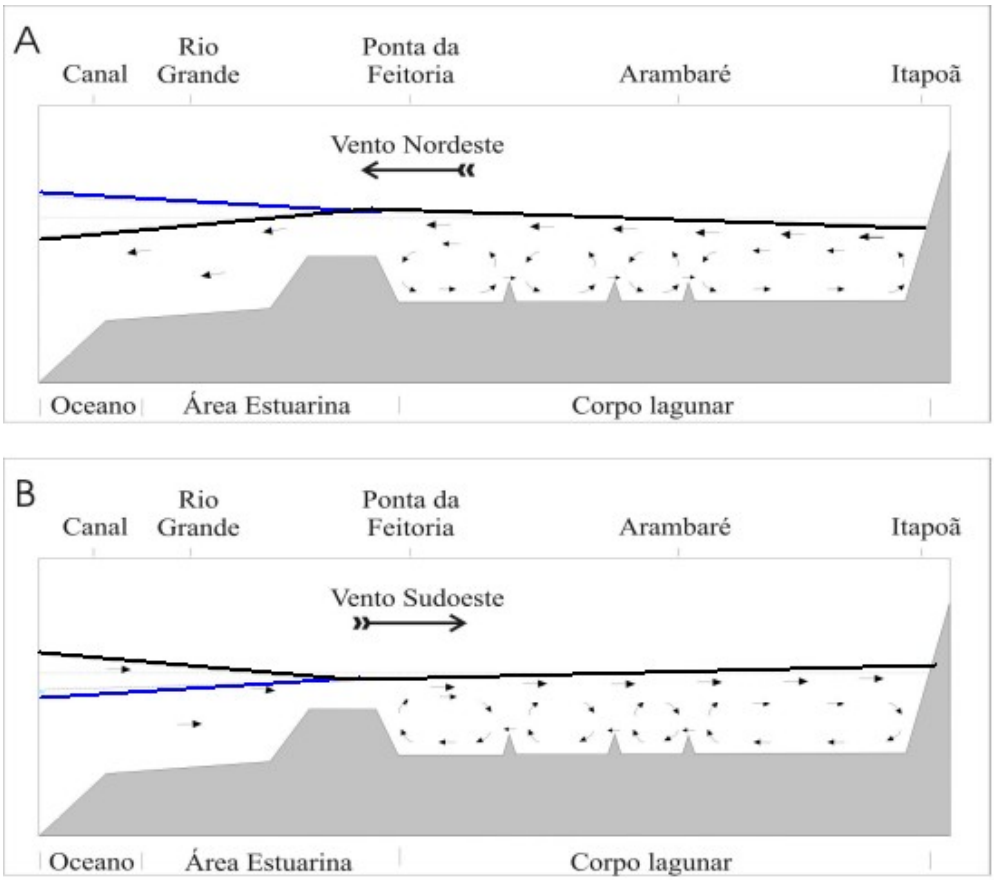


Figura 3: Oscilação do nível do mar na Lagoa dos Patos em função dos ventos NE (A) e SO (B). A linha azul representa a elevação da superfície forçada pelo vento considerando a Lagoa dos Patos fechada nas duas extremidades. Os vetores representam o sentido das correntes (Castelão e Möller Jr, 2003).

Todavia, este padrão de circulação não se verifica em presença de elevadas descargas (>2000 $m^3s^{-1}$), pois a ação do vento SO é dominada pela descarga continental (Möller Jr e Canstaing, 1999), impondo um gradiente de pressão para o

oceano, fato que confina a zona estuarina a ocorrer na região costeira adjacente (Möller Jr et al., 2001).

Segundo Piola et al. (2005) e Marques et al. (2009), ventos de S/SO, predominantes no inverno, forçam a pluma para norte durante períodos de baixa descarga fluvial, mantendo-a restrita à costa e relativamente estreita (60 km), além de produzir um intenso gradiente de salinidade perpendicular à costa. Em contrapartida, ventos de NE retém a pluma ao sul dos Molhes da Barra e a espalham sobre a plataforma continental, deixando o restante da plataforma sob influência das massas de água Tropical (AT), Subtropical de Plataforma (ASTP) e Central do Atlântico Sul (ACAS).

A lagoa recebe água de drenagem continental de vários rios afluentes localizados na sua porção superior fornecendo cerca de 85 % do volume total de água da lagoa (Odebrecht et al., 2005). Os 3 principais tributários são: o rio Guaíba bem ao norte, o rio Camaquã na porção central da lagoa, e as águas da Lagoa Mirim ao sul, através do Canal São Gonçalo (Figura 1). A lagoa apresenta uma descarga média anual de cerca de 2400 $m^3s^{-1}$ (Möller Jr e Fernandes, 2010). As elevadas descargas verificam-se no final do inverno e início de primavera e as baixas à moderadas entre o verão e outono (Marques e Möller Jr, 2009), apresentando consistentes anomalias em escalas interanuais (Távora et al., 2019), pois a região apresenta clima temperado associado à eventos ENOS (Möller Jr et al., 2001; Fernandes et al, 2002; Möller Jr et al., 2009). A ocorrência dos eventos ENOS causa anomalias na descarga, observando-se que em anos de ocorrência de El Niño, o período de primavera tende a ser mais úmido com elevadas descargas e em anos de ocorrência de La Niña no mesmo período, fortes anomalias secas e baixas descargas são registradas (Grimm et al., 1998, Montecinos et al., 2000). Variações sazonais levam ao registro de médias de descargas de 700 $m^3s^{-1}$ durante o verão (dezembro a março), e acima de 3000 $m^3s^{-1}$ durante o inverno (setembro ao início de dezembro), tendo sido observado por Möller Jr et al. (1996) um pico máximo de descargas variando entre 12.000 e 25.000 $m^3s^{-1}$ durante períodos de El Niño (Möller Jr et al., 2001; Lisboa e Fernandes, 2015). A ocorrência do fenômeno ENSO na região sul do Brasil, que ocasiona alterações no regime hidrológico e na dinâmica da Lagoa dos Patos com as anomalias na precipitação e consequentemente nas

descargas, também causa aumento ou redução da intrusão salina confinando a região estuarina junto a boca da lagoa. (Fernandes et al., 2002; Odebrecht et al., 2005; Seiler et al., 2015).

No aspecto meteorológico, a região litorânea do Rio Grande do Sul apresenta um clima que é afetado por sistemas sinóticos e fatores associados à circulação de larga escala. A circulação atmosférica é dominada por dois sistemas meteorológicos de alta pressão, o anticiclone do Atlântico Sul que transporta massas de ar quentes e úmidas acompanhado dos ventos NE que atingem em média cerca de 5 $ms^{-1}$, e o anticiclone de origem polar que transporta para a região massas de ar frias e secas, acompanhadas de ventos do quadrante S, podendo registrar ventos de SO que chegam a 8 $ms^{-1}$. As frentes frias chegam à região num intervalo 3 a 15 dias (Moler et al., 2001; Fernandes et al., 2002; Marques, 2009; Möller Jr e Fernandes, 2010).

A salinidade na Lagoa dos Patos oscila com a variabilidade das marés, porém varia em função da força do vento e das descargas dos rios em escalas de horas a semanas, devido à reduzida influência das marés (Garcia, 1997 citado por Fernandes et al, 2005). O limite médio de intrusão salina abrange apenas uma porção de cerca de 10% da lagoa atingindo cerca de 60 km (Ponta da Feitoria), embora os limites superior e inferior das águas salinas migrem sazonalmente e de ano para ano dependendo dos balanços hidrológicos (Möller Jr et al., 2001). Todavia, o seu alcance máximo na lagoa atinge cerca de 180 km da boca da lagoa durante períodos de baixas descargas e ventos SE e SW, e o alcance mínimo ocorre em períodos de alta descarga combinando com ventos NE, reduzindo significativamente a salinidade, limitando-se a região estuarina e podendo permanecer totalmente doce por dias (Odebrecht et al., 2005; Fernandes et al., 2005).

### 1.3. Recrutamento de ictioplâncton para estuários

Áreas costeiras rasas, como estuários, baías e outros sistemas semi-fechados são vitais no mundo, por serem altamente produtivos e capazes de sustentar grande diversidade e densidade de organismos, e também servirem de habitat e berçário para os organismos (Norcross e Shaw, 1984; Dugan et al., 2011; Costa et al., 2013; Araujo et al., 2016; Liu e Chan, 2016).

A dinâmica do recrutamento de peixes em regiões costeiras é muito variável e depende da complexa combinação de fatores bióticos e físicos ou abióticos, resultando em consequências tanto ecológicas quanto econômicas (Brown et al., 2000). Segundo alguns autores, os fatores bióticos incluem a abundância sazonal de adultos e larvas, preferências ambientais, disponibilidade de alimento, potenciais predadores e o próprio comportamento das larvas (Norcross e Shaw; 1984; Muelbert et al., 2010). Complementar a esses, os fatores físicos do ambiente incluem a oceanografia ou hidrologia, e o clima da região, especialmente a temperatura, salinidade, estratificação, turbidez, descarga, padrões do tempo e do fluxo da água, bem como sua direção e anomalias (Norcross e Shaw; 1984; Muelbert et al., 2010). Logo, a sua variabilidade interanual determina o transporte, retenção e consequentemente a sobrevivência de ovos e larvas (Bruno e Muelbert, 2009).

De forma a compreender o processo de recrutamento de organismos, Harden e Jones (1968), guiados pelas ideias de Hjort (1914), desenvolveram o chamado “triângulo de migração”, definindo áreas de desova, locais de crescimento e estoque de adultos. Os autores presumiram que na fase passiva os ovos e larvas são dependentes das correntes, e na fase de recrutamento os juvenis já são nadadores ativos. A teoria veio a ser comprovada por vários autores, constatando-se que as áreas de desova e crescimento no primeiro estágio de vida de muitos organismos marinhos é definida pelos padrões de circulação local, que envolvem movimentos oceânicos de ampla escala espacial e temporal (Brown et al. 2000; Vaz et al, 2005; Martins et al., 2007; Dugan et al. 2011; Franzen et al., 2019). Mesmo sendo definidos os locais de desova dos organismos junto à costa, o seu transporte para locais protegidos como estuários, baias e regiões costeiras rasas é essencial, pois é durante esse processo que ocorre a dispersão e morte das larvas (Norcross e Shaw, 1984; Vaz et al, 2005; Vieira et al., 2010).

A costa da região sul do oceano Atlântico Sul apresenta um ecossistema costeiro de grande importância do ponto de vista ecológico e socio-econômico que é influenciado principalmente pela interação de características oceanográficas, condições climáticas e descargas continentais (Kjerfve et al. 2001). O estuário da Lagoa dos Patos é um importante habitat para ovos e larvas de peixes e crustáceos por ser um estuário do tipo pouco profundo (Muelbert e Weiss, 1991), e cerca de

80% da região estuarina ter menos de 2 m de profundidade (Möller Jr et al., 2001). Estas condições são consideradas apropriadas para o crescimento de organismos estuarinos dependentes, que são os organismos que se reproduzem em águas costeiras, e seus ovos e larvas são transportados pela água do mar para o estuário, onde passam o seu estágio inicial de vida (Ibagy e Sinque, 1995; Martins, 2007; Salvador e Muelbert, 2019). O estuário da Lagoa dos Patos e sua região costeira adjacente são um importante viveiro para espécies de importância econômica, sendo as mais abundantes a *Brevoortia pectinata, Lycengraulis grossidens e Micropogonias furnieri*, representando 88% dos ovos e 66% das larvas do ictioplâncton presente no estuário (Muelbert e Weiss, 1991; Filgueiras, 2009).

Os estudos do ictioplâncton no estuário da Lagoa dos Patos começaram na década de 70, analisando-se a influência da hidrodinâmica na distribuição espacial e temporal, e no ciclo de vida das espécies (Castello, (1976) citado por Muelbert et al., 2010). Até a década de 90, o estuário apresentava uma composição de cerca de 17 espécies, agrupadas em 2 gêneros e 2 famílias. E de forma similar a outros estuários temperados, a ocorrência da abundância do ictioplâncton é determinada principalmente pelas variações sazonais de salinidade e temperatura (Muelbert e Weiss, 1991; Garcia et al., 2003; Muelbert et al., 2010).

### 1.4. Corvina *Micropogonias furnieri*

A corvina *Micropogonias furnieri* (Figura 4) encontra-se ao longo de toda costa do Rio Grande do Sul em águas pouco profundas de 4 m a 10 m, desova preferencialmente na região costeira próximo ao canal de acesso e é uma das espécies mais abundante do ictioplâncton do estuário da Lagoa dos Patos, (Oliveira e Bemvenuti, 2006; Martins et al. 2007; Muelbert et al., 2010). Os ovos e larvas são encontrados durante todo o ano na região costeira adjacente (Ibagy e Muelbert, 2009), usa o estuário durante seu primeiro estágio de vida com o recrutamento ocorrendo principalmente entre a primavera e verão (Bruno e Muelbert, 2009; Costa et al., 2014).


Figura 4: Corvina *Micropogonias furnieri* (modificado da FAO, 2020)

No estuário da Lagoa dos Patos, o ciclo da corvina (Figura 5) ocorre durante a primavera até o outono, coincidindo com o seu estágio de desova e larval, sendo recrutados os ovos e larvas da região costeira adjacente do Rio Grande até a isóbata de 60 m para o interior do estuário, e a saída para a região costeira ocorre no inverno (época chuvosa) (Oliveira e Bemvenuti, 2006; Bruno e Muelbert, 2009). Os juvenis com tamanhos <30 mm de Comprimento Total (CT) podem concentrar-se em águas rasas (áreas com vegetação e não vegetação) e águas profundas. Os juvenis com tamanhos entre 30-90 mm CT e 90-160 mm CT podem ser encontrados em todo o estuário, em habitats estuarinos rasos e profundos (Costa et al., 2014). Juvenis maiores que 160 mm CT são registrados nas praias estuarinas durante o primeiro período, mas aparentemente estão mais relacionados às águas profundas (Vieira, 2006), indicando a migração inicial para a plataforma continental para desova (Figura 5). Castello (1986) citado por Costa et al., (2014) demonstrou que juvenis maiores que 160 mm são registrados mais em águas profundas com tendência a migrarem para a plataforma continental, subsequentemente juvenis entre 180-205 mm CT, são os que mais migram, estando o padrão associado à primeira maturidade sexual, notando-se ainda diferenças no comportamento alimentar e nas preferências alimentares entre áreas profundas e rasas de ELP (Figueiredo e Vieira, 1998).

Estudos constataram que parte das corvinas tem o seu ciclo de vida completo dentro do estuário, e é possível capturar corvina adulta dentro do estuário da Lagoa dos Patos, o que leva a crer que parte das larvas são retidas (Oliveira e Bemvenuti, 2006; Castro et al., 2014).

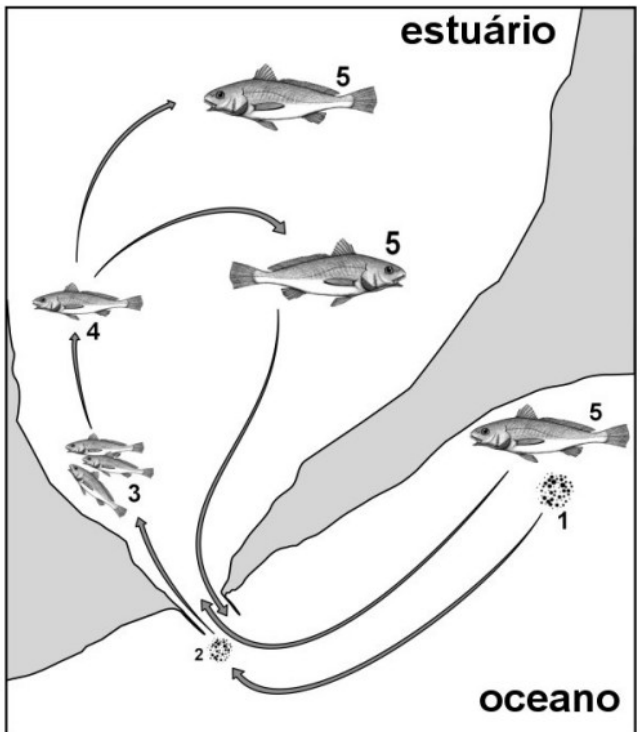


Figura 5: Ciclo de vida da corvina *Micropogonias furnieri,* no estuário da Lagoa dos Patos. (1) desova realizada na zona costeira adjacente; (2) ovos e larvas sãoo advectadas para o estuário; (3) juvenis se desenvolvem nas zonas razas; (4) indivíduos maturos com cerca de 20-25 cm; (5) adultos aptos para desovar, deslocam-se para o mar ou desovam dentro do estuário. (Fonte: Oliveira e Bemvenuti, 2006).

A corvina *Micropogonias furnieri* apresenta uma variação sazonal na abundância de ovos, e a maior abundância média de ovos ocorre no verão (32 +- 16 ovos por 100 $m^3$) e a mais baixa no inverno (1 +- 2 ovos por 100 $m^3$), havendo um aumento significativo da abundância em direção ao canal de acesso do ELP e consequentemente a maior concentração na parte inferior (desembocadura) do estuário (Bruno e Muelbert, 2009). Similar aos ovos, as larvas também apresentam sua maior abundancia média no verão (5 +-4 larvas por 100 $m^3$) com uma diminuição da ordem de 10 vezes no inverno e outono, estando a maior concentração junto à desembocadura do estuário e diminuindo para o interior do estuário, porém não

apresentam variação interanual significativa da sua abundância (Bruno e Muelbert 2009).

Uma variação positiva da abundância de ovos e larvas de *M. furnieri* no estuário da Lagoa dos Patos é registrada em função da temperatura e a salinidade (Costa et al., 2014). A abundância da corvina durante a primavera e o verão no ELP está associada ao fato da espécie ter como preferência águas com temperaturas mais quentes (Harris et al., 2001). Período coincidente com os ventos em direção a costa que propiciam condições polihalinas e entrada de ovos e larvas para o interior do estuário e áreas favoráveis a alimentação e crescimento do ictioplâncton, demostrando que a salinidade é o fator ambiental mais crucial para a distribuição nas diferentes áreas do estuário, e elevada precipitação e vazão são fatores que contribuem para baixa abundância do ictioplâncton numa determinada região (Muelbert et al., 2010).

Os eventos ENOS associados ao regime dos ventos também influenciam na variabilidade interanual dos organismos como a corvina e na atividade pesqueira na Lagoa dos Patos em geral (Möller Jr et al., 2009), sendo determinantes no recrutamento de espécies marinhas (Garcia et al., 2003; Bruno e Muelbert, 2009; Muelbert et al., 2010). Associado as elevadas correntes de vazante do estuário, grandes são as implicações do ENOS no transporte e migração de ovos, larvas e organismos, na pescaria bem como em processos ecológicos da região (Garcia et al., 2001; Fernandes et al., 2002; Odebrecht et al., 2005; Möller Jr et al., 2009; Seeliger (2004) citado por Seeliger e Odebrecht, 2010; Seiler et al., 2015).

### 1.5. Dinâmica do transporte de ovos e larvas

Dependendo da dinâmica da circulação das áreas de desova até os berçários, a maior ou menor retenção dos primeiros estágios de vida nestes ecossistemas é definida e contribuiu para um maior ou menor sucesso no recrutamento, bem como o sucesso reprodutivo das futuras gerações de uma espécie (Brown et al., 2000). Logo, alterações morfológicas mudam as características da hidrodinâmica e circulação estuarina e impactam no processo de recrutamento e no ciclo de vida dos organismos que dependem destes ecossistemas (Sherwood et al., 1990; Brown et al., 2000; Dugan et al., 2011; Liu e Chan, 2016).

Na Lagoa dos Patos, a construção dos Molhes da Barra do Rio Grande no início do século XX, além de alterar a intensidade do fluxo de entrada e saída de água no estuário (Cunha e Calliari, 2009; Möller Jr e Fernandes 2010; Lisboa e Fernandes, 2015) podem ter alterado o transporte de organismos entre o estuário e a região costeira, e modificado os padrões de composição, distribuição e de recrutamento de ovos e larvas no estuário (Muelbert et al., 2010). Diversas causas com enfoques na causa antrópica levaram a um acentuado declínio da pesca artesanal no estuário da Lagoa dos Patos, desde a configuração dos Molhes à alta velocidade da vazão que dificulta a penetração da água do mar, e consequentemente a entrada de juvenis de crustáceos e peixes marinhos (Seeliger e Costa, 2010; Vieira et al., 2010; Muelbert et al. 2010). Fato a ressaltar é que a ação antrópica também pode alterar a dinâmica dos ecossistemas marinhos, e outras intensas e multidisciplinares atividades de recuperação de populações marinhas super-exploradas ou destruídas antropogenicamente, que é um processo moroso e de extrema importância para a pesca e conservação (Dugan et al., 2011; Costa et al., 2013; Barletta e Lima, 2019).

Como forma de garantir o controle das populações pesqueiras, problema que ainda carece de solução, para uma reversão do declínio de estoques pesqueiros marinhos mundiais, o estudo da dinâmica de populações de organismos marinhos ganhou foco devido a extrema pressão da pesca no início do século XX (Norcross e Shaw, 1984; Brown et al., 2000; Vaz et al., 2007; Dugan et al., 2011; Costa et al., 2013; Liu e Chan, 2016;), pois entender esse recrutamento garante uma boa gestão e padrões de sustentabilidade na exploração.

Segundo Miller (2007), um elevado número de estudos tem sido publicados nas últimas décadas a respeito do acoplamento de modelos físicos e biológicos para o estudo do recrutamento de peixes, pois a sua compreensão garante uma boa gestão e padrões de sustentabilidade na exploração e regulamento da pesca. Os avanços da oceanografia física e ecológica dos peixes no acompanhamento do desenvolvimento do primeiro estágio individual dos peixes foi crescendo, e o acoplamento de modelos físicos e biológicos para o estudo do estágio precoce do ciclo de vida dos peixes iniciaram no fim dos anos 1980, tendo evoluído rapidamente

(Able, 2005;  Miller, 2007; Dugan et al., 2011; Costa et al., 2013; Barletta e Lima, 2019).

Aliados a essa tendência, experimentos numéricos tem investigado a relação das principais forçantes hidrodinâmicas e meteorológicas do estuário da Lagoa dos Patos, com particular enfoque para a corvina da espécie *Micropogonias furnieri,* no processo de transporte, dispersão e no recrutamento dos seus ovos e larvas (Martins et al., 2007; Franzen et al., 2019). Estes autores constataram que os ventos de SO e a desova na região central da desembocadura da lagoa são os catalisadores do melhor recrutamento de ovos e larvas da corvina. Todavia, após as recentes obras de modernização dos Molhes da Barra, nenhum estudo foi feito de modo a avaliar os efeitos das mudanças na geomorfologia da desembocadura do estuário da Lagoa dos Patos sobre a hidrodinâmica e sobre a dinâmica de transporte de ovos e larvas de organismos estuarino-dependentes como a corvina da espécie *Micropogonias furnieri.*

# Capítulo II:

# Hipótese

**2. HIPÓTESE**

A nova configuração da desembocadura dos Molhes da Barra do Rio Grande de 2010 alterou a hidrodinâmica local e consequentemente o transporte de ovos e larvas de corvina no estuário da Lagoa dos Patos.

# Capítulo III:
# Objetivos

## 3. OBJETIVOS

### 3.1. Geral

Estudar o efeito da alteração da configuração dos Molhes da Barra do Rio Grande na circulação estuarina e no transporte de ovos e larvas da corvina *Micropogonias furnieri* no estuário da Lagoa dos Patos.

### 3.2. Específicos

1. Analisar as mudanças hidrodinâmicas induzidas através das alterações nos Molhes da Barra do Rio Grande na hidrodinâmica do estuário da Lagoa dos Patos;
2. Avaliar o efeito da alteração da configuração dos Molhes da Barra sobre a extensão de penetração dos ovos e larvas no estuário da Lagoa dos Patos;
3. Analisar o efeito da estratificação lateral na entrada de ovos e larvas da corvina *Micropogonias furnieri* antes e depois da modificação dos Molhes da Barra.

# Capítulo IV:
# Material e Métodos

### 4.1. Modelo hidrodinâmico – TELEMAC-3D

O modelo TELEMAC (http://www.opentelemac.org/) foi desenvolvido no *Laboratoire National d'Hidraulique et Environment*, no departamento de *Division for Research and Development of the French Electricity Board* (EDB R&D). O TELEMAC é um sistema de programas computacionais desenhado para estudos de processos ambientais em fluxos transitórios em superfícies livres. É aplicado para domínios

costeiros, oceânicos, estuários, rios e lagos. O modelo TELEMAC-MASCERET (versão v7p0) apresenta módulos em duas e três dimensões para estudos em hidrodinâmica, sedimentologia, qualidade de água e evolução da superfície livre durante ação de ondas curtas. O modelo TELEMAC-3D calcula também os fluxos em superfícies livres em corpos de água naturais no transporte de substâncias dissolvidas e em suspensão.

O pré-processamento do Sistema TELEMAC-MASCARET concentra módulos de digitalização de dados batimétricos (MATISSE, BLUEKENUE, JANET), gerando uma malha de elementos finitos para discretizar o domínio do modelo no espaço e estabelecer o tipo de condições de contorno (MATISSE), especificando os parâmetros físicos a utilizar na simulação (EDAMOX).

Todos módulos de sistema TELEMAC são baseados em uma biblioteca interna de solucionadores numéricos de elementos finitos (BIEF library). O modelo resolve as equações de fluxo em superfície livre da água, aplicando a técnica de elementos finitos e usando o sistema de coordenadas sigma para a discretização vertical. As variáveis computacionais são definidas em cada ponto da malha tridimensional, incluindo o fundo e a superfície.

A discretização espacial horizontal bi-dimensional do domínio do fluxo é baseada em malhas não-estruturadas de elementos triangulares de vários tamanhos e formas. Por outro lado, os domínios tri-dimensionais são representados por elementos prismáticos de base triangular ou tetraedros. Para preparar a malha do domínio em 3D, primeiro uma malha bidimensional compreendendo triângulos que cobrem o domínio computacional em um plano é construída. O segundo passo consiste em duplicar essa malha ao longo da direção vertical em várias superfícies curvas conhecidas como planos. Entre dois desses planos, os elos entre os triângulos entrelaçados formam prismas (Figura 6).

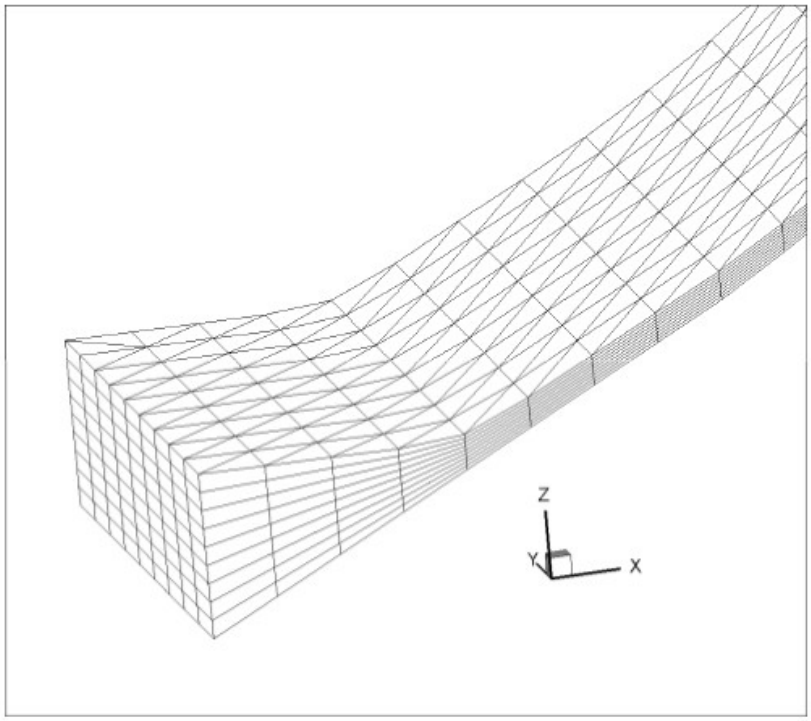


Figura 6: Malha tridimensional do Telemac-3D.

Outro aspecto do TELEMAC-3D, é que o tipo de malha permite introduzir um maior refino garantido uma resolução espacial mais alta em torno das zonas de interesse ou zonas de alto gradiente de batimetria. É o caso, por exemplo, das regiões próximas à desembocadura do estuário da Lagoa dos Patos, canais de navegação, e locais com elevada variação batimétrica.

### 4.1.1. Equações e principais parâmetros físicos

O modelo hidrodinâmico resolve as equações diferenciais parciais de segunda ordem de Navier-Stokes, considerando variações locais da superfície livre do fluido, negligenciando as variações da densidade na equação de conservação de massa (equação de continuidade), considerando a pressão hidrostática ou não-hidrostática, bem como a aproximação de Boussinesq para resolver a equação de movimento (Hervouet, 2007). Dadas estas suposições, as seguintes equações 3D são resolvidas:

- Conservação de movimento:

$$\frac{\partial u}{\partial x}+\frac{\partial v}{\partial y}+\frac{\partial w}{\partial z}=0 \quad (1)$$

- Conservação de quantidade de momento: $\nu$ (2)

$$\frac{\partial u}{\partial t}+u\frac{\partial u}{\partial x}+v\frac{\partial u}{\partial y}+w\frac{\partial u}{\partial z}=-\frac{1}{\rho}\frac{\partial P}{\partial x}+\nu\nabla^2 u+F_x$$

$$\frac{\partial v}{\partial t}+u\frac{\partial v}{\partial x}+v\frac{\partial v}{\partial y}+w\frac{\partial v}{\partial z}=-\frac{1}{\rho}\frac{\partial P}{\partial y}+\nu\nabla^2 v+F_y$$

$$\frac{\partial w}{\partial t}+u\frac{\partial w}{\partial x}+v\frac{\partial w}{\partial y}+w\frac{\partial w}{\partial z}=-\frac{1}{\rho}\frac{\partial P}{\partial w}-g+\nu\nabla^2 w+F_z$$

Pressão hidrostática:

$$P=P_{atm}+\rho_0 g(\eta-z)+\rho g\int_z^\eta \frac{\Delta\rho}{\rho_0}dz \quad (3)$$

Onde: *U, V e W* são as componentes das velocidades nas direções x, y, e z, respectivamente; P é a pressão; $P_{atm}$ é a pressão atmosférica; η é o nível do mar; z é a profundidade total; $\rho_0$ é a densidade inicial da água; ρ é a densidade da água; $\nu$ é o coeficiente de viscosidade cinemática; *g* é a aceleração da gravidade; $\nabla^2$ é o operador Laplaciano; *Fx*, *Fy* e *Fz* são termos fonte horizontais (arrasto do vento, força de Coriolis e fricção do fundo).

### 4.1.2. Lei de Estado

Duas leis de estado podem ser usadas como padrão através do TELEMAC-3D. Na maioria das simulações, a salinidade e a temperatura tornam possível calcular as variações de densidade. A primeira lei expressa a variação de densidade apenas com os dois parâmetros, sendo a lei escolhida para aplicação neste estudo, e é escrita da seguinte forma:

$$\rho=\left[1-\left(7\left(T-T_{ref}\right)^2-750\,S\right)10^{-6}\right] \quad (4)$$

Onde: $T_{ref}$ é a temperatura de referência de 4°C e $\rho_{ref}$ é a densidade de referência a essa temperatura, e quando a salinidade S é zero, então $\rho_{ref}$ = 999.972 kg/m$^3$. Essa lei permanece válida para 0°C < T < 40°C e 0 g / L < S < 42 g / L.

A segunda lei é mais geral e permite construir todas as variações de densidade com os marcadores ativos sendo levados em consideração no cálculo:

$$\rho=\rho_{ref}[1-\sum_i \beta_i(T_i-T_i^0)] \quad (5)$$

Onde: $\rho_{ref}$, a densidade de referência, e pode ser modificada pelo usuário juntamente com os coeficientes de expansão volumétricos $\beta_i$ relacionados aos marcadores $T_i$.

### 4.1.3. Modelos de turbulência

A implementação do TELEMAC-3D requer a definição de dois modelos de turbulência horizontal e vertical. O sistema do modelo TELEMAC-3D disponibiliza vários modelos de turbulência vertical e horizontal, os quais são aplicados às velocidades, bem como aos traçadores ativos e passivos.

A fim de definir o modelo de turbulência a ser utilizado na horizontal e na vertical, no presente estudo, simulações teste foram feitas com o TELEMAC-3D. Nos conjuntos das simulações utilizou-se o Modelo de comprimento de mistura na vertical e o Modelo Smagorinsky na horizontal.

A difusividade vertical das velocidades é automaticamente calculada pelo TELEMAC-3D por meio do modelo de comprimento de mistura, levando em consideração ou não os efeitos da densidade. O modelo de comprimento de mistura expressa a viscosidade turbulenta (ou coeficiente de difusão) em função do gradiente de velocidade média e do comprimento de mistura (Teoria de Prandtl):

$$v_{tz}=f(R_i)L_m^2\sqrt{(\frac{\partial U}{\partial Z})^2+(\frac{\partial V}{\partial Z})^2} \quad (6)$$

$$v_{zt}=f_T(R_i)L_m^2\sqrt{(\frac{\partial U}{\partial Z})^2+(\frac{\partial V}{\partial Z})^2} \quad (7)$$

$$R_i = \frac{-g}{\rho_0} \frac{\frac{\partial \rho}{\partial z}}{\rho_0 \left(\frac{\partial U}{\partial z}\right)^2 + \left(\frac{\partial V}{\partial z}\right)^2}$$

Onde: é o número de Richardson e $L_m$ é o parâmetro de comprimento de mistura; f e $f_T$ são as funções de atenuação das velocidades e dos traçadores, que ajudam a ajustar o modelo e adaptá-lo a casos especiais.

O Modelo *Smagorinsky* (*Smagorinsky,* 1963), fundamenta-se no modelo de comprimento de mistura, e pertence a categoria de modelos de turbulência de sub-grid, permitindo a representação de processos físicos que ocorrem em escalas de comprimento com resolução limitada na malha computacional. Neste sentido *Smagorinsky* adiciona à viscosidade molecular uma viscosidade turbulenta deduzida do Modelo Comprimento de mistura.

O atrito da parte inferior ou lateral reflete a continuidade da restrição na interface fluido-sólido. Ao equacionar a fricção é importante conhecer o fluxo nas proximidades do fundo e das bordas laterais e inferiores. Os modelos de turbulência fornecem uma solução para diferentes fluxos.

A tensão de cisalhamento (fricção do fundo) atua no fluido se opondo a direção da velocidade de corrente, e pode ser escrita como:

$$\vec{\tau} = -\mu \frac{\partial \vec{v}}{\partial \eta} \tag{8}$$

A partir da análise dimensional da tensão de cisalhamento de fundo, a expressão passa a ser expressa por:

$$\vec{\tau} = \frac{-1}{2} C_f \sqrt{u^2 + v^2} \tag{9}$$

Onde: $C_f$ é o coeficiente adimensional de fricção; e $\vec{V}$ é o campo de velocidade de fundo.

O cálculo da tensão turbulenta na parte inferior depende do perfil de velocidade acima da parte inferior (dentro da camada limite), que pode ser rugoso ou suave. Essa opção altera a padrão do perfil de velocidade e, consequentemente, a velocidade de

atrito. O TELEMAC-3D oferece parametrizações de alguns coeficientes de fricção do fundo, sendo: Chézy (Equação 10), Strickler (Equação 11), Manning (Equação 12) e Nikuradse (Equação 13). No estudo foi usado o Manning.

$$C_h = 7.831 \ln\left(12\frac{h}{k_s}\right) \tag{10}$$

$$C_s = \frac{2g}{h^{1/3}S^2} \tag{11}$$

$$C_m = \frac{2gm^2}{h^{1/3}} \tag{12}$$

$$C_n = 2gC_{h^{-2}} \tag{13}$$

Onde: g é o coeficiente de gravidade; h é a espessura da coluna de água; $k_s$ é o tamanho do grão; e (C, S, m) são os coeficientes.

### 4.1.4. Força do vento

A influência dos ventos é considerada no modelo como uma condição bi-dimensional no contorno superficial, levando-se em consideração a influência de um vento soprando na superfície da água. A tensão de cisalhamento gerada pelo vento é dada por:

$$F_{wx} = \frac{1}{h}\frac{\rho_{ar}}{\rho} a_{vento} u_{vento} \sqrt{u_{vento}^2 + v_{vento}^2}$$

$$F_{wy} = \frac{1}{h}\frac{\rho_{ar}}{\rho} a_{vento} v_{vento} \sqrt{u_{vento}^2 + v_{vento}^2} \tag{14}$$

Onde: $F_{wx}$ e $F_{wy}$ são as componentes zonais e meridionais das tensões de cizalhamento ou força de fricção do vento; $\rho_{ar}$ é a densidade do ar equivalente a 1.29 $kgm^{-3}$; u e v são as componentes zonais e meridionais da velocidade horizontal do vento na superfície do domínio; $a_{vento}$ é o coeficiente adimensional de influência do vento, e é dado por Flather (1976) como sendo:

$$a_{vento} = 0{,}565 \cdot 10^{-3} \quad \text{Se} \quad |\overrightarrow{u_{vento}}| < 5\, m.s^{-1}$$

$$a_{vento} = \left(-0{,}12 + 0{,}137\,|\overrightarrow{u_{vento}}|\right) \cdot 10^{-3} \quad \text{Se} \quad 5 < |\overrightarrow{u_{vento}}| < 19{,}22\, m.s^{-1}$$

$$a_{vento} = 2{,}513 \cdot 10^{-3} \quad \text{Se} \quad |\overrightarrow{u_{vento}}| > 19{,}22\, m.s^{-1}$$

O coeficiente de influência do vento oculta fenômenos complexos. De forma que, a sua influência depende da suavidade ou rugosidade da superfície livre e da distância sobre a qual ele atua.

Ao modelar grandes domínios, a influência da força de inércia de Coriolis deve ser levada em consideração. Isso é feito ativando a palavra-chave lógica CORIOLIS. Nesse caso, o valor do coeficiente de Coriolis foi considerado constante de 7,27 x $10^{-5}$ rad $s^{-1}$ considerando a latitude média da aréa aplicada no modelo.

### 4.1.5. Traçadores

TELEMAC-3D resolve as equações de advecção e difusão de traçadores ativos, que são os que interagem na densidade ou com o fluído, sendo eles, temperatura, salinidade, sedimentos em suspensão, bem como traçadores passivos para estudo do processo de transporte, que não afetam o fluxo e são apenas transportados (partículas passivas). A evolução espaço-temporal dos traçadores depende das correntes que controlam os processos de advecção, e dos processos de difusão que são na maioria das vezes processos turbulentos, e por fim dependem de fontes ou sumidouros de traçadores.

A forma conservativa da evolução dos traçadores considerando a advecção e difusão em três dimensões é dada por:

$$\frac{\partial}{\partial t}(\rho T) + divergente\left(\rho T \vec{U} + \vec{q}\right) = F_{fonte} \qquad (15)$$

A equação da evolução dos traçadores na forma não-conservativa é dada por:

$$\frac{\partial T}{\partial t} + u\frac{\partial T}{\partial x} + v\frac{\partial T}{\partial y} + w\frac{\partial T}{\partial z} = V_T \nabla^2 T + Q \quad (16)$$

Onde: T é traçador passivo ou ativo; $v_T$ é o coeficiente de difusão do traçador; t é o tempo; x, y e z são as componentes do espaço; u, v e w são as componentes da velocidade; Q é a fonte ou sumidouro do traçador.

A aplicação das condições de contorno nas fronteiras sólidas, o fluxo dos traçadores é considerado zero:

$$v\frac{\partial T}{\partial n} = 0 \quad (17)$$

Onde: $\frac{\partial T}{\partial n}$ expressa $\vec{\nabla} T \cdot \vec{n}$ e $\vec{n}$ é o versor perpendicular a fronteira apontando para fora.

Em contrapartida nas condições de contorno das fronteiras líquidas a condição do fluxo dos traçadores é dada por:

$$v\frac{\partial T}{\partial n} = aT + b \quad (18)$$

Onde: a é o coeficiente de fricção na fronteira e b é um coeficiente linear de fricção.

### 4.2. Domínio numérico e Malha batimétrica

O domínio numérico do estudo que abrange toda Lagoa dos Patos e região costeira adjacente, está compreendido entre as latitudes de 28° e 36°S e as longitudes de 46° e 54°O.

A batimetria da Lagoa dos Patos, do estuário e da região costeira adjacente foram obtidas a partir de dados históricos. Cartas náuticas do Diretório de Hidrografia e Navegação (DHN, Marinha do Brasil) antes de 2010 foram usadas como as informações batimétricas antigas (antes das alterações na configuração dos Molhes). Os dados do projeto de expansão dos Molhes foram utilizados para definir a batimetria após a alteração dos Molhes da Barra. Duas malhas numéricas

foram geradas, e a principal diferença entre as malhas é o comprimento dos Molhes e a profundidade do canal de acesso ao estuário (Figura 7).

O Programa BlueKenue (http://www.nrc-cnrc.gc.ca/eng/solutions/advisory/blue_kenue_index.html) foi usado para gerar as malhas batimétricas não-estruturadas de elementos triangulares. A otimização da malha foi feita nos locais de morfologia complexa e nas áreas de acentuados gradientes batimétricos. As duas malhas resultantes foram usadas para simular a hidrodinâmica antes e após a modificação dos Molhes da Barra (Figuras 7B e 7C). As malhas abrangem toda a área de estudo até cerca de 2500 m de profundidade para melhor representar a dinâmica costeira, e contêm um total de 17868 e 17575 nós para o antigo e novo cenário, respectivamente. Um total de 11 níveis sigma foram considerados na vertical e distribuídos do fundo à superfície. Os maiores triângulos localizados em mar aberto (menor refinamento) têm arestas de cerca de 27 km de comprimento, enquanto os menores triângulos no canal de acesso (maior refinamento) têm cerca de 50 m.

### 4.3. Condições iniciais e de contorno para a modelagem hidrodinâmica

De forma a reproduzir as condições observadas no ambiente, o modelo necessita de condições iniciais e de contorno. Para que os resultados das simulações para os diferentes cenários sejam comparáveis, foram aplicadas as mesmas condições iniciais e de contorno em ambas simulações (Figura 7A).

As fronteiras abertas do domínio foram forçadas com resultados de modelos globais, regionais e dados de campo. As condições iniciais consideradas foram: a elevação da superfície do mar, velocidade das correntes, salinidade, temperatura, descarga continental e o efeito do vento.

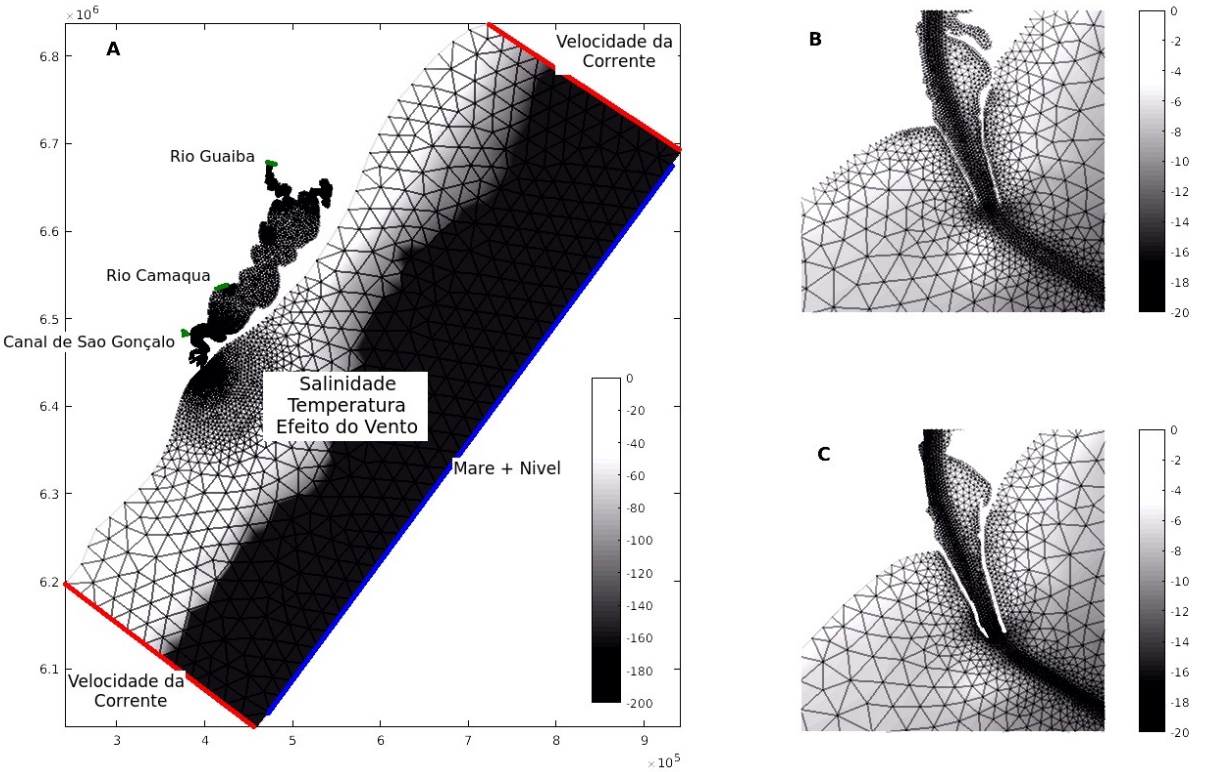


Figura 7: (A) Malha batimétrica da área de estudo, e a aplicação das condições iniciais e de contorno (B) Antiga e (C) Nova configuração dos Molhes da Barra de Rio Grande.

### 4.3.1. Fronteira Oceânica

Dados de altura da superfície do mar e velocidade de corrente regional, obtidos no TPXO Project (acoplado internamente ao modelo TELEMAC), foram usados como condição inicial nas fronteiras oceânicas.

De forma complementar, dados de salinidade (Figura 8A) e temperatura (Figura 8B) obtidos do projeto HYCOM + NCODA (Hybrid Model Coordinate Oceanic, https://hycom.org/), com a resolução temporal de 3 horas e espacial de 1/12°, foram prescritos tridimensionalmente em todos pontos da malha.

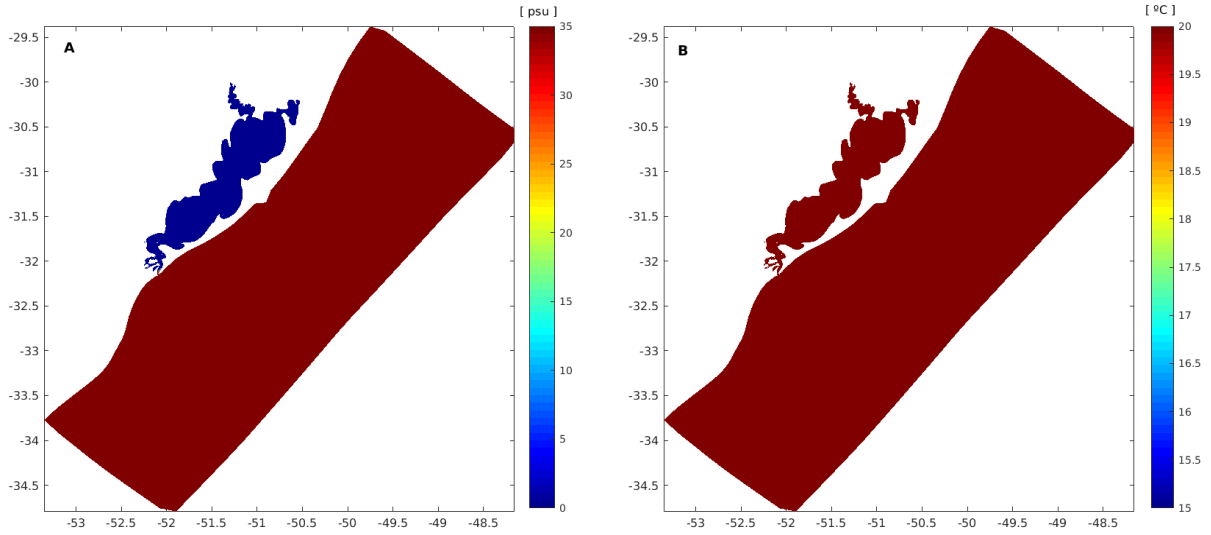


Figura 8: Campo inicial de (A) Salinidade e (B) Temperatura para todo o domínio em estudo.

### 4.3.2. Fronteira Continental

Nas fronteiras continentais, séries temporais de média diárias de descarga dos principais tributários da Lagoa dos Patos (rio Guaíba e rio Camaquã) foram obtidas da Agência Nacional de Águas (ANA, http://www.ana.gov.br), e prescritos nas condições de fronteira continentais para os períodos de elevada (Figura 9A) e baixa (Figura 9B) descargas. Para o Canal São Gonçalo, foi considerada uma descarga média constante de 700 $m^3.s^{-1}$ (Vaz et al., 2006) devido a falta de séries temporais no período em estudo.

### 4.3.3. Fronteira Superficial

As fronteiras superficiais do domínio numérico foram forçadas com dados de vento obtidos na ECMWF (European Center for Medium-Range Weather Forecasts, http://www.ecmwf.int), ERA-Interim, com resolução espacial de 0.75º e temporal de 6 horas, interpolados espacialmente para cada ponto da malha para antiga (Figura 10A) e nova (Figura 10B) configuração dos Molhes da Barra.

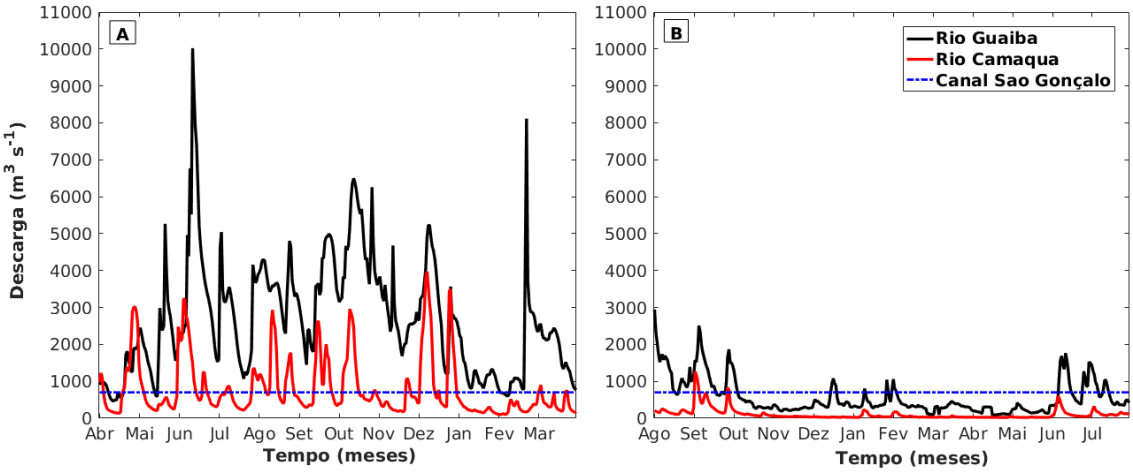


Figura 9: Séries temporais da descarga dos rios Guaíba, Camaquã e do Canal São Gonçalo para os períodos estudados de A) alta (2002-2003) e B) baixa (2011-2012) descarga continental.

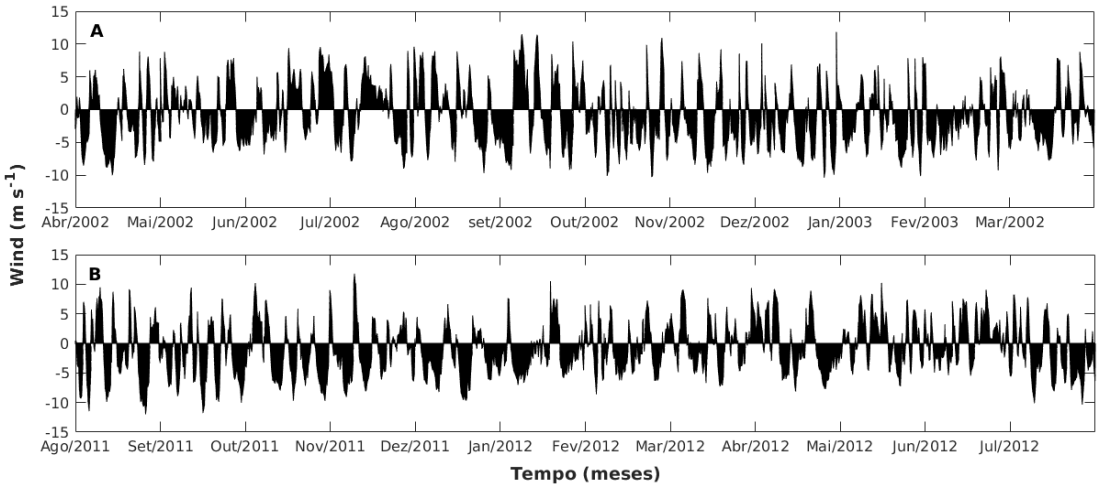


Figura 10: Séries temporais de intensidade do vento para os períodos estudados na (A) alta (2002-2003) e (B) baixa (2011-2012) descarga continental.

### 4.4. Calibração e Validação do modelo

O modelo TELEMAC já foi extensivamente calibrado e validado, e aplicado na Lagoa dos Patos (Fernandes et al., 2001; 2002; Marques et al., 2009. 2010a; 2010b; 2011; Paula Kirinus e Marques 2015). Os exercícios de calibração e validação são executados de forma a demonstrar a habilidade do modelo em reproduzir as condições

ambientais observadas neste região em particular. De forma a demonstrar a capacidade do modelo em reproduzir as condições ambientais observadas, antes e após a modificação dos Molhes da Barra, processos de calibração e validação do modelo hidrodinâmico TELEMAC-3D para os anos em estudo (2006 e 2010) foram realizados. Os teste de calibração e validação foram feitos para ambos cenários (antigo e novo, Figura 8), considerando as mesmas condições iniciais e de fronteira na configuração, e foram conduzidos com os mesmos conjuntos de parâmetros físicos e escolhido o conjunto que apresentou a melhor reprodução. Dados de campo (velocidade, salinidade e elevação) coletados nos períodos de outubro a novembro de 2006, e outubro a novembro de 2010, disponibilizados pelo Laboratório de Oceanografia Costeira e Estuarina (LOCOSTE) do IO – FURG (Tabela 1), foram usados para calibrar e validar o modelo na antiga e nova configuração, respectivamente.

Tabela 1: Dados in situ, coordenadas, local de coleta e o tipo de teste realizado.

| **Parâmetro** | **Latitude** | **Longitude** | **Local** | **Teste** |
|---|---|---|---|---|
| Velocidade | 32.136º S | 52.1024ºW | Praticagem | Calibração |
| Salinidade | 32.136º S | 52.1024ºW | Praticagem | Validação |
| Elevação | 31.325º S | 51.909º W | São Lourenço | |
| Elevação | 30.880º S | 51.453º W | Arambaré | |
| Elevação | 30.136º S | 51.243º W | Ipanema | |
| Velocidade | 32.307º S | 52.098º W | Zona Costeira | |

O exercício de calibração e validação foi feito para os períodos de outubro a novembro de 2006 para a configuração antiga e de outubro a novembro de 2010 para a nova configuração. Uma vez determinados os parâmetros físicos que melhor representam a hidrodinâmica da região, através dos testes de calibração para as duas malhas (Tabela 2), exercícios de validação do modelo foram realizados.

O desempenho do modelo foi avaliado pela comparação estatística entre os dados medidos em campo e os resultados do modelo utilizando Erro Médio Quadrático (Root Mean Square Error - RMSE) e o Erro Médio Absoluto (Relative Mean Absolute

Error – RMAE). O RMAE pode ser classificado de acordo com Walstra et al., (2001) (Tabela 3).

O RMSE determina a magnitude do módulo do erro médio quadrático sem levar em conta o sinal entre as observações e os valores calculados pelo modelo, sendo calculado pela seguinte expressão:

$$RMSE = \sqrt{\frac{\sum_{i=1}^{N} (m_i - o_i)^2}{N}} \tag{19}$$

Onde: “m” é o resultado do modelo; “o” é o dado medido ou observações de campo e “N” é o número de pontos.

O RMAE indica o erro relativo médio entre os dados de campo e os resultados obtidos pelo modelo (Wastra et al., 2001), e é expresso da seguinte forma:

$$RMAE = \frac{\langle |Y - X| \rangle}{\langle |X| \rangle} = \frac{MAE}{\langle |X| \rangle} \tag{20}$$

Onde: MAE é o Erro Absoluto Médio; X é o conjunto de N valores observados; Y é o conjunto de N valores modelados, extraídos em uma mesma posição espacial e temporal.

Tabela 2: Parâmetros que apresentaram melhores resultados na calibração do modelo

| Configuração | Modelo de Turbulência Horizontal | | Modelo de Turbulência Vertical | | Lei de Fricção do Fundo | | Coeficiente de Influência do Vento | Coeficiente de Coriolis |
|---|---|---|---|---|---|---|---|---|
| Teste 1 (Antiga) | Smagorinsky | $10^{-6}$ | Mixing length (Prandtl) | $10^{-6}$ | Manning | 0.03 | $1x10^{-5}$ N $m^{-1}$ $S^{-1}$ | $-7,7x10^{5}$ N $m^{-1}$ $S^{-1}$ |
| Teste 2 | Smagorinsky | $10^{-6}$ | Mixing length (Prandtl) | $10^{-6}$ | Manning | 0.03 | $2x10^{-5}$ N $m^{-1}$ $S^{-1}$ | $-7,7x10^{5}$ N $m^{-1}$ $S^{-1}$ |
| Teste 3 (Nova) | Smagorinsky | $10^{-6}$ | Mixing length (Prandtl) | $10^{-6}$ | Manning | 0.03 | $5x10^{-5}$ N $m^{-1}$ $S^{-1}$ | $-7,7x10^{5}$ N $m^{-1}$ $S^{-1}$ |
| Teste 4 | Smagorinsky | $10^{-6}$ | Mixing length (Prandtl) | $10^{-6}$ | Manning | 0.04 | $1x10^{-5}$ N $m^{-1}$ $S^{-1}$ | $-7,7x10^{5}$ N $m^{-1}$ $S^{-1}$ |
| Teste 5 | Smagorinsky | $10^{-6}$ | Mixing length (Prandtl) | $10^{-6}$ | Manning | 0.04 | $2x10^{-5}$ N $m^{-1}$ $S^{-1}$ | $-7,7x10^{5}$ N $m^{-1}$ $S^{-1}$ |
| Teste 6 | Smagorinsky | $10^{-6}$ | Mixing length (Prandtl) | $10^{-6}$ | Manning | 0.04 | $5x10^{-5}$ N $m^{-1}$ $S^{-1}$ | $-7,7x10^{5}$ N $m^{-1}$ $S^{-1}$ |
| Teste 7 | Smagorinsky | $10^{-6}$ | Mixing length (Prandtl) | $10^{-6}$ | Manning | 0.02 | $1x10^{-5}$ N $m^{-1}$ $S^{-1}$ | $-7,7x10^{5}$ N $m^{-1}$ $S^{-1}$ |
| Teste 8 | Smagorinsky | $10^{-6}$ | Mixing length (Prandtl) | $10^{-6}$ | Manning | 0.02 | $2x10^{-5}$ N $m^{-1}$ $S^{-1}$ | $-7,7x10^{5}$ N $m^{-1}$ $S^{-1}$ |
| Teste 9 | Smagorinsky | $10^{-6}$ | Mixing length (Prandtl) | $10^{-6}$ | Manning | 0.02 | $5x10^{-5}$ N $m^{-1}$ $S^{-1}$ | $-7,7x10^{5}$ N $m^{-1}$ $S^{-1}$ |
| Teste10 | Smagorinsky | $10^{-2}$ | Mixing length (Prandtl) | $10^{-6}$ | Manning | 0.03 | $1x10^{-5}$ N $m^{-1}$ $S^{-1}$ | $-7,7x10^{5}$ N $m^{-1}$ $S^{-1}$ |
| Teste 11 | Smagorinsky | $10^{-2}$ | Mixing length (Prandtl) | $10^{-6}$ | Manning | 0.03 | $2x10^{-5}$ N $m^{-1}$ $S^{-1}$ | $-7,7x10^{5}$ N $m^{-1}$ $S^{-1}$ |
| Teste 12 | Smagorinsky | $10^{-2}$ | Mixing length (Prandtl) | $10^{-6}$ | Manning | 0.03 | $5x10^{-5}$ N $m^{-1}$ $S^{-1}$ | $-7,7x10^{5}$ N $m^{-1}$ $S^{-1}$ |
| Teste 13 | Smagorinsky | $10^{-2}$ | Mixing length (Prandtl) | $10^{-6}$ | Manning | 0.04 | $1x10^{-5}$ N $m^{-1}$ $S^{-1}$ | $-7,7x10^{5}$ N $m^{-1}$ $S^{-1}$ |
| Teste 14 | Smagorinsky | $10^{-2}$ | Mixing length (Prandtl) | $10^{-6}$ | Manning | 0.04 | $2x10^{-5}$ N $m^{-1}$ $S^{-1}$ | $-7,7x10^{5}$ N $m^{-1}$ $S^{-1}$ |
| Teste 15 | Smagorinsky | $10^{-2}$ | Mixing length (Prandtl) | $10^{-6}$ | Manning | 0.04 | $5x10^{-5}$ N $m^{-1}$ $S^{-1}$ | $-7,7x10^{5}$ N $m^{-1}$ $S^{-1}$ |
| Teste 16 | Smagorinsky | $10^{-1}$ | Mixing length (Prandtl) | $10^{-6}$ | Manning | 0.03 | $1x10^{-5}$ N $m^{-1}$ $S^{-1}$ | $-7,7x10^{5}$ N $m^{-1}$ $S^{-1}$ |
| Teste 17 | Smagorinsky | $10^{-1}$ | Mixing length (Prandtl) | $10^{-6}$ | Manning | 0.03 | $2x10^{-5}$ N $m^{-1}$ $S^{-1}$ | $-7,7x10^{5}$ N $m^{-1}$ $S^{-1}$ |
| Teste 18 | Smagorinsky | $10^{-1}$ | Mixing length (Prandtl) | $10^{-6}$ | Manning | 0.03 | $5x10^{-5}$ N $m^{-1}$ $S^{-1}$ | $-7,7x10^{5}$ N $m^{-1}$ $S^{-1}$ |
| Teste 19 | Smagorinsky | $10^{-1}$ | Mixing length (Prandtl) | $10^{-6}$ | Manning | 0.04 | $1x10^{-5}$ N $m^{-1}$ $S^{-1}$ | $-7,7x10^{5}$ N $m^{-1}$ $S^{-1}$ |
| Teste 20 | Smagorinsky | $10^{-1}$ | Mixing length (Prandtl) | $10^{-6}$ | Manning | 0.04 | $2x10^{-5}$ N $m^{-1}$ $S^{-1}$ | $-7,7x10^{5}$ N $m^{-1}$ $S^{-1}$ |
| Teste 21 | Smagorinsky | $10^{-1}$ | Mixing length (Prandtl) | $10^{-6}$ | Manning | 0.04 | $5x10^{-5}$ N $m^{-1}$ $S^{-1}$ | $-7,7x10^{5}$ N $m^{-1}$ $S^{-1}$ |
| Teste 22 | Smagorinsky | $10^{-1}$ | Mixing length (Prandtl) | 5 | Manning | 0.02 | $1x10^{-5}$ N $m^{-1}$ $S^{-1}$ | $-7,7x10^{5}$ N $m^{-1}$ $S^{-1}$ |
| Teste 23 | Smagorinsky | $10^{-1}$ | Mixing length (Prandtl) | 5 | Manning | 0.02 | $2x10^{-5}$ N $m^{-1}$ $S^{-1}$ | $-7,7x10^{5}$ N $m^{-1}$ $S^{-1}$ |
| Teste 24 | Smagorinsky | $10^{-1}$ | Mixing length (Prandtl) | 5 | Manning | 0.02 | $5x10^{-5}$ N $m^{-1}$ $S^{-1}$ | $-7,7x10^{5}$ N $m^{-1}$ $S^{-1}$ |
| Teste 25 | Smagorinsky | $10^{-1}$ | Mixing length (Prandtl) | 5 | Manning | 0.03 | $1x10^{-5}$ N $m^{-1}$ $S^{-1}$ | $-7,7x10^{5}$ N $m^{-1}$ $S^{-1}$ |
| Teste 26 | Smagorinsky | $10^{-1}$ | Mixing length (Prandtl) | 5 | Manning | 0.03 | $2x10^{-5}$ N $m^{-1}$ $S^{-1}$ | $-7,7x10^{5}$ N $m^{-1}$ $S^{-1}$ |

| | | | | | | | | |
|---|---|---|---|---|---|---|---|---|
| Teste 27 | Smagorinsky | $10^{-1}$ | Mixing length (Prandtl) | 5 | Manning | 0.03 | $5x10^{-5}$ N $m^{-1}$ $S^{-1}$ | $-7,7x10^{5}$ N $m^{-1}$ $S^{-1}$ |
| Teste 28 | Smagorinsky | $10^{-1}$ | Mixing length (Prandtl) | 5 | Manning | 0.04 | $1x10^{-5}$ N $m^{-1}$ $S^{-1}$ | $-7,7x10^{5}$ N $m^{-1}$ $S^{-1}$ |
| Teste 29 | Smagorinsky | $10^{-1}$ | Mixing length (Prandtl) | 5 | Manning | 0.04 | $2x10^{-5}$ N $m^{-1}$ $S^{-1}$ | $-7,7x10^{5}$ N $m^{-1}$ $S^{-1}$ |
| Teste 30 | Smagorinsky | $10^{-1}$ | Mixing length (Prandtl) | 5 | Manning | 0.04 | $5x10^{-5}$ N $m^{-1}$ $S^{-1}$ | $-7,7x10^{5}$ N $m^{-1}$ $S^{-1}$ |
| Teste 31 | Smagorinsky | $10^{0}$ | Mixing length (Prandtl) | 5 | Manning | 0.03 | $1x10^{-5}$ N $m^{-1}$ $S^{-1}$ | $-7,7x10^{5}$ N $m^{-1}$ $S^{-1}$ |
| Teste 32 | Smagorinsky | $10^{0}$ | Mixing length (Prandtl) | 5 | Manning | 0.03 | $2x10^{-5}$ N $m^{-1}$ $S^{-1}$ | $-7,7x10^{5}$ N $m^{-1}$ $S^{-1}$ |
| Teste 33 | Smagorinsky | $10^{0}$ | Mixing length (Prandtl) | 5 | Manning | 0.03 | $5x10^{-5}$ N $m^{-1}$ $S^{-1}$ | $-7,7x10^{5}$ N $m^{-1}$ $S^{-1}$ |
| Teste 34 | Smagorinsky | $10^{0}$ | Mixing length (Prandtl) | 5 | Manning | 0.04 | $1x10^{-5}$ N $m^{-1}$ $S^{-1}$ | $-7,7x10^{5}$ N $m^{-1}$ $S^{-1}$ |
| Teste 35 | Smagorinsky | $10^{0}$ | Mixing length (Prandtl) | 5 | Manning | 0.04 | $2x10^{-5}$ N $m^{-1}$ $S^{-1}$ | $-7,7x10^{5}$ N $m^{-1}$ $S^{-1}$ |
| Teste 36 | Smagorinsky | $10^{0}$ | Mixing length (Prandtl) | 5 | Manning | 0.04 | $5x10^{-5}$ N $m^{-1}$ $S^{-1}$ | $-7,7x10^{5}$ N $m^{-1}$ $S^{-1}$ |

Tabela 3: Escala da classificação do coeficiente do RMAE para o desempenho do modelo (Walstra *et al.,* 2001).

| QUALIDADE DOS RESULTADOS | COEFICIENTE |
|---|---|
| **Excelente** | < 0.2 |
| **Boa** | 0.2 - 0.4 |
| **Razoável** | 0.4 – 0.7 |
| **Pobre** | 0.7 – 1.0 |
| **Ruim** | > 1.0 |

A calibração do modelo hidrodinâmico foi feita com séries temporais de velocidade na superfície e no fundo para os períodos entre outubro a novembro de 2006 para a antiga configuração dos Molhes da Barra (Figura 11A e 11B), e outubro a novembro de 2010 para a nova configuração dos Molhes da Barra (Figura 11C e 11D).

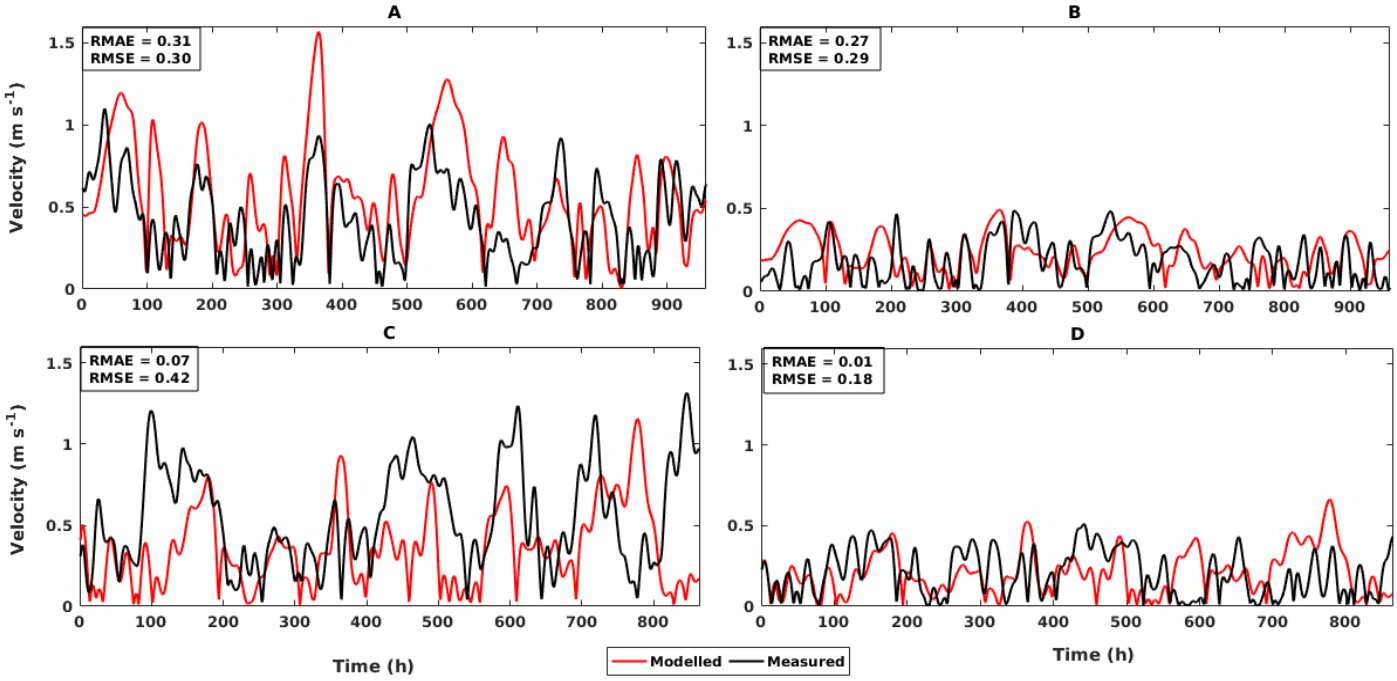


Figura 11: Exercício de calibração – Comparação entre velocidade da corrente modelada (linha vermelha) e medida (linha preta) na superfície (painel esquerdo) e no fundo (painel direito), nos meses de Outubro a Novembro de 2006 para antiga configuração (A e B) e nos meses de Outubro a Novembro de 2010 para nova configuração (C e D) dos Molhes da Barra.

A validação do modelo TELEMAC também foi realizada para ambos os cenários com as mesmas condições iniciais e de contorno para as duas simulações e considerando o mesmo conjunto de parâmetros físicos que geraram o melhor desempenho do modelo nos testes de calibração. Os dados de salinidade, elevação e velocidade resultantes da modelagem foram comparados com dados de campo para

os períodos entre outubro a novembro de 2006 para a antiga configuração dos Molhes da Barra (Figura 12), e outubro a novembro de 2010 para a nova configuração dos Molhes da Barra (Figura 13). O teste de validação para ambos cenários resultou em um desempenho do modelo classificado entre Bom a Excelente (Tabela 4).

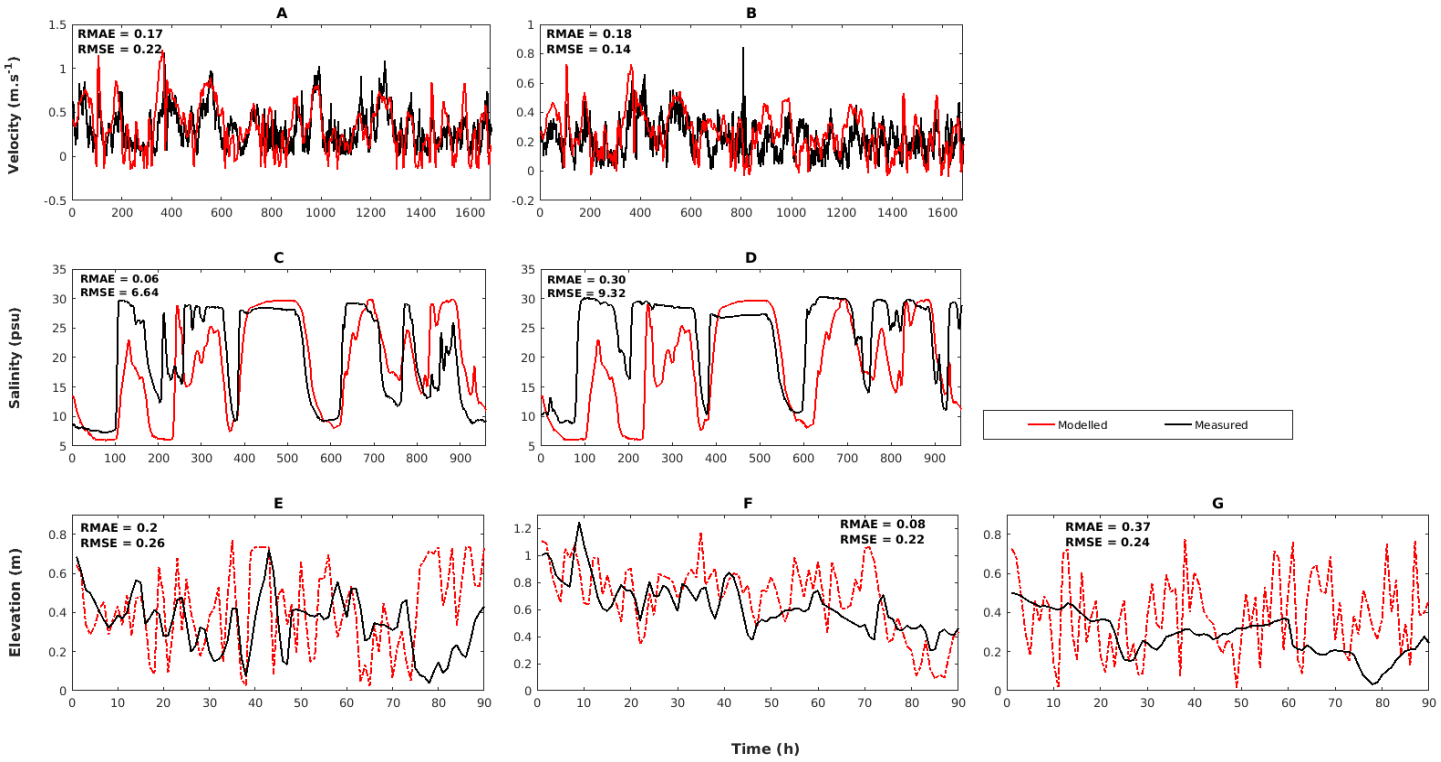


Figura 12: Resultado da validação - comparação entre dados de velocidade de corrente, salinidade e elevação modelado (linha vermelha) e observado (linha preta) para a antiga configuração dos Molhes da Barra nos meses de Outubro a Novembro de 2006. Velocidade (A) e salinidade (C) da superfície, velocidade (B) e salinidade (D) do fundo. (E - G) Dados da elevação da superfície nos pontos E1 (São Lourenço), E2 (Arambaré) e E3 (Ipanema).

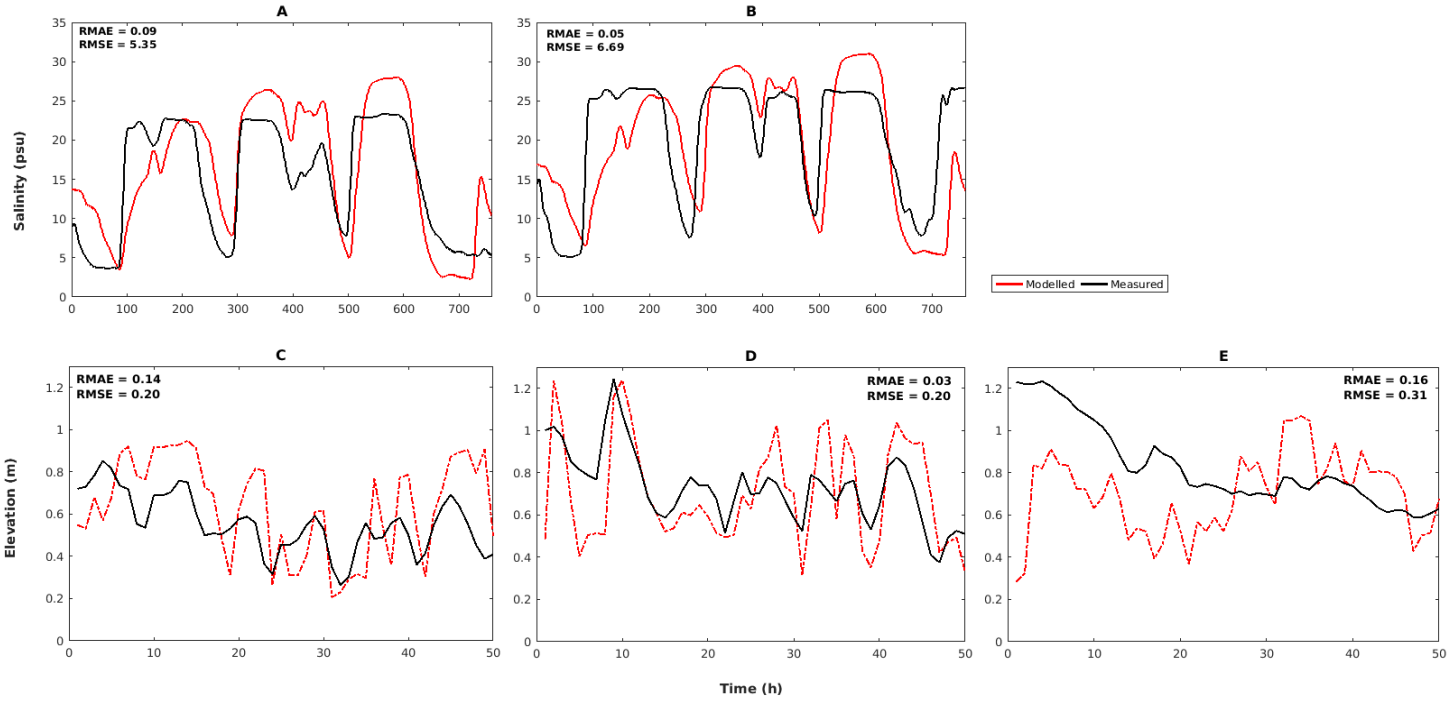


Figura 13: Resultado da validação - comparação entre dados de salinidade e elevação modelado (linha vermelha) e observado (linha preta) para a nova configuração dos Molhes nos meses de Outubro a Novembro de 2010. Salinidade da superfície (A) e salinidade do fundo (D). (C - E) Dados da elevação da superfície nos pontos E1 (São Lourenço), E2 (Arambaré) e E3 (Ipanema).

Tabela 4: Resultados do Erro Absoluto Médio Relativo dos testes de validação do modelo hidrodinâmico nas duas configurações dos Molhes da Barra.

| Parâmetro | Posição | Antiga configuração | Nova configuração |
|---|---|---|---|
| | | RMAE | RMAE |
| Velocidade | Superfície | 0,17 | - |
| | Fundo | 0,18 | - |
| Salinidade | Superfície | 0,06 | 0,09 |
| | Fundo | 0,03 | 0,05 |
| Elevação | São Lourenço | 0,02 | 0,014 |
| | Arambaré | 0,08 | 0,03 |
| | Ipanema | 0,27 | 0,16 |

### 4.5. Modelagem lagrangeana do transporte de ovos e larvas

Para as simulações lagrangeanas do transporte dos ovos e larvas como partículas passivas, ventos de quadrante sul (Sudoeste, Sul e Sudeste) com intensidade constante nos primeiros 2 dias e linearmente decrescentes até o quinto dia (Figura 14) foram usados no modelo para ambas configurações (antiga e nova, Figura 7), nos períodos característicos de alta (01 a 05/01/2003) e baixa (01 a 05/01/2012) descarga continental, respectivamente.

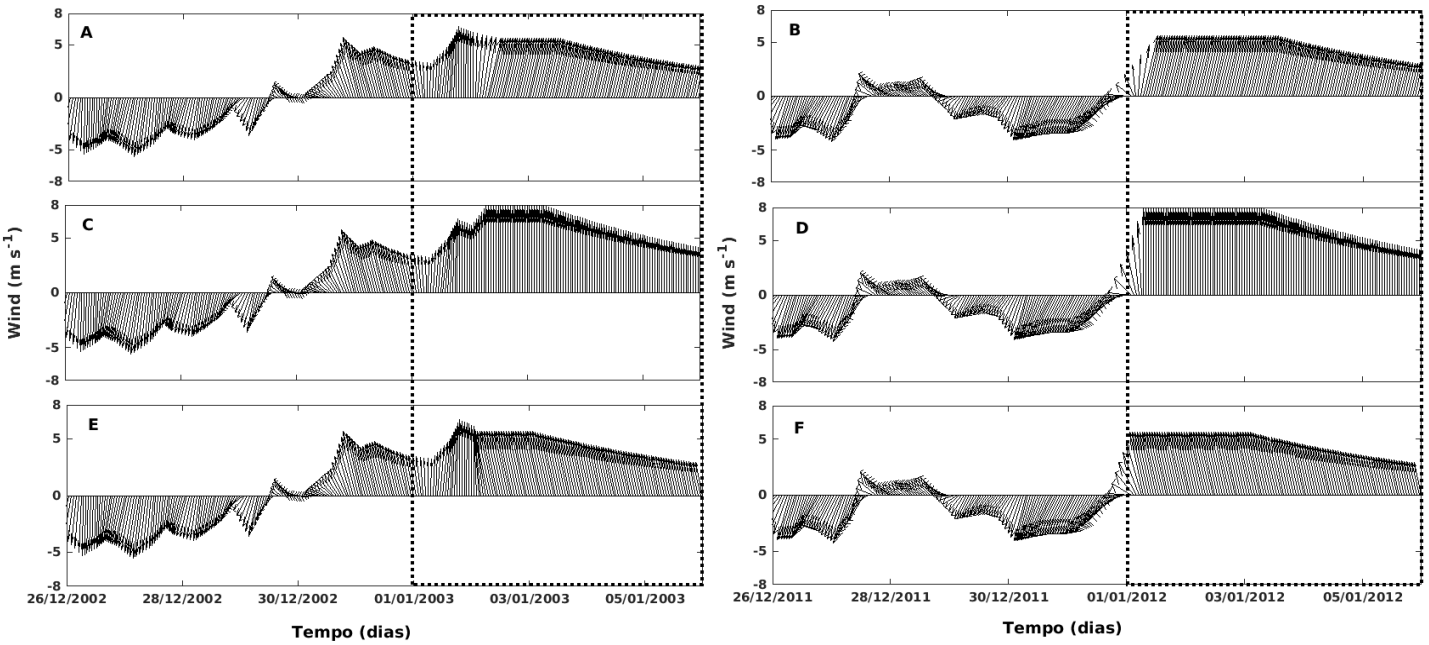


Figura 14: Séries temporais da intensidade do vento SO (A, B), S (C, D) e SE (E, F), para os períodos estudados em anos característicos de alta (painel esquerdo) e baixa (painel direito) descargas continentais.

Durante uma simulação hidrodinâmica, o TELEMAC-3D oferece a oportunidade de seguir os caminhos de uma série de partículas (drogues) que são lançadas no fluido a partir de pontos de descarga. O modelo de partículas é uma sub-rotina do modelo hidrodinâmico TELEMAC-3D, que é simulado internamente a cada passo de tempo após a componente hidrodinâmica. Desta forma, para reproduzir o transporte dos ovos e larvas na fase passiva e simular sua dispersão no estuário da Lagoa dos Patos, o modelo lagrangeano foi acoplado ao modelo hidrodinâmico TELEMAC-3D.

Para a configuração do modelo, alguns parâmetros são inseridos no arquivo de direção, a destacar, a definição do número de partículas por meio das palavras-chave “NUMBER OF DROGUES” cujo valor padrão é 0, e no estudo foram definidas 7000 partículas. As coordenadas tridimensionais iniciais (x, y, z) do ponto de liberação das partículas (XFLOT, YFLOT, ZFLOT e TAGFLO), e a introdução de um identificador da

partícula (drogue). Outro parâmetro a configurar é o tempo de saída desse arquivo (valor padrão = 1), esse valor é expresso em várias etapas de tempo e pode ser independente do período de saída dos outros resultados do TELEMAC-3D. No presente estudo foi definido o mesmo tempo para a saída dos resultados hidrodinâmicos e lagrangeanos, que foi de 60 segundos. Portanto, a cada 60 segundos o TELEMAC-3D rodou a componente hidrodinâmica, e instantaneamente os resultados eram inseridos no modelo de partículas, sendo calculado o deslocamento das partículas tridimensionalmente na grade numérica.

O acoplamento de partículas ao fluido permite que as características de fluxo médio em grande escala ao longo da costa sejam calculadas de forma eficiente com um modelo Euleriano (Joly et al., 2012). O modelo de partículas obtém as informações lagrangeanas a partir das informações das velocidades eulerianas, calculadas pelo modelo hidrodinâmico para determinar a trajetória das partículas advectadas pelo fluxo a cada passo de tempo, e as trajetórias tridimensionais são computadas usando as informações de posição calculadas. Desta forma, o movimento de advecção horizontal e vertical considera o esquema de Euler e a flutuabilidade da partícula baseia-se nas componentes zonal, meridional e vertical (u, v e w), e é dado pela seguintes expressão:

$$X_i\left(x_0, y_0, z_0\right)^{n+1} = X_i\left(x_0, y_0, z_0\right)^n + \int_{t_0+n\Delta t}^{t_0+(n+1)\Delta t} u_i\left(x_0, y_0\, z_0, t\right) dt \qquad (21)$$

Onde $X_i$ é a posição, para a posição horizontal ($x_0$, $y_0$) e vertical ($z_0$) do movimento da partícula; $u_i$ é a velocidade para componente de velocidade zonal ($x_0$), meridional ($y_0$) e vertical ($z_0$), u, v e w, respectivamente; t é o tempo e Δt é o intervalo de tempo.

O cálculo das componentes hidrodinâmicas é levado em conta de forma discreta tridimensionalmente em cada ponto da grade numérica. Durante a simulação, as partículas são livres para se movimentar para qualquer posição entre os pontos da grade, sem interferir no fluido. O modelo prevê o movimento das partículas em fluxos

ambientais com movimento browniano e nenhuma das características físicas do corpo é levada em consideração. Por outro lado, forças atuantes sobre as partículas são levadas em consideração como o caso da  força histórica de Basset, que considera que o movimento de um corpo depende da evolução anterior do corpo sólido e da velocidade do fluido (Joly et al., 2012), assim como a flutuabilidade das partículas, força essa considerada importante em fluxos tridimensionais, como aplicado no presente trabalho. Desta forma, a cada novo passo de tempo, a velocidade é interpolada de forma instantânea para cada posição em que as partículas se localizam. A precisão e resolução dos cálculos de transporte das partículas é extremamente dependente dos termos hidrodinâmicos.

O tempo de liberação final das partículas também é definido, na sub-rotina inserida no arquivo hidrodinâmico (FORTRAN). Os resultados são armazenados no arquivo especificado com as coordenadas tridimensionais das diferentes posições das partículas ao longo do seu transporte.

# Capítulo V:

## Resultados e Discussões

Os resultados e a discussão serão apresentados em forma de artigos neste Capítulo. O primeiro artigo, de autoria de Maria Helena Paulo António, Elisa Helena Fernandes e José Henrique Muelbert, é intitulado "**Impact of jetties configuration changes on the hydrodynamics of the subtropical Patos Lagoon Estuary, Brazil***"* foi submetido para publicação no periódico "*Estuarine, Coastal and Shelf Sciences"*. O segundo artigo, de autoria de Maria Helena Paulo António, José Henrique Muelbert e Elisa Helena Fernandes é intitulado "**Human induced changes in the estuarine hydrodynamic and its influence on eggs and larval fish transport and dispersion**" e foi submetido para publicação no periódico "*Journal of the European Geosciences Union: Biogeosciences"*.

# Impact of jetties configuration changes on the hydrodynamics of the subtropical Patos Lagoon Estuary, Brazil

**Maria Helena P. António[a,c,@], Elisa H. Fernandes[a] and José H. Muelbert[b]**

[a]Laboratório de Oceanografia Costeira e Estuarina, Instituto de Oceanografia. Universidade Federal do Rio Grande, CP 474, CEP 96201-900, Brazil

[b]Laboratório de Ecologia do Ictioplâncton, Instituto de Oceanografia. Universidade Federal do Rio Grande, CP 474, CEP 96201-900, Brazil

[c]Escola Superior de Ciências Marinhas e Costeiras. Universidade Eduardo Mondlane, Mozambique

[@]Corresponding author: mhbeula2@gmail.com (Maria Helena P. António)

## Abstract

Coastal infrastructure alterations, such as jetty expansions, are designed to provide improvements to natural dredging and safety of marine access and to maximize the management and efficiency of ports. Furthermore, these alterations have the potential to cause significant environmental changes to the estuaries and adjacent coastal areas. Here, the Patos Lagoon hydrodynamics were investigated before and after the jetty alterations, which were increased by approximately 10 - 18%, and the mouth width was reduced by 15%. Hydrodynamic simulations of the system were performed with the TELEMAC-3D numerical model. The model was first calibrated and then validated using the field data for each jetty configuration. The characteristic low and high extremes of the discharge conditions were simulated for the old and new jetty configurations. The results showed a flow reduction of approximately 20% both in the ebb and flood conditions in the new configuration, which was accompanied by a slight change in the propagation angle of the western jetty current. Reduction of the saltwater intrusion was registered during both the high and low discharge conditions with the new jetty configuration. During the high discharge periods with NE winds, the saltwater intrusion did not reach the previous estuarine inland boundary. During the periods of low discharge with SW wind, the salinity did not reach further than 180 km inland. Reduced saltwater intrusion was observed landwards and in the shallow embayments. The horizontal stratification structure of the salinity changed, with the partial centralization of the flow in the access channel. The observed hydrodynamic changes from the infrastructure modifications could affect the estuarine ecosystem by increasing the sediment retention, reducing the transport of marine organisms and water properties into the estuary. This study contributes not only to the understanding of hydrodynamic changes but also to the potential optimization of estuarine and coastal management strategies.

***Keywords:*** Hydrodynamic, continental discharge, TELEMAC-3D model, coastal structures, man-induced alteration.

## 1. INTRODUCTION

Approximately 60% of the world's population inhabits coastal regions (Adger et al., 2005), and most of it is located around estuarine areas. Important ports and large cities are located inside estuaries, making them vulnerable to changes by natural processes and anthropogenic alterations associated with economic development (Prumm and Iglesias, 2016; Zhao et al., 2018). Changes in the geomorphology, river discharge, and circulation patterns, however, influence pollution and the distribution of nutrients and suspended sediments (Prumm and Iglesias, 2016). The ecological consequence of these alterations is enhanced because estuaries serve as habitats and nursery for the initial stages of the development of many species (Braverman et al. 2009; Salvador and Muelbert, 2019), are rich in nutrients, influence primary production (Abreu et al., 2010), and provide abundant food and protection against predators (Able, 2005; Sheaves et al., 2015).

Studies on human-induced impacts on the hydrodynamics, saltwater intrusion, sediment transport, pollutant dispersion, and ecology of coastal systems have been gaining ground during the last century. Port expansions can increase sedimentation and the migration of tidal delta and infill of channels (Prumm and Iglesias, 2016). Jetty construction can change the direction of the tidally induced currents, the evolution of the bed level and induce sedimentation and erosion (Ghashemizadeh and Tajziehchi, 2013) and can also significantly reduce the wave height and flushing rates and increase sedimentation and pollution (Azarmsa *et al.*, 2009). It has also been reported that the extension of jetties does not change inlet flow propagation and water quality; however, changes in the topography increase current velocities and salinity values (Yuk and Aoki, 2007). Dredging activities can cause significant variations in the estuarine physical parameters and suspended sediment concentration; moreover, they can promote fast siltation in the harbor waterway after the end of the dredging operations (Martelo et al., 2019).

The port of Rio Grande which is located in the Patos Lagoon estuary (Figure 1) in the southernmost part of Brazil, is the third-largest port in Brazil (Esteves et al., 2003). To respond to the commercial demands for port expansion, human interventions have been necessary since the last century to ensure safety and navigation conditions. The first alteration to the access channel was the construction of two 4 km long jetties at the mouth of the Patos

Lagoon in 1907 (Silva et al., 2015). In 2010, the adjustments in the original project were carried out, and the jetties were lengthened by 370 m (east) and 700 m (west). This alteration aimed to improve the navigation conditions by allowing a progressively deeper channel, which reached a depth of 16 m inside and 18 m outside of the estuarine access channel, and by reducing the width of the estuary mouth. The concept behind this last modification was to converge the jetties at the mouth to increase the flood velocities and promote natural dredging (Lisboa and Fernandes, 2015).

The Patos Lagoon is the largest choked coastal lagoon in the world (Kjerfve, 1986) and extends 250 km with a 40 km width and a total area of 10,360 $km^2$ (Figure 1). The lagoon connects to the Atlantic Ocean through a 700 m wide channel. The southern estuarine portion of the lagoon represents 10% of the total area and has an average depth of 5 m (Castelão and Möller Jr, 2006) and natural and dredged channels of up to 16 m (Möller Jr et al., 2009). The estuary is microtidal, and its dynamics are controlled by wind action and freshwater discharge (Fernandes et al., 2002; Garcia et al., 2003; Lisboa and Fernandes, 2015). The tides are mixed with diurnal predominance, and with an amplitude of approximately 0.23 m (Möller Jr et al., 2001), which is restricted to the coast and the lower estuary (Fernandes et al., 2004) and contributes to the mixing of the water column and the landward water transport (Fernandes et al., 2005; Möller Jr and Fernandes, 2010). The freshwater discharge is typical of that in the temperate regions, with a historical annual mean runoff of approximately 2400 $m^3s^{-1}$. ENSO (El Niño-Southern Oscillation) variability plays an important role in changing the river flow behavior, with high discharge values of approximately 12000 $m^3s^{-1}$ during El Niño years and low values of 500 $m^3s^{-1}$ during La Niña (Möller Jr et al., 2009).

Most studies on the hydrodynamics of the Patos Lagoon estuary were carried before 2010 (Castelão and Möller Jr, 2006; Fernandes et al., 2005; Marques et al., 2009) or were based on the old access channel configuration (Marques et al., 2011, Seiler et al., 2015). Only a few studies focused on the environmental consequences of the jetty modernization, which concluded in 2010. Silva et al. (2015) investigated the changes in the fine sediment dynamics in the access channel of the Patos Lagoon and indicated that the changes in the deposition pattern and the redistribution at the bottom occurred due to the new configuration. Lisboa and Fernandes (2015) concluded that the access channel modification resulted in changes in the

erosion and deposition rates and the longitudinal growth of the sand spits. However, investigations of the hydrodynamic characteristics after the modernization of the jetties have not yet been conducted.

This study investigated changes in the hydrodynamics of the Patos Lagoon after the alteration concluded in 2010. A three-dimensional numerical model was used to test the hypothesis that even small infrastructure alterations in the coastal environments can lead to hydrodynamic changes. If proven correct, these changes could lead to alterations in the flow pattern and modification of the saltwater intrusion, stratification, and mixing characteristics that could have potential environmental consequences.

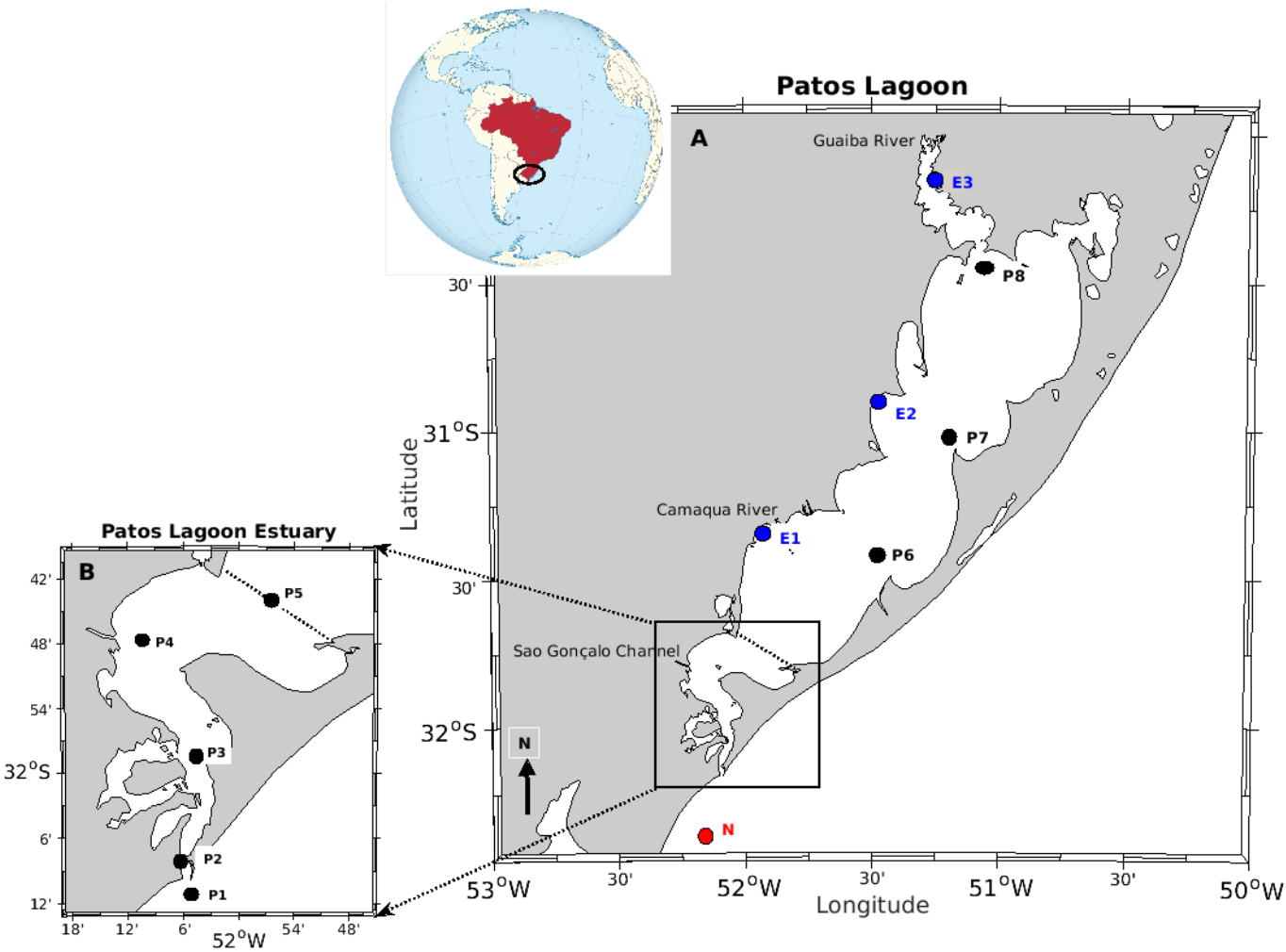

Figure 1: The study site located in Southeast South America, depicting A) The Patos Lagoon and its main tributaries, where the three blue points (E1 – São Lourenço, E2 - Arambaré and E3 - Ipanema) indicate the position where the water level was obtained and one red point (N) where current velocity was obtained at the coastal region. Dotted line indicates the estuarine limit (Ponta da Feitoria). B) Patos Lagoon estuary, where eight black points (P1 – P8) show the location where the model results were extracted.

## 2. NUMERICAL MODEL

This study was carried out with the TELEMAC-3D model (www.opentelemac.org) to simulate the hydrodynamics of the Patos Lagoon system with the old and new jetties configurations of the lagoon access channel. The model was run with high and low freshwater discharge conditions, which coincided with the El Niño (2002 to 2003) and La Niña (2011 to 2012) simulated periods (Figure 2).

### 2.1. Model Description

The TELEMAC-MASCARET model (V7P0 version) presents modules in two and three dimensions to study the hydrodynamics, sediment transport, waves and water quality of the coastal and oceanic regions. The hydrodynamic model solves the Navier-Stokes equations and considers the local variations in the free surface of the fluid, neglecting the variation of density in the mass conservation equation and considering the hydrostatic or nonhydrostatic pressure and the Boussinesq approximation to solve the motion equation. This model applies the finite element method to solve the hydrodynamic equations and uses the sigma coordinate system for vertical discretization; its domain is discretized by a nonstructured grid of finite elements (triangular elements), which allows the concentration of a higher number of elements in the regions of interest and/or significant bathymetric variations and lower resolutions in the regions of more homogeneous bathymetry, which reduces computational time. Details about the model formulations are presented by Hervouet (2007).

### 2.2. Model Grid

The bathymetry of the Patos Lagoon, the estuary, and the adjacent coastal region was obtained from historical data. Nautical charts from the Directory of Hydrography and Navigation (DHN, Brazilian Navy) for before 2010 were used as the “old” bathymetric

information (before changes in configuration). Data from the jetty expansion project were used to define the bathymetry after the alteration of the jetties. The main difference between the two grids was the length of the jetties and the depth of the access channel to the estuary (Figure 3). The BlueKenue Software was used to generate the unstructured bathymetric grids of the triangular elements. Grid optimization was conducted on the complex morphology and the shallow areas inside the estuary and in the adjacent coastal regions, which allowed higher resolution in the regions of interest (Figure 3).

Two resulting meshes were used to reproduce the hydrodynamics before and after the modification of the jetties (Figures 3B and 3C). The meshes encompassed the entire study area up to approximately 2500 m depth to better represent the coastal dynamics. The generated meshes contained a total of 17868 and 17575 node points for the old and new scenarios, respectively. The largest triangles located in the open sea (lowest refinement) had edges of approximately 27 km in length, while the smallest triangles in the access channel (highest refinement) were approximately 50 m.

### 2.3. Initial and Boundary Conditions

The open boundaries of the domain were run with the results from the global models and the field data (Figure 3). To ensure comparability, the simulations for both scenarios used the same settings. The altimeter sea level and velocity data were obtained from the TPXO Project (internally coupled to the TELEMAC model) and were used to set up the conditions at the oceanic boundary. Time series of the daily averaged river discharges of the main tributaries (Guaíba River and Camaquã River) were obtained from the National Water Agency (http://www.ana.gov.br) and prescribed for the northern and central continental boundaries. The mean discharge data for the São Gonçalo Channel was considered constant at 700 $m^3 s^{-1}$ (Vaz et al., 2006) due to the lack of available data for the studied periods. The temperature and salinity fields obtained from the HYCOM model (Hybrid Model Coordinate Oceanic, https://hycom.org/), with a temporal resolution of 3 h and a spatial resolution of 1/12.5°, were prescribed tridimensionally for all grid points. Wind time series data with spatial and temporal resolutions of 0.75º and 6 h, respectively, were obtained from the ECMWF (European Center for Medium-Range Weather Forecasts, http://www.ecmwf.int).

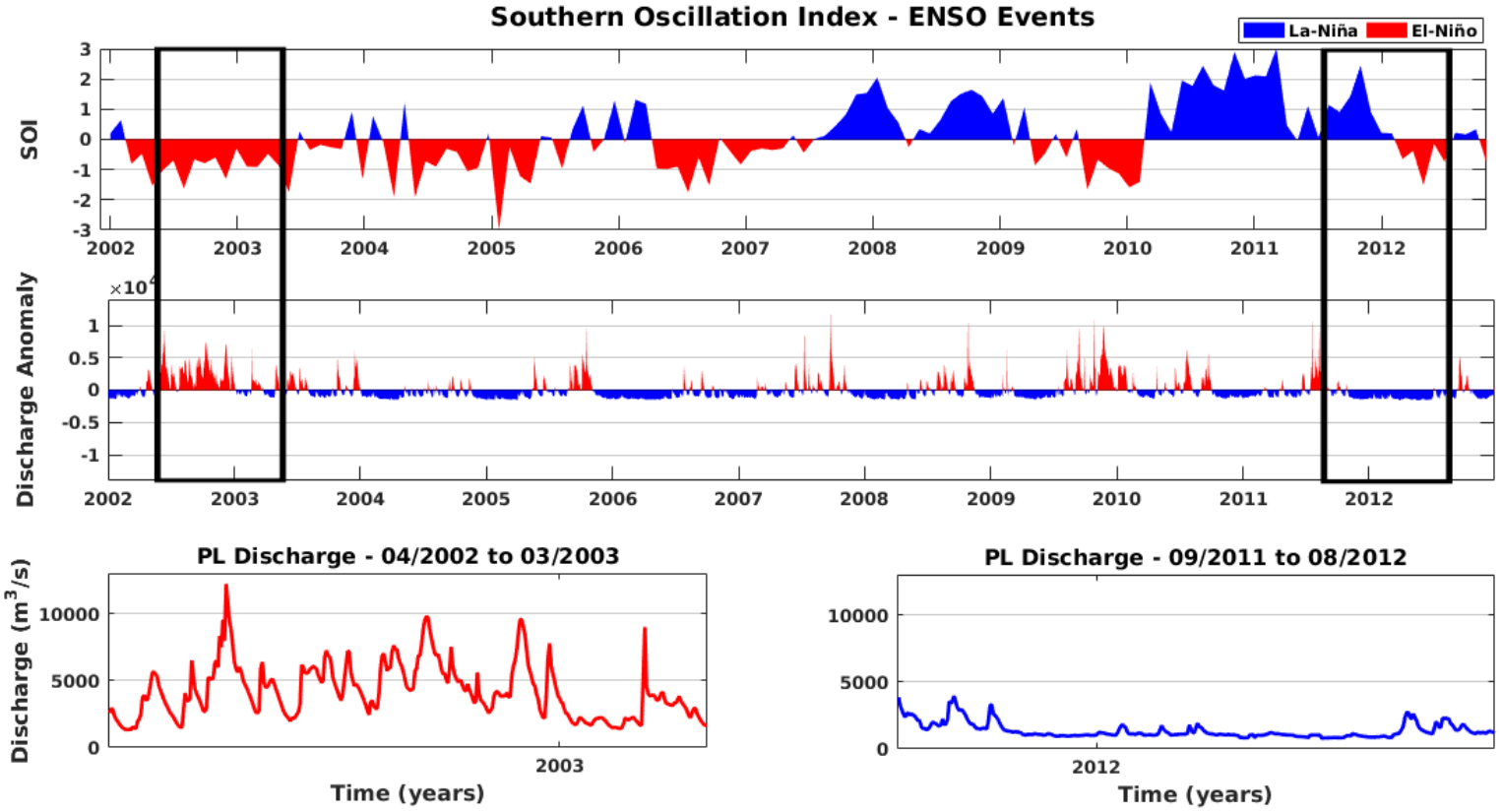


Figure 2: Southern Oscillation Index (SOI) and discharge anomaly for the 2002-2012 period (top and middle panels). Black rectangles represent periods of Patos Lagoon high discharge during El-Niño (bottom left) and low discharge during La-Niña (bottom right), the years that were simulated in this study.

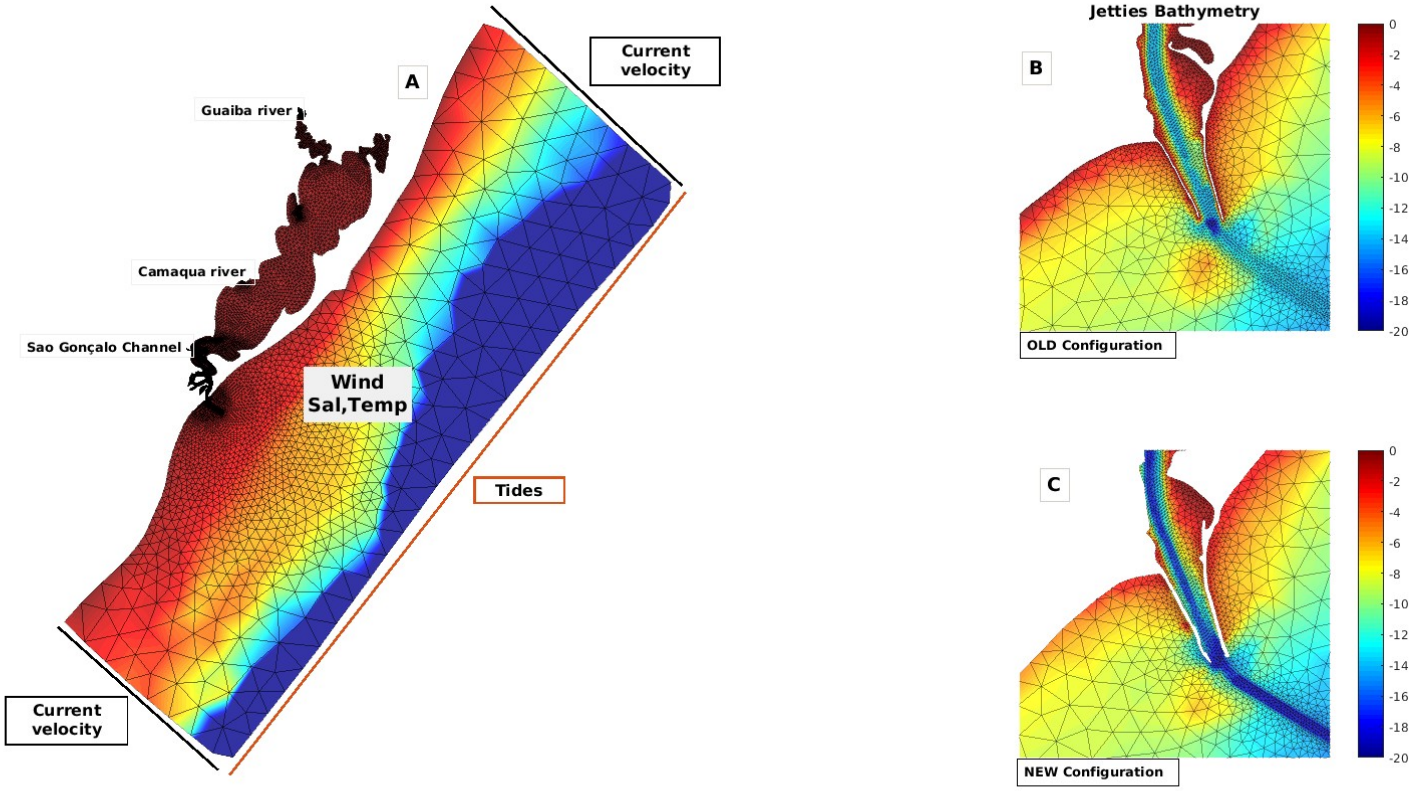


Figure 3: A) The model domain and the finite element mesh highlighting the initial and boundary conditions applied to the old and new configuration of Barra Jetties. The lower Patos Lagoon estuary in the (B) old, and (C) new jetty configuration.

Eleven (11) sigma levels were considered vertical direction and were distributed from the bottom to the sea surface.

## 2.4. Calibration and Validation

Previous studies (Fernandes et al., 2002; Marques et al., 2010) using TELEMAC in Patos Lagoon performed calibration and validation exercises to demonstrate the ability of the model to reproduce the observed environmental conditions. In the present study, calibration tests were carried out for both scenarios with the same initial and boundary conditions settings. The tests were conducted with the main physical parameters (Supplementary Table 1), and the best model reproduction was obtained with Smagorinsk = $10^{-6}$ as the horizontal turbulent model, mixing length (Prandtl) = $10^{-6}$ as the vertical turbulent model, Manning = 0.03 as law of bottom friction, the Coriolis constant = $-7{,}7*10^{-5}$ $Nm^{-1}s^{-1}$ and the wind influence coefficient = $1*10^{-5}$ $Nm^{-1}s^{-1}$ for the old and $5*10^{-5}$ $Nm^{-1}s^{-1}$ for the new jetty configuration during both simulation periods.

The model performance was classified as excellent when the values of RMAE were smaller than 0.2; good, when the values were between 0.2 and 0.4; reasonable, when the values were between 0.4 and 0.7; poor, when the values were between 0.7 and 1; and bad, when the values were greater than 1 (Walstra et al., 2001). The model calibration tests for both scenarios resulted in model performances ranging from good to excellent for the current velocity time series at the surface (old RMAE = 0.31 and new RMAE = 0,07) and bottom (old RMAE = 0.27 and new RMAE = 0.01) (Figure 4).

The TELEMAC model validation was also carried out for both scenarios with the same initial and boundary conditions settings for both simulations and considered the same set of physical parameters that generated the best model performance in the calibration tests. The salinity, elevation and current velocity modeling results were compared with the field data for the period between October and November 2006 for the old jetty configuration (Figure 5) and October to November 2010 for the new configuration (Figure 6). The model validation tests for both scenarios resulted in model performances ranging from good to excellent (Table 1).

Table 1: Relative Mean Absolute Error (RMAE) results for the hydrodynamic model validation.

| Parameters | Position | Old Configuration | New Configuration |
|---|---|---|---|
| | | RMAE | RMAE |
| Velocity | Surface | 0.17 | - |
| | Bottom | 0.18 | - |
| Salinity | Surface | 0.06 | 0.09 |
| | Bottom | 0.30 | 0.05 |
| Elevation | E1 | 0.02 | 0.014 |
| | E2 | 0.08 | 0.03 |
| | E1 | 0.27 | 0.16 |

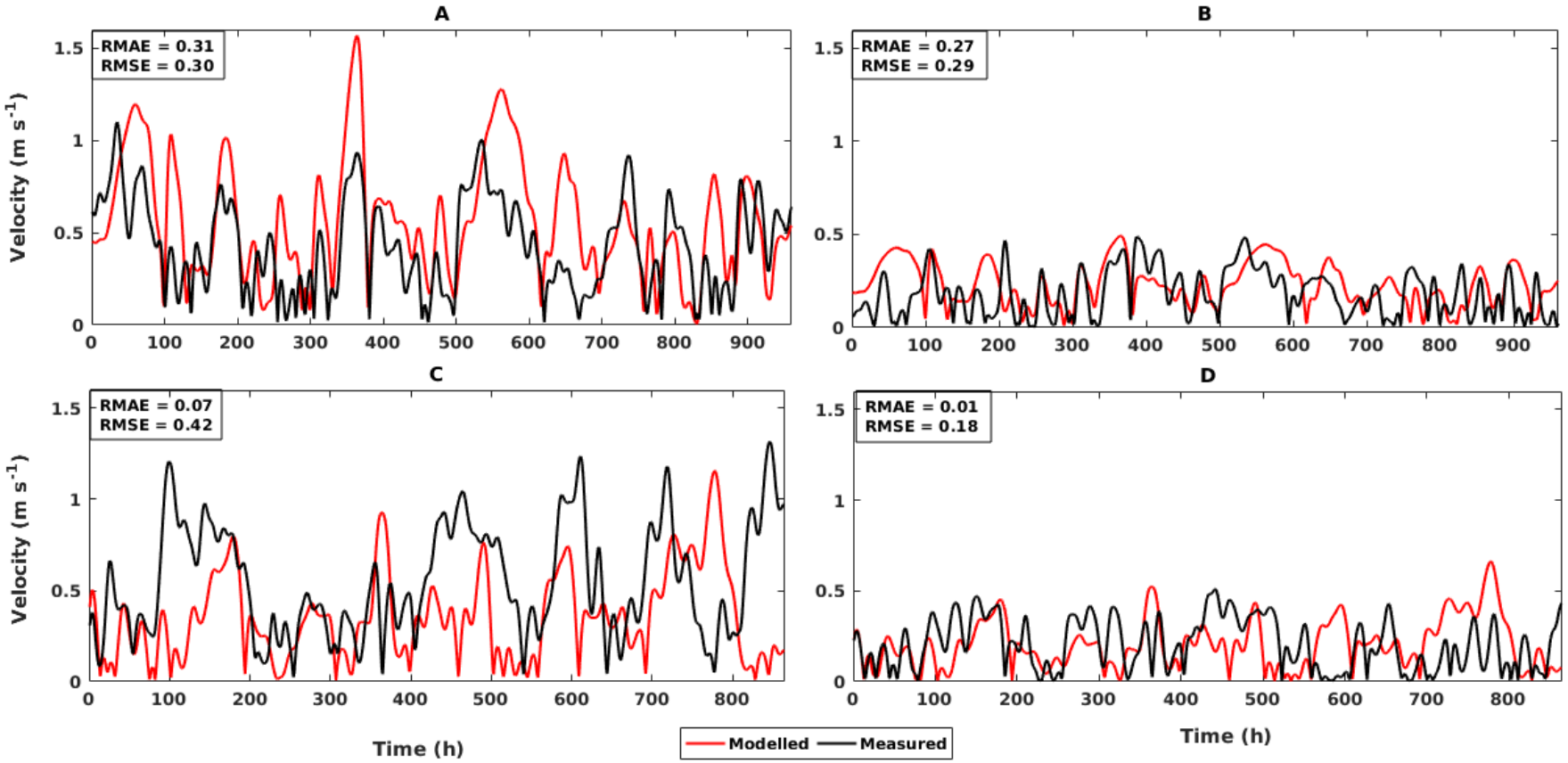


Figure 4: Calibration exercise - comparison between modeled (red line) and measured (black line) current velocity at the surface (left panel) and bottom (right panel), in the old (A and B) and new (C and D) jetty configurations.

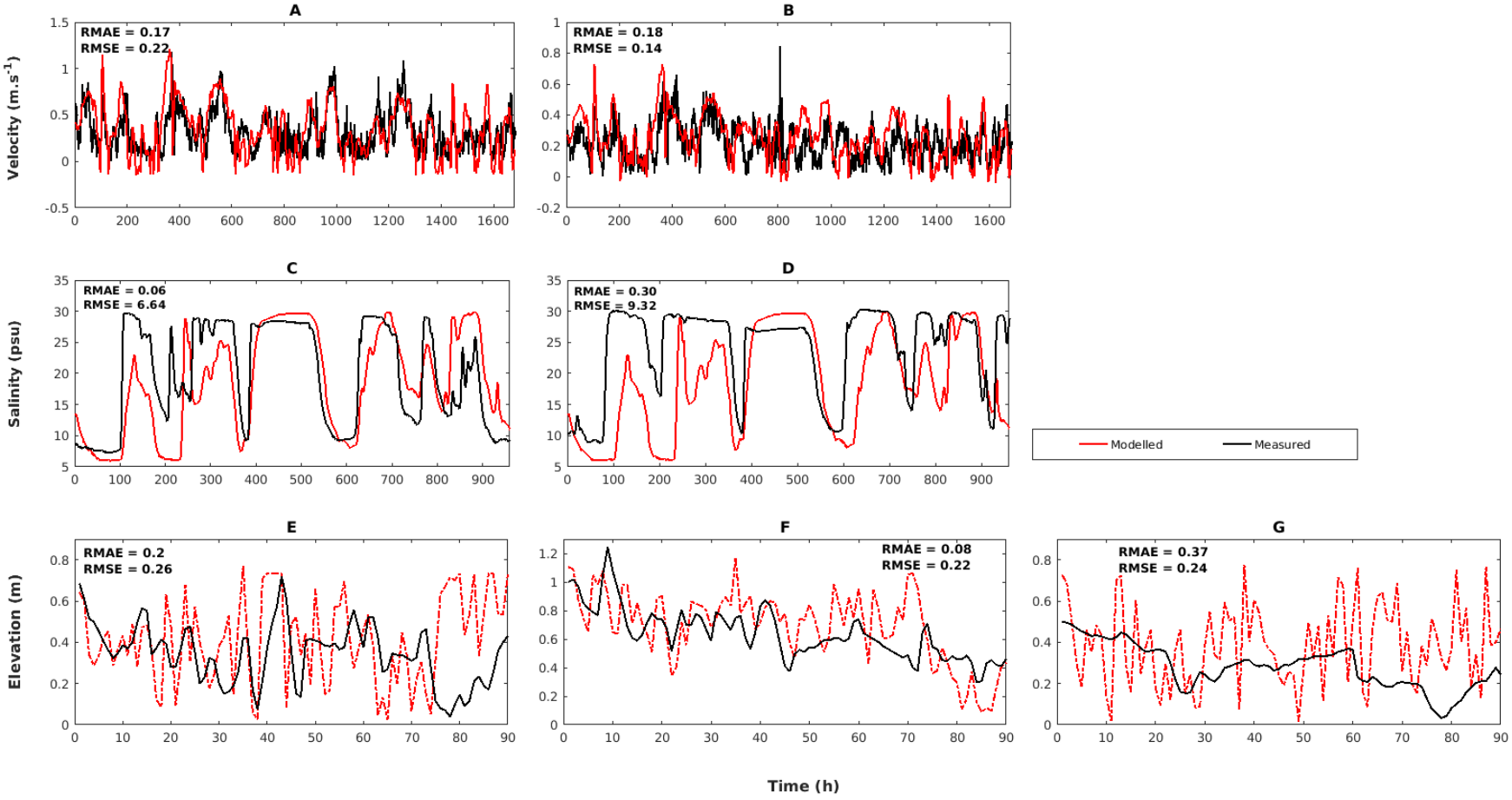


Figure 5: Validation results, comparison between modeled (red line) and measured (black line) current velocity, salinity and water elevation for the old jetty configuration. Surface velocity (A) and salinity (C) and bottom velocity (B) and salinity (D). (E-G) water elevation for points E1 (São Lourenço), E2 (Arambaré) and E3 (Ipanema).

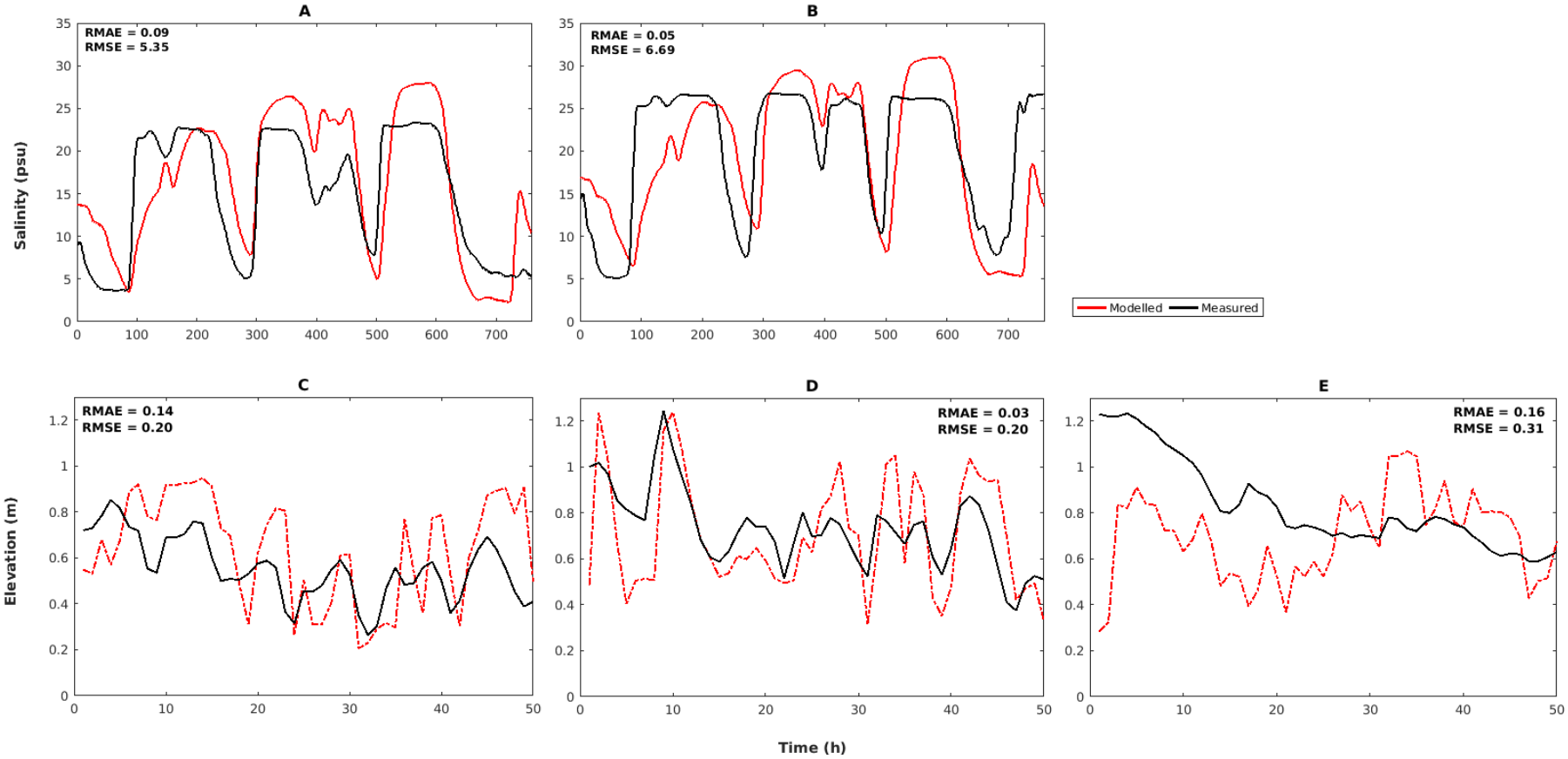


Figure 6: Validation results, comparison between modeled (red line) and measured (black line) salinity and water elevation for new jetty configuration. Surface (A) and bottom (B) salinity data. (C-E) Water elevation for points E1 (São Lourenço), E2 (Arambaré) and E3 (Ipanema), respectively.

## 2.5. Data Analysis

To analyze the effect of alteration of the Patos Lagoon estuary access channel on the hydrodynamics and saltwater intrusion, the difference between the velocity and salinity fields, respectively, in the configurations were calculated and analyzed in terms of the discharge and wind (direction and intensity) variability. The time series of the velocity and salinity were also extracted from the model results for points P1, P2, P3, P4 and P5 during the high discharge simulations and P1, P2, P3, P4, P5, P6, P7 and P8 during the low discharge simulations at the surface and bottom (Figure 1). The salinity fields of representative time steps were chosen for the periods of high and low discharge during the maximum flood and ebb conditions.

The time scale of the effect of wind on the saltwater behavior into the estuary during high and low discharge was investigated. The spectral contents and the correlations between the daily time series of the salinity were carried out using Morlet wavelet analysis (Torrence and Compo, 1998) at points P1, P2, P3, P4 and P5 and P1, P2, P3, P4, P5, P6, P7, and P8. A background Fourier red noise spectrum ($\alpha$ = 0,72) was assumed at each scale, and then the chi-squared distribution was used to find the 95% confidence (5% significance) contour.

To investigate the changes in the lateral and vertical stratification between the jetty configurations, profiles of salinity were extracted during the periods of lateral ebb and flood. The spatial differences between the old and new configurations were calculated. In addition, the changes in the intensity and incidence angle of the current velocities between the jetties were investigated.

## 3. RESULTS

The numerical simulations considering the new and old jetty configurations at the mouth of the Patos Lagoon estuary between periods of high and low continental discharge were analyzed comparatively. The high discharge simulation (El-Niño 2002-2003) was marked by an average discharge of 4200 $m^3s^{-1}$, with a maximum of 12300 $m^3s^{-1}$ during mid-June 2002 and a minimum of 1336 $m^3s^{-1}$ during February 2003. The predominant wind was from the north, with the NE winds reaching a maximum intensity of approximately 8 $ms^{-1}$. During the low discharge simulation (La Niña 2011-2012), the minimum discharge was approximately 806 $m^3s^{-1}$ for several months, with an average of 1370 $m^3s^{-1}$ and a maximum of 4000 $m^3s^{-1}$. The winds were mainly from the north and south quadrants, with the NE and SW wind intensities close to 10 $ms^{-1}$ (Figure 7).

### 3.1. Hydrodynamics

To analyze the effects of the access channel modifications on the dynamics of the Patos Lagoon estuary, the current velocity time series at the surface and bottom were extracted from the modeling results for both the old and new jetty configurations. The model results were obtained for several points from the access channel landwards for the low and high discharge conditions (Figure

1). The difference between the current velocities of the old and new jetties configuration was calculated and analyzed as a function of discharge and wind direction and intensity.

### 3.1.1. High Discharge Simulation

The predominant winds during the simulated period were from the NE, and the mean river discharge was approximately 4,200 $m^3s^{-1}$, with peaks of 10,000 $m^3s^{-1}$ (P1, Figure 7A).

The differences in the current velocity between the old and new configurations were higher at the bottom than at the surface and generally decreased landwards (Figure 7). The exception was at the estuarine limit (P5, Figure 1), where the difference increased at the surface (Figure 7J). The maximum difference in flood velocities was approximately 1 $ms^{-1}$ at the entrance of the estuary (P1 and P2, Figures 7C and 7E). At the estuarine limit (P5, Figures 7J and 7K), however, the differences at the surface were approximately 0.5 $ms^{-1}$, while those at the bottom were almost nonexistent. Overall, the reduction in the current velocity between the old and new configurations ranged from 10% to 20% at the surface and up to 50% at the bottom, mainly in the estuarine mouth region.

### 3.1.2. Low Discharge Simulations

During the simulated period, the wind pattern presented alternation between the NE and SW directions, and the river discharge varied from approximately 1,370 $m^3s^{-1}$ to 4,000 $m^3s^{-1}$. The differences in current velocity between the old and new configurations were higher at the bottom than at the surface near the estuary entrance and decreased landwards (Figure 8). The difference in the ebb flow values between the old and new configurations was highest at the bottom, with a value of approximately -1.1 $ms^{-1}$ at the estuarine entrance (P1 and P2, Figure 8C and 8E), and reached approximately 0.2 $ms^{-1}$ at the surface and was almost null at the bottom in the estuarine limit (P5, Figure 8J, and 8K). The reduction in the current velocity between the old and new configuration was similar to the reduction estimated in the high discharge simulation, with between a 10% to 20% reduction at the surface and up to 50% at the bottom at the estuary mouth. The analysis of the additional points inside the Patos Lagoon revealed that the differences in current velocity between the old and new configurations were more pronounced in the interior of the lagoon (P8, Supplementary Figure 1). The reduction in the current velocity from the old to the new configuration was similar in the other points at the surface (10%) and bottom (20%) (P6 and P7, Supplementary Figure 1).

At point P8 (Figure 1), the difference in the current velocities between the two configurations was higher at the surface, with twice the difference of the other points, where the range was -1 to 0.5 $ms^{-1}$, and the difference in the ebb flow was more than 50%.

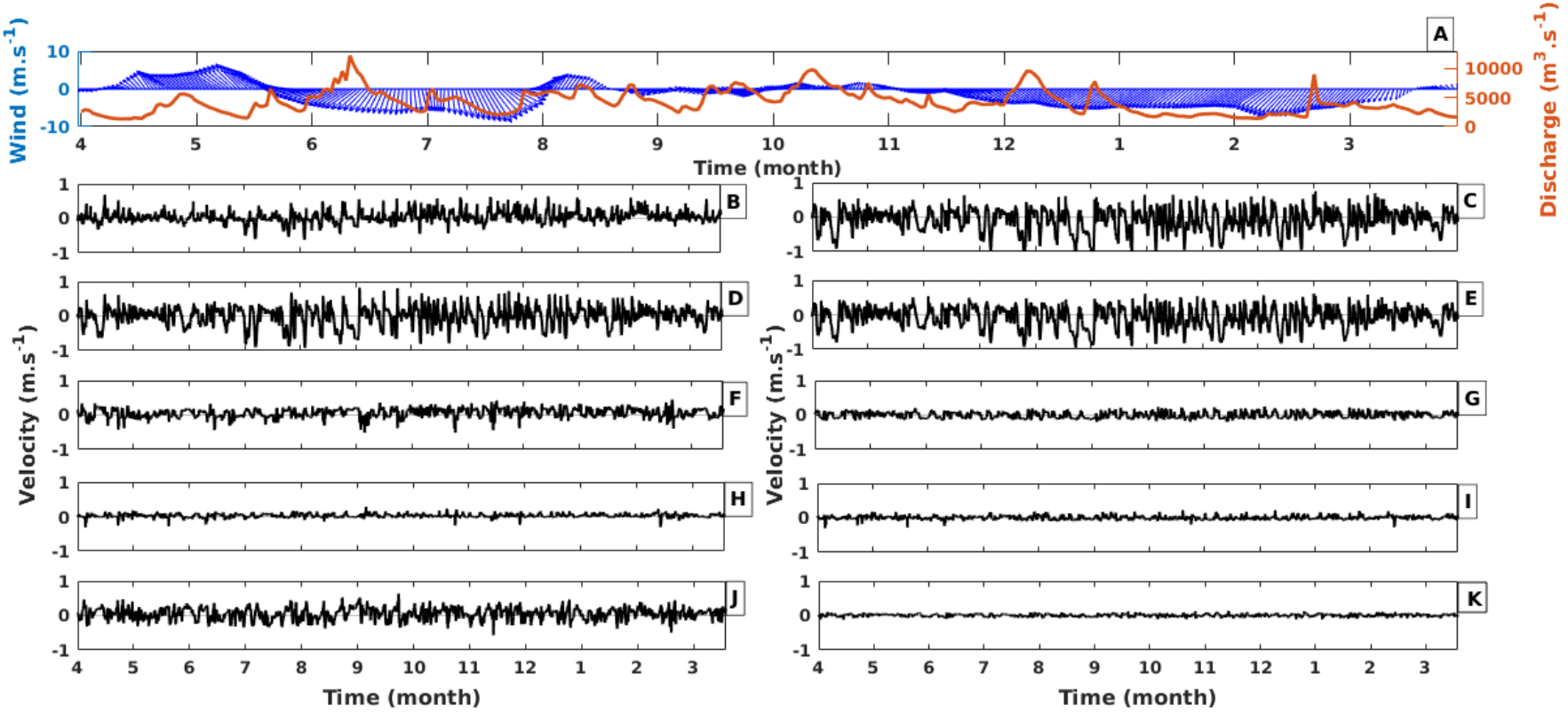


Figure 7: Time series of river discharge and wind for the period between 4/2002 and 3/2003. South (North) winds are positive (negative) (A). Current velocity time difference between the old and new jetty configuration at surface (left) and bottom (right) at points P1 (B and C), P2 (D and E), P3 (F and G), P4 (H and I) and P5 (J and K), during 4/2002 and 3/2003. Positive (negative) values denote inflow (outflow).

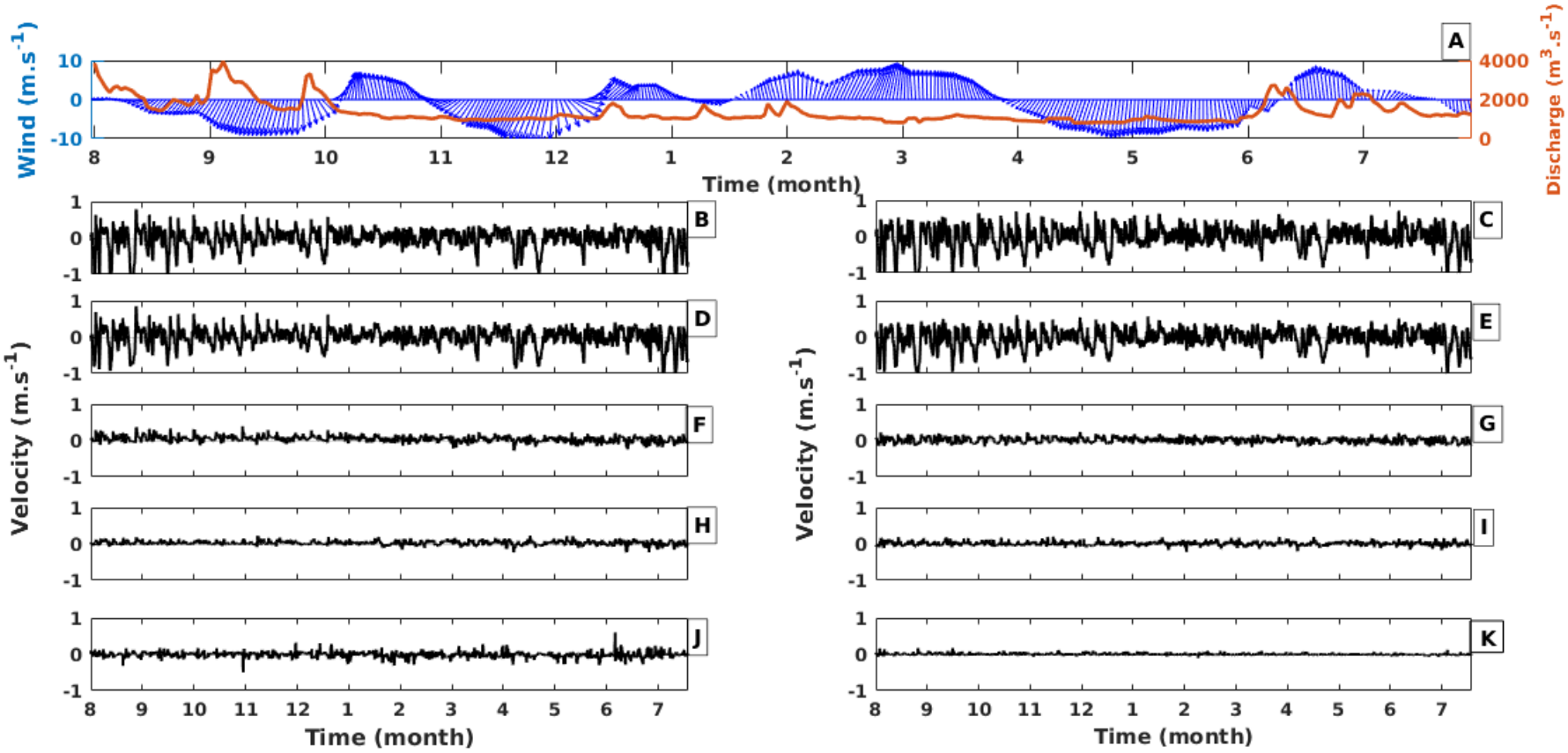


Figure 8: Time series of river discharge and wind for the period between 8/2011 and 7/2012. South (North) winds are positive (negative) (A). Current velocity time series difference between the old and new jetty configuration at surface (left) and bottom (right) at points P1 (B and C), P2 (D and E), P3 (F and G), P4 (H and I) and P5 (J and K) during 8/2011 and 7/2012. Positive (negative) values denote inflow (outflow).

### 3.2. Alterations in Saltwater Distribution

#### 3.2.1. High Discharge Simulation

The salinity behavior throughout both simulations (old and new scenarios) responded to the wind and freshwater discharge. The differences in salinity between the scenarios indicated that the saltwater excursion throughout the estuary decreased after the jetty alterations during the simulated period, with the differences ranging between a few units to almost 25 units of salinity. The largest differences were estimated near the estuarine limit (P5, Figures 9J, and 9K) at the surface and bottom. These results highlighted that the sporadic events of salinity intrusion towards the estuarine limit were reduced with the new jetty configuration (P5, Figures 9J, and 9K).During flood conditions, the salinity was reduced in more than 30% of the estuarine region with the new configuration (Figure 10C, F). During ebb conditions, a salinity reduction of up to 5 units was verified in the shallow embayments.

The variability in the salinity presented significant periodicity of approximately 10-15 days, with a similar response for both the old (Figures 11A, 11B, 11C) and new scenarios (Figures 11D, 11E, 11F) at the estuary entrance. The global power spectrum showed that only the frequencies at time scales < 15 days were significant for the old and new configurations (Figures 11C, 11F). The results for the middle estuary (P4, Figures 11I, 11L), indicated that this periodicity of < 15 days existed only during the first period of the simulation (April-June, August). The upper limit of the estuary (P5) presented a similar behavior (not shown). The signal of salinity intrusion lost strength towards the interior of the lagoon, and this decrease in energy was most evident with the new jetty configuration. A power value of 2500 $C^2$ in the overall power at 15 days was estimated at the entrance of the estuary for both the old and new configurations (Figures 11C, 11F), but in the interior of the estuary experienced a reduction from 1250 $C^2$ to 300 $C^2$ from the old (Figure 11I) to the new (Figure 11L) configuration.

#### 3.2.2. Low Discharge Simulation

Similar to the behavior in the high discharge simulation, the salinity behavior during the low discharge simulations for the old and new scenarios were influenced by the wind and freshwater discharge. An increase in salinity was estimated in the Patos Lagoon under the continued predominance of the S and SW winds and the low discharge. The maximum salinity was estimated close to the estuarine mouth (P1, Figure 12) from mid-December to March. The maximum salinity was verified at point P3 (Figure 12F and 12G) after January and at point P5 (Figures 12J and 12K) at the end of April as a response to the saltwater intrusion from the ocean to the inner lagoon (approximately 250 km). This response lasted until the end of June and reached the northern region of the lagoon (P8, Supplementary Figure 2), even during the period from April to May, when the

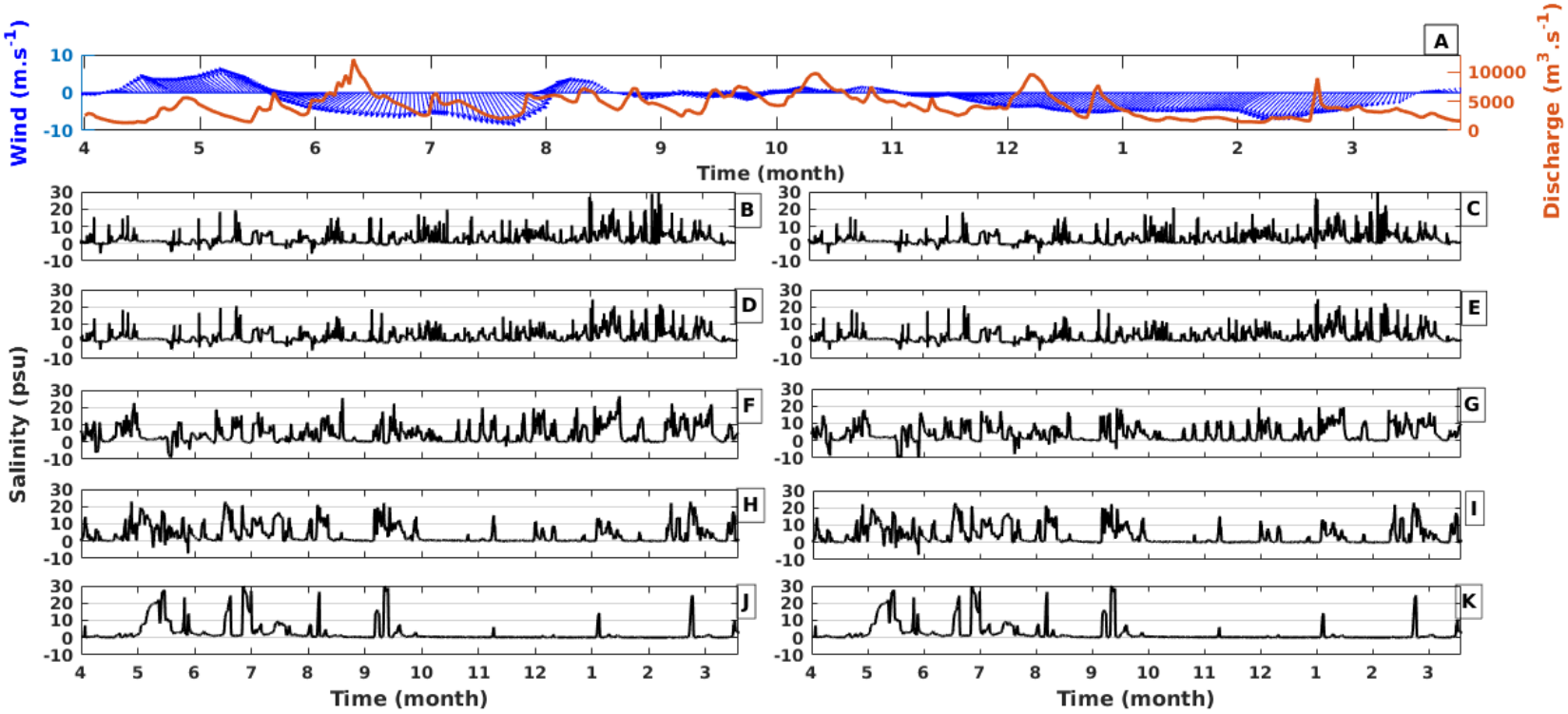


Figure 9: Time series of river discharge and wind for the period between 4/2002 and 3/2003. South (North) winds are positive (negative)(A). Salinity time series difference between the old and new jetty configuration at surface (left) and bottom (right) at points P1 (B and C), P2 (D and E), P3 (F and G), P4 (H and I) and P5 (J and K), during 2002-2003 (El Niño).

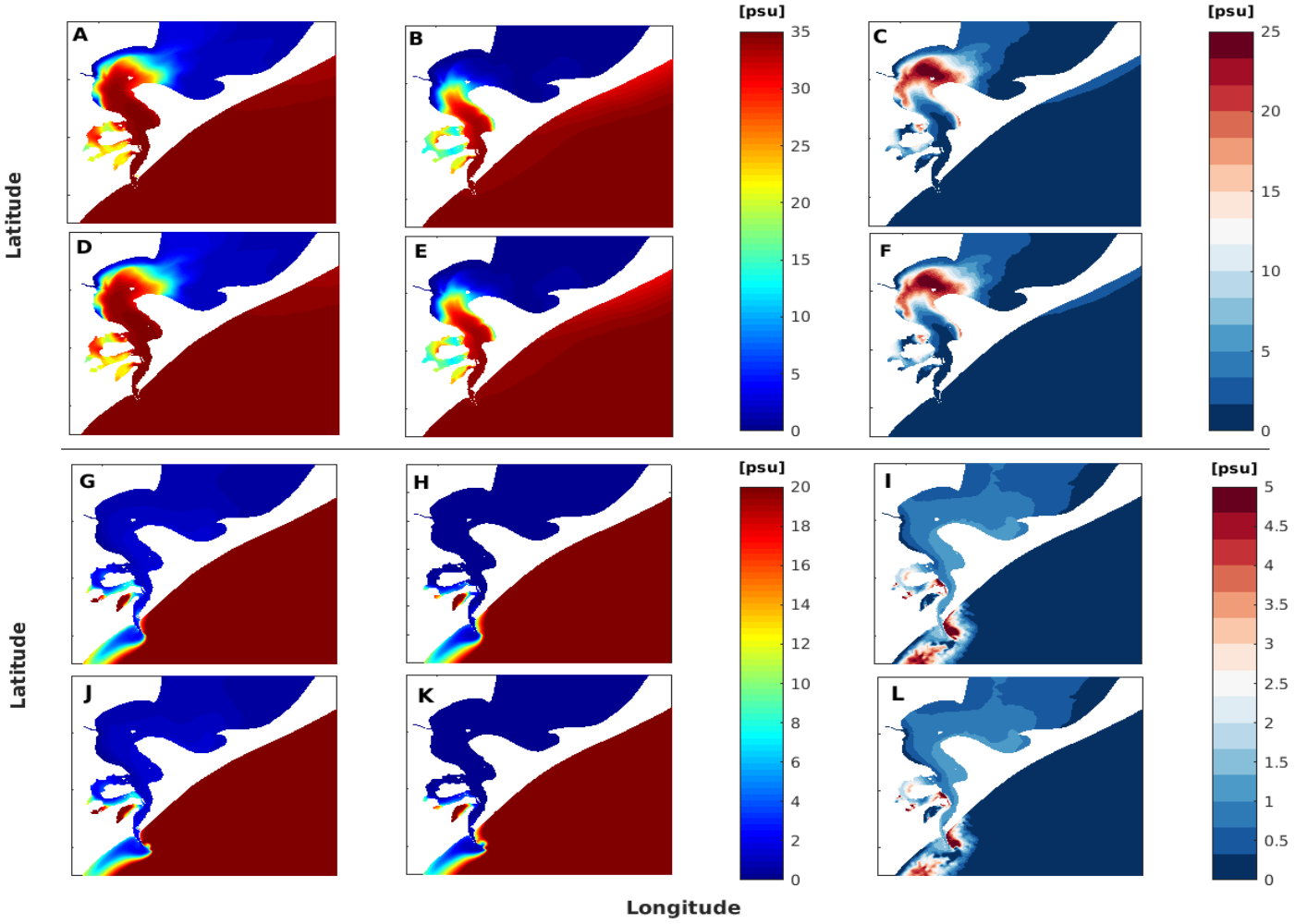


Figure 10: Spatial distribution of salinity during maximum flood (top panels) and maximum ebb (bottom panels) during the period of high discharge (2002-2003), considering the old (left) and new (center) scenarios and the calculated difference in salinity distribution (right). Results are presented for the surface (A, B, C, G, H, I) and for bottom (D, E, F, J, K, L).

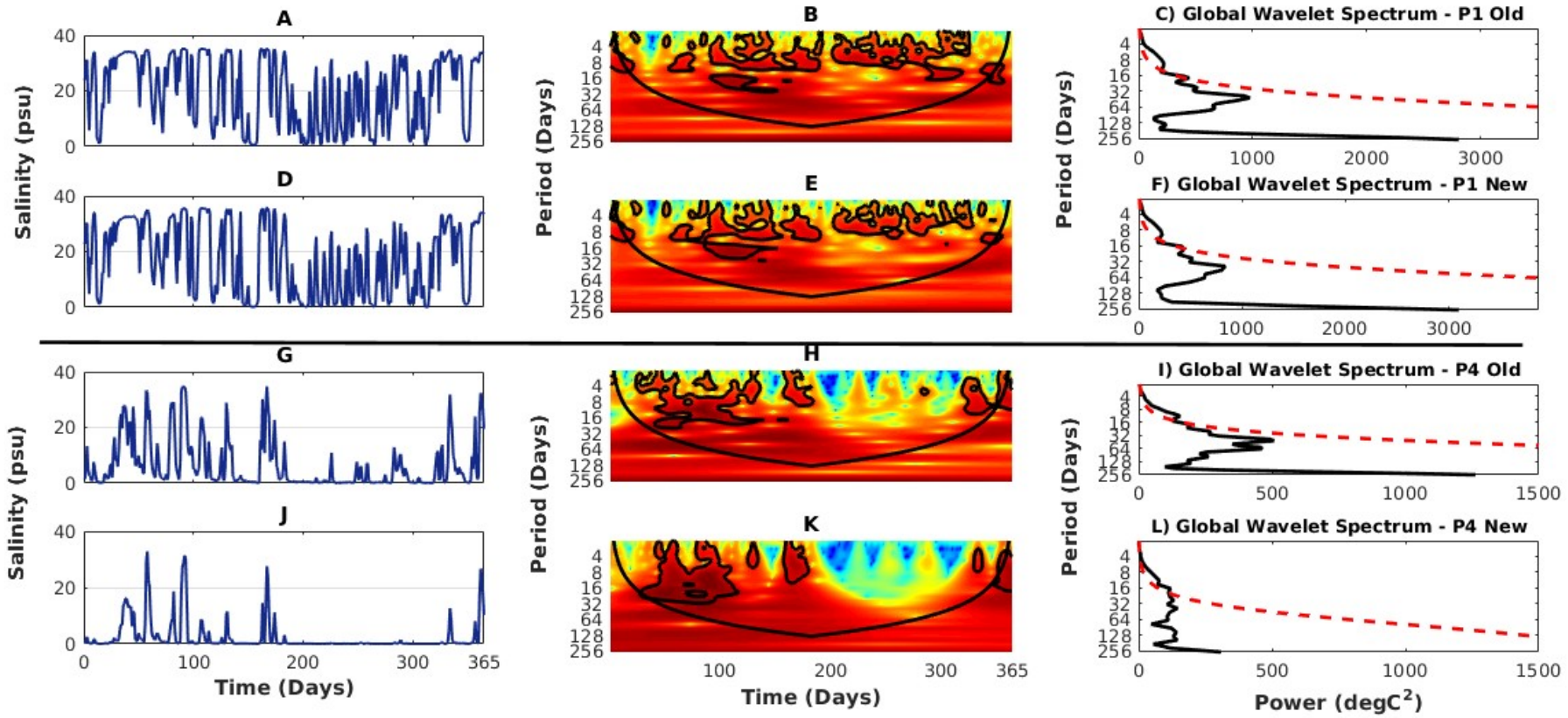


Figure 11: (A, D, G and J) Time series of salinity and (B, E, H and K) wavelet power spectrum of the time series for the estuary entrance (P1, top 2 panels) and near estuary limit (P4, bottom 2 panels), during the high discharge 2002-2003 period for the old (A, B, G and H) and for the new (D, E, J and K) jetties configuration. Thick contour line enclosed regions of greater than 95% confidence. Dash-dot regions indicate the cone of influence.

wind changed to the NE. In contrast to the old scenario, in the new jetty configuration, salinity values greater than 20 seldom reached the estuary limit. At approximately 120 km from the estuary mouth, w salinity increase was registered in mid-January with the old configuration but only increased in April with the new configuration (P6 where edge effect become important. (C, F, I and L). The global wavelet power spectrum of the time series and the dotted red line indicate the 95% confidence level. and P7, Supplementary Figures 2M, 2N, 2O, and 2P). With the old configuration, saltwater only reached the mouth of the Guaíba River, but was never recorded in the new scenario (P8, Supplementary Figures 2Q, and 2R).

The lagoon was less saline in the new than in the old scenario at all points in both the surface and the bottom. The differences in salinity between both scenarios ranged from a few units to just over 20 units. Large differences in salinity were estimated at the surface and the bottom near the estuarine limit after the incidence of the increased saltwater intrusion due to the southerly winds from February to July. The sporadic salinity events that were registered with the old configuration were not verified with the new configuration (P4 and P5, Figures 12H, 12I, 12J, and 12K). The results for the Patos Lagoon revealed that salinity differences of up to 10 units can propagate to the northern limit of the lagoon (approximately 250 km from the estuary mouth) (Supplementary Figure 2). The differences in salinity decreased towards the northern end of the lagoon, from 10 at point P6 at the bottom (Supplementary Figure 2N) to less than 5 at the Guaíba River mouth (Supplementary Figures 2Q and 2R).

The simulations with low river discharge revealed an increased difference in salinity between the old and the new jetty configuration (Figure 13). During the flood conditions, the salinity differences were the strongest, and decreased to approximately 25 in the southern lagoon, surpassing the northern limit of the estuary, and decreasing towards the interior of the lagoon to approximately 5 at the Guaíba River mouth, both at the surface and bottom (Figures 13C, 13F, 13I and 13L). Differences in salinity of approximately 20 were evident inside the shallow estuarine embayments. During the ebb conditions, the lagoon also became less saline with the new jetty configuration than with the old configuration. Differences in salinity of approximately 10 were evident in the coastal regions and the shallow embayments close to the estuary mouth, while from the estuary limit to the north of the lagoon, the difference did not exceed 5 units (Figures 13I and 13L) and had the same spatial dimension as during the flood period.

Similar to the high discharge results, during the low river discharge conditions, the salinity presented a periodicity of approximately 10-15 days for both the old and new jetty configurations (Figures 14A, 14B, 14C, 14D, 14E, 14F) at P1 to P3 (not shown). The results of the global power spectrum analysis highlighted that the time scale frequencies < 15 days were significant for the old

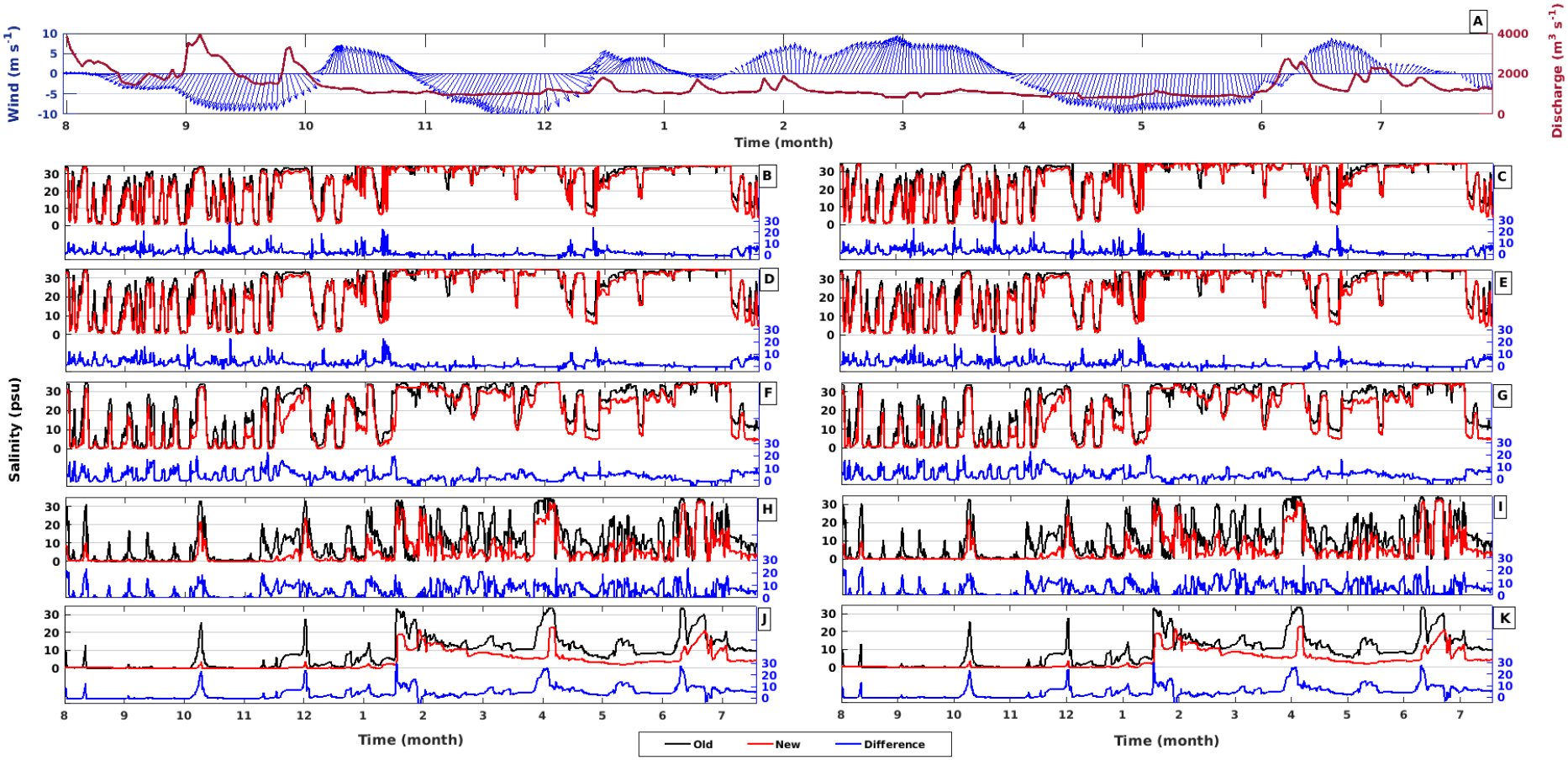


Figure 12: Time series (top) of river discharge and wind for the period between 08/2011 and 07/2012. South (North) winds are positive (negative) (A). Salinity time series at surface (left) and bottom (right) at points P1 (B and C), P2 (D and E), P3 (F and G), P4 (H and I) and P5 (J and K), for the old (black) and new (red) jetties configuration during 2011-2012 (La Niña). The blue line in all plots shows the difference between the old and new jetties configuration.

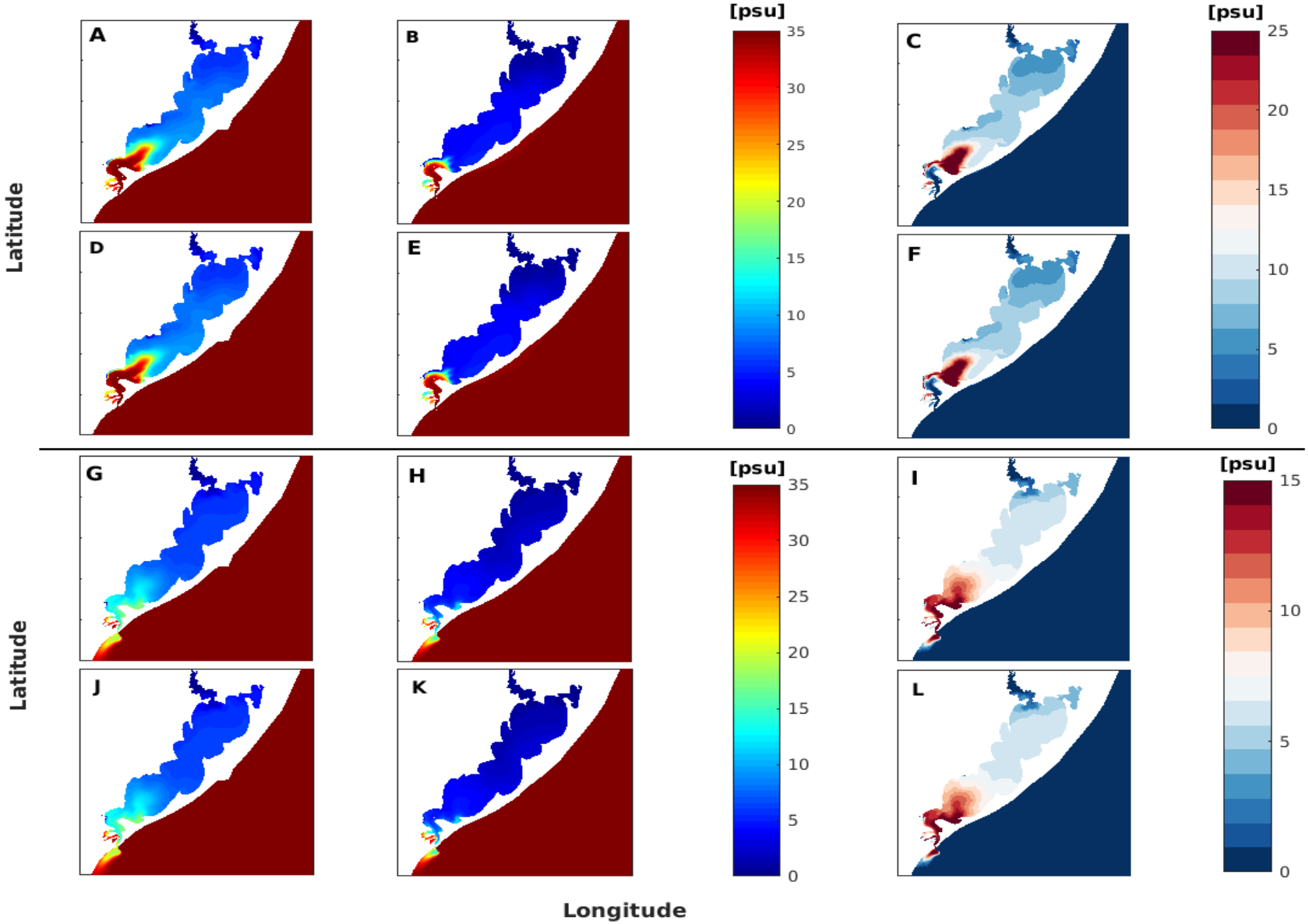
A
B
C
D
E
F
G
H
I
J
K
L
[psu]
35
30
25
20
15
10
5
0
[psu]
25
20
15
10
5
0
[psu]
35
30
25
20
15
10
5
0
[psu]
15
10
5
0
Latitude
Latitude
Longitude

Figure 13: Spatial distribution of salinity during maximum flood (top panels) and maximum ebb (bottom panels) during the period of low discharge (2011-2012), considering the old (left) and new (center) scenarios, and the calculated difference in salinity distribution (right). Results are presented for the surface (A, B, C, G, H, I) and for the bottom (D, E, F, J, K, L).

and new configurations (Figures 14C, 14F). The results indicated significant salinity variability in the first 150 days of the simulation in the southern lagoon region (P1, P2, and P3, Figure 1) during August-September and November-December. After 150 days, the salinity did not present significant variability (Figures 14B and 14E). From the limit of the estuarine region (P5, Figures 14H and 14K) to the northern lagoon, the daily salinity variability did not occur during the studied period. The salinity intrusion signal lost strength towards the interior of the lagoon, and a decrease in energy was most evident in the new jetty configuration. The overall power at 15 days at the entrance of the estuary decreased from approximately 1700 $C^2$ (Figure 14C) to 1100 $C^2$ in the old configuration (Figure 14I) and from 2500 $C^2$ (Figure 14F) to 580 $C^2$ in the new configuration (Figure 14L).

### 3.3. Changes in Salinity Stratification at the Mouth of the Estuary

Lateral stratification was evident between the jetties during the flood and ebb conditions, both at the surface and bottom for the old (Figures 15A, 15D, 15G, 15J) and new (Figures 15B, 15E, 15H, 15K) scenarios. Lateral stratification occurred at the estuary mouth, with higher salinity near the eastern than the western jetty. It was also evident that the range of salinity values between the jetties changed after the modification. In the old scenario, during flooding, the lateral salinity between the jetties ranged from 30-35 and was reduced to 23-27 after the jetty modification. During the ebb conditions, the lateral salinity values changed from 27-30 to 20-25 after the jetty modification.

After the changes in the jetty configuration, the lateral stratification time was reduced. During the flood flow at the same time step were observed in the old configuration (Figures 15A and 15D), more salted water near the eastern than the western jetty. In contrast, in the new configuration (Figures 15B and 15E), the flood current already dominated every navigation channel. On the other hand, in the western jetty during the ebb time step with the new configuration (Figures 15H and 15K), the estuary lost less saline water (approximately 20) to the ocean. In the old configuration (Figures 15G and 15J), the estuary lost a greater quantity of saline water (approximately 25).

The differences in salinity between the old and new scenarios for the flood results were significant in the region adjacent to the coast and in the shallow regions inside the estuary. A decrease of up to 15 units in the salinity was observed in the coastal and shallow embayments, and a decrease of approximately 5 was observed in the navigation channel (Figures 15C and 15F). During the ebb flow, the highest differences were along the navigation channel and the coastal plume, with a decrease of approximately 7 units of salinity (Figures 15I, 15L). No changes were observed in the eastern coastal region.

Figure 16 presents the vertical cross sections of salinity between the jetties at point P1 (Figure 1), during the ebb time step of Figures 15G and 15H, for the old (Figure 16A) and the new configuration (Figure 19B). The salinity values presented a vertical mixed structure and horizontal stratified water column in both configurations. The horizontal structure from the western jetty to the eastern jetty showed salinity values ranging from 26.5 to approximately 30 in the old scenario (Figure 16A) and from approximately 20 to 27 in the new scenario (Figure 16B). The lateral salinity gradient was approximately 3.5 units in the old jetty configuration and approximately 7 in the new configuration. The results demonstrated a characteristic lateral salinity gradient with more salted water in the eastern side than in the west during the NE winds.

The ebb flow velocities were approximately twice the flood intensities between the jetties, but the center ebb velocity was highest with values above -6 $ms^{-1}$ (Figure 17). The ebb current velocities were reduced in the western jetty and eastern jetty. In contrast, the flood velocity was more intense from the center of the channel to the eastern jetty, with currents faster than 2 $ms^{-1}$. The ebb velocities were more intense from August to October. The velocity intensity for both the ebb and flood conditions was reduced by approximately 20% at the surface with jetty modification. At the bottom, the reduction was up to 50% at the center of the channel and near the eastern jetty.

Lateral stratification was also observed in the current velocity time series. The frequency distribution of the current velocities also revealed lateral stratification at the mouth of the estuary and indicated velocities higher than 6 $ms^{-1}$ at the surface and close to 3 $ms^{-1}$ at the bottom during flood conditions (Figures 18 and 19). Reductions in the ebb and flood velocities occurred in the center of the channel and in the eastern channel from the old to new jetty configurations, both for the surface (Figures 18B, 18E and 18C, 18F) and the bottom (Figures 19B, 19E and 19C, 19F). In contrast, in the new western configuration, the intensification of the ebb and flow was registered at the surface (Figures 18A and 18D) and bottom (Figures 19A and 19D). The frequency of high velocities was reduced in the central area and the eastern side, while the maximmum flood and

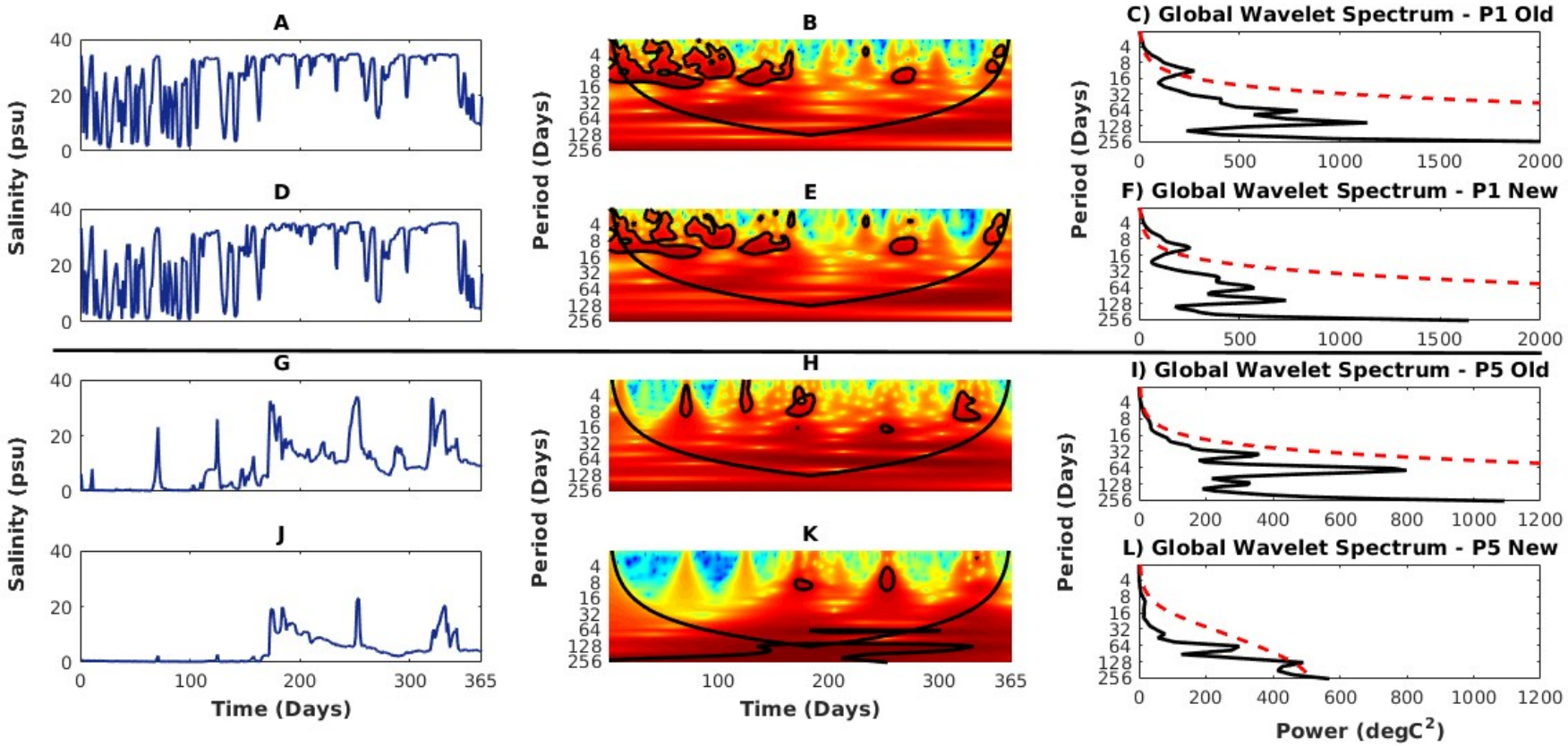


Figure 14: (A, D, G and J) Time series of salinity and (B, E, H and K) wavelet power spectrum of the time series for the estuary entrance (P1, top 2 panels) and estuary limit (P5, bottom 2 panels), during the low discharge 2011-2012 period for the old (A, B, G and H) and for the new (D, E, J and K) jetties configuration. Thick contour line enclosed regions of greater than 95% confidence. Dash-dot regions indicate the cone of influence where edge effect becomes important. (C, F, I and L). The global wavelet power spectrum of the time series and the dotted red line indicate the 95% confidence level.

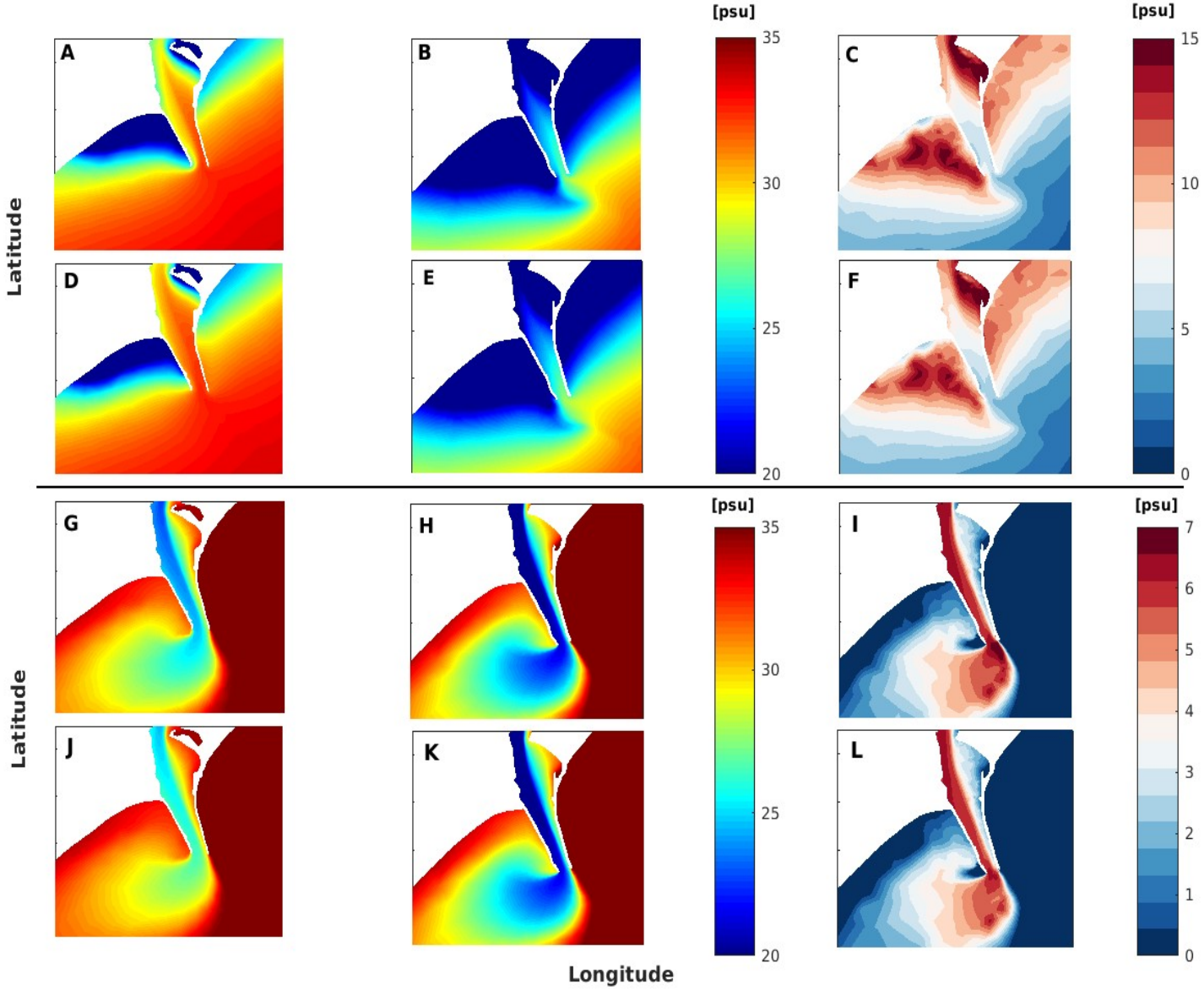
A
B
C
D
E
F
G
H
I
J
K
L
[psu]
35
30
25
20
[psu]
15
10
5
0
[psu]
35
30
25
20
[psu]
7
6
5
4
3
2
1
0
Latitude
Latitude
Longitude

Figure 15: Spatial distribution of salinity at the mouth of the estuary depicting changes in intensity and the lateral stratification between the jetties during the high discharge period 2002-2003. Flood (top panels) and ebb (bottom panels), for the old (left) and new (center) scenarios, and the calculated difference in salinity distribution (right) at the surface (A, B, C, G, H, I) and bottom (D, E, F, J, K, L).

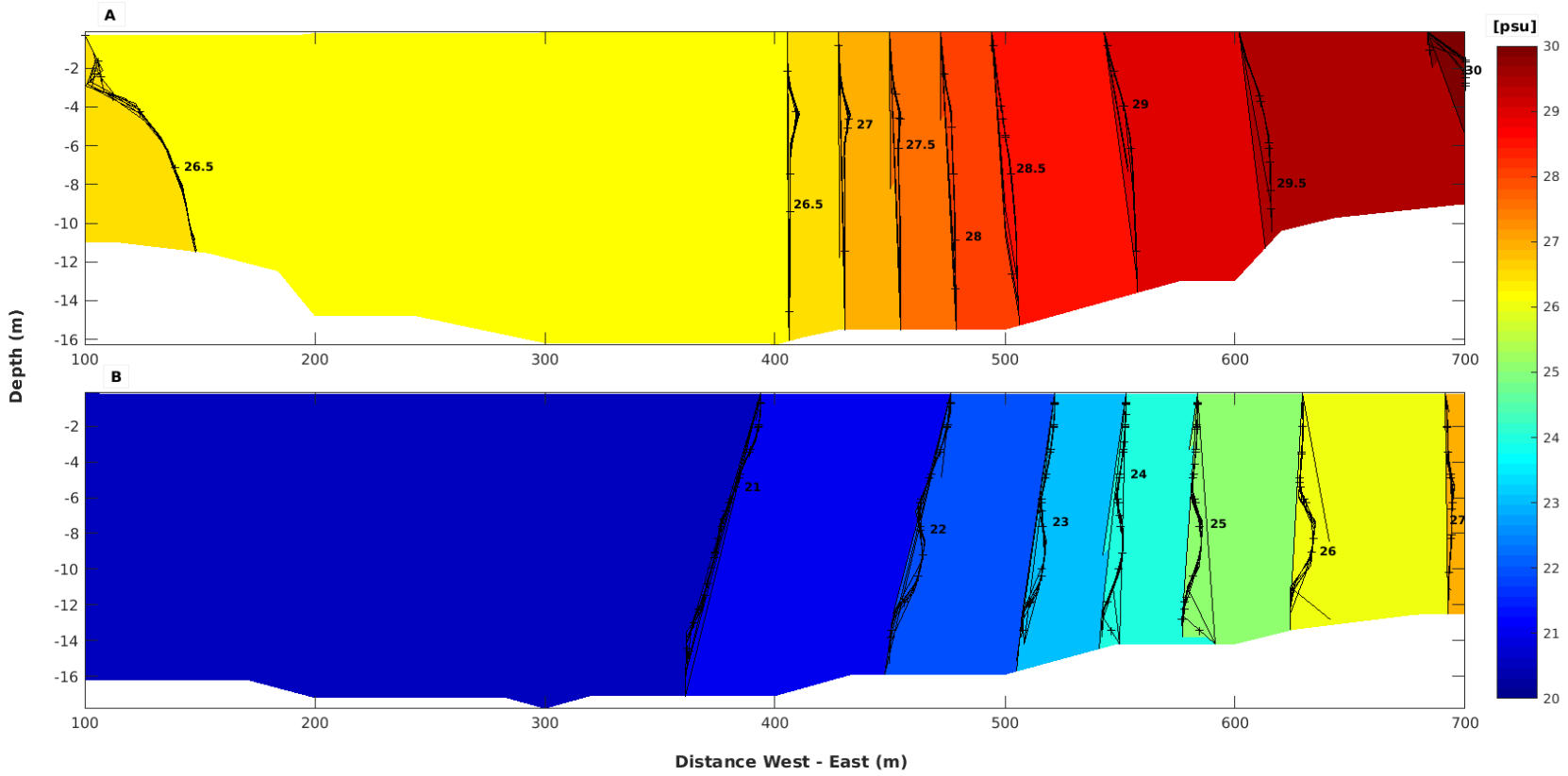


Figure 16: Vertical cross-section distribution of salinity during ebb flow at the estuary entrance (P1) from west (left) to east (right) jetties, for the old (A) and new (B) jetties configuration, during high discharge period 2002-2003 (El Niño).

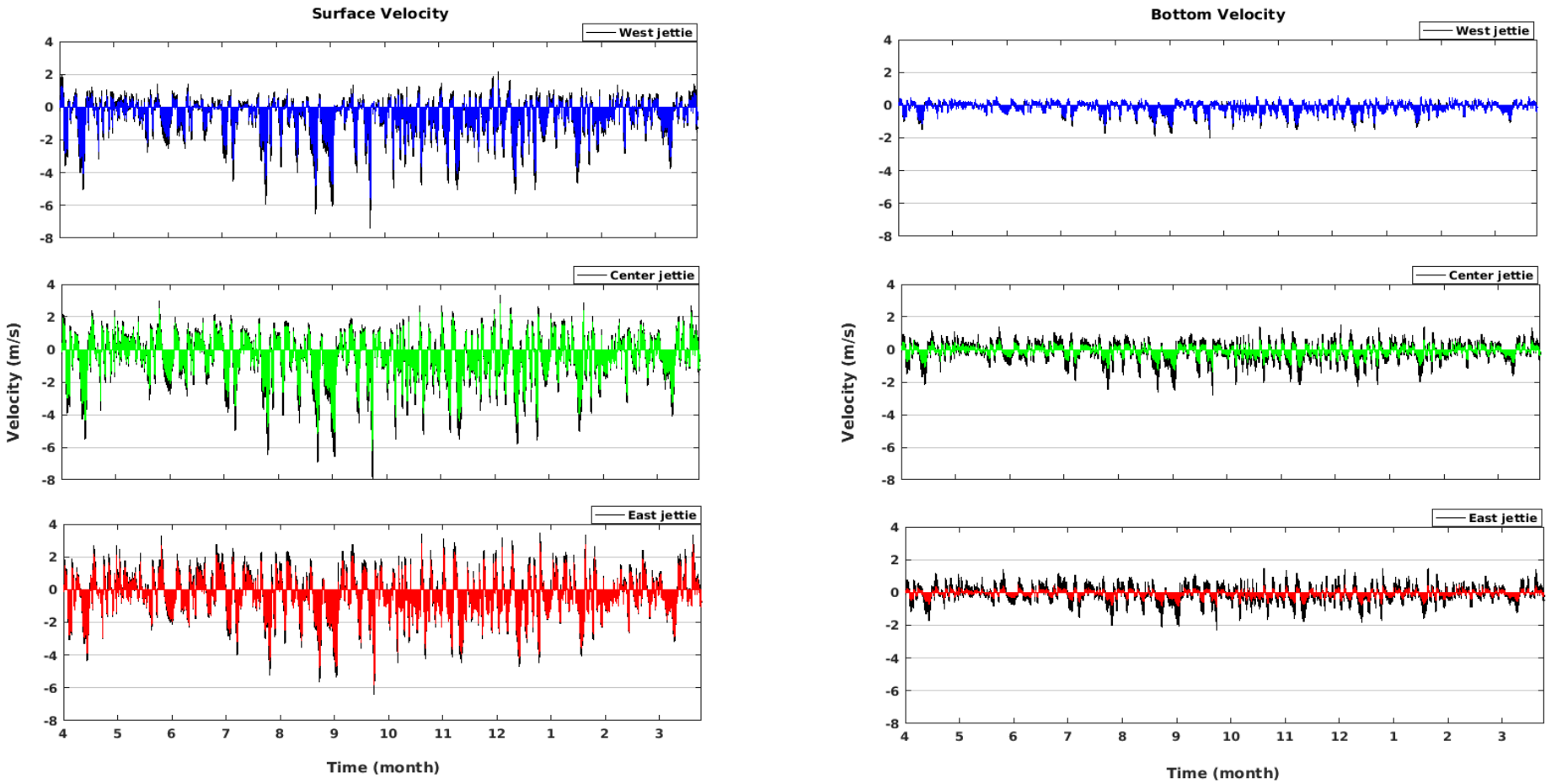


Figure 17: Current velocity time series from 3 points between the jetties (point P1) for the old (black line) and the new (colored lines) jetties configuration, during high discharge period of 2002-2003 (El Niño). The points are located at: first near the west jetty (top panel), second at the center oh the channel (center panel) and the third near the east jetty (bottom panel), both for surface (left panel) and bottom (right panel). Positive (negative) values denote inflow (outflow).

ebb velocities were increased on the western side, both at the surface and bottom.

At the surface area by the eastern jetty (Figures 18C and 18F), the maximum ebb velocity decreased from approximately 5 to 4 $ms^{-1}$, a reduction of approximately 20%. However, at the bottom (Figures 19C and 19F), the maximum flood and ebb velocities decreased from 2 to 1 $ms^{-1}$, a reduction of 50%. Similar velocity behavior was observed at the bottom during the flood period in the center of the channel, but during the ebb period (Figures 19B and 19E), the maximum velocities did not exceed 2 $ms^{-1}$ in the new configuration, in comparison with the 3 $ms^{-1}$ registered in the old scenario, a reduction of approximately 33%. At the surface (Figures 18B and 18E), the maximum ebb velocity decreased from approximately 6 to 5 $ms^{-1}$, a reduction of approximately 16%, and no visible change was observed in the flood velocities. In contrast, at the surface near the western jetty (Figures 18A and 18D), the maximum ebb velocities increased from approximately 3 $ms^{-1}$ to more than 5 $ms^{-1}$ from the old to the new scenario (an increase of 66%). In the flood stage, the velocities doubled in intensity, from approximately 1 to 2 $ms^{-1}$ (an increase of 100%). At the bottom (Figures 19A and 19D), the velocities up to 1 $ms^{-1}$ and higher than 1 $ms^{-1}$ doubled in frequency of occurrence in the flood and ebb periods, respectively.

Changes in the jetty configuration also promoted changes in the angle of incidence of the velocity from the old to the new configuration, which was more evident in the western jetty. The angle of incidence of the ebb flow from the western jetty changed from W to NW, while the angle of incidence of the flood flow changed from SE to E (Figures 18A, 18D, 19A and 19D).

## 4. DISCUSSION

This paper applied the TELEMAC-3D model to investigate the effects of the recent modernization work on the jetties of the Patos Lagoon mouth on the hydrodynamics of the system during the high discharge period in 2002-2003 (El Niño) and the low discharge period in 2011-2012 (La Niña). As the model results agreed well with the in situ data during the calibration and validation processes, the model was considered adequate for the simulation of current velocity, water level and salinity behavior, both at the bottom and surface, for both configurations (new and old).

The hydrodynamic characteristics of the estuaries were subject to several forces that could determine their spatio-temporal variability (Freitas et al., 2015; Seiler et al., 2015). In this study, we presented changes in the hydrodynamic behavior of the Patos Lagoon estuary due to alterations in the jetty configurations and the entrance channel to the Patos Lagoon. The study evaluated the changes in the currents and the salinity excursion and distribution in the scenarios with different geomorphologies, freshwater inflow and local and non-local wind effects.The scenarios of high and

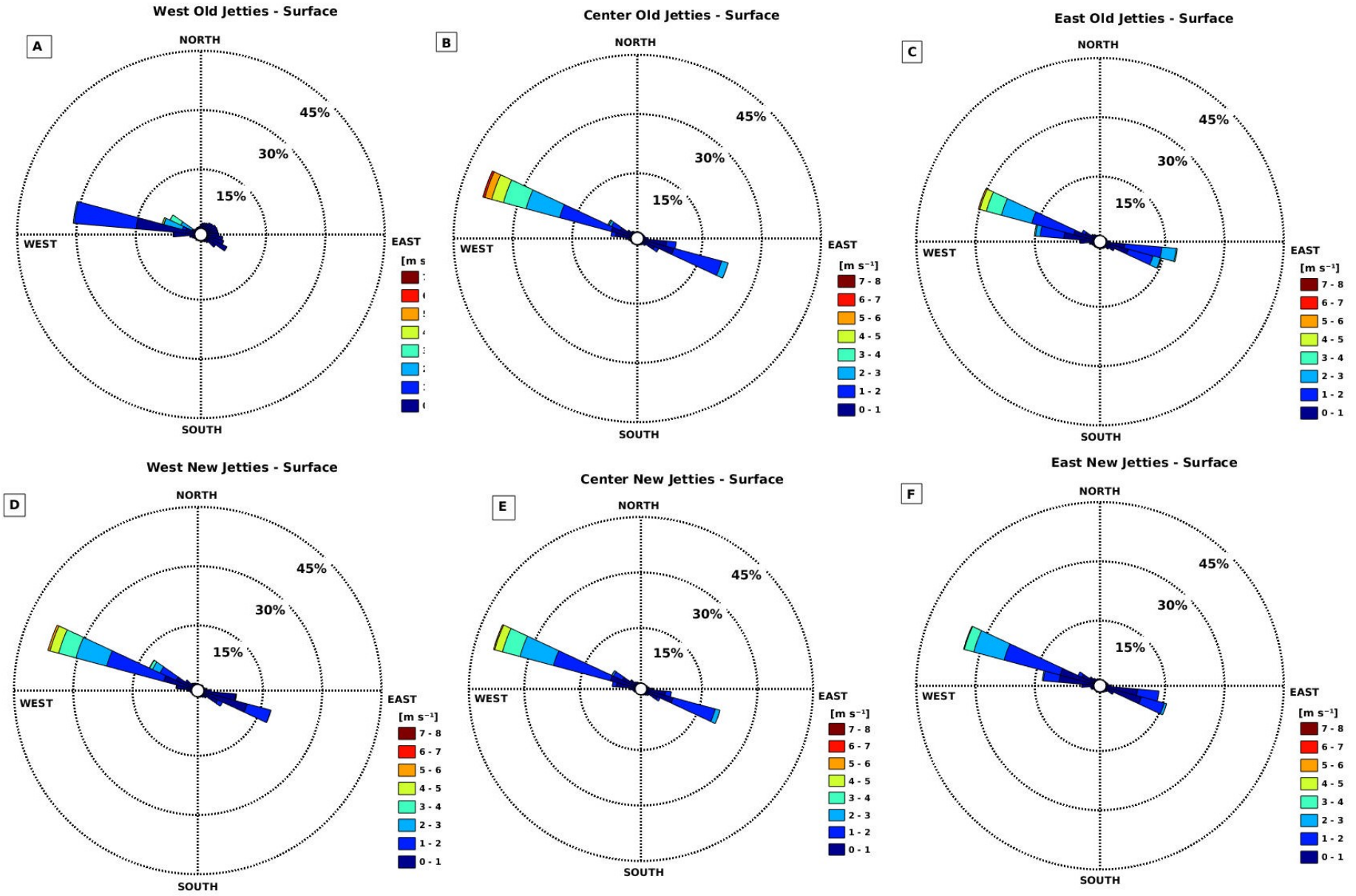
West Old Jetties - Surface
A
NORTH
45%
30%
15%
WEST
EAST
SOUTH
Center Old Jetties - Surface
B
NORTH
45%
30%
15%
WEST
EAST
SOUTH
[m s⁻¹]
7 - 8
6 - 7
5 - 6
4 - 5
3 - 4
2 - 3
1 - 2
0 - 1
East Old Jetties - Surface
C
NORTH
45%
30%
15%
WEST
EAST
SOUTH
[m s⁻¹]
7 - 8
6 - 7
5 - 6
4 - 5
3 - 4
2 - 3
1 - 2
0 - 1
West New Jetties - Surface
D
NORTH
45%
30%
15%
WEST
EAST
SOUTH
[m s⁻¹]
7 - 8
6 - 7
5 - 6
4 - 5
3 - 4
2 - 3
1 - 2
0 - 1
Center New Jetties - Surface
E
NORTH
45%
30%
15%
WEST
EAST
SOUTH
[m s⁻¹]
7 - 8
6 - 7
5 - 6
4 - 5
3 - 4
2 - 3
1 - 2
0 - 1
East New Jetties - Surface
F
NORTH
45%
30%
15%
WEST
EAST
SOUTH
[m s⁻¹]
7 - 8
6 - 7
5 - 6
4 - 5
3 - 4
2 - 3
1 - 2
0 - 1

Figure 18: Frequency distribution of velocity and incidence angle at surface for points at the west (A and D), center (B and E) and east (C and F) jetties in the estuary entrance (P1), for the old (top) and new (bottom) jetties configurations, during the high discharge period 2002-2003 (El Niño). Northward (southward) velocities denote outflow (inflow).

low river discharge were used since freshwater inflow is a major controlling force of the dynamics of the Patos Lagoon (Möller Jr e al., 2001; Möller Jr and Fernandes, 2010), and the region is subject to El Niño/La Niña cycles (Garcia et al., 2003).

These periods of extreme high and low discharge were accompanied by dynamic winds that predominantly came from the N and S quadrants, which were also important for the local hydrodynamic (Fernandes et al., 2002; Odebrecht et al., 2005), mainly when discharge was lower than 3,000 $m^3s^{-1}$ (Möller Jr et al., 2001; Möller Jr and Fernandes, 2010).

The range of the intensity of the current velocity had an inverse relationship with the area of the cross section, as reported by Fernandes et al. (2002); this behavior was also reflected in the velocity difference between the two configurations. The ebb current velocities were more intense during the first portion of the simulated periods, especially when combined with the occurrence of the NE winds during the high river discharge period. The velocities of the flood currents, on the other hand, were more intense during the low discharge period, combined with the SW winds during the second portion (summer and autumn) of the simulated periods. These results agreed with those of with Fernandes et al. (2005) and Marques (2005).

Contrary to what was anticipated and used as the motivation for the jetty elongation and the narrowing of its mouth, the results revealed a decrease in the current velocity throughout the estuary and in the inner lagoon after the alteration. A more significant decrease of approximately 20% was observed at the estuary mouth and has also been observed by Silva et al. (2015). These authors suggested that the causes could be related to changes in the dynamics of the coastal currents and in the coastal plume direction and the intensification of the recirculation zones, which occur at the north and south of the jetties. Other factors, such as the prolongation and intensification of the funnel (Yuk and Aoki, 2007), and the convergence of the jetty edges, could have contributed to the decrease in the current velocity. Möller Jr and Fernandes (2010) assumed that changes in the morphology induced by dredging, embankment, jetty or bridge construction can alter wave propagation, modify vertical salinity stratification, and decrease or increase the saltwater penetration into the estuary.

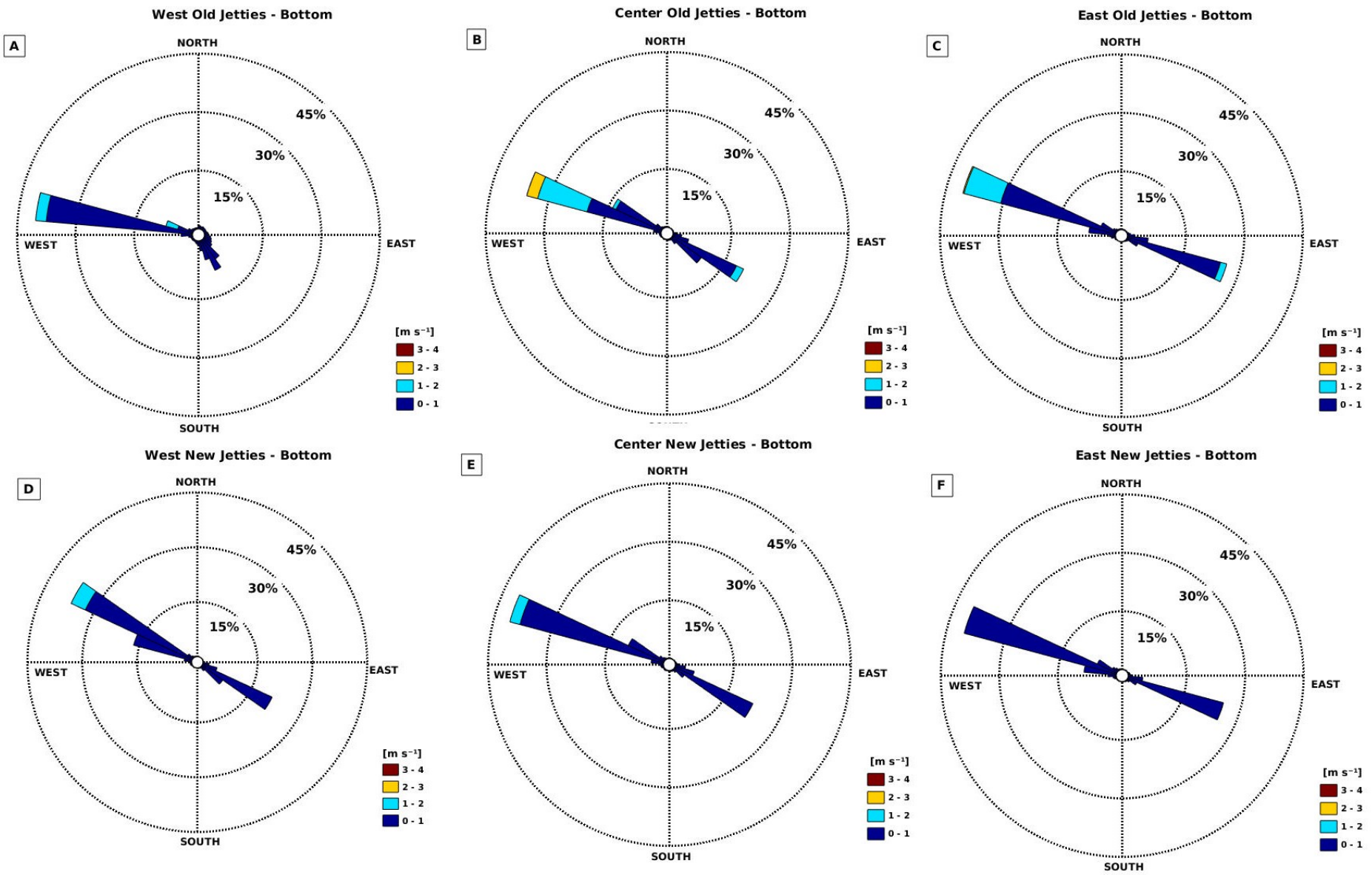
A
West Old Jetties - Bottom
NORTH
45%
30%
15%
WEST
EAST
SOUTH
[m s⁻¹]
3 - 4
2 - 3
1 - 2
0 - 1
B
Center Old Jetties - Bottom
NORTH
45%
30%
15%
WEST
EAST
[m s⁻¹]
3 - 4
2 - 3
1 - 2
0 - 1
C
East Old Jetties - Bottom
NORTH
45%
30%
15%
WEST
EAST
SOUTH
[m s⁻¹]
3 - 4
2 - 3
1 - 2
0 - 1
D
West New Jetties - Bottom
NORTH
45%
30%
15%
WEST
EAST
SOUTH
[m s⁻¹]
3 - 4
2 - 3
1 - 2
0 - 1
E
Center New Jetties - Bottom
NORTH
45%
30%
15%
WEST
EAST
SOUTH
[m s⁻¹]
3 - 4
2 - 3
1 - 2
0 - 1
F
East New Jetties - Bottom
NORTH
45%
30%
15%
WEST
EAST
SOUTH
[m s⁻¹]
3 - 4
2 - 3
1 - 2
0 - 1

Figure 19: Frequency distribution of velocity and incidence angle at bottom for points at the west (A and D), center (B and E) and east (C and F) jetties in the estuary entrance (P1), for the old (top) and new (bottom) jetties configurations, during the high discharge period 2002-2003 (El Niño). Northward (southward) velocities denote outflow (inflow).

In estuaries that present a significant contribution of freshwater, the salinity decreases with high river flow, reflecting the effect of river discharge on the salinity distribution in coastal environments (Azevedo et al., 2014; Seiler et al., 2015); the opposite effect is observed for low discharges. The model results showed decreasing salinity with the increase of discharge during 2002-2003, and the opposite was observed during 2011-2012. Similar results were observed during 1997-1998 and 2011, which were high discharge periods (Fernandes et al., 2002; Garcia et al., 2003; Möller Jr et al., 2009; Seiler et al., 2015), where the salinity decrease resulted by high precipitation occured during the El Niño events and NE wind, which promoted intense ebb flows, making the estuarine region sometime unsalted. This event may persist for months because the continental waters are forced towards the mouth, preventing the salinization of the lagoon (Möller Jr and Fernandes, 2010). In contrast, salinization of the Patos Lagoon occurred during 2011-2012, and Odebrecht et al. (2005) and Seiler et al. (2015) studied the 1988 and 2006 La Niña events, respectively, and attributed the enhanced saltwater intrusion to the low precipitation combined to SW wind and reported that the oligohaline limit reached approximately 180 km, from the Patos Lagoon mouth, near point P7 (Figure 1), which was in agreement with our results.

The jetties modernization work changed the salinity distribution by reducing the saltwater intrusion and removing the occurrence of the sporadic peaks of salinity observed with the old configuration. The direct analyses of the daily salinity time series revealed strong variability in the salinity patterns on a timescale of approximately 16 days. This modulation is characteristic of the passage of a meteorological front over the area (Möller Jr et al., 2001; Marques et al., 2010). Significant differences in the power variability from the estuary entrance region to the northern limit of the lagoon were registered. Near the estuary mouth for both high and low discharge simulations, the global power spectrum was approximately one order of magnitude higher than in the estuarine limit and close to Guaíba River mouth in the old configuration. However, in

the new configuration, the global power spectrum decreased two orders of magnitude for the same locations. This behavior can be associated with the reduction of the most energetic events in the exchange region between the estuary and the coastal regions (Marques et al., 2010) as a consequence of the jetty modification.

The power variation analyses also indicated the influence of the local wind close to the Patos Lagoon mouth as the main factor that controlled the salinity propagation in the coastal and southern estuarine regions, with the direct transfer of momentum to the water column (Marques et al., 2010). On the other hand, from the north of the lagoon towards the estuary, the discharge controlled the salinity events. Previous studies based on in situ measurements and model results have noted that the Patos Lagoon circulation was mainly controlled by the combination of discharges and local and non-local wind action (Fernandes et al., 2002, 2005; Marques et al., 2010; Möller Jr et al., 2001).

The salinity signal lost strength and significantly decreased in power towards the lagoon as a consequence of the reduced saltwater intrusion with the new configuration compared to with old jetty configuration. The modification of the jetty configuration also seemed to contribute to the reduction of the propagation of the tides into the estuary.

The lateral flow stratification characterized by flooding near the eastern jetty and ebb near the western jetty in the Patos Lagoon access channel was already present in the old jetty configuration (Fernandes et al., 2005). This behavior was attributed to the asymmetry of the jetty length and the anthropogenic dredging activity in the navigation channel located near the eastern jetty and the channel depth (Fernandes et al., 2005; Möller Jr and Fernandes, 2010). The jetty modification maintained this behavior but decreased the occurrence of lateral stratification by half. Despite the presence of lateral stratification, the vertical water column presented a mixed characteristic, which is typical of estuaries (Möller Jr et al., 2001). Dyer (1989) suggested that when the lateral density gradient was at a maximum, vertical mixing was supposed to be least efficient.

With the new jetty configuration, the higher velocities observed from the center of the channel to the eastern jetty during the ebb and flood currents were reduced. Associated with the other findings of this study, this trend highlights the decrease in velocity, which was mainly observed near the estuary mouth. The western shift in the ebb and flood propagation angle was also observed and indicated a result of the

engineering work, as suggested by Ghashemizadeh and Tajziehchi (2013) at the eastern coast of Bandar Abbas. Changes in the propagation velocity direction changed the bed level evolution and induced sedimentation on the eastern and erosion on the western jetty.

The influence of the jetty configuration in the saltwater intrusion were reflected in the flow characteristic. The indentation of the maximum saltwater intrusion on the new configuration contributed to the reduced transfer of momentum and promoted stratification by weak vertical shear action at the new less than with the old configuration (Fernandes et al., 2005). The weak action of the hydrodynamic agents and the condition that was directly related to lower depth and smaller tidal range have as a consequence weaker turbulence and tidal current action (Freitas et al., 2015).

The results supported the hypothesis that the jetties modernization work caused changes in the Patos Lagoon hydrodynamics. As a consequence, the changes in the transport and distribution of the estuarine properties and organisms in the whole lagoon could also be expected. Azarmsa et al. (2009) explained that changes in the circulation pattern could also negatively impact the navigation of large vessels and the pollution and sedimentation processes (by the reduction of the ebb currents and natural dredging in the access channel). Other effects, such as the migration of the tidal delta as a result of the changes in the morphodynamics of the central channel and the infilling or formation of banks on the jetty sides, which could influence the maintenance of adequate water depth, were mentioned by Prumm and Iglesias (2016) after the Ribadeo port expansion in Spain. Ecologically, the reduction of the saltwater intrusion and sporadic saltwater peak events could greatly impact the entrance of oceanic organisms, which contribute to the increase of recruitment of estuarine dependent species and are essential for maintaining the fish stocks in the Rio Grande do Sul coastal region.

The presence of lateral stratification in the access channel was expected to be an important factor because it influences the stratification, mixing, and distribution of the organisms and properties in the areas of the estuary. Dyer (1989) considered that this effect occurs when a maximum lateral density gradient is observed and that the transverse mixing should be less efficient. This lateral stratification could define the distribution of the eggs, larvae, sediments and other water properties during the ebb and flood currents, indicating possible locations of maximum and minimum concentrations.

## 5. CONCLUSIONS

The effect of the recent modernization works on the jetties at the access channel to the Rio Grande port was investigated through TELEMAC-3D numerical modeling in extreme freshwater discharge conditions. The validation and calibration demonstrated that the applied model provided acceptable simulations.

The jetty modernization did not contribute to the propagation of the inflow and outflow through the narrow inlet, and the ebb and flood velocity ranges were reduced by approximately 20%. With the new configuration, the saltwater intrusion decreased, sporadic salinity peaks disappeared, and the strength of the salinity signal decreased by more than one order of magnitude in the interior of the estuary and lagoon.

The changes in the mouth configuration contributed to the partial centralization of the access channel flow, reducing the occurrence time of lateral stratification by one-third.

The modifications induced a reduction of approximately 20% for the ebb and flood surface velocities, and a reduction of over 50% in the bottom velocities was observed near the eastern jetty. A relative increase in the velocity at the western jetty during flooding was observed. The modernization of the jetties also changed the flow characteristic into the estuary by altering the angle of propagation of the ebb and flood currents near the western jetty.

## ACKNOWLEDGEMENTS

The authors would like to acknowledge CAPES (*Coordenação de Aperfeiçoamento Pessoal de Ensino Superior*) for sponsoring the first author's (MHA) PhD's grant through the *Programa de Pós-Graduação Ciência para o Desenvolvimento* (PGCD), and CNPq (*Conselho Nacional de Desenvolvimento Científico and Tecnológico*) for the research grants 308274/2011-3 (EHF) and Proc. 310047/2016-1 (JHM). This study was partially funded by the Brazilian Long-Term Ecological Research Program (PELD) from CNPq (Proc.441492/2016-9) and the Fundação de Amparo à Pesquisa do Estado do Rio Grande do Sul (Proc. 16/2551-0000102-2). We are also grateful to the LOCOSTE (*Laboratório de Oceanografia Costeira e Estuarina)* team for giving support during this research and to Prof. Dr. Osmar Möller Jr for providing the in situ data used to calibration and validation of TELEMAC-3D model. Thanks again to CAPES for support PPGO during my tesis.

SUPPLEMMENT A

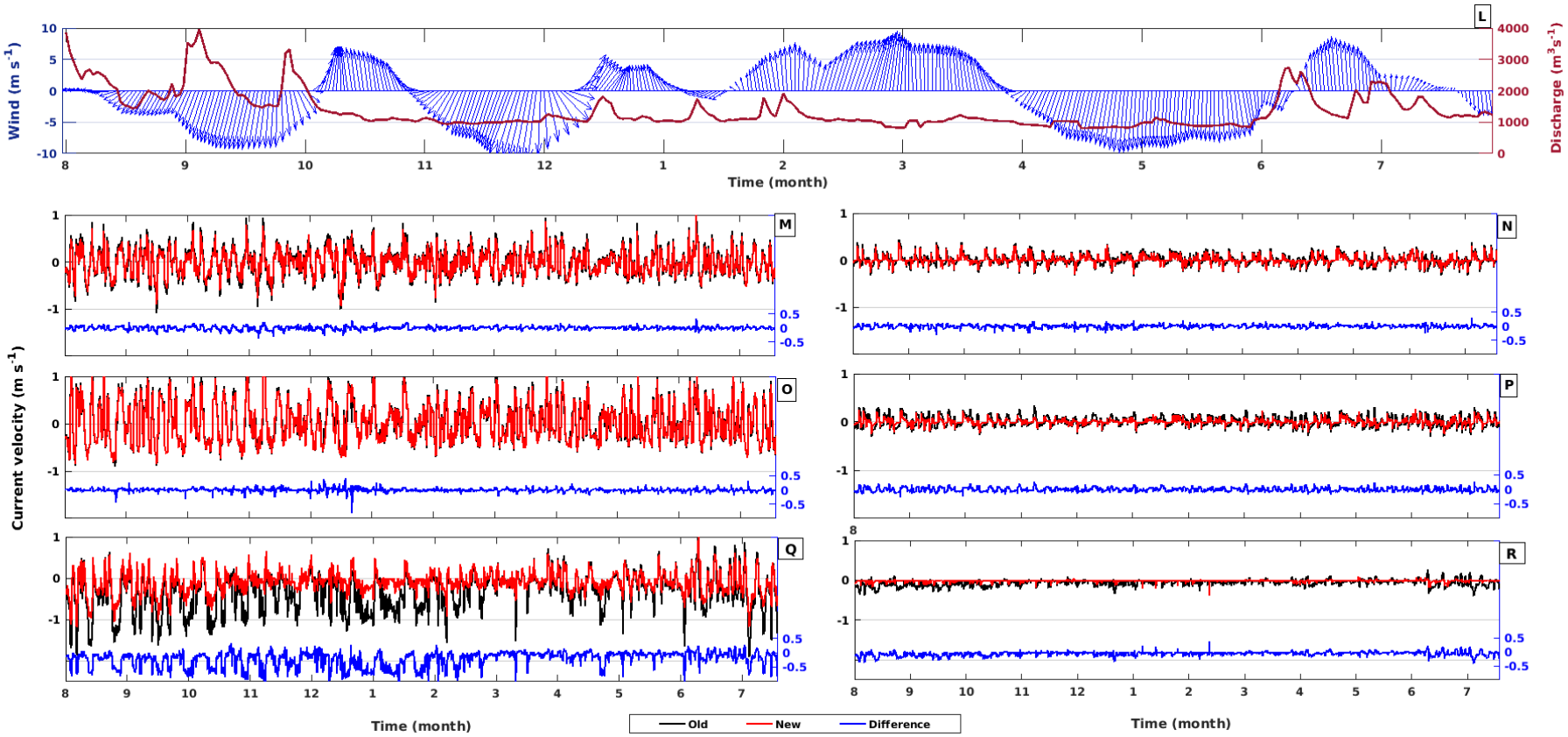


Figure 1: Time series of river discharge and wind for the period between 8/2011 and 7/2012. South (North) winds are positive (negative) (L). Current velocity time series at surface (left) and bottom (right) at points P6 (M and N), P7 (O and P), P8 (Q and R) for old (black line) and new (red line) jetties

configuration during 8/2011 and 7/2012. Positive (negative) values denote flood (outflow). The blue line in all plots shows the difference between the old and new  jetties configuration.

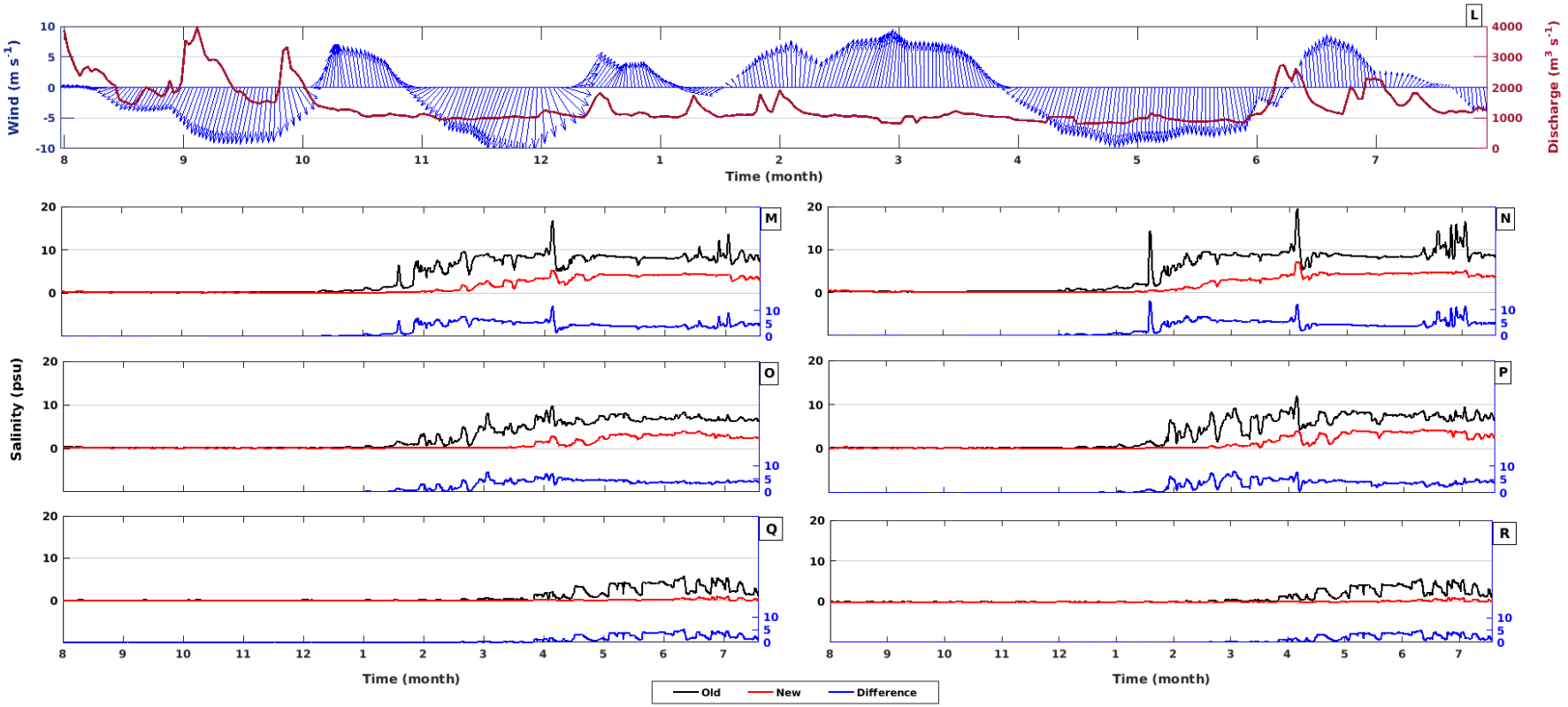


Figure 2: Time series (top) of river discharge and wind for the period between 8/2011 and 7/2012. South (North) winds are positive (negative)(L). Salinity time series at surface (left) and bottom (right) at points P6 (M and N), P7 (O and P), P8 (Q and R), of old (black) and new (red) jetties configuration during 2011-2012 (La Niña). The blue line in all plots shows the difference between the old  and new jetties configuration.

# Human-induced influence on eggs and larval fish transport in a subtropical estuary

**Maria Helena Paulo António[a,c,d,e,@], José H Muelbert[b,e] and Elisa H. L. Fernandes[a,e]**

[a]Laboratório de Oceanografia Costeira e Estuarina, Instituto de Oceanografia, Universidade Federal do Rio Grande, Brasil

[b]Laboratório de Ecologia do Ictioplâncton, Instituto de Oceanografia, Universidade Federal do Rio Grande, Brasil

[c]Escola Superior de Ciências Marinhas e Costeiras, Universidade Eduardo Mondlane, Moçambique

[d]Pós-graduação Ciência para o Desenvolvimento, Instituto Gulbenkian de Ciência,

Oeiras, Portugal

[e]Programa de Pós-Graduação em Oceanologia, Instituto de Oceanografia, Universidade Federal do Rio Grande, Brazil

[@]E-mail: mhbeula2@gmail.com

## Abstract

Transport during the early stages of life to the nursery areas is one of the main processes in the maintenance of the marine fish population, and human interventions can influence this process. In this work, a Lagrangian model coupled to the hydrodynamic model TELEMAC-3D was used to evaluate the effect of the change in the configuration of the Barra Jetties of the Rio Grande to the transport of eggs and larvae of the croaker *Micropogonias furnieri* in the Patos Lagoon estuary (PLE). Twelve experiments of 5 days with periods of extreme high and low discharge combined with winds from the south quadrant (SW, S, and SE) were carried out to test the hypothesis that human interventions in the coastal region alter the transport patterns of fish eggs and larvae. SW winds ensured the most efficient recruitment into the estuary, in terms of both entry time and maximum reach for both configurations. However, the recent modernization of the Barra Jetties has changed the pattern of transport and dispersal of larvae and has reduced the amount and reach of incursion of croaker eggs and larvae into the estuary compared to their old configuration. With the new configuration and high water discharge, 25% reduction in larval concentration and abundance was registered in the estuary for SW and S winds, and 68.6% for SE winds. At low discharge, the decrease was only between 0.5% to 1% for the wind conditions evaluated. L Predominant wind direction was decisive in defining the initiation time of lateral stratification in the access channel, and was shown to be an important parameter in larval transport and distribution between the jetties.. For the old configuration, lateral stratification was established at 1 h, 7 h, and 10 h after the start of the simulation with the incidence of SW, S and SE winds, respectively. For the new configuration, lateral stratification was established at a later time for all tree incident winds. Delay in establishment of lateral stratification at the entrance of the estuary influenced the intrusion of saline water and resulted in a smaller number of larvae between the jetties and consequently their transport into the estuary. With the new configuration, a reduction of 1.6 km at high and 2.3 km at low water discharge was observed for the maximum excursion of the larvae in the estuary.. The results obtained corroborate the hypothesis that human interventions in coastal regions change the patterns of transport of fish eggs and larvae. Furthermore, the findings suggest that small alterations in coastal structures

contribute to reduce the transport of dependent estuarine species to their nursery grounds. Coupled with current knowledge about this species, the results can be used to support better management of fishery resources in the region.

**Keywords:** *Micropogonias furnieri*, larvae transport, anthropogenic effects, ports, Patos Lagoon, TELEMAC-3D

## 1. INTRODUCTION

Coastal and estuarine environments are extremely important for the life cycle of various marine organisms (Muelbert and Weiss, 1991; Able, 2005; Whitfield, 2016), which are the most important aquatic resources in the world (Liu and Chan, 2016). In addition to their ecological wealth and capability of providing high rates of primary production and abundance of food, estuaries also serve as a habitat, nursery and protection against predators in early life stages and facilitate the development of numerous marine species (Liu and Chan, 2016; Teodosio et al., 2016).

The planktonic phase of species demands attention as a research topic, as it is a characteristic component of the life cycle of many marine organisms (Tiessen et al., 2013). In fish, the planktonic phase is marked by the stages of egg and larva, and changes in their transport has been suggested as one of the important factors that affect variability of recruitment in marine fish stocks (Brown et al., 2000; Houde, 2008). The survival of fish larvae depends on the pattern of circulation and transport from the spawning to the nursery area, and local biological and physical events can explain the patterns of growth and survival in the early stage of fish life (Lough et al., 1994; Brown et al., 2000; Hinrichsen, 2009; Endo et al., 2019).

Studies to understand the pattern of transport and dispersion of eggs and larvae in estuaries and coastal regions have been of great importance for understanding the reduction in the stock of adults in different regions around the world. Lough et al. (1994) evaluated the influence of advection promoted by wind in the interannual variability and distribution of cod eggs and larvae in the Georges Bank region. Blanton et al. (1999) reported the use of passive larvae of white shrimp and blue crab megalopae to understand the response of wind to transport generation over a shallow estuary channel in the southeastern United States. Brown et al. (2000) investigated the importance of tidal forces in the transport of larvae through a narrow channel under the effect of jetties in the bay of Aransas Pass. Sentchev and Korotenko (2007) evaluated the effect of physical forcing and vertical migration on the transport and

dispersion of sole larvae in the region of freshwater influence in the east of the English Channel. Tiessen et al. (2013) determined the importance of passive transport by advection in the dispersion of eggs and larvae of plaice fish in the south of the North Sea and the English Channel. Teodosio et al. (2016) described the biophysical processes involved in the recruitment of fish larvae in the Ria Formosa lagoon estuary. Joyeux (2001) evaluated the influence of wind, tide, and meteorological forces in the retention of fish larvae transported to estuaries by the Beaufort channel in North Carolina.

The croaker *Micropogonias furnieri* is one of the most important fisheries resources in Brazil, with approximately 43.369 tons of catch per year (MPA, 2011). Along the coast of Rio Grande do Sul, in the Patos Lagoon estuary, *M. furnieri* is one of the 3 most abundant species of Sciaenidae (Ibagy and Sinque, 1995) and is considered one of the species with the greatest commercial value in the region (Haimovici and Cardoso, 2017). The species is in decline in the Patos Lagoon region and its catch was reduced from 22,500 tons between 1970-1974 to 7,000 tons captured between 2007-2010 (Haimovici and Cardoso, 2017). Croaker spawns preferentially along the internal continental shelf, near estuarine entrance, and can spawn an average of 3 to 7 million eggs over a breeding season (Acha et al., 2008; Alburquerque, 2008; Albuquerque et al., 2009; Bruno and Muelbert, 2009; Acha et al., 2012). It is present throughout the year, with greatest spawning and egg and larval abundance during summer (November to April) (Muelbert and Weiss, 1991; Ibagy and Sinque, 1995). Winds and low river discharge are the physical mechanisms that determine the success of transport and recruitment of the early stages of croaker in coastal regions of South America (Muelbert and Weiss, 1991; Ibagy and Sinque, 1995; Acha et al., 1999; Martins et al., 2007; Acha et al., 2012; Costa et al., 2014; Franzen et al., 2019).

The recruitment of eggs and larvae in the Patos Lagoon estuary occurs during the spring and summer (Ibagy and Sinque, 1995; Martins et al., 2007; Vaz et al. 2007; Bruno and Muelbert, 2009; Franzen et al., 2019) when Ekman transport resulting from the south quadrant winds rises sea level on the coast and pushes water into the estuary he (Vaz et al. 2007). Residual baroclinic current resulting from the contribution of continental discharge promotes the retention and accumulation of ichthyoplankton inside the estuary (Vaz et al. 2007). The dynamics of transport and dispersion of eggs and larvae of *Micropogonias furnieri* in the Patos Lagoon estuary are determined by the direction, intensity and duration of the

southwest winds combined with low freshwater discharge, that modulate the distribution of different stages of development in different estuarine environments (Martins et al., 2007; Bruno and Muelbert, 2009; Franzen et al., 2019).

Changes in topography and natural geomorphological structure of access channels impact the dynamics and ecology of estuaries (Yuk and Aoki, 2007; Liu and Chan, 2016). Specifically, concerning fish eggs and larvae, a direct correlation between recruitment and environmental conditions during their transport makes anthropic contribution one of the processes that limit stock and recruitment (Hinrichsen, 2009; Acha et al., 2012). In 2010, the Barra Jetties at the entrance of the Patos Lagoon estuary, built-in 1915, had an increase in the length of approximately 10% and 18% (370 m and 700 m) on the east and west side, respectively, as well as a reduction of approximately 15% in the opening width (currently with 700 m) (Moller and Fernandes, 2010).. An increase in the depth in the navigation channel was followed by a reduction in saline intrusion and the current speed that was associated with the modifications made (Lisboa and Fernandes, 2015; Silva et al., 2015). Recently, António et al. (2020) found that changes in the access channel and Barra Jetties caused a reduction in saline intrusion, a reduction of approximately 20% in both flooding and ebbing speeds, and a reduction in the time of occurrence of lateral stratification events between the jetties by approximately 1/3 from the old to the new jetty configuration. These changes in the characteristics of estuarine circulation, due to small changes in coastal structure, may have an impact on the transport and dispersion of eggs and fish larvae in the PLE.

High cost and difficulty in obtaining data in situ with adequate space-time resolution have limited the analyses and the studies of complex coastal ecosystems. Numerical modeling techniques, coupling hydrodynamic and biological models, have been increasingly used as a tool to solve this limitation (Lough et al., 1994; Brown et al. 2000; Seiler et al., 2015; Franzen et al., 2019). The physical-biological coupling has ensured better coverage by interpolation and extrapolation of data in the space-time domain, assisting in fish dynamics studies at an early stage of life. These advances have enabled us to understand the causes of mortality of larval and juvenile fish during transport, focusing on the effects of advective and trophodynamic processes ( Brown et al. 2000; George et al, 2011; Seiler et al., 2015).

The main objective of the present study is to determine if the modification of the Barra Jetties of the Rio Grande influences transport of eggs and larvae of the croaker,

*Micropogonias furnieri,* in the Patos Lagoon estuary. For this, a Lagrangian model coupled to the hydrodynamic model TELEMAC-3D will be used. The novelty is to demonstrate that even small alterations in coastal structures can result in circulation changes that have an impact on the transport of planktonic organisms. The results of this study aim to contribute to an understanding of the dynamics of recruitment process and management of fishery resources from the Patos Lagoon and the adjacent coastal region.

## 1.1. Study Area

The Patos Lagoon (Figure 1) is located in the southwestern region of Brazil between 30º and 32º South. It is classified as a strangled coastal lagoon (Kjerfve, 1986) that is 250 km long, 40 km wide, and has an average depth of 5 m, occupying an area of approximately 10,360 $km^2$ (Moller et al., 2001). The lagoon is connected to the South Atlantic Ocean by a narrow channel less than 1 km wide (Martins et al., 2007). The estuarine region of the Patos Lagoon, which represents approximately 10% of the total area of the lagoon, has more than 80% of its area with depths below 2 m with diverse and abundant flora and fauna, which makes these shallow embayments suitable for the development of estuarine-dependent organisms (Moller et al., 2001; Odebrech et al., 2010).

The lagoon has 3 main tributaries, the Guaíba and Camaquã Rivers, and the São Gonçalo Channel, with an average discharge of approximately 2400 $m^3s^{-1}$, ranging between 700 $m^3s^{-1}$ during the summer and 3000 $m^3s^{-1}$ during spring (Moller et al., 2001; Moller and Fernandes, 2010). Tides have little influence on the estuary's dynamic, with a diurnal predominance of approximately 0.3 m that is attenuated during propagation into the estuary (Moller et al., 2001; Fernandes et al ., 2004; Moller et al., 2009). Tidal's greatestTidal contribution is in modulating the mixture of the water column and transporting water further to the north of the estuary during periods of less intense winds and discharge (Moller and Fernandes, 2010). WWinds and the regime of freshwater discharge determine the range of saline intrusion in the Patos Lagoon. During periods of low discharge, saline waters can pass the northern limit of the estuarine region, while high discharges can act as physical barriers and prevent the intrusion of saltwater into the estuary (Moller et al., 2001; Moller and Fernandes, 2010; Seiler et al., 2015). These dynamic conditions may affect the pattern of

recruitment, immigration, and emigration of organisms of estuarine species (Garcia et al., 2001; Salvador and Muelbert, 2019).

## 2. METHODOLOGY

The present study was based on the application of the hydrodynamic numerical model TELEMAC-3D (www.opentelemac.org) and its Lagrangian module to investigate the influence of the change in the configuration of the Barra Jetties on the transport and dispersion of eggs and larvae of the croaker, *Micropogonias furnieri*, in the Patos Lagoon estuary. Controlled simulations were carried out, considering extreme discharge conditions and winds from the south quadrant.

### 2.1. Hydrodynamic Numerical Model

The TELEMAC-MASCARET model (V7P0 version) was developed by *Laboratoire National d'Hydraulique et Environnement of the Company Electricité of France (©EDF)*. The model presents two and three dimension modules to study hydrodynamics, sediment transport, waves, and water quality of coastal regions. The hydrodynamic model solves the Navier-Stokes Equations, considers local variations of the free surface of the fluid, neglects the variation of density in the mass conservation equation, and considers the hydrostatic or non-hydrostatic pressure and the Boussinesq approximation to solve the equation of motion. The model applies the Finite Element Method in order to solve the hydrodynamic equations, using the Sigma Coordinate System for vertical discretization. The model domain is discretized by a non-structured grid of finite elements (triangular elements), which allows concentrating a large number of elements in regions of interest and/or significant bathymetric variations, and low resolution in regions of more homogeneous bathymetry, reducing computational time. Details about the model formulation are presented by Hervouet (2007).

The bathymetry of the Patos Lagoon, the estuary, and the adjacent coastal region was obtained from historical data. Nautical charts from the Directory of Hydrography and Navigation (DHN, Brazilian Navy) previous to 2010 were used as the "old" bathymetric information (before changes in configuration). Data from the jetty expansion project were used to define the bathymetry after the alteration of the jetties. The main difference between the two grids is the length of the jetties and the depth of the access channel to the estuary (Figure 1D and 1E). The BlueKenue Software was used to generate the unstructured

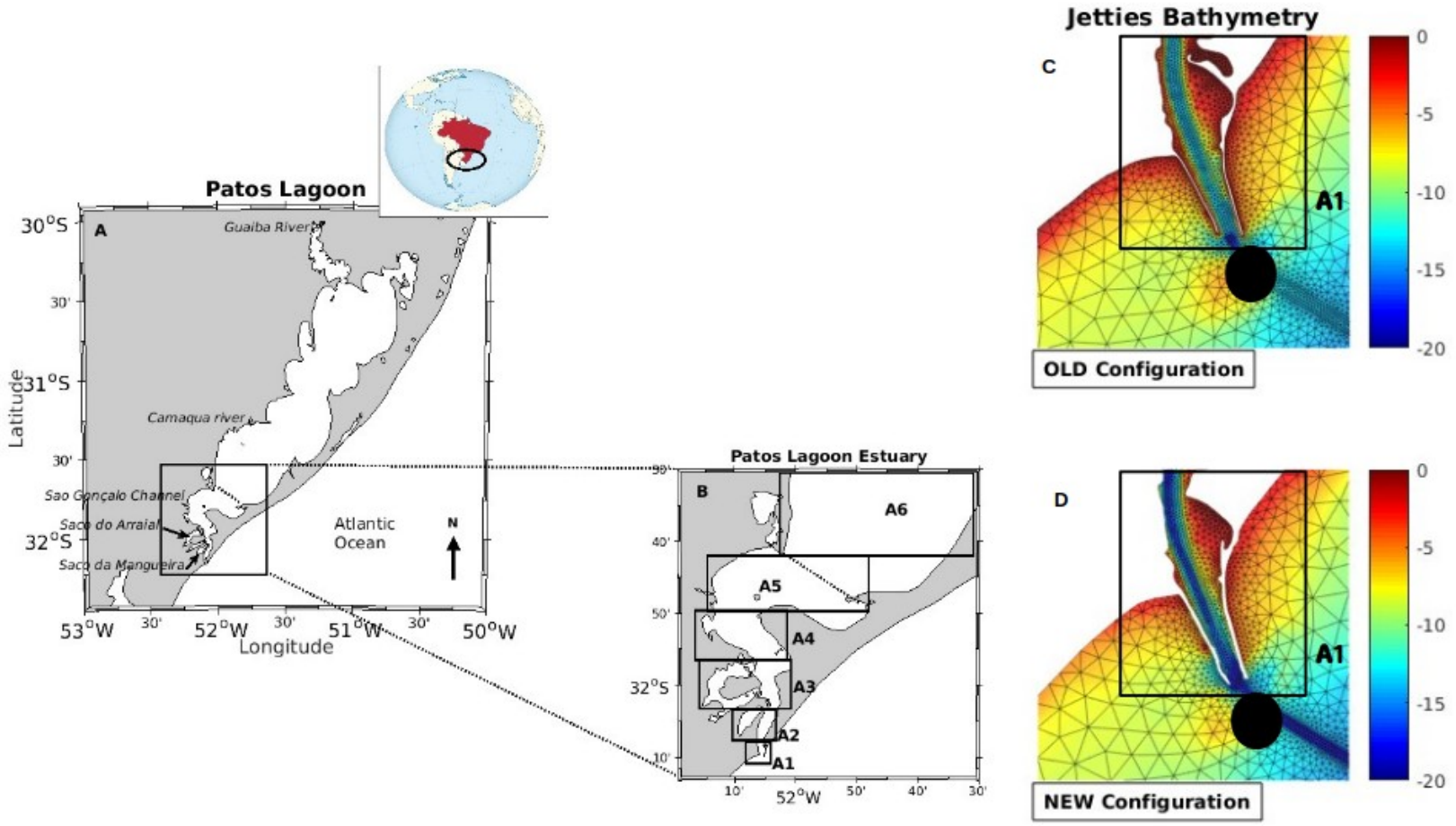


Figure 1: The study site located in Southeast South America, depicting the Patos Lagoon (A) and the estuary (B). Dotted line indicates the estuarine limit (Ponta da Feitoria). Five rectangle areas (A1 – A5) show locations where modeled organism concentration results were

extracted. The lower Patos Lagoon estuary in the (C) old, and (D) new jetty configuration. Black points indicate the position where M. furnieri eggs were released.

bathymetric grids of triangular elements. Grid optimization was made for the complex morphology and shallow areas inside the estuary and for the adjacent coastal region, allowing higher resolution in regions of interest. Two resulting meshes were used to reproduce the hydrodynamics before and after the modification of the jetties (Figures 1D and 1E). The meshes encompass the entire study area up to about 2500 m depth to better represent the coastal dynamics.

The open boundaries of the domain were forced with results from regional and global models and field data. To be comparable, simulations for both scenarios had the same set-up. Time series of daily averaged river discharge of the main tributaries (Guaíba and Camaquã rivers, Figure 1) were obtained from the National Water Agency (www.ana.gov.br) and prescribed at the northern and central continental boundaries. The discharge for the São Gonçalo Channel was considered constant at 700 $m^3/s$ (Vaz et al., 2006) as there were no time series available for the studied periods. Temperature and salinity fields obtained from the HYCOM model (Hybrid Model Coordinate Oceanic, https://hycom.org/), with a temporal resolution of 3h and spatial resolution of 1/12.5°, were prescribed tridimensionally in all grid points. Wind time series, with a spatial and temporal resolution of 0.75º and 6h, respectively, were obtained from theEuropean Center for Medium-Range Weather Forecasts (ECMWF, www.ecmwf.int). Eleven (11) sigma levels were considered in the vertical and distributed from bottom to sea surface. The model ran for a minimum of 6 months before producing the present results.

The model calibration and validation for both scenarios (Supplement A) are presented in more detail by António et al. (2020). The calculated results were compared with field data for the period between October and November 2006 for the old jetty configuration, and between October and November 2010 for the new configuration. Root Mean Square Error (RMSE) and Relative Mean Absolute Error (RMAE) were used to evaluate model performance (Table 1, Supplement A) which ranged from Good to Excellent (Wastra et al., 2001). Current velocity time series were used for calibration tests (Figure A1, Supplement A)

and salinity, sea surface elevation and current velocity time series were used for validation tests (Figure A2 and A3, Supplement A) for both configurations.

## 2.2. Particle Tracking Model

The particle model is a subroutine of the hydrodynamic model TELEMAC-3D, which is simulated internally at each time step after the hydrodynamic component. Therefore, to reproduce the transport of eggs and larvae in the passive phase and simulate their dispersion in the Patos Lagoon estuary, the Lagrangian model was coupled to the hydrodynamic model TELEMAC-3D. The particle model obtains the Lagrangian information from the Eulerian velocity information that is calculated by the hydrodynamic model to determine the particle trajectory caused by the flow at each time step, and the three-dimensional trajectories are computed using the position information calculated at each step of the time. The horizontal and vertical advection movements consider that the Euler scheme and the particle buoyancy are based on the zonal, meridional and vertical components (u, v and w) and are given by the following expressions:

$$X_i(x_0, y_0, z_0)^{n+1} = X_i(x_0, y_0, z_0)^n + \int_{t_0+n\Delta t}^{t_0+(n+1)\Delta t} u_i(x_0, y_0 z_0, t)\, dt$$

where $X_i$ is the position, for horizontal ($x_0$, $y_0$) and vertical ($z_0$) position of the particle movement; $u_i$ is the velocity for a zonal ($x_0$), meridional ($y_0$) and vertical ($z_0$), u, v and w velocity component, respectively; t is the time and $\Delta t$ is the time step.

The calculation of hydrodynamic components is taken into account in a discrete three-dimensional way at each point of the numerical grid. During the simulation, the particles are free to move to any position between the grid points. In each new time step, the velocity is interpolated instantly for each position where the particles are located. The accuracy and resolution of particle transport calculations are extremely dependent on hydrodynamic terms.

In this study, a time step of 60 s was applied, with the particle model in phase with the time step of the hydrodynamic model. Thus, at every 60 seconds, TELEMAC-3D runs the

hydrodynamic component, and the results are instantly inserted into the particle model, with the displacement of the particles being calculated three-dimensionally in the numerical grid.

### 2.3. Model Experiments

To investigate the effect of the modifications made in the Barra Jetties in the transport and dispersion of eggs and larvae of *Micropogonias furnieri* in the Patos Lagoon estuary, a total of 12 controlled experiments were carried out, with dynamic forces from extreme conditions of river discharge combined with constant south quadrant winds (SW, S, and SE), considering the old and the new configuration of the Barra Jetties (Table 1).

Table 1: Controlled experiments simulations

| Wind | High Discharge (El Niño, 2003) | | Low Discharge (La Niña, 2012) | |
|---|---|---|---|---|
| Direction | Old Configuration | New Configuration | Old Configuration | New Configuration |
| SW | X | X | X | X |
| S | X | X | X | X |
| SE | X | X | X | X |

The simulations were carried out for the first 5 days of January, which represented the passage of cold fronts and ensured the continuous incidence of winds from the south quadrant in the region. Extreme high and low river discharge regimes for the years 2003 and 2012, respectively, were considered. These extreme discharge regimes are associated with ENSO, with high discharge characteristics during El Niño (2003) and low discharges during La Niña (2012) (Moller and Fernandes, 2010). Constant SW, S, and SE winds were also considered with an initial intensity of 8 $m.s^{-1}$, decreasing linearly after the second day of incidence until reaching 4 $m.s^{-1}$ on day 5. Only south quadrant winds were considered because they facilitate the entry of saltwater into the estuary (Moller et al, 2001).

The simulation time of 5 days considered the growth rate of the larvae of the species under study and their passive period in the plankton. Eggs of the *Micropogonias furnieri* hatch in approximately 24 hours (Albuquerque, 2008), and the larvae are approximately 1.85 mm. The average growth rate is 0.36 mm/day (Albuquerque et al., 2009), and at the end of 5 days

the larvae will be approximately 3.29 mm. One spawning eventeggs at the entrance of the Patos Lagoon estuary (Figure 1D and 1E) was used and considered the grouped spawning characteristic of the species. The spawning site was defined at the estuary entrance to guarantee the best recruitment of eggs and larvae of the croaker to the Patos Lagoon estuary (Martins et al., 2007; Franzen et al., 2019), who concluded that the spawning  Due to the computational limitation of the TELEMAC-3D version V7P0, the maximum particle concentration per spawning was 7000 eggs for each simulation, and represents approximately 25% of the maximum average concentration of eggs per cubic meter (497 eggs/100 $m^3$) (Bruno and Muelbert, 2009). For each experiment run, 7000 particles were placed at a depth of 5 m at 00:00 on January 1, 2003 (high discharge) and January 1, 2012 (low discharge). The evolution of the larvae was monitored for 5 days. Eggs and larvae were considered passive and neutral particles, assuming that fish eggs are transported by the flow without depositing. During the simulation, the particles were considered eggs from the spawning site for up to 24 hours, and shortly afterward, the occurrence of hatching of the eggs was considered when the particles started to be considered larvae of the *Micropogonias furnieri* croaker.

### 2.4. Data Processing

Numerical simulations that considered the old and the new configuration of the Barra Jetties of the Rio Grande and the incidence of constant winds of the south quadrant (Figures 2A - 2F) in periods of high (Figure 2G) and low (Figure 2H) continental discharge were analyzed comparatively for the 6 simulated scenarios (Table 1).

The results were analyzed in relation to the extension of entry of larvae and eggs and their distribution in the estuary. Maps of spatial patterns of the salinity field and the final distribution of the larvae in the estuary in the last step of the simulations for the periods of high and low discharge during the incidence of southern winds were selected for presentation.

Based on the sampling techniques proposed by Cochran (1976) and based on simple significant sampling calculations made by Miaoulis and Michener (1976), stratified random samples of 99 larvae, which represented a 10% precision level (sampling error), a 95% confidence level and a variability degree (proportion) P = 0.5, were extracted from the total of 7000 placed in the simulations (Cochran, 1976; Miaoulis and Michener, 1976; Israel, 1992).

To determine the average path taken by the larvae at the end of each day in the two configurations (old and new), the weighted distances traveled by each of the larvae that compose the sample were calculated from the spawning place (in the mouth of the estuary) until the end of each of the 5 days of simulation. Then, the center of mass was found, calculating the average distance covered at the end of each day. Finally, the mean standard deviation of the individual distances from the center of mass (mean distance) was calculated. The Student's t-test was applied to verify the significance between the average distances in the two configurations in the simulated scenarios (Louangrath, 2015; Padovani, 2012). At random, another reduced sample of 10 larvae (P1, P2, P3, P4, P5, P6, P7, P8, P9, and P10) was extracted at the end of each day, and the trajectories of larvae were tracked from the spawning site to the final location in the two configurations (old and new) of the Barra Jetties, at the end of each of the five simulation days.

The abundance of larvae for each hydrodynamic simulation was extracted from the model result for 6 areas (A1, A2, A3, A4, A5 and A6 (Figure 1C)) at the end of each of the five simulation days and analyzed in terms of the distribution of the spatio-temporal concentration along the estuary.

To investigate changes promoted by lateral stratification in the distribution of eggs and larvae between the Barra Jetties, profiles of the spatial distribution of salinity and eggs and larvae were extracted between the Barra Jetties during the flood period. Changes in the time of occurrence of lateral stratification and the salinity gradient were observed in the hydrodynamic study with dynamic winds (António et al., 2020, submitted). In this way, the aim is to evaluate the effect of the difference in the direction of the incident wind (SW, S, and SE) on the variability of the behavior of the lateral stratification, and consequently on the changes in the distribution of eggs and larvae that occurred due to the recent modernization works.

To associate the direction of the incident wind and the position (west, center channel and east) of the eggs and larvae among the jetties, the internal area between the west and east Jetties was divided into 3 (three) regions: root, center and mouth of the jetties (mouth). Each of these areas was subdivided into 3 other areas (west, center channel and east jetties), totaling

9 areas, where the concentrations of eggs and larvae were counted during the occurrence of lateral stratification and incidence of SW, S and SE winds.

## 3. RESULTS

The periods of extreme discharges used in the experiments (Figure 2) presented different characteristics. During the high discharge period (El Niño, January 2003), the average discharge was 6340 $m^3s^{-1}$, the maximum was 8000 $m^3s^{-1}$ (on January 2), and the minimum was 5000 $m^3s^{-1}$ (on January 5). In contrast, in the low discharge period (La Niña, January 2012), it was practically constant at 1200 $m^3s^{-1}$ over the 5 days.

### 3.1. Saltwater Distribution

During the period of high continental discharge, the penetration of saltwater was relatively less in the new configuration in the 3 simulated wind scenarios (Figure 3). During SW winds, the salinity in the new configuration (Figure 3D) reached 54 km, approximately 3 km less than the old configuration, which reached 57 km (Figure 3A). During the S wind, salinity reached 43 km in the old configuration (Figure 3B) and 41 km in the new configuration (Figure 6E). During the SE wind, the salinity reached 36 km and 34 km in the old (Figure 3C) and the new (Figure 3F) configuration, respectively.

In the low discharge period, the extent of saltwater intrusion passed from the northern limit of the Patos Lagoon estuary in all simulations (Figure 4). The results indicate that the lagoon was less saline in the new configuration in relation to the old configuration during the SW wind, and during the S and SE wind, the saltwater intrusions did not present any noticeable differences. At the end of the 5 days of simulation, the 5 psu isohaline reached approximately 106 km in length in the old configuration (Figure 4A) during the incidence of the SW wind. In the new configuration, the saline intrusion was reduced to 97 km (Figure 4D). During the S wind, the saline intrusion had an extension of approximately 96 km both in the old (Figure 4B) and in the new configuration (Figure 4E). The SE wind was the one that presented the least saline intrusion. The salinity for the old (Figure 4C) and new (Figure 4F) configuration reached approximately 79 km.

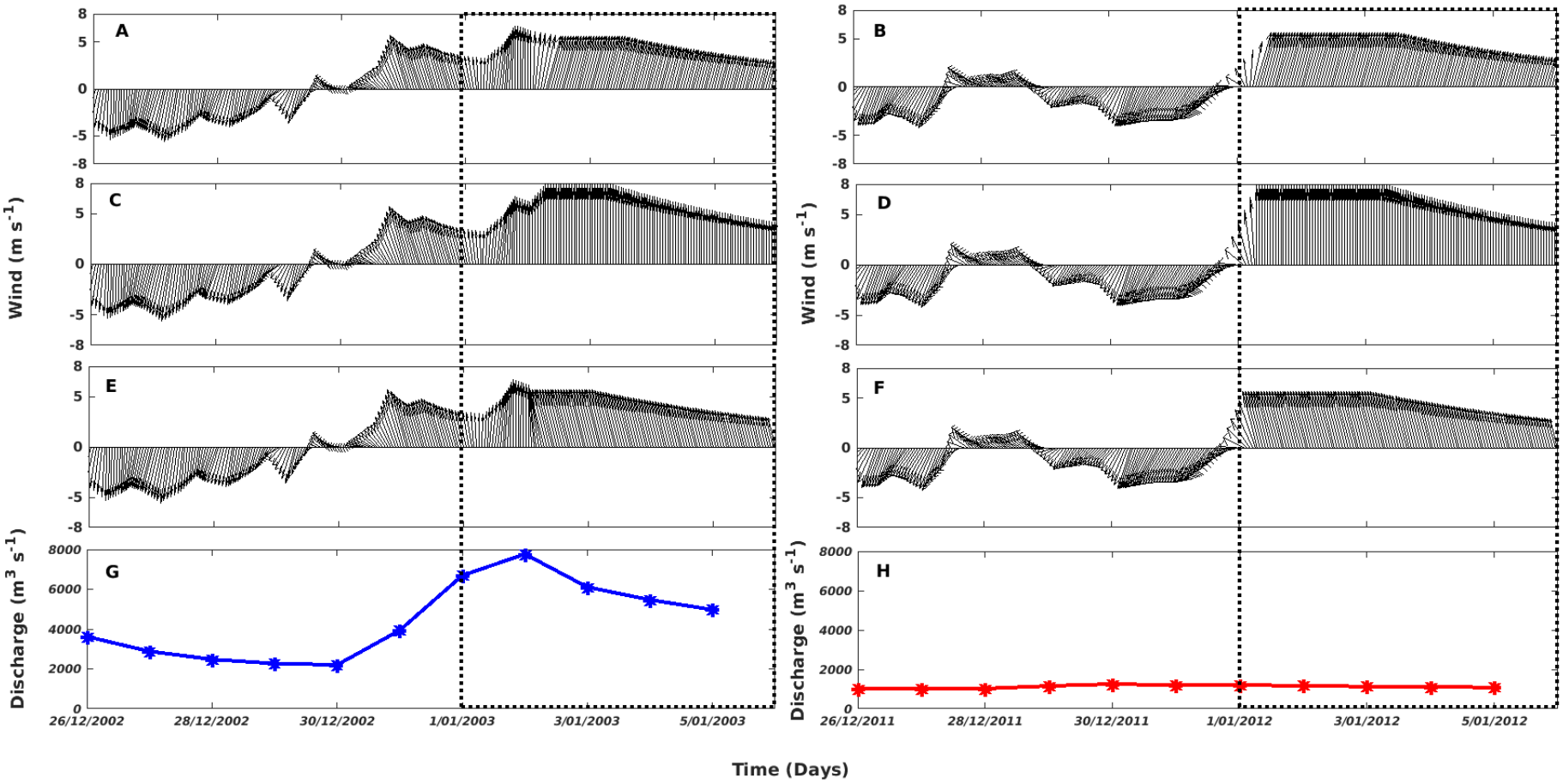


Figure 2: Wind and discharge from 26/12/2002 to 05/01/2003 (left panel) and from 26/12/2011 to 05/01/2012 (right panel). (A and B) SW wind, (C and D) S wind and (E and F) SE wind. Black doted rectangles represent characteristic periods of Patos Lagoon high discharge (G) during El-Niño during El-Niño (left panel) and low discharge (H) during La-Niña (right panel) that were simulated in this study.

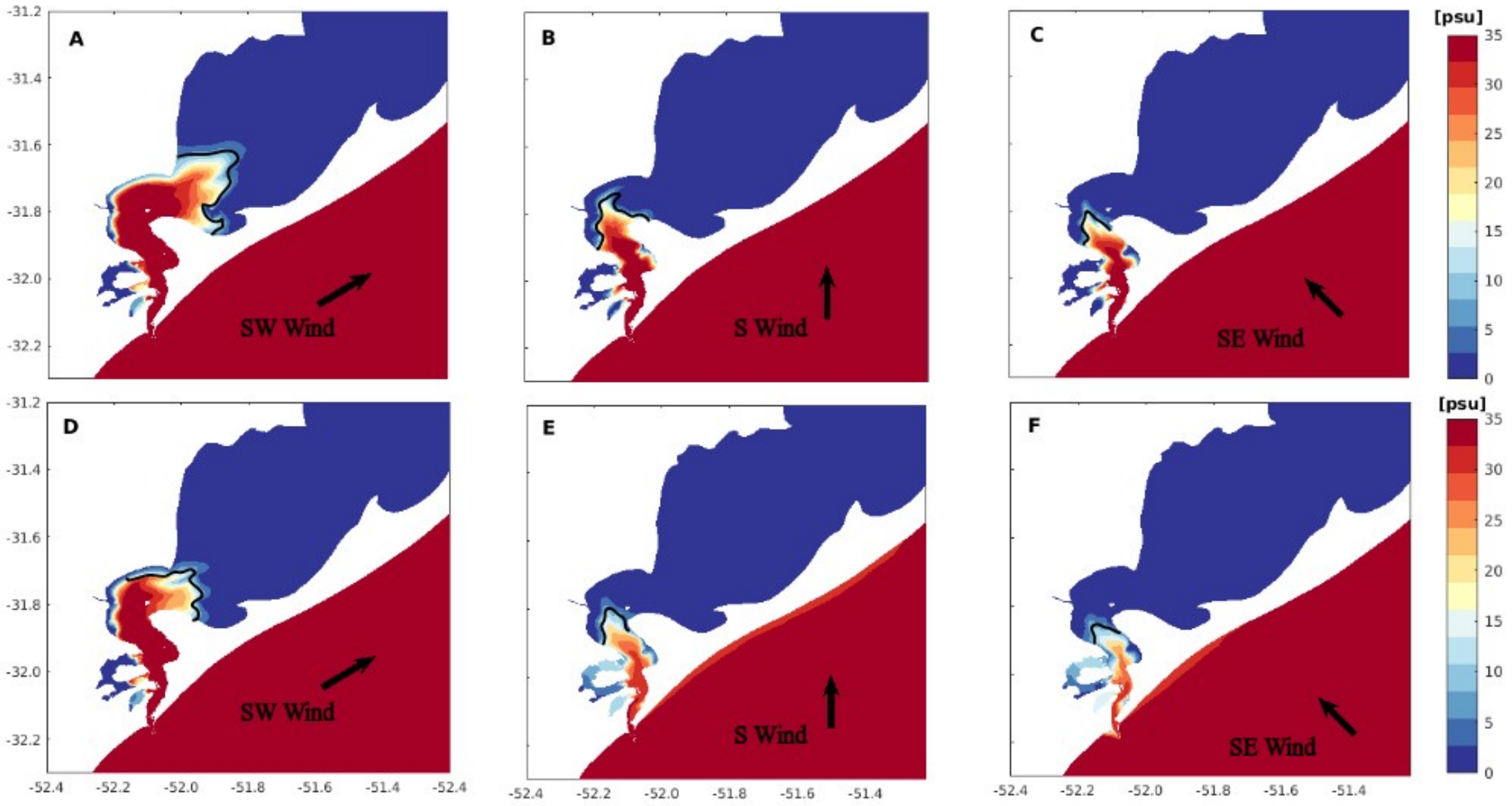


Figure 3: Spatial distribution of salinity excursion at the end of 5 days of simulation during the high continental discharge condition, considering SW (A and D), S (B and E) and SE (C and F) wind experiments (black arrows). Results are presented for the old (top panel) and for the new (bottom panel)

jetty configurations. Black line indicates salinity reference of 5 psu.

### 3.2. Transport and Dispersion of Larvae

A reduction in the extent of larval transport after the modernization works was observed in the 3 simulated wind scenarios for the period of high (Figure 5) and low continental discharge (Figure 6). The SW winds were the ones that guaranteed the largest incursion of the larvae in the high and low discharge, both for the old configuration (Figures 5A and 6A) and the new configuration (Figures 5D and 6D).

At high discharge, during the SW wind, the larvae extension was approximately 58 km and 56 km for the old and new configuration, respectively (Figure 5A and 5D). The S and SE winds did not show great differences in their extension between the old and the new configuration. The length varied between 42 km and 40 km for the S wind (Figure 5B and 5E) and between 38 km and 37 km for the SE wind (Figure 5C and 5F) for the old and new configuration, respectively. Differences in the larvae final location were observed that were associated with the direction of the incident wind because, during the SW and S wind, the larvae were closer to the east side of the lagoon, while the opposite was observed during the SE wind incidence.

Differences in the extension of larvae penetration were noticeable mainly in low discharge, with their pattern associated with the variability of the direction and intensity of the incident wind (Figure 6). The highest concentrations were observed along the navigation channel, with few larvae entering the shallow region of the bags (Arraial and Mangueira, Figure 1). The larvae showed a greater extension than that defined by the 5-psu salinity isohaline into the estuary in both configurations, with greater emphasis on low discharge. At low discharge, the maximum larvae penetration was approximately 109 km from the spawning site to the old (Figure 6A) and approximately 104 km to the new (Figure 6D) configuration of the Barra Jetties. During the incidence of the S wind, the larvae were transported up to approximately 102 km in the old configuration (Figure 6B), and in the new configuration (Figure 6E) up to approximately 101 km. On the other hand, during SE winds, the larvae were transported up to less than 79 km, reaching approximately 78 km in both configurations (old and new, Figure 6C and 6F, respectively). During the incidence of SW winds, the larvae were transported along the central region of the lagoon with different

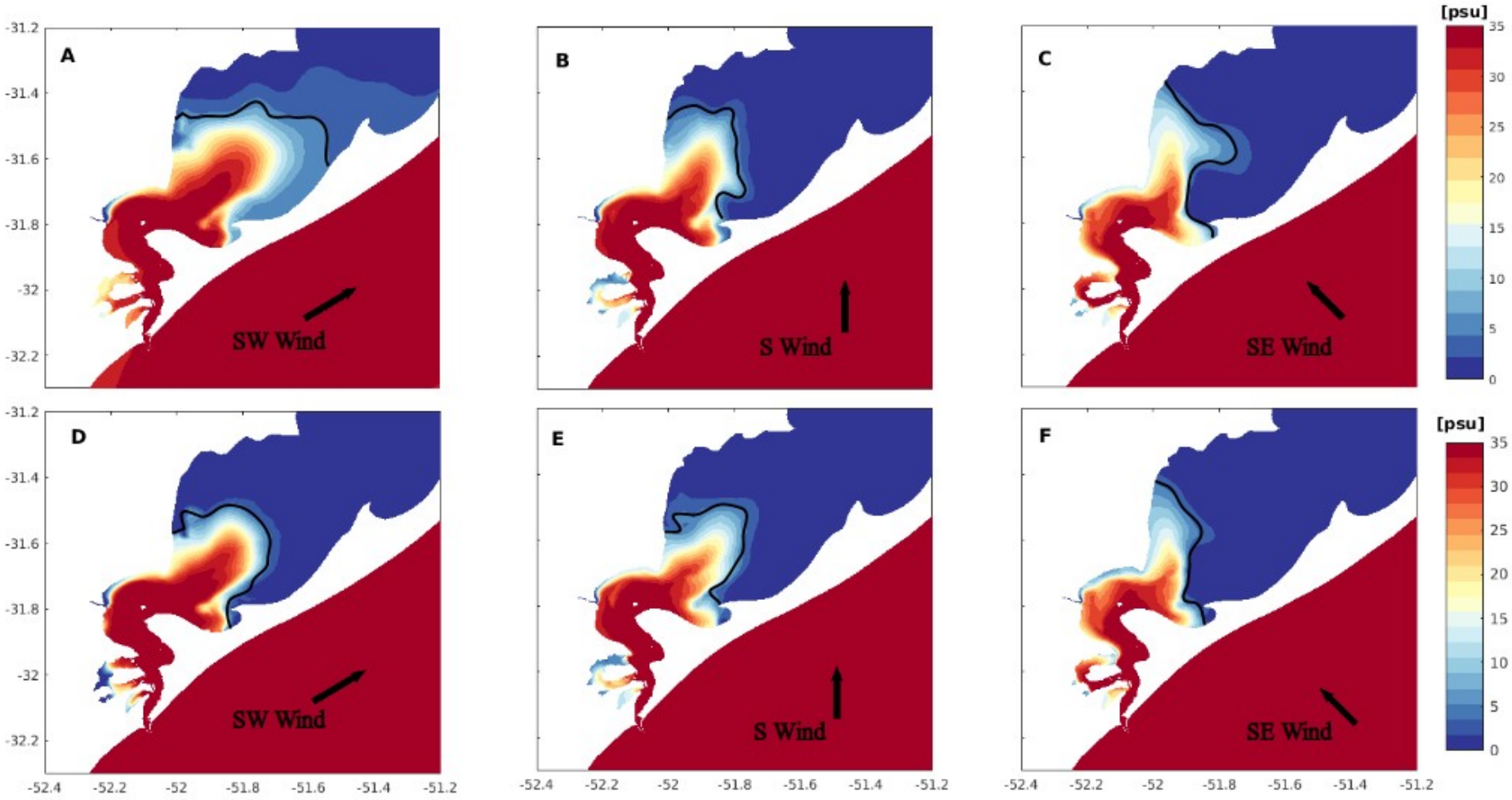


Figure 4: Spatial distribution of salinity excursion at the end of 5 days of simulation during the low continental discharge condition, considering SW (A and D), S (B and E) and SE (C and F) wind experiments (black arrows). Results are presented for the old (top panel) and for the new (bottom panel) jetty configurations. Black line indicates salinity reference of 5 psu.

dispersion patterns. In contrast, during the incidence of the S wind, the larvae were transported along the west side of the lagoon in the new configuration (Figure 6E) and through the central cell of the lagoon in the old configuration (Figure 6B). Similarly, during SE winds, the larvae were transported closer to the west side of the lagoon (Figure 6C and 6F) with little dispersion.

The total number of larvae transported to the interior of the estuary differed from the old to the new configuration in each incident south wind (Table 2). At high discharge, the transport was greater in the old configuration, with more than 6000 (approximately 87%) larvae inside the estuary in each incident wind (SW, S, and SE). On the other hand, in the new configuration, there was a reduction in the number of larvae transported according to the incident winds. SW and S winds carried slightly more than 4000 (~ 61.5%) larvae, differing by approximately 25.5% from the old configuration, while the SE wind wind carried only 1287 (~ 18.4%) larvae, a difference of approximately 68.6% from the old configuration. In contrast to the high discharge, in the low continental discharge, the difference in the transport of larvae to the lagoon between the old and the new configuration of the jetties fluctuated between 0.5% and 1% according to the winds. SW and SE winds were the ones that transported the most larvae to the interior of the estuary in both configurations (old and new), with more than 6000 (~ 86%) larvae each. The S wind carried just over 5000 (~ 72%) larvae in both configurations.

Table 2: Total number and percentage of lavae of *Micropogonias furnieri* transported towards the estuary at the end of the 5 days of simulation, during south quadrant winds for the old and new configurantions.

| Wind Direction | Configuration | High Descharge | Low Descharge |
|---|---|---|---|
| SW | Old | 6100 (87%) | 6000 (85%) |
| | New | 4400 (62.9%) | 6003 (85.8%) |
| S | Old | 6016 (86.9%) | 5101 (72.9%) |
| | New | 4210 (60.1%) | 5003 (71.5%) |
| SE | Old | 6101 (87.2%) | 6200 (88.6%) |
| | New | 1287 (18.4%) | 6102 (87.2%) |

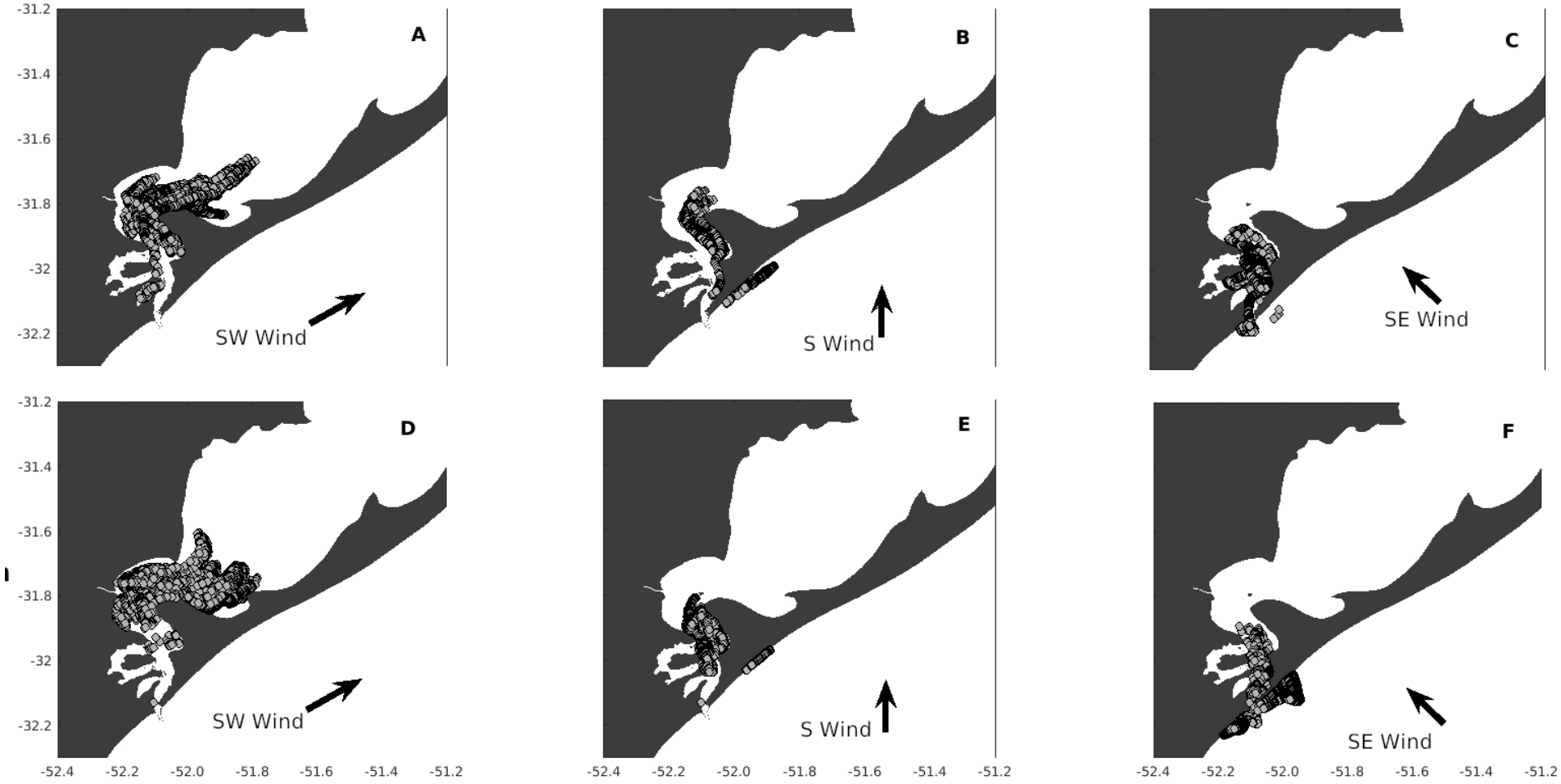


Figure 5: Spatial distribution pattern of excursion of *Micropogonias furnieri* larvae at the end of 5 days of transport, during the period of high continental discharge, considering the SW (A and D), S (B and E) and SE (C and F) wind experiments. Results are presented for the old (top panel) and for the new (bottom panel) jetty configurations. Black arrows indicate the wind direction.

In the adjacent coastal region, it was observed that some larvae that did not enter the estuary were transported to the north during SW winds (Figure 5A and 5D, 6A, and 6D), leaving the range of the area of interest in both configurations. During the S winds (Figure 5B and 5E, 6B and 6E), a portion of the larvae was trapped at the mouth of the estuary in the coastal region adjacent to the east of the Barra Jetties. During the incidence of SE winds (Figure 5C and 5F, 6C and 6F), the larvae were also concentrated in the coastal region adjacent to the mouth of the estuary. In contrast to the high discharge, in the low discharge, the old and the new configuration did not present notable differences in the dispersion of the larvae in the coastal region. However, as in the high discharge, at low discharge, larvae that did not enter the estuary showed a similar dispersion pattern.

### 3.3. Larvae Travel Distance

Figure 7 shows the evolution of the average distance traveled by the particles at the end of each simulation day for the high (Figure 7A) and low (Figure 7B) discharge period during SW winds. This wind condition was chosen because it guaranteed the largest incursion of larvae into the estuary in comparison to the S and SE winds (Figures 5 and 6).

During the high discharge period, at the end of the first day, the eggs covered an average of 13 km in the old and 9.5 km in the new configuration of the Barra Jetties (Figure 7A). On the second day, the distance covered reached approximately 22.5 km and 19 km in the old and the new configuration, respectively. On the third day, they passed the central region of the estuary, reaching 35 km and 30.5 km. On the fourth day, the distance covered was reduced; in the old configuration, the larvae reached approximately 39.5 km, and in the new configuration, they reached approximately 35.5 km. This trend was maintained, with the fifth day being the shortest route for the larvae, reaching an average distance of 45 km and 43 km in the old and the new configuration, respectively. These differences in the mean distance were not statistically significant ($p = 0.6857$).

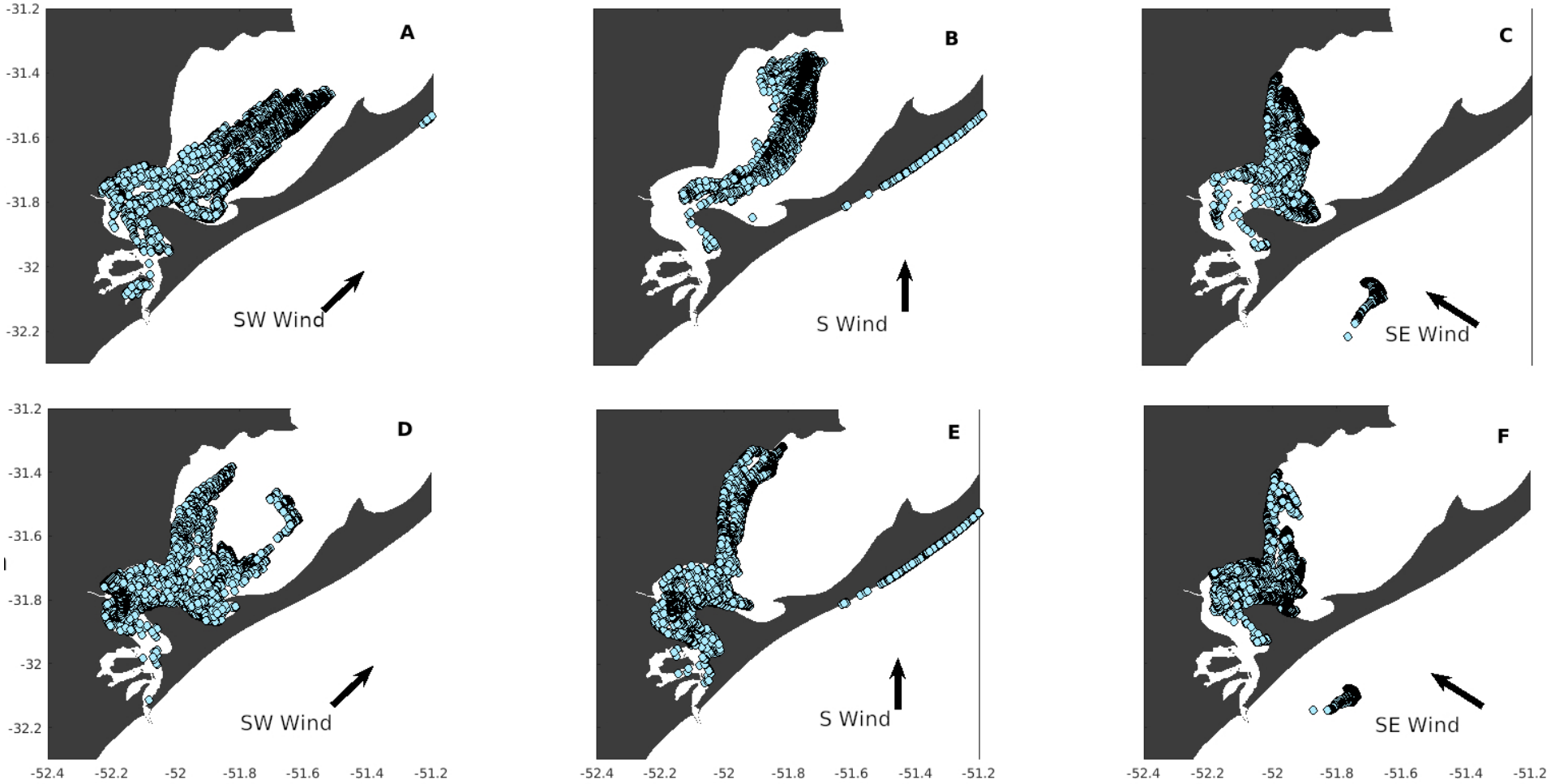
A
B
C
D
E
F
SW Wind
S Wind
SE Wind
-31.2
-31.4
-31.6
-31.8
-32
-32.2
-52.4
-52.2
-52
-51.8
-51.6
-51.4
-51.2

Figure 6: Spatial distribution pattern of excursion of *Micropogonias furnieri* larvae at the end of 5 days of transport, during the period of low continental discharge, considering the SW (A and D), S (B and E) and SE (C and F) wind experiments. Results are presented for the old (top panel) and for the new (bottom panel) jetty configurations. Black arrows indicate the wind direction.

At low discharge (Figure 7B), the particles passed the northern limit of the estuary (Ponta de Feitoria, Figure 1A). On the first day, the particles traveled approximately 17.5 km in the old configuration and approximately 13.5 km in the new configuration. On the second day, they reached approximately 31 km and 26 km away, in the central region of the estuary, in the old and new configuration, respectively. On the third day, they reached approximately 49.5 km and 45 km. On the fourth day, different from what was observed in the high discharge, the distance covered increased in both configurations (old and new), and the larvae reached approximately 65.5 km and 60.5 km. This trend was maintained, and on the fifth day, the larvae reached an average distance of 94 km and 89 km in the old and new configurations, respectively. Similar to the high discharge, at low discharge, the differences in the average distance between the old and the new configuration were not statistically significant ($p = 0.8099$).

At the end of each day, the larvae traveled long distances in the old configuration of the Barra Jetties, at both high and low discharge. At high discharge (Figure 7A), the distances traveled by the larvae in the two configurations decreased from day 1 to day 5. The difference on the first day was approximately 3.5 km, gradually reducing to approximately 2 km on the fifth day. The average distance traveled at the end of each day was similar for both configurations, ranging from approximately 9.5 km from the first to the second day, increasing by approximately 12.5 km from the second to the third, and then decreasing to 4.5 km and 5.5 km in the old and new configuration, respectively. At low discharge (Figure 7B), the average travel difference between the two configurations was approximately 4 km on the first and second days. On the third day, the difference between the two configurations increased to 4.5 km, while reducing on the fourth day to 4 km. On the fifth day, the difference was fixed at 5 km.

### 3.4. Larvae Trajectories

To study the evolution of the particle trajectory over time, the transport behavior of 10 larvae were analyzed from the first hour (1 hour) to the end of 5 days of simulation for both configurations of the Barra Jetties, during the high and low period (Figure 8) discharge.

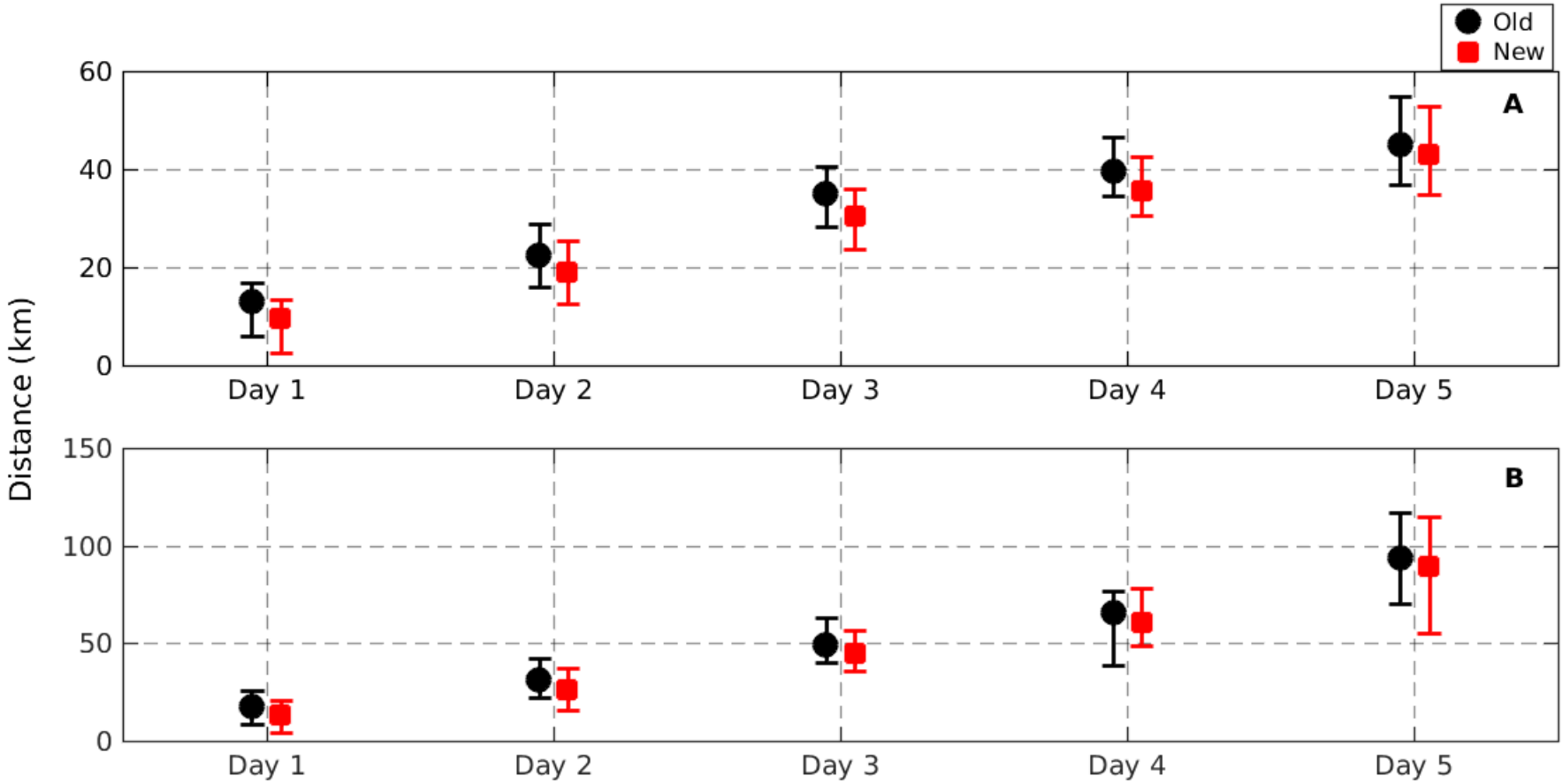


Figure 7: Distribution of the mean distance traveled by *Micropogonias furnieri* larvae sampled during the SW wind experiment at the end of each of the 5 days (day 1, day 2, day 3, day 4 and day 5), simulated during the period of high water discharge (A) and low water discharge (B), for the old (black) and the new (red) jetty configuration.

Experiments with an incidence of the SW wind were analyzed because they ensured the largest incursion of larvae into the interior of the Patos Lagoon compared to the S and SE winds.

The largest length of the trajectory traveled by the larvae was observed in the old configuration both at high (Figure 8A and 8B) and low (Figure 8C and 8D) discharge. During the period of high continental discharge, most of the tracked larvae entered the estuary in the old (Figure 8A) configuration compared to the new (Figure 8B) configuration of the Barra Jetties. The other larvae stayed in the adjacent coastal region (Figures 8A and 8B) and moved to the north. The greater extension in the daily trajectory traveled by the same larva at the end of each day led the larvae to position themselves in distant locations between the two configurations, a fact that was reflected in the final position. Of the larvae that entered the estuary, it was also observed that in the old configuration of the jetties (Figure 8A), some larvae had their trajectory in the bags of Mangueira and Arraial (Figure 1A), while in the new configuration of the jetties (Figure 8B), none of the larvae entered into the bags. At low discharge, the tracked larvae behaved similarly to the high discharge. The larvae that entered the estuary differed in length by covering greater distances in the old configuration, and it was also observed that larvae entered into the bags only in the old configuration of the jetties (Figure 8C).

### 3.5. Spatiotemporal Distribution of Eggs and Larvae

Figure 9 shows the spatiotemporal evolution of eggs and larvae concentration in 6 areas of the Patos Lagoon estuary (Figure 1C) over the 5 days of simulation during the period of high continental discharge. For all tested wind scenarios (SW, S, and SE), the number of larvae that reached regions A1, A2, A3, A4, A5, and A6 differ from each other when comparing results for the old and the new configuration of the jetties.

During the beginning of the simulation of the high discharge, the two days preceding the simulations (day 30 and 12/31/2002) presented winds from the south quadrant (Figure 2A, 2C, 2D), driving the early entry of the plume into the interior of the estuary. One hour after the start of the simulation, area A1 showed approximately 100% (~ 7000) of eggs in the old configuration and approximately 61% (~ 4300) of eggs in the new configuration, and no eggs were recorded in the remaining estuary areas during SW winds (Figure 9A); a similar situation was verified during S and SE winds (Figure 9G and 9M). At low discharge, one hour after the simulation started, area A1 showed only a concentration of approximately 36% (~ 2500 of 7000) of eggs in the old configuration, while in the new one, there were no eggs in the estuary for any of the incident winds (Figure 9A, 9G and 9M).

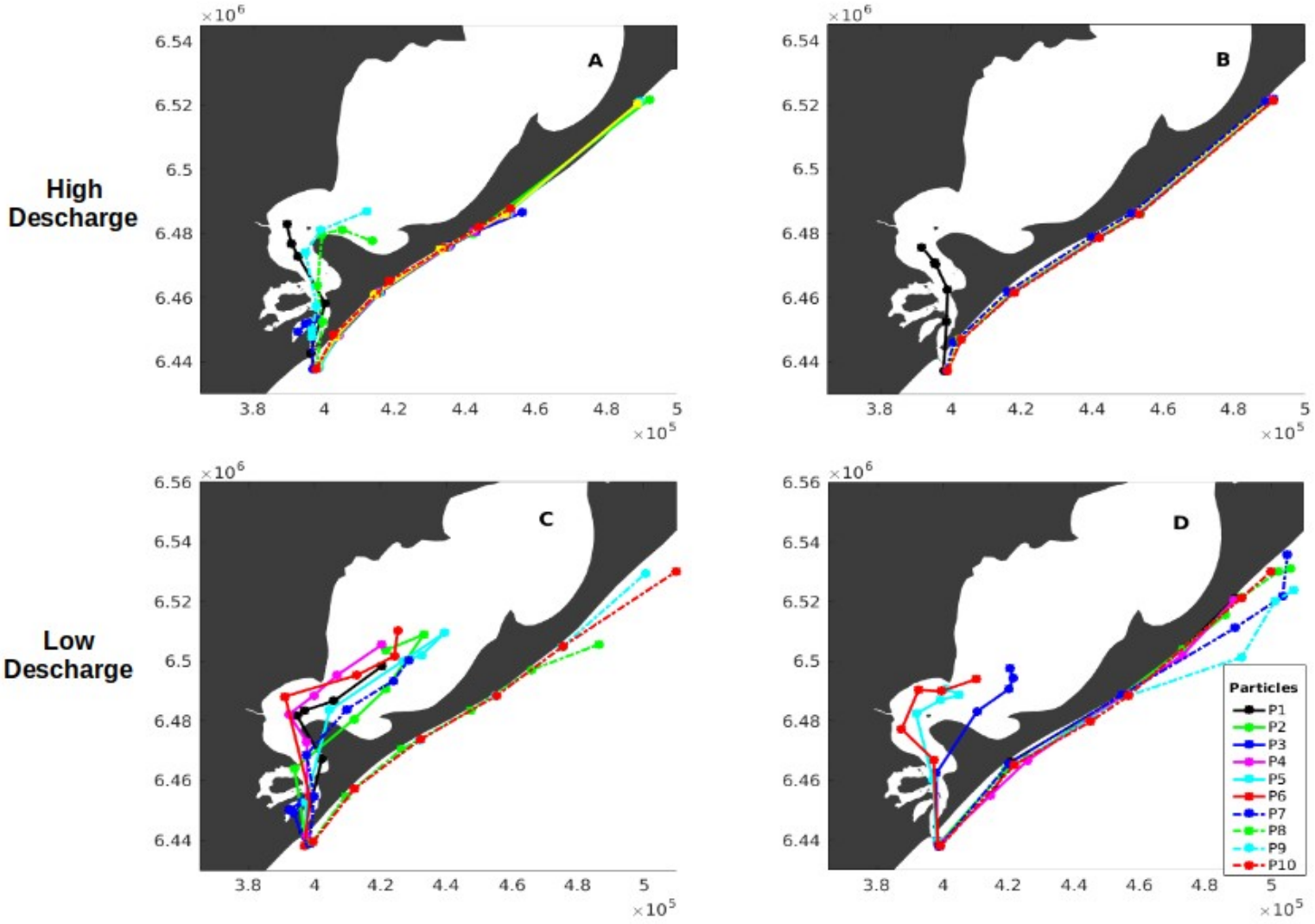


Figure 8: Trajectory of *Micropogonias furnieri* eggs and larvae for the SW wind experiment at the end of each of the 5 days ( 1h, day 1, day 2, day 3, day 4 and day 5), during the period of high (top panel) and low (bottom panel) water discharge for the old (A,C) and new (B, D) jetty

configuration. Particle tracking trajectory during the SW wind experiment, at the end of each of the 5 days of simulation (1h, 1 day, 2 days, 3 days, 4 days and 5 days, marked dots).

On day 1, during the SW wind (Figure 9B), the larvae reached area A3, concentrating the largest number of larvae in area A2 in both the old and the new configuration. However, different from the old configuration that already concentrated more than 75% of the larvae, in the new configuration, the total of the larvae in areas A1, A2 and A3 represented less than 50%. During the S wind (Figure 9H), in both configurations, the larvae reached area A2 where they concentrated their greatest abundance of approximately 94% and 84% for the old and new configuration, respectively. On the other hand, during the SE wind (Figure 9N) at the end of the day1, in the old configuration, the larvae reached area A2, and almost 100% of the larvae concentrated in these 2 areas. However, in the new configuration, the larvae were restricted to area A1 with only approximately 26% of the larvae.

On day 2, during the SW wind (Figure 9C), the larvae reached area A4, with the greatest abundance in area A3 in both configurations; an abundance of approximately 85% in the old configuration was shown, while that in the new configuration was approximately 64%. During the S wind (Figure 9I), the larvae reached area A3, registering the greatest abundance in this area, but a reduction in the total number of larvae in the areas within the estuary was observed compared to day 1. The old configuration presented approximately 71%, and the new configuration presented only approximately 15% of the larvae. During the SE wind (Figure 9O), the distribution of the larvae did not pass from area A2 in both configurations, and similar to the S wind, a reduction in the total number of larvae inside the estuary was observed, reducing to approximately 54% in the old configuration and approximately 20% for the new configuration.

On day 3, concentrations increase again in the 3 winds studied (Figures 9D, 9J, 9P). During the SW wind (Figure 9D), the larvae reached area A5 (northern limit of the estuary, Figure 1C), with a greater abundance in area A4 in both configurations. A total of approximately 87% (~ 6,100) of the larvae were recorded in the old configuration and approximately 60% (~ 4,200) in the new configuration. During the S wind (Figure 9J), the larvae reached area A4 in both configurations, and the abundance in the old configuration was approximately 86% (~ 6050), and in the new configuration, the total larvae did not exceed

15% (~ 1030). During the SE wind (Figure 9P), the larvae reached area A4 in the old configuration where the greatest abundance occurred, while in the new configuration, area A3 was restricted, and the greatest abundance was observed in area A1. The total number of larvae was approximately 86% (~ 6060) in the old configuration and approximately 61% (~ 4300) in the new configuration.

On day 4, during the SW wind (Figure 9E), the larvae did not pass area A5, showing only an increase in abundance in area A5, and the total larvae did not change in both configurations. During the S wind (Figure 9K), the larvae reached area A5 despite the greater abundance being concentrated in area A4, as observed on day 3 in both configurations. The total number of larvae inside the estuary did not change in the old configuration, remaining at approximately 86% (~ 6050), while the new configuration registered an increase of approximately 62% (~ 4400). During the SE wind (Figure 9Q), the larvae did not pass area A4 in both configurations, concentrating approximately the total of the larvae in this area in the old configuration with an abundance of approximately 86% (~ 6060). In contrast, in the new configuration, the larvae were distributed in all areas with a total abundance of approximately 18% (~ 1260).

On the last day of the simulation (day 5), the total number of larvae did not change from day 4 in both configurations for the 3 winds studied. During the SW wind (Figure 9F), the larvae passed from the northern limit of the estuary (Figure 1C) and reached area A6 in both configurations, with their greatest abundance in area A5. During the S wind (Figure 9L), the larvae distribution was limited to area A5 in both configurations, concentrating their abundance between areas A4 and A5. During the SE wind (Figure 9R), the old configuration showed a decrease in the larvae incursion, and the greatest abundance was observed in area A3 in the new configuration, where the distribution of abundance was approximately similar in all areas.

In the low continental discharge, 1 h after starting the simulations for the 3 winds studied (SW, S, and SE) (Figure 10A, 10G, 10M), only in the old configuration did the larvae enter the estuary, concentrating the larvae in area A1 with an abundance of approximately 36% (~2500).

On day 1, during the SW wind (Figure 10B), the larvae in the old configuration passed from the northern limit of the estuary (A5, Figure 1C) and reached area A6 in the old

configuration, with a greater abundance in area A4. In contrast, in the new configuration, the larvae did not pass area A3 where the greatest abundance was observed. Unlike the old configuration that had the largest incursion of larvae in the estuary, the new configuration presented the largest number of larvae in approximately 81% (~5700) compared with approximately 71% (~5000) of the old configuration. During the S wind (Figure 10H), the larvae reached area A4 in the old configuration, while in the new configuration, the larvae did not pass area A3 where the greatest abundance was observed in both configurations. The total abundance was approximately 76% (~5300) in the old configuration and approximately 24% (~1700) in the new configuration. During the SE wind (Figure 10N), in the old configuration, the larvae also reached the northern limit of the estuary, area A5, concentrating their greatest abundance in area A4. In contrast, in the new configuration, the larvae did not pass area A3, concentrating the greatest abundance in the areas A1 and A2 on the lower estuary. As observed during the SW wind, in the SE wind, the new configuration presented the highest total abundance of approximately 92% (~6500) compared to approximately 85% (~ 6100) in the old configuration despite the lesser incursion.

From day 2 (Figure 10C, 10I, 10O), the larvae in the old configuration passed from the northern limit of the estuary (area A5, Figure 1C) during all winds (SW, S, and SE), spreading toward the north of the Lagoon, whereas in the new configuration, this only occurred during the SW wind. The concentration of larvae declined from region A1 until up to the limit of the estuary (area A5), with total abundance declining to 57% (~4000) and 47% (~3300) for the old and new configuration, respectively, concentrating the largest number of larvae in area A4 (Figure 10C) in both configurations. The S wind showed the same behavior only for the old configuration, where the abundance declined to approximately 74% (~5150), while in the new configuration, the larvae were limited and concentrated their greatest abundance in area A4, and their total abundance registered an increase of approximately 73% (~5100) (Figure 10I). The SE wind showed almost no larvae from area A4 (Figure 10O) in the new configuration, whereas the old configuration showed its greatest abundance in area A6. The new configuration presented its abundance distributed in areas lower than A4 (A1, A2, and A3).

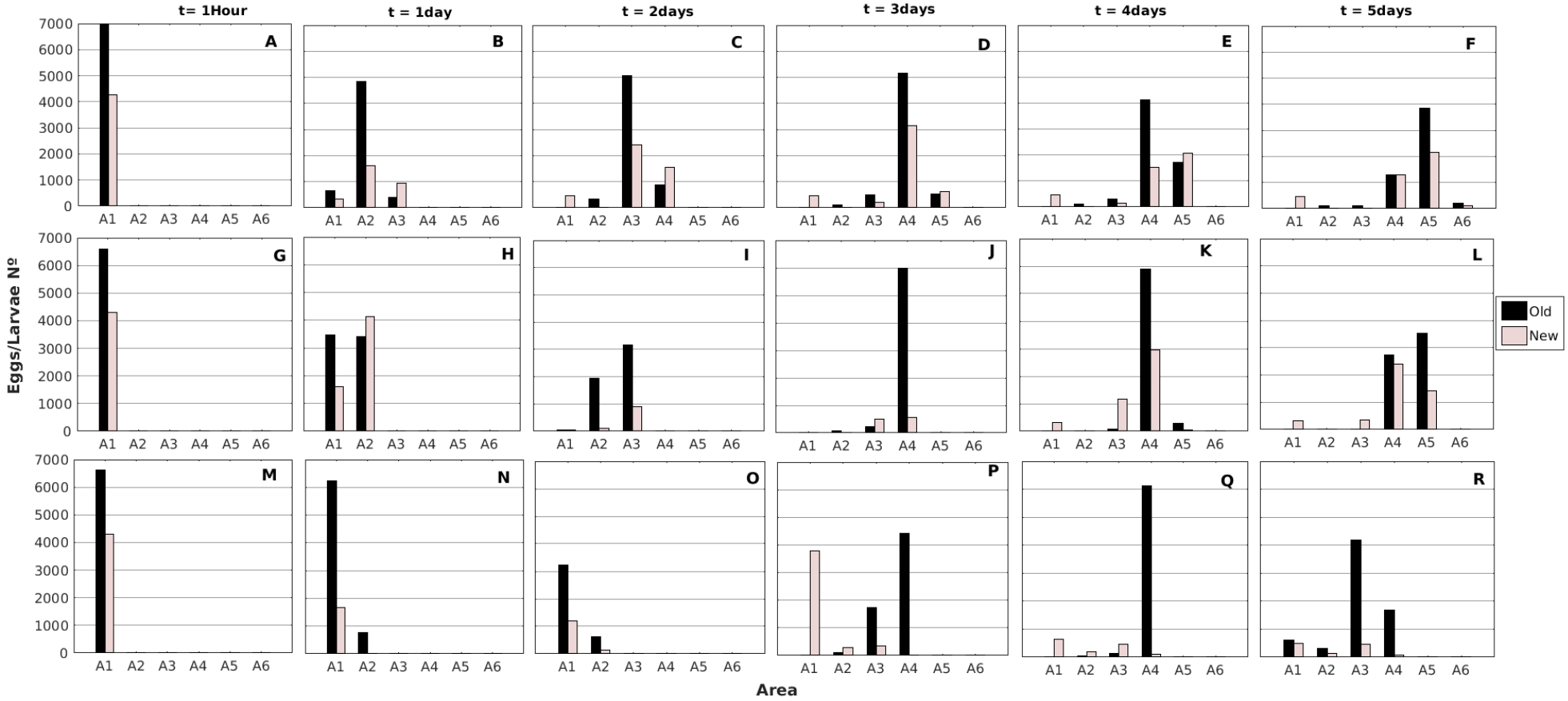


Figure 9: Spatio-temporal distribution of the abundance of eggs and larvae of *Micropogonias furnieri* in the 5 areas (A1, A2, A3, A4 and A5) at the end of each of the 5 days of simulation (day 1, day 2, day 3, day 4 and day 5), for old (blue) and new (yellow) jetty configuration, during the period of high continental discharge. Considering the SW (Top panel), S (center panel) and SE (bottom panel) wind experiments.

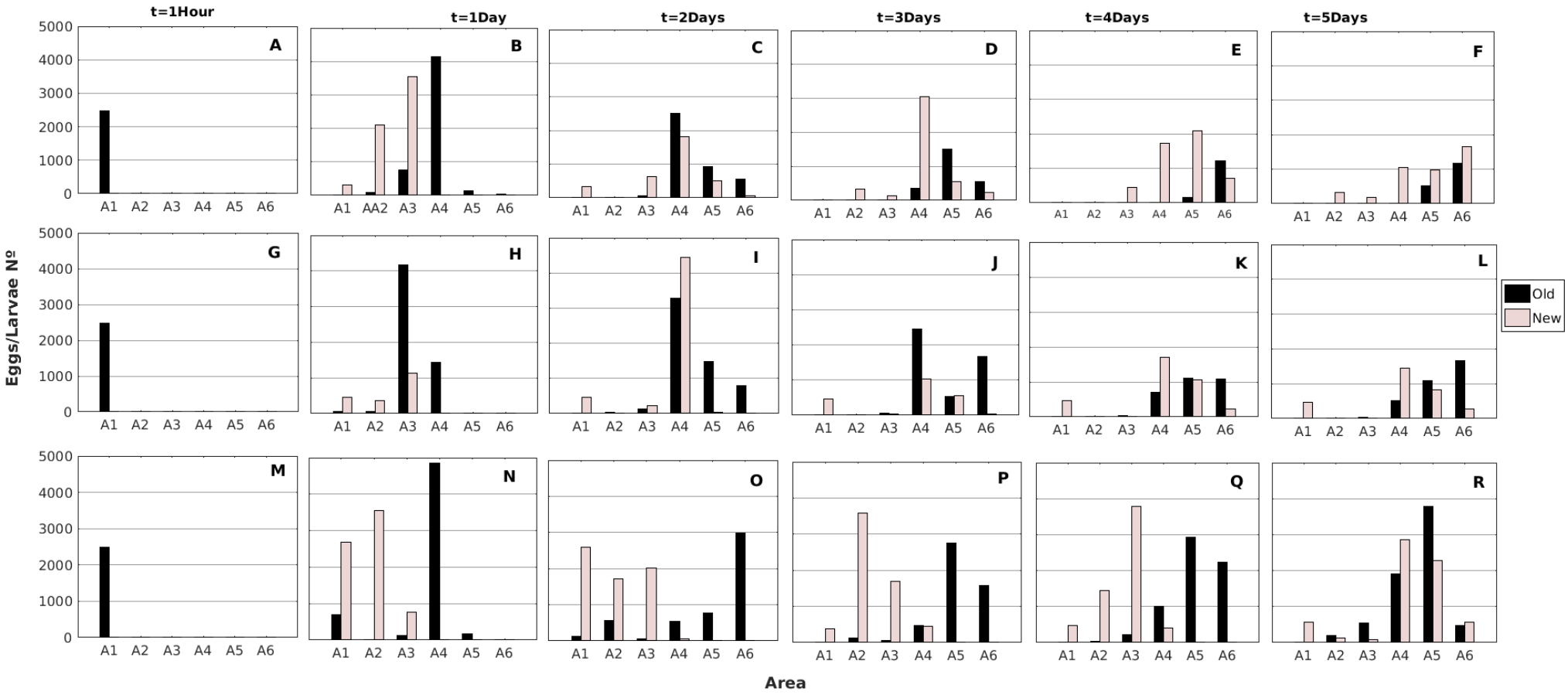


Figure 10: Spatio-temporal distribution of the abundance of eggs and larvae of *Micropogonias furnieri* in the 5 areas (A1, A2, A3, A4 and A5)at the end of each of the 5 days of simulation (day 1, day 2, day 3, day 4 and day 5), for old (black) and new (blue) jetty configuration, during the period of low continental discharge. Considering the SW (Top panel), S (center panel) and SE (bottom panel) wind experiments.

Similar to the SW wind, the SE wind showed a decline in total abundance to approximately 71% (~ 5000) in the old and approximately 86% (~6000) in the new configuration.

On day 3 (Figure 10D, 10J, 10P), the decay of larvae abundance continued in the region of the estuary (A1 to area A5) for all winds, demonstrating the incursion of the larvae beyond the estuarine region. During the SW wind (Figure 10D), in the old configuration, the abundance dropped to 36% (~2500), and in the new configuration, the larvae reached and passed the northern limit of the estuary, with their total abundance dropping to 60% (~4200). During the wind S (Figure 10J), the abundance declined to approximately 69% (~4800) and approximately 31% (~2200) in the old and the new configuration, respectively. However, during SE winds (Figure 10J), both configurations did not show changes in their total abundance, maintaining approximately 71% (~ 5000) in the old and approximately 86% (~6000) in the new configuration, with an advance of larvae to area A4.

From day 4 (Figure 10E, 10K, 10Q) onward, the new configuration followed the same decay behavior, similar to the old configuration for the SW and S wind. The southern areas of the estuary (A1, A2, and A3), showed low and/or almost no larvae and higher concentrations in the northern areas (A5 and A6) (Figure 10E, 10F, 10K, 10L), demonstrating that part of the larvae may have crossed the northern limit of area A6 (Figure 1C) because, as illustrated in Figure 6, the maximum range of the larvae during the simulated winds exceeded 75 km (northern limit of area A6). The total abundance on the 4th and 5th days decreased to approximately 23% (~1600) in the old configuration and approximately 59% (~4100) in the new configuration during the SW wind, and approximately 44% (~3000) for both configurations during S wind. Larvae during the SE wind only reached the northern limit of the estuary (area A5) on day 5 (Figure 10R) in the new configuration. The total larvae abundance was approximately 93% (~ 6500) and approximately 90% (~ 6300) in the old and new configuration, respectively, and the greatest abundance was concentrated in areas A4 and A5.

### 3.6. Lateral Stratification at the mouth of testuary

#### 3.6.1. Changes on Salinity Stratification

The lateral stratification between the jetties was analyzed only for low discharge experiments because at the beginning of the experiments, the plume of the Patos Lagoon was

in the adjacent coastal region, allowing the lateral stratification process to be more evident between the jetties (António et al., submitted). The lateral stratification varied from the old (Figure 11A, 11B, 11C) to the new (Figure 11D, 11E, 11F) configuration for each incident wind direction. The lateral stratification was more evident during the incidence of the SW wind, both for the old and the new configuration. The beginning of the flood, and consequently the establishment of lateral stratification in both the old and in the new configuration of the Barra Jetties, occurred 1 hour after the beginning of the experiment (Figures 11A and 11D). In the SW wind experiment, the highest salinity was observed near the east jetty and the lowest near the west jetty, both in the old and the new configuration. In the new configuration, however, the salinity gradient was smaller, as the difference in salinity between the east and west was 2.5 psu, while in the old configuration this difference was 5 psu.

With the S wind experiment, a clear pattern of lateral stratification was not observed in the two configurations of the Barra Jetties. It should be noted that in the old configuration (Figure 11B) the lateral stratification between the jetties was not established, but the flow of saltwater was present between the jetties 7 hours after the beginning of the experiment, dominating the entire navigation channel. In the new configuration (Figure 11E) at 7 hours, the stratification had not been established, observing the beginning of the entry of saline water from the coastal region into the mouth of the jetties. In the old configuration, the highest salinity was observed more centralized, decreasing for the jetties (Figure 11B). During the SE wind, the lateral stratification was observed only 10 hours after the beginning of the experiment with the highest salinity in the east jetty (Figure 11C). In the new configuration, 10 hours after the beginning of the experiment, the navigation channel still did not have lateral stratification (Figure 11F). In general, the beginning of floods and consequently the establishment of lateral stratification occurred faster in the old than in the new configuration, resulting in a difference of 2 hours during S winds and 5 hours during SE winds.

### 3.6.2. Larvae Distribution

Analyzing the larvae abundance among the jetties (Figure 12), the dispersion results corroborate with the salinity gradient (Figure 11). During SW winds (Figure 12A, 12D, 12G), stratification was observed 1 h after the beginning of the experiment for both configurations.

In the old configuration, the largest number of larvae was concentrated at the root of the jetties, spreading from the central channel toward the east jetty region (Figure 12A). In the new configuration, despite stratification also occurring 1 hour after the beginning of the experiment, the largest number of larvae was concentrated in the center of the jetties, in the east jetty region (Figure 12D). During the S wind (Figure 12B, 12E, 12H), the stratification occurred after 7 hours of simulation. In the old configuration, the largest number of larvae was observed in the mouth of jetties in the central channel region (Figure 12H), concentrating the largest number of larvae in the east jetty and decaying to the west jetty during transport to the interior of the estuary (Figure 12B and 12E). In the new configuration, the larvae were observed only in the region of the mouth of the jetties in the central channel of the jetties (Figure 12H). During the SE wind (Figure 12C, 12F, 12I), the stratification occurred 10 hours after the beginning of the experiment. In the old configuration, the largest number of larvae was observed in the mouth region in the central channel of the jetties (Figure 12I), decreasing linearly from the west to the east jetty during transport to the interior of the estuary (Figure 12C and 12F). In contrast, in the new configuration, no larvae were recorded between the jetties 10 h after the beginning of the experiment (Figure 12I).

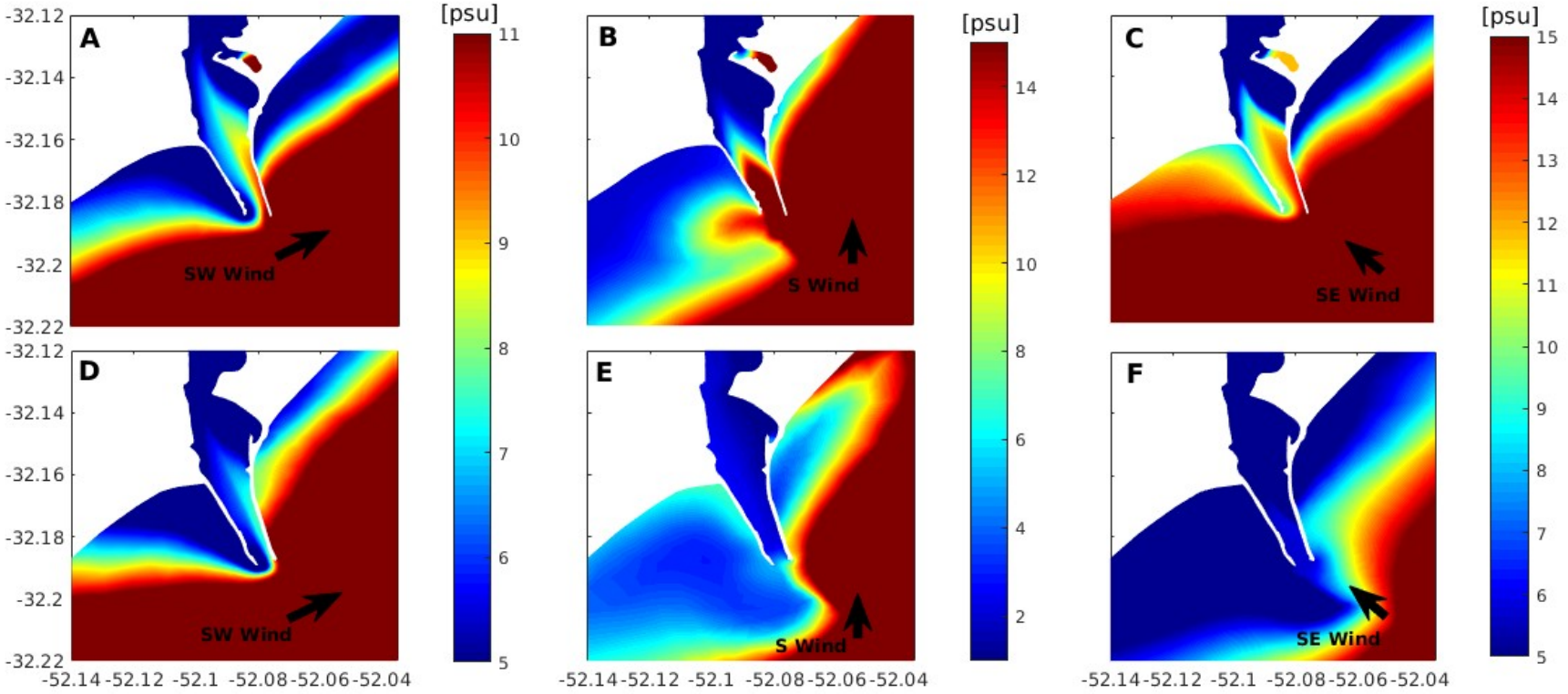


Figure 11: Spatial distribution of salinity in the estuarine mouth during low continental discharge at: 1h (A and D), 7h (B and E), 10h (C and F)., considering the SW (A and D), S (B and E) and SE (C and F) wind experiments. Results are presented for the old (top panel) and for the new (bottom panel) jetty configurations. Black arrows indicate the wind direction.

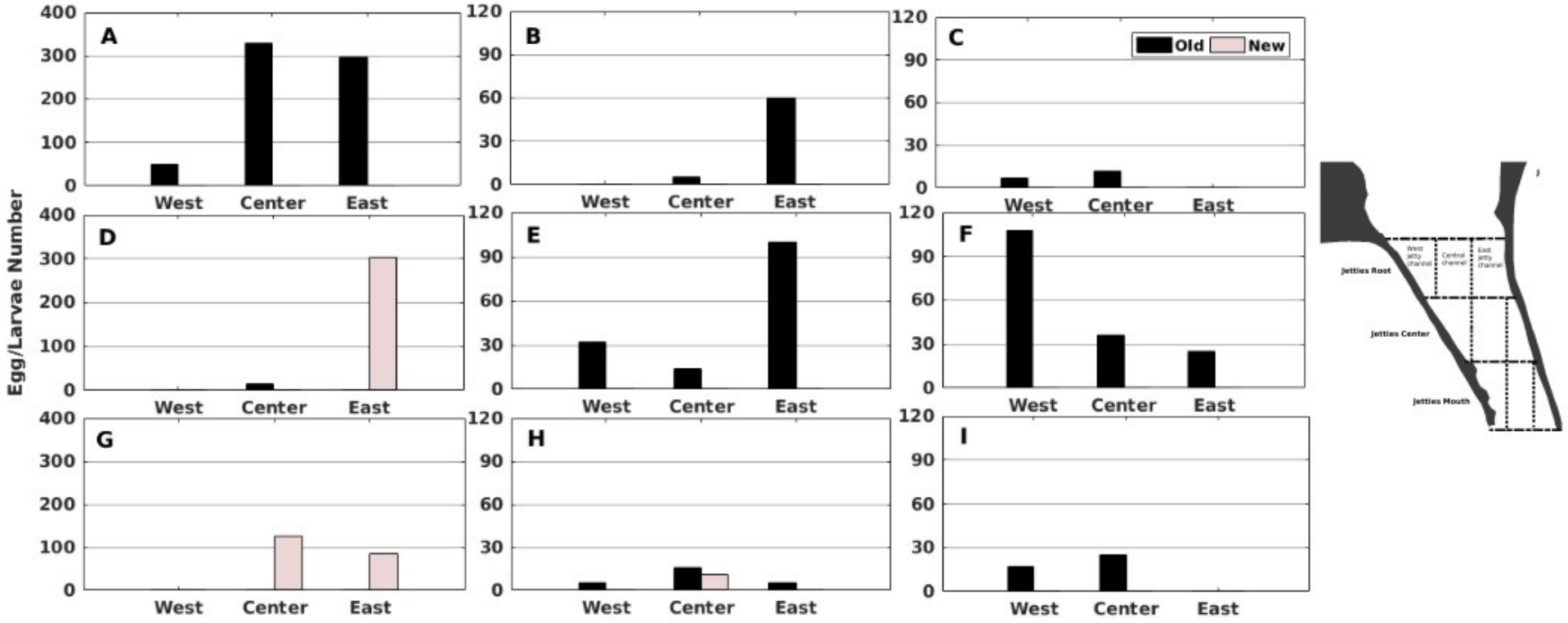


Figure 12: Egg abundance of *Micropogonias furnieri* between the jetties during lateral stratification, considering the SW (A, D and G), S (B, E and H) and SE (C, F and I) wind experiments, at: jetties root (A, B, C), jetties center (D, E, F), an jetties mouth (G, H, I), during the period of low water discharge.

## 4. DISCUSSION

The present study analyzes the effects of changes in the configuration of coastal structures in the transport and dispersion of eggs and larvae of the croaker, *Micropogonias furnieri*. This study is the first Lagrangean 3D model study with an emphasis on the dispersion of organisms (eggs and larvae), and builds on previous work conducted with 2D models of particle dispersion in the region by Silva et al, (2019), Franzen et al, (2019) and Martins et al, (2007). These studies have been used to try to overcome the lack of observational data on the transport of eggs and larvae in the study region. The novelty of this study is to demonstrate that even small alterations in coastal structures can result in hydrodynamic changes that have an impact on the transport of planktonic organisms. The study analyzed the case of the Barra Jetties on the access channel to the Patos Lagoon in southern Brazil. River discharge and wind control circulation in the Patos Lagoon estuary (Moller et al., 2001; Fernandes et al., 2005; Moller and Fernandes, 2010; Odebrecht et al., 2010). The analysis considered two extreme discharge conditions, high in 2003 (El Niño) and low in 2012 (La Niña), which produce extreme circulation conditions (Moller et al., 2001; Marques and Möller, 2009) and consequently influence the transport of fish eggs and larvae (Muelbert and Weiss, 1991). Situations with winds from the south quadrant were simulated because they favor the entry of saltwater (Hartmann and Schettini, 1991; Moller et al., 2001; Moller and Fernandes, 2010; Marques et al., 2011) and consequently maximize the transport of marine organisms to the estuary (Muelbert and Weiss, 1991). In each of these situations, only changes in depth and jetty shape were simulated, which were induced by humans in the project to alter the jetties at the entrance to the Patos Lagoon estuary. The duration of 5 days of the experiments, with a continuous incidence of south winds, was defined according to the passage of cold fronts in the region (Moller and Fernandes, 2010), and because it represents the passive stage in the life span of the croaker when they do not yet present active movement (Weiss, 1981).

Differences, both in saltwater intrusion and in the pattern of transport and dispersal of larvae to the interior of the estuary, were observed between the old and the new configuration of the jetties in the different scenarios analyzed. According to Dugan et al. (2011), the design and inclusion of engineering structures in coastal environments alter hydrodynamics, modify water flow, wave regime and propagation, sediment dynamics, grain size and deposition processes. Despite the use of coastal structures around the world for thousands of years, studies on the physical, environmental and economic effects of these structures in open and sheltered coastal regions are recent (Yuk and Aoki, 2007; Azarmsa et al., 2009; Cunha and Caliari, 2009; Ghashemizadeh and Tajziehchi, 2013; Lisboa and Fernandes, 2015; Silva et al., 2015; Prumm and Iglesias, 2016). The ecological effects resulting from the construction of these structures have been little studied and understood, and even

less about how they alter the functions and services of these natural ecosystems (NRC, 2007; Dugan et al., 2011).

Differences in the final location of the larvae were observed associated to the direction of the incident wind because, during the SW and S wind, the larvae were closer to the east side of the lagoon, while the opposite was observed with SE winds. Recent jetty modernization has reduced the incursion of eggs and larvae into the estuary in the new configuration compared to the old jetty configuration. The morphology of the Patos Lagoon entrance plays a fundamental role in the transport and dispersion of eggs (Martins et al., 2007). As a consequence, larvae took longer to be transported from one area to another as the incursion into the estuary occurred. Transport of fish eggs and larvae to estuarine breeding sites is important to ensure the recruitment and maintenance of fishing resources (Castro et al. 2005; Vieira et al. 2010). According to Robins et al. (2013), the larval transport pattern, whether promoting self-recruitment (retention) or high connectivity among local populations, is fundamentally important for species that live in irregular habitats, such as reefs, zones between tides or estuaries.

The differences observed in the pattern and extension of larvae incursion in the Patos Lagoon estuary may be due to differences in the bathymetry of the access channel, symmetry and length of the jetties between the two configurations, as well as the convergence and funneling of the jetties in the new configuration (Cunha and Caliari, 2009; Lisboa and Fernandes, 2015). The recent modernization of the jetties changed the hydrodynamics of the estuary, reducing saline intrusion as well as the intensity of flood and ebb currents by approximately 20%, along the access channel between the jetties (António et al., 2020; Silva et al., 2015). Such factors modyfy the flood flows that are responsible for the transport of eggs and larvae in their passive phase to the interior of the estuary (Castro et al., 2005; Martins et al., 2007; Franzen et al., 2019). Additionally, a partial centralization of the flow along the navigation channel (António et al., 2020) opposed to the previous circulation pattern in which the east jetty was more dynamic than the west jetty (Cunha and Caliari, 2009) can cause different residual currents and influence the transport of eggs and larvae as observed in the Aransas Pass estuary in the Gulf of Mexico (Brown et al., 2000). Human interventions in estuarine geomorphology changes the natural flow of saltwater, leading to the loss of habitat and disturbing the ecocline throughout the estuarine system, preventing fish from moving between previously connected habitats, especially in early ontogenetic phases (Barletta and Lima, 2019). Results from our study demonstrated that the influence of the local geomorphology in the variation of circulation conditioned the way that the fish larvae are transported to the estuary, a crucial parameter when associated with other physical and biological factors that are determinant for transport during the initial stage of life of the larvae (Able, 2005; Barletta and Lima, 2019). The

factors mentioned also affected the larvae trajectory, and differences were observed in the estuary between the two configurations.

The number of larvae that entered the estuary also differed between the old and the new jetty configuration. The reduction of flood currents along the navigation channel combind with the reduction of the cross-sectional area by approximately 15%entrance, despite the increase in depth by approximately 2 m (António et al., 2020; Silva et al., 2015) and the extension of the jetties after the recent modernization, may limit the incursion of the passively transported larvae to the estuary. Moreover, increasing or decreasing the current velocities has a direct impact on the transport of particles and water properties (Castro et al., 2005; Cunha and Caliari, 2009). These may be the case withI eggs and larvae of species such as croaker that enter estuaries withestuaries the intrusion of saltwater from the adjacent coastal region where the species spawn (Castello, 1986; Sinque and Muelbert, 1997; Vieira and Castello 1997; Odebrecht et al. 2017).

The reduced incursion caused by the delay in the entry of eggs and larvae into the estuary in the new configuration of the jetties will contribute to a greater loss due to their dispersion in the adjacent coastal region. The reduction in the number of organisms that enter the estuary, which is a nursery (Odebrecht et al. 2017) and contains favorable conditions for development, could result in negative impacts for the croaker population. Ramos et al. (2006) found that environmental parameters such as increased river flow can prevent the recruitment of marine species, leading to a decrease in diversity in the estuarine region as well as variations in abundance, total diversity, and in the structure of the larval fish assembly. In the coastal region adjacent to the study, ocean currents, tides, and meteorological conditions are the main forces responsible for the transport and dispersion of planktonic organisms (Acha et al., 2004; Muelbert et al., 2008). Environments with high tidal energy and high variability in oceanographic conditions, such as coastal regions, lead to greater dispersion of larvae to places far from the population (Robins et al., 2013) as well as to areas with conditions that are not appropriate for their development. Although unfavorable environmental conditions rarely induce direct larval mortality, they contribute indirectly by prolonging the planktonic phase, so that the larvae are more exposed to planktonic dispersion, predation, or lack of food (Ellien et al., 2004). playve(,Such findings demonstrate that anthropic changes can lead to a reduction in the incursion, structure, and composition of organisms in the estuary.

Furthermore, the maximum final distance and abundance of larvae to reach inside the estuary was also reduced in the new configuration of the jetties at both high and low river discharge. A reduced penetration of organisms will result in the reduction of the diversity of organisms and will change the structure and composition of the fauna and the environment inside the estuaries. This may directly affect the observation and occurrence of organisms of estuarine-dependent

species further north of the estuary over distances previously recorded. Odebrecht et al. (2005) found that the reduced limit of the salinity range reduces the oligohaline region of the Patos Lagoon, an important characteristic for the distribution of species and biodiversity. Fish abundance has decreased in the last three decades (1990–2010) in Sepetiba Bay, and more pronounced changes have been observed in the inner and middle bays, noting that changes in the salinity gradient have led to spatial changes in fish communities due to the expansion of the port (Araújo et al., 2017). Such port expansion activities, which included dredging to deepen the navigation channel, contribute to the degradation of the coast, the impoverishment of natural habitats, and an increase in the pollutant load in the bay.

The circulation observed between the jetties in the access channel to the Patos Lagoon forces the establishment of lateral stratification, a pattern that was also observed in the access channel to the bay of Aransas Pass (Bown et al., 2000; Cunha and Calari, 2009; Marques et al., 2011). The recent jetty modernization has also affected the establishment of lateral stratification in periods of low discharge. A delay in the time of occurrence of lateral stratification in the new configuration promotes a decrease in the number of eggs and larvae transported during the incidence of SW and S winds. Asymmetry in the length of the jetties, coincident with weakening of flood currents, due to changes in the configuration at the entrance of the estuary seems to be the cause for this delay  is the (Cunha and Caliari, 2009; Moller and Fernandes, 2010; Silva et al. 2015; António et al,  2020). A similar result was found on the jetties at Aransa Pass (Bown et al., 2000). What justifies the delay in the start time of the occurrence of lateral stratification, combining symmetry and the increase in the length of the jetties in the new configuration, which results in the reduction of the intensity of the currents between the jetties (António et al., 2020; Silva et al., 2015). In this way, it is expected that the location that holds the highest concentrations of eggs and larvae will be altered as a consequence of the reduction in the daily distance and the maximum extent covered by eggs and larvae toward the interior of the estuary. During the lateral stratification between the jetties, each incident wind presented a specific characteristic in the larvae distribution pattern during the incursion into the estuary and the location of greater concentration in the new configuration did not change significantly; however, there is still a need for further analysis since the lateral stratification was not fully established in the time observed for the old configuration for the 3 winds studied. This fact meant that the variations in the region with the highest concentration of eggs and larvae observed were mainly determined by the direction of the incident wind.

Figure 13 presents the conceptual model of eggs and larvae transport during the incidence of southern winds (SW, S, and SE) for the old and the new configuration of the Barra Jetties. The transport and dispersion of eggs and larvae in the first moments after the start of the simulations are

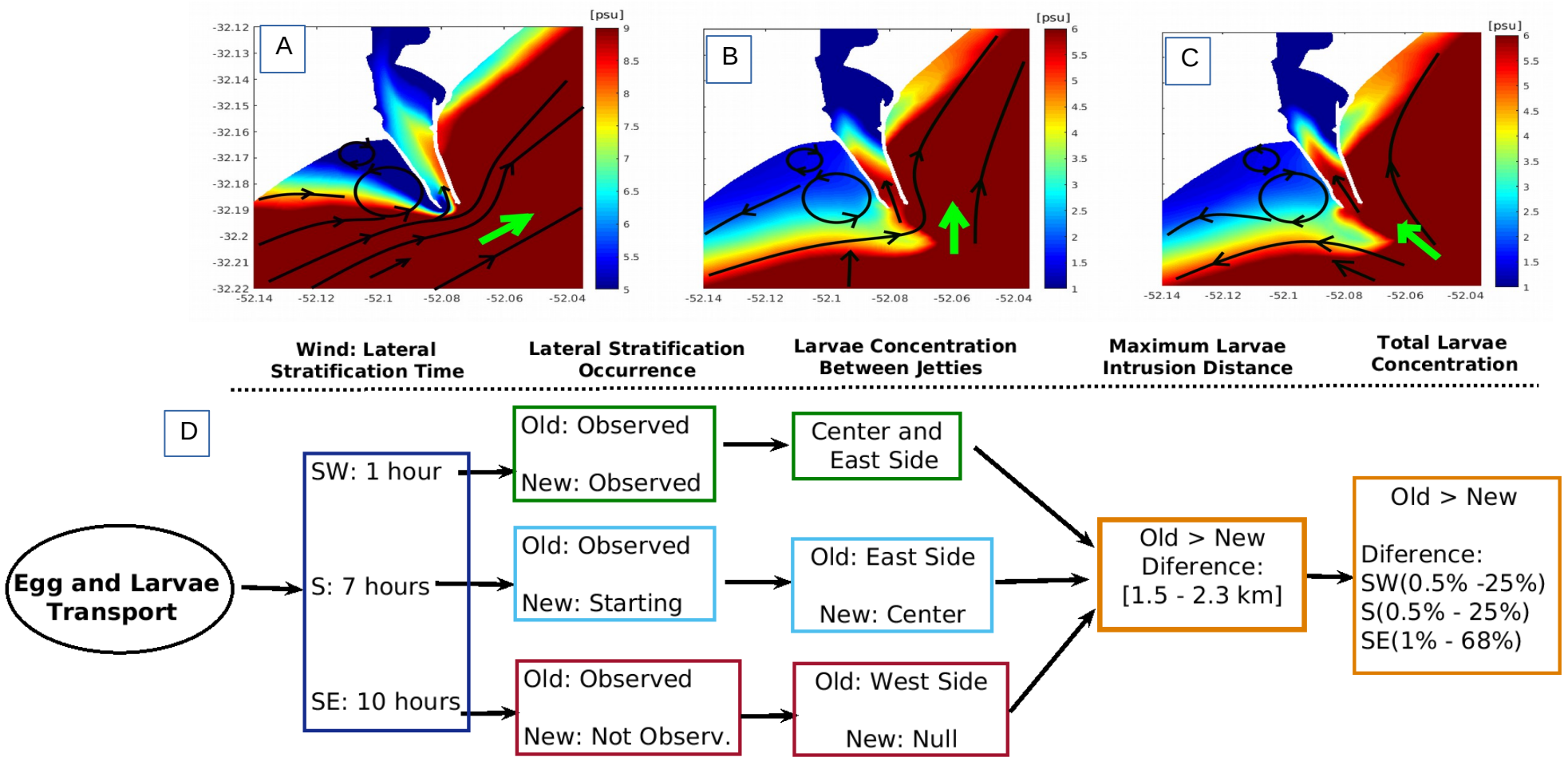


Figure 13: Schematic diagram of the differences in the transport of eggs and larvae of *Micropogonias furnieri* from the coastal region to the Patos Lagoon estuary induced by changes in the configuration of the jetties. Coastal circulation induced by SW (A), S (B) e SE (C) winds. Black lines and arrows indicate the current velocity. Green arrows indicate the wind direction. (D) Diagram of the resulted effects in the eggs and larvae transport.

forced by the pattern of velocity currents in the coastal region (Figure 13A, 13B, and 13C), which are determined by the direction of the incident wind. In the experiments in both configurations, re-circulation zones with turns are formed at the root of the west jetty, a place that can concentrate and/or retain larvae in the central region of the turns, both cyclonic and anti-cyclonic, due to the trapping conditions in the protected region. The coastal circulation forms lines of currents that skirted the jetties which, depending on the wind, favor the transport of organisms to the interior of the estuary. The contribution of these physical conditions conditioned the differentiated transport of eggs and larvae (Figure 13D). The differences in the jetty configurations determined the extension of penetration and abundance of eggs and larvae within the estuary. A shorter incursion time and a greater range and concentration of larvae stood out in the old configuration, while in the new configuration, a delay in stratification time, a reduction of the maximum incursion, and the concentration of larvae were registered.

## 5. CONCLUSION AND REMARKS

The study results demonstrated that the recent modernization of the Barra Jetties of Rio Grande affected the extension of incursion, abundance, and distribution of eggs and larvae in years of extreme contrasting dynamics, 2003 (El Niño) and 2012 (La Niña). A reduction in these parameters was notable in the new configuration during transport to the estuary with SW, S and SE winds. The recent modernization also changed the time for the start of lateral stratification and how the eggs and larvae enter the estuary, with a delay in the new configuration for the 3 simulated winds (SW, S, SE).

The present study concludes, therefore, that the differences in transport, the dispersion of eggs and larvae to the Patos Lagoon, and the extension and its variability are attributed to hydrodynamic changes caused by alterations in the geomorphology of the estuarine environment imposed by the jetty configuration changes. The study demonstrates that even small alterations in coastal structures can result in circulation changes that have an impact on the transport of planktonic organisms. The results of the study shed some light to the problem

of declining abundance and capture of the adult stocks in the Patos Lagoon estuary, but it is important to consider limitations of modeling results and the complexity of the life cycle of the *Micropogonias furnieri*. Future work should investigate biological characteristics of the species, such as growth and mortality rate, and predation, which are fundamental factors for the real dimension of successful recruitment.

## ACKNOWLEDGMENTS

The authors would like to acknowledge CAPES (*Coordenação de Aperfeiçoamento Pessoal de Ensino Superior*) for sponsoring the first author's (MHA) PhD's grant through the *Programa de Pós-Graduação Ciência para o Desenvolvimento* (PGCD), and provided resources support to the Postgraduate Program in Oceanology. We thank the CNPq (*Conselho Nacional de Desenvolvimento Científico and Tecnológico*) for the research grants 308274/2011-3 (EHF) and Proc. 310047/2016-1 (JHM). This study was partially funded by the Brazilian Long-Term Ecological Research Program (PELD) from CNPq (Proc.441492/2016-9) and the Fundação de Amparo à Pesquisa do Estado do Rio Grande do Sul (Proc. 16/2551-0000102-2). We are also grateful to the LOCOSTE (*Laboratório de Oceanografia Costeira e Estuarina)* team for giving support during this research and to Prof. Dr. Osmar Möller Jr for providing the in situ data used to calibration and validation of TELEMAC-3D model.

SUPPLEMENT B

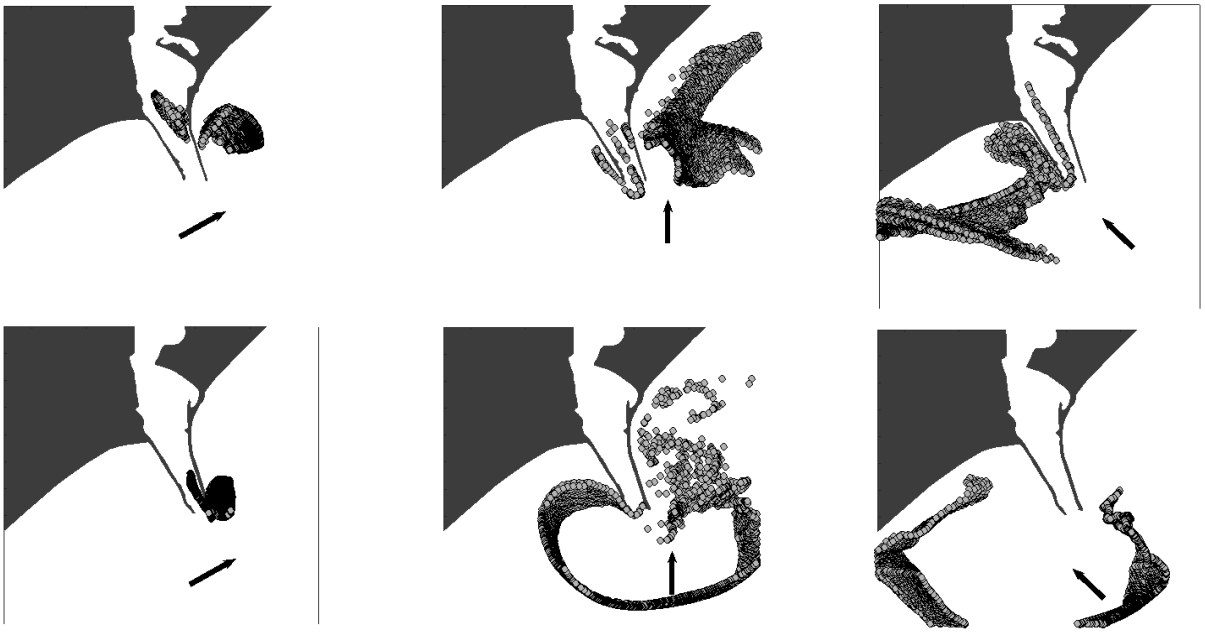

Figure 1: Spatial distribution pattern of larvae during lateral stratification at 1h (A and D), 7h(B and E), 10h (C and F). During the period of low water discharge, considering the SW (A and D), S (B and E), and SE (C and F) wind experiments. Results are presented for the old (top panel) and the new (bottom panel) jetty configurations. The black arrow indicated the wind direction.

# Capítulo VI:
# Considerações Finais

## Considerações Finais

A obra de modernização dos Molhes da Barra na desembocadura do canal de navegação do Porto do Rio Grande realizada em 2010 alterarou a hidrodinâmica do estuário da Lagoa dos Patos. As mudanças hidrodinâmicas observadas tiveram efeito sobre o transporte de ovos e larvas, reduzindo sua abundância e alcance máximo no interior do estuário na nova configuração dos Molhes da Barra. Fatos esses que são reflexos da redução da extensão máxima da intrusão salina, e das correntes tanto de enchente como de vazante, associados à centralização parcial do fluxo no canal de navegação e às mudanças no tempo de início e de duração da estratificação lateral que foi reduzida na nova configuração, implicando na forma e no tempo de transporte para o interior do estuário.

As mudanças observadas têm efeitos no processo de transporte, distribuição e alcance não apenas de ovos e larvas da corvina *Micropogonias furnieri* mas também de propriedades e de outros organismos estuarino-dependentes durante o processo de recrutamento. Estas alterações poderão ter consequências na abundância de estoques pesqueiros na região costeira e estuarina, requerendo especial atenção dos órgãos de gestão. Estudos subsequentes são necessários levando em consideração aspectos mais detalhados como as características biológicas e comportamentais de cada espécie, de modo a garantir informações robustas que permitam a aplicação de medidas adequadas na reversão do cenário do declínio da pesca na região costeira adjacente à Lagoa dos Patos.

## Referências Bibliográficas


Able, K.W. 2005. A re-examination of fish estuarine dependence: evidence for connectivity between estuarine and ocean habitats. Estuarine, Coastal and Shelf Science 64 (1): 5–17. https://doi.org/10.1016/j.ecss.2005.02.002.

Abreu, P. C., Odebrecht, C. e Niencheski, L. F. 2010. Nutrientes Dissolvidos. In: Seeliger, U. and Odebrecht, C. (Eds.). O Estuário da Lagooa dos Patos: Um século de transformações. Rio Frande, FURG, P180. ISBN: 978-85-7566-144-4, pp 43-48.

Adger, W. N., Hughes, T. P., Folke, C., Carpenter, S. R. and Rockstrom, J. 2005. Social-Ecological Resilience to Coastal Disasters. Science, 309(5737), 1036–1039. Doi:10.1126/science.1112122

Azarmsa, S. A., Esmaeili, M. and Khaniki, A. K. 2009. Impacts of Jetty construction on the wave heights of the Kiashahr lagoon. Aquatic Ecosystem Health & Management, 12(4):358-363. ISSN: 1463-4988. DOI: 10.1080/14634980903354726.

Azevedo, I.C., Bordalo, A.A. and Duarte, P. 2014. Influence of freshwater inflow variability on the Douro estuary primary productivity: a modelling study. Ecol. Model. 272, 1–15, http://dx.doi.org/10.1016/j.ecolmodel.2013.09.010

Able, K.W. 2005. A re-examination of fish estuarine dependence: evidence for connectivity between estuarine and ocean habitats. Estuarine, Coastal and Shelf Science 64 (1): 5–17. https://doi.org/10.1016/j.ecss.2005.02.002.

Acha, E.M., Simionato, C.G., Carozza, C., Mianzan, H. 2012. Climate-induced year-class fluctuations of whitemouth croaker Micropogonias furnieri (Pisces, Sciaenidae) in the Rio de la Plata estuary, Argentina–Uruguay. Fish. Oceanogr. 21 (1), 58–77.

Acha, E. M., Mianzan, H., Guerrero, R., Carreto, J., Giberto, D., Montoya, N. and Carignan, M. 2008. An overview of physical and ecological processes in the Rio de la Plata Estuary. Continental Shelf Research. Volime 28, Issue 13, Pp.1579-1588. Doi.org/10.1016/j.csr.2007.01.031

Acha, E. M., Mianzan, H., Lasta, C. A. and Guerrero, R. A.. 1999. Estuarine spawning of the whitemouth croaker Micropogonias furnieri (Pisces: Sciaenidae), in the Río de la Plata, Argentina.Mar. Freshwater Research. 50, 57-65. DOI: 10.1071/MF98045.

Albuquerque, C.Q., Muelbert, J.H. and Sampaio, L.A.N. 2009. Early developmental aspects and validation of daily growth increments in otoliths of Micropogonias furnieri (Pisces, Sciaenidae) larvae reared in the laboratory. Pan-American Journal of Aquatic Sciences, 4(3): 259-266.

Albuquerque, C.Q. 2008. Bionomia da corvina Micropogonias furnieri no extremo sul de sua área de ocorrência, através da análise química de otólitos. Tese de Doutorado. Programa de Pós-Graduação em Oceanografia Biológica. Universidade Federal do Rio Grande, Rio Grande, RS. Brasil.

António, M. H. P., Fernandes, E. H. and Muelbert, J. H. 2020. Impact of jetties configuration changes on the hydrodynamics of the subtropical Patos Lagoon Estuary, Brazil. Water, 12, 3195. doi:10.3390/w12113197.

Araújo, G. F., Azevedo, M. C. C. Guedes, A. P. P. 2016. Inter-decadal changes in fish communities of a tropical bay in southeastern Brazil. Regional Studies in Marine Science. http://dx.doi.org/10.1016/j.rsma.2015.06.001.

Araújo, F. G., Pinto, S. M., Neves, L. M., Azevedo, M. C. C. 2017. Inter-annual changes in fish communities of a tropical bay in southeastern Brazil: What can be inferred from anthropogenic activities? Marine Pollution Bulletin, 114(1), 102–113. DOI:10.1016/j.marpolbul.2016.08.063

Braverman, M. S., Acha, E. M., Gagliardini, D. A. and Rivarossa, M. 2009. Dsitrubution of Whitemouth croaker (Micropoginias furnieri, Desmarest 1823) larvae in the Rio de La Plata estuarine front. Estuar. Coast. Shelf Sci, doi:10.1016/j.ecss.2009.02.018.

Barletta, Mário, and Lima, André R. A. 2019. Systematic Review of Fish Ecology and Anthropogenic Impacts in South American Estuaries: Setting Priorities for Ecosystem Conservation. Frontiers in Marine Science, Volume 6:237. DOI: 10.3389/fmars.2019.00237.

Blanton, J. O., Werner, F. E., Kapolnai, A., Blanton, B. O., Knott, D. and Wenner, E. L. 1999. Wind-generated transport of fictitious passive larvae into shallow tidal estuaries. Fish. Oceanogr. 8(Suppl. 2), 210-223.

Brown, Cheryl A., Jackson, George A. and Brooks, David A. 2000. Particle transport through a marraw tidal inlet due to tidal forcing and implications for larval transport. Journal of Geophysaical Research, Vol. 105, nº C10, Pages 24, 141-24, 156.

Bruno, Marcelo A. e Muelbert, José H. 2009. Distribuição Espacial e Variações Temporais da Abundância de Ovos e Larvas de Micropogonias Furnieri, no Estuário da Lagoa dos Patos: Registros Históricos e Forçantes Ambientais. Atlantica, Rio Grande. 51-68.doi: 10.5088/atl. 2009.31.1.51

Calliari, L.J., Winterwerp, J.C., Fernandes, E., Cuchiara, D., Vinzon, S.B., Sperle, M. & Holland, K.T. 2009. Fine grain sediment transport and deposition in the Patos Lagoon–Cassino beach sedimentary system. Continental Shelf Research. 23: 515-529. Doi:10.1016/j.csr.2008.09.019

Calliari, L., Cunha, R. P., e Antiqueira, J.A.F. 2010. Geomorfologia e dinâmica sedimentar. In: SEELIGER, U.; ODEBRECHT, C. (Eds.). O estuário da Lagoa dos Patos: Um século de transformações. 1.ed. p. 31-41, Rio Grande: FURG. (ISBN: 978-85-7566-144-4).

Castelão, R. M and Möller Jr, O. O. 2006. A modeling study of Patos Lagoon (Brazil) Flow response to idealized wind and river discharge dynamical analysis. Brazilian journal of oceanography, 54(1): 1-17.

Castelão, R. M. and Möller Jr Jr, O. O. 2003. Sobre a circulação tridimensional forçada por ventos na lagoa dos patos, Revista Atlantica, 25(2001), pp. 91–106.

Castello, J. P. (1986). Distribución, crecimiento y maduración sexual de la corvina juvenil (Micropogonias furnieri) en el estuario de la 'Lagoa dos Patos', Brasil. Physis 44, 21-36.

Castro, Marcia S., Bonecker, Ana C. T., and Valentin, Jean L. 2005. Seasonal Variation in Fish Larvae at the Entrance of Guanabara Bay, Brazil. Brazilian Archives of Biology And Technology. Vol. 48, n.1, pp. 121-128, ISSN 1516-8913.

Clark, B. M. 1997. Variation in Surf-sone fish community structure across a wave-exposure gradient. Estuar Coast Shelf Sci 44, 659-674.

Cochran, Wiliam G. 1976. Samplig Techniques. Third edition. By John Wiley and Sons, Inc., 1977. ISBN 0-471-16240-X. Pp. 77-728.

Costa, M.D.P., Muelbert, J.H., Moraes, L.E., Vieira, J.P. and Castello, J.P. 2014. Estuarine early life stage habitat occupancy patterns of whitemouth croaker *Micropogonias furnieri* (Desmarest, 1830) from the Patos Lagoon, Brazil. Fisheries Research 160. Pp. 77–84. http://dx.doi.org/10.1016/j.fishres.2013.10.025.

Costa, Sónia, Azeiteiro, Ulisses M., Pardal, Miguel A. 2013. The contribution of scientific research for integrated coastal management: The Mondego estuary as study case. Journal of Integrated Coastal Zone Management 13(2):229-241 (2013). DOI:10.5894/rgci391.

Cunha, R.M.P. and Calliari, L.J. 2009. Natural and antropic geomorphological changes in the inlet of Patos Lagoon before and after its fixation. Journal of Coastal Research, SI 56 (Proceedings of the 10th International Coastal Symposium), 708 – 712. Lisbon, Portugal, ISSN 0749-0258

D'Incao, F. 1991. Pesca e biologia de Penaeus paulensis na Lagoa dos Patos, RS. Atlântica, Rio Grande, 13(1): 159-169.

Dugan, J. E., Airoldi, L., Chapman, M. G., Walker, S.J. and Schlacher, T. 2011. Estuarine and Coastal Structures: Environmental Effects, A Focus on Shore and Nearshore Structures. Treatise on Estuarine and Coastal Science, Vol.8, 17-41, https://doi.org/10.1016/B978-0-12-374711-2.00802-0

Dyer, K. R. 1989. Estuarine flow interaction with topography - lateral and longitudinal effects. In: Neilson, B. J.; Kuo, A., and Brubaker, J. (eds), Estuarine Circulation, Tototowa, New Jersey: Human Press, pp. 39-59.

Ellien, C., Thiébaut, E., Dumas, F., Salomon, J-C. And Nival, P. 2004. A modeling study of the respective role of hydrodynamic processes and larval mortality on larval dispersal and recruitment of benthic invertebrates: example of Pectinaria koreni (Annelida: Polychaeta) in the Bay of Seine (English Channel). Journal of Plankton Research Vol. 26 No. 2, Pp. 117-132. https://doi.org/10.1093/plankt/fbh018.

Endo, Clarissa A. K., Gherardi, Douglas F. M., Pezzi, Luciano P. and Lima L. N. 2019. Low connectivity compromises the conservation of reef fishes by marine protected areas in the tropical South Atlantic. Nature, Scientific Reports, 9:8634. https://doi.org/10.1038/s41598-019-45042-0.

Esteves, L. S., Da Silva, A. R. P., Arejano, T. B., Pivel, M. A. G. and Vranjac, M. P. 2003. Coastal Development and Human Impacts Along the Rio Grande do Sul Beaches, Brazil. Journal of Coastal Research, SI 35 (Proceedings of the Brazilian Symposium on Sandy Beaches; Morphodynamics, Ecology, Uses, Hazards and Management), 548-556. Itajaí, SC – Brazil, ISSN 0749-0208.

FAO. 2020. The State of World Fisheries and Aquaculture 2020. Sustainability in action. Rome.

Fernandes, E.H.L.; Möller, O.O.; Cuchiara, D.; Marques, W.C. 2012. Avaliação das Condições de Navegabilidade do Canal de Acesso ao Porto de Rio Grande Após as Obras de Modernização. Reporte Tecnico, Rio Grande, RS, Brazil. Não pubicado.

Fernandes, E. H. L., Dyer, K. R. and Möller Jr, O. O. 2005. Spatial Gradients in Flow of Southern Patos Lagoon. *Journal of Coastal Research*, 21(4), 759-769, West Palm Beach (Florida), ISSN 0749-0208.

Fernandes, E. H. L,. Tapia, I. M., Dyear, K. R. and Möller Jr, O. O. 2004. The attenuation of tidal and subtidal oscillations in the Patos Lagoon Estuary. Ocean Dynamic, 54:348-359.

Fernandes, E. H. L, Dyer, K. R., Möller Jr, O. O. and Niencheski, L. F. H. 2002. The Patos Lagoon hydrodynamics during El Niño event (1998). *Continental Shelf Research*, 22, 1699-1713.

Fernandes, E. H. L., Dyer, K. R., e Möller Jr, O. O. 2001. On the hydrodynamics of the world's largest choked coastal lagoon: Patos Lagoon (Brazil). Estuaries.

Filgueras, Andre S. 2009. Condições oceanograficas e as assembleias Ictioplanctonicas no Estuário da Lagoa dos Patos. Universidade Federal do Rio Grande. PPGOB. Dissertação de Mestrado.

Figueiredo, G. M. e Vieira, J. P. 1998. Cronologia alimentar e dieta da corvina, Micropogonias furnieri, no estuário da Lagoa dos Patos, RS, Brasil. Atlântica, v. 20, p. 55-72.

Franzen, M. O., Muelbert, J. H. and Fernandes, E. H.. 2019. Influence of wind events on the transport of early stages of Micropogonias furnieri (Desmarest, 1823) to a subtropical estuary. Latin American Journal of Aquatic Research, 47(3): 536 - 546. https://doi.org/10.3856/vol47-issue3-fulltext-15

Freitas, P. P., Menezes, M. O. B. and Schettini, C. A. F. 2015. Hydrodynamics and Suspended Particulate matter transport in a shallow and highly urbanized estuary: The Cocó Estuary, Fortaleza, Brazil. Revista Brasileira de Geofísica, 33(4): 579-590. ISSN 0102-261X

Garcia, A. M., Vieira, J. P. and Winemiller, K. O. 2003. Effects of 1997-1998 El-Niño on the dynamics of the shallow-water fish assemblage of the Patos Lagoon Estuary (Brazil). Estuarine, Coastal and Shelf Science 57 (2003) 489–500. https://doi.org/10.1016/s0272-7714(02)00382-7

Garcia, A. M.; Vieira, J. P. and K.O., Winemiller. 2001. Dynamics of the shallow-water fish assemblage of the Patos Lagoon estuary (Brazil) during cold and warm ENSO episodes. Journal of Fish Biology. 59:1218-1238.

George, G., Vethamony, P., Sudheesh, K. and Babu, M. T. 2011. Fish larval transport in a macro-tidal regime: Gulf of Kachchh, west coast of India. Fisheries Research 110. Pp. 160–169. https://doi.org/10.1016/j.fishres.2011.04.002

Ghashemizadeh, N. and Tajziehchi, M. 2013. Impact of Long Jetty on Shoreline Evaluation (Case Study: Eastern Coast of Bandar Abbas). Journal of Basic and Applied Scientific Research. ISSN 2090-4304,Pp 1256-1266.

Grimm, A. M., Ferraz, S. E. T., and Gomes, J. 1998. Precipitation anomalies in southern Brazil assiciated with El Nino and La niña events. J Clim 11, 2863-2880.

Gong, W.P., Lin, Z.Y., Chen, Y.Z., Chen, Z.Y., and Zhang, H. 2018. Effect of winds and waves on salt intrusion in the Pearl River estuary. Ocean Sci 14, 139–159.

Haimovici, Manuel and Cardoso, Luís G. 2017. Long-term changes in the fisheries in the Patos Lagoon estuary and adjacent coastal waters in Southern Brazil, Marine Biology Research, 13:1, 135-150. https://doi.org/10.1080/17451000.2016.1228978

Harden-Jones F. R. 1968. Fish Migration. London: Edward Arnold Ltd.

Harris, S. A; Cyrus, D. P.; Beckley, L. E. 2001. Horizontal Trends in Larval Fish Diversity and Abundance Along an Ocean-Estuarine Gradient on the Northern KwaZulu-Natal Coast, South Africa. Estuarine, Coastal and Shelf Science. ELSIEVER. Vol. 53. Pp. 221-235. doi:10.1006/ecss.2001.0803

Hartmann, C., and Schettini, C. A. F. 1991. Aspectos hidrológicos na desembocadura da Laguna dos Patos, RS, Rev. Bras. Geocienc., 21, 371–377.

Hervouet, J. M. 2007. Hydrodynamics of Free Surface Flows: Modeling with the Finite Element Method, Wiley, Chichester.

Hinrichsen, Hans-Harald. 2009. Biological processes and links to the physics. Deep-Sea Research II 56. Pp. 1968–1983. https://doi.org/10.1016/j.dsr2.2008.11.008

Houde, E. D. 2008. Emerging from Hjort's Shadow. J. Northw. Atl. Fish. Sci., 41: 53–70. https://doi.org/10.2960/J.v41.m634

Hoguane, A. M., Gammelsrod, T., Mazzilli, S., António, M. H. e Da Silva, N. F. 2020. The hydroynamic of the Bons Sinais Estuary: The value of simple hydrodynamic tidal models in understanding circulatios in estuaries of central Mozambique. Regional Studies in Marine Science 37. https://doi.org/10.1016/j.rsma.2020.101352

Huggett, J.A., Freon, P., Mullon, C. and Penven, P. 2003. Modelling the transport success of anchovy Engraulis encrasicolus eggs and larvae in the southern Benguela: the effect of spatio-temporal spawning patterns. Marine Ecology Progress Series. Vol. 250:247–262.

Ibagy, A.S. e Sinque, C. 1995. Distribuição de ovos e larvas de Sciaenidae (Perciformes-Teleostei) da região costeira do Rio Grande do Sul-Brasil. Arquivos Biologia e Tecnologia 38 (1), 249–270.

Israel, Glenn D. 1992. Determining Sampling Size. IFAS Extension. PEOD6. Univercity of Florida.

Ivanoff, M. D., Toldo Jr, E. E., Figueira, R. C. L. and Ferreira, P. A. L. 2020. Use of $^{210}$Pb and $^{137}$Cs in the assessment of recent sedimentation in Patos Lagoon, southern Brazil. Geo-Marine Letters. https://doi.org//10.1007/s00367-019-00633-8

Ji, X., Sheng, J., Tang, L., Liu, D. and Yang, X. 2011. Process study of circulation in the Pearl River Estuary and adjacent coastal waters in the wet season using a triply-nested circulation. Ocean Modelling 38, 138-160. doi:10.1016/j.ocemod.2011.02.010.

Joly, A., Violeau, D., Moulin, F., Astruc, D. and Kassiotis, C. 2012. Transport of isotropic particles in a partially obstructed channel flow, Journal of Hydraulic Research, 50:3, 324-337. DOI: 10.1080/00221686.2012.686457

Joyeux, Jean-Christophe. 2001. The retention of ¢sh larvae in estuaries: among-tide variability at Beaufort Inlet, North Carolina, USA. Journal Mar. Biol. Ass. U.K. (81), Pp 857-868.

Kjerfve, B. and K.E. Magill. 1986. Comparative oceanography of coastal lagoons, p. 63-81. In: Wolfe, D. A. ed. Estuarine variability. New York, Academic Press. 509p.

Kjerfve, Bjorn. 1994. Chapter 1: Coastal Lagoons. Coastal Lagoon Processes edited by B. Kjerfve. Elsever Science Publisher B. V.

Kjerfve, B. Seeliger, U., Lacerda, L. D. 2001. A summary of natural and human induced variables in coastal marine ecosystems of Latin America. In: Seeliger U.Kjerfve B. (eds). Coastal marine ecosystems of Latin America. Springer-Verlag, Heidelberg. Pp 341-353.

Kriauciūnienė, J., Zilinskas, G., Pupienis, D., Jarmalavicius, D., and Gailiusis, B. 2013. Impact of Šventoji port jetties on coastal dynamics of the Baltic sea. Journal of Environmental Engineering and Landscape Management, 21(2), 114-122. https://doi.org/10.3846/16486897.2012.695736

Lett, C; Verley, P.; Mullon, and C.; Parada, C. 2008. A Lagrangian tool for modelling ichthyoplankton dynamics. Environmental Modelling & Software.science Direct. Pp 1210 - 1214

Lisboa, P. V. and Fernandes, E. H. 2015. Anthropogenic influence on the sedimentary dynamics of a sand spit bar, Patos Lagoon Estuary, RS, Brazil. Journal of Integrated Coastal Zone Management, 15(1):35-46. https://doi.org/10.5894/rgci54 .

Liu, Wen-Cheng and Chan, Wen-Ting. 2016. Assessment of Climate Change Impacts on Water Quality in a Tidal Estuarine System Using a Three-Dimensional Model. Water 2016, 8, 60; https://doi.org/10.3390/w8020060.

Louangrath, Paul. 2015. Common Statistical Tables. https://doi.org/10.13140/RG.2.1.2206.5769

Lough, R. G., Smith, W. G., W erner, F. E., Loder, J. W., Page, F. H., Hannah, C. G., Naimie, C. E., Perry, R. I., Sinclair, M., and Lynch, D. R. 1994. Influence of wind-driven advection on interannual variability in cod egg and larval distributions on Georges Bank: 1982 vs 1985. - ICES mar. Sei. Symp., 198: 356-378.

Marques W. C., Fernandes, E. H. L., and Rocha, L. A. O. 2011. Straining and advection contributions to the mixing process in the Patos Lagoon estuary, Brazil. *J. Geophys. Res.,*115,C03016, https://doi.org/10.1029/2010JC006524 .

Marques, W. C., Fernandes, E. H. L., e Möller Jr, O. O. 2010a. Straining and advection contributions to the mixing process of the Patos Lagoon coastal plume, Brazil. Journal of Geophysical Research, 115(C6).

Marques, W. C., Fernandes, E. H. L., Moraes, B. C., Möller, O. O., e Malcherek, A. 2010b. Dynamics of the Patos Lagoon coastal plume and its contribution to the deposition pattern of the southern Brazilian inner shelf. Journal of Geophysical Research: Oceans, 115(10):C10045.

Marques, W.C.; Monteiro, I.O.; Fernandes, E.H. 2009. Numerical modeling of Patos Lagoon plume, Brazil. Continental Shelf Re-search. 29(3):556-571. DOI: 10.1016/j.csr.2008.09.022

Marques, W. C. 2005. Padrões de variabilidade temporal nas forçantes da circulação e seus efeitos na dinâmica da Lagoa dos Patos, Brasil, M.Sc thesis, Univ. of Rio Grande, Rio Grande, Brazil.

Marques, W.C.; Monteiro, I.O. and Fernandes, E.H. 2009. Numerical modeling of Patos Lagoon plume, Brazil. Continental Shelf Re-search. 29(3):556-571. DOI: 10.1016/j.csr.2008.09.022

Marques, W. C., and Möller, O. O. 2009. Variabilidade temporal em longo período da descarga fluvial e níveis de água da Lagoa dos Patos, Rio Grande do Sul, Brasil, Rev. Bras. Recursos Hídricos, 13, 155-163.

Martins, I.M.S., Dias, J.M., Fernandes, E.H.L. and J.H. Muelbert. 2007. Numerical modelling of fish eggs dispersion at the Patos Lagoon estuary -Brazil. Journal of Marine Systems, 68: 537-555.

Martelo, A. F., Trombetta, T. B., Lopes, B. V., Marques, W.C. and Möller Jr, O.O. 2019. Impacts of dredging on the hydromorphodynamics of the Patos Lagoon estuary, southern Brazil. Ocean Engineering, Volume 188, https://doi.org/10.1016/j.oceaneng.2019.106325

Miaoulis, George, and R. D. Michener. 1976. An Introduction to Sampling. Dubuque, Iowa: Kendall/Hunt Publishing Company.

Miller, Thomas J. 2007. Contribution of individual-based coupled physical-biological models to undertanding recruitment in marine fish population. Chesapeake Biological Laboratory, University of Maryland Center for Environmental Science,

Solomons, Mar Ecol Prog Ser, Vol 347, Pp 127–13, USA. doi: 10.3354/meps06973

Möller Jr, O. O. and Fernandes, E. H. L. 2010. Hidrologia e Hidrodinâmica. In: Seeliger, U. and Odebrecht, C. (Eds.). O Estuário da Lagooa dos Patos: Um século de transformações. Rio Frande, FURG, P180. ISBN: 978-85-7566-144-4, pp 17-27.

MPA, 2011. Boletim Estatístico da Pesca e Aquicultura – Brasil. Ministério da Pesca e Aquicultura, Brasília.

Möller Jr, O. O., Castello, J. P. and Vaz, A. C. 2009. The Effect of river discharge and winds on the interannual variability of the Pink Shrimp *Farfantepeneaus paulensis* Production in Patos Lagoon;Estuaries and Casts, 787-796. Doi: 10.1007/s12237-009-9168-6.

Möller Jr, O. O., Castaing, P., Salomon, S. and Lazure, P. 2001. The Influence of Local and Non-local Forcing Effects on the Subtidal Circulation Of Patos Lagoon. Estuaries, Vol. 24, Nº2, p. 297-311.

Möller O. O. e Castaing, P. 1999. Hydrographical characteristics of the estuarine area of Patos Lagoon (30ºS, Brazil). In Estuaries of South America-Their Geomorphology and Dynamics, pages 83–100.

Möller, O.O., Lorenzetti, J.A., Stech, J.L. and Mata, M.M. 1996. The Patos Lagoon summertime circulation and dynamics. Continental Shelf Research, 16: 335-351.

Montecinos, A., Diaz, A., and Aceituno, P. 200. Seasonal Diagonostic and Predictability of Rainfall in subtroical South America Based on Tropica Pacific SST. Journal of Climate. American Meteorological Society.p. 746-758.

Muelbert, J. H., Muxagata, E., & Kaminski, S. M. 2010. As comunidades zooplanctonicas. In: Seeliger, U. e Odebrecht, C (eds). O estuário da Lagoa dos Patos: Um século de transformações. 1ª Edição. FURG. Rio Grande, Brasil. Pp 67-75

Muelbert, J. H., Acha, M., Mianzan, H., Guerrero, R., Reta, R., Braga, E. S., Garcia, V. M.T. Berasategui, A., Gomez-Erache, M. and Ramı´rez, F. 2008. Biological, physical and chemical properties at the Subtropical Shelf Front Zone in the SW Atlantic Continental Shelf. Continental Shelf Research, 28. Pp.1662–1673. DOI:10.1016/j.csr.2007.08.011.

Muelbert, J.H. and Weiss, G., 1991. Abundance and distribution of fish larvae in the channel area of Patos Lagoon estuary, Brazil. In: NOAA Technical Report NMFS, vol. 95., pp. 43–5.

NRC, 2007. Mitigating Shoreline Erosion along Sheltered Coasts. Ocean Study Board, National Research Council. National Academies Press, Washington, DC.

Norcross, B.L. and Shaw, R. F. 1984. Oceanic and estuarine transport of fish eggs and larvae: a review. T Am Fish Soc. 113: 153-165.

Oliveira, Antonio F. and Bemvenuti, Marlise A. 2006.O Ciclo De Vida De Alguns Peixes Do Estuário Da Lagoa Dos Patos, Rs, Informações Para O Ensino Fundamental E Médio. Vol 1. Nº 2. Cadernos De Ecologia Aquática.

Odebrecht, C., Abreu, P. C., Möller Jr Jr, O. O., Niencheski, I. F., Proença, L. A. and Torgan, L. C. 2005. Drought Effect on Pelagic Properties in the shallow and turbid Patos Lagoon, Brazil. Estuaries. Vol. 28. No. 5, p. 675-685.

Odebrecht, C., Secchi, E., Abreu, P. C, Muelbert, J. H., and Uiblein, F. 2017. Biota of the Patos Lagoon estuary and adjacent marine coast: long-term changes induced by natural and human-related factors, Marine Biology Research, 13:1, 3-8, DOI: 10.1080/17451000.2016.1258714.

Odebrecht, C., Bergesch, M., Medeanic, S. and Abreu, P. C. 2010. A cominidade de microalgas. In: Seeliger, U. and Odebrecht, C. (Eds.). O Estuário da Lagooa dos Patos: Um século de transformações. Rio Frande, FURG, P180. ISBN: 978-85-7566-144-4, pp 51-63.

Parada C., Van Der Lingen, C.D., Mullon, C. and Penven, P.. 2003. Modelling the effect of buoyancy on the transport of anchovy (*Engraulis capensis)* eggs from spawning to nursery grounds in the southern Benguela: an IBM approach. *Fisheries Oceanography,* 12(3):170-184.

Padovani, Carlos R. 2012. Bioestatística. São Paulo: Cultura Acadêmica: Universidade Estadual Paulista, Pró-Reitoria de Graduação, 2012.112 p. ISBN 978-85-7983-265-9.

Paula Kirinus E. and Marques, W.C. 2015. Viability of the application of marine current power generators in the South Brazilian shelf. Appl Energy 155:23–34

Piola, A. R., Matano, R. P., Palma, E. D., Möller Jr, J. O. O., e Campos, E. J. D. 2005. The influence of the Plata River discharge on the western South Atlantic shelf. Geophysical Research Letters, 32(1):1–4.

Pritchard, D. W. 1956. The dynamic structure of a coastal plain estuary. Journal of Marlne Research 15, 33-42.

Prumm, M and Iglesias, G. 2016. Impacts of port development on estuarine morphodynamics: Ribadeo (Spain). Ocean and Coastal Management 130, 58-72.

Ramos, S., Cowen, R. K., Ré, P., and Bordalo, A. A. 2006. Temporal and spatial distribution of larval fish assemblages in the Lima estuary (Portugal). Estuarine, Coastal and Shelf Science 66, 303-314. DOI:10.1016/j.ecss.2005.09.012.

Robins, Peter E., Neill, Simon P., Giménez, L., Jenkins, Stuart R. and Malham, Shelagh K. 2013. Physical and biological controls on larval dispersal and connectivity in a highly energetic shelf sea. Limnol. Oceanogr., 58(2), Pp. 505–524. DOI:10.4319/lo.2013.58.2.0505.

Salvador, N.L.A. and Muelbert, J.H. 2019. Environmental variability and body condition of Argentine menhaden larvae, *Brevoortia pectinata* (Jenyns, 1842), in estuarine and coastal waters. Estuaries and Coasts 42, 1654–1661. https://doi.org/10.1007/s12237-019-00604-3

Schmidt, N. and Luther, M.E. 2002. ENSO impacts on salinity in Tampa Bay, Florida. *Estuaries*, 25, No. 5, 976–984.

Seeliger, U. e Costa, C. S. B. 2010. Lições ecológicas e futuras tendências. In: Seeliger;Odebrecht. (Org.) O estuário da Lagoa dos Patos: um século de transformações. Rio Grande: FURG, p. 147-149;

Seiler, L. M. N, Fernandes, E. H. L., Martins, F. and Abreu, P. C. 2015. Evolution of hydrologic influence on water quality variation in a coastal lagoon through numerical modeling. Ecological Modelling 314, 44-61, Elsevier.

Sheaves, M., Baker, R., Nagelkerken, I. and Connolly, R.M. 2015. True value of estuarine and coastal nurseries for fish: incorporating complexity and dynamics. Estuaries and Coasts 38, 401-414. DOI 10.1007/s12237-014-9846-x.

Sherwood, C.R., D.A. Jay, R.B. Harvey, P. Hamilton, and C.A. Simenstad. 1990. Historical changes in the Columbia River estuary. Progress in Oceanography 25: 299-352.

Sentchev, Alexei and Korotenko, Konstantin, 2007. Modelling distribution of flounder larvae in the eastern English Channel: sensitivity to physical forcing and biological behaviour. Marine Ecology Progress Series. Vol, 347:233-245. doi:10.3354/meps06981.

Silva, P. D., Lisboa, P. V. and Fernandes, E. H. 2015. Changes on the fine sediment dynamics after the Port of Rio Grande expansion. Advances in Geosciences 39, 123–127. DOI:10.5194/adgeo-39-123-2015.

Student (William Sealy Gosset). 1908. The probable error of a mean. *Biometrika*, 6 (1). Pp. 1–25. doi:10.1093/biomet/6.1.1.

Tavora, J., Fernandes, E. H. L., Thomas, A. C., Weatherbee, R. and Schettini, C. A. F. 2019. The influence of river discharge and wind on Patos Lagoon, Brazil, Suspended Particulate Matter, International Journal of Remote Sensing, DOI:10.1080/01431161.2019.1569279.

Teodósio, M.A., Paris, C.B., Wolanski, E., and Morais, P.. 2016. Biophysical processes leading to the ingress of temperate fish larvae into estuarine nursery areas. Estuarine, Coastal and Shelf Science (2016), doi: 10.1016/j.ecss.2016.10.022.

Tiessen, M. C. H., Fernard, L., Gerkema, T., van der Molen, J., Ruardij, P. and van der Veer, H. W. 2013. Numerical modelling of physical processes governing larval transport in the Southern North Sea. Ocean Science Discuss, 10, 1765–1806. doi:10.5194/osd-10-1765-2013.

Toldo Jr, E. E, Ayup-Zouain, R. N., Correia, I. C. S., and Dillen-Burg, S. R. 1991. Barra Falsa: Hipótese de um paleocanal Holocênico de comunica-ção entre a Laguna dos Patos e o Oceano Atlântico. Pesquisas, 18(2), 99-103.

Toldo Jr., E. E., Dillenburg, S., Corrêa, I., Almeida, L., Weschenfelder, J., and Gruber, N. 2006. Sedimentação de Longo e Curto Período na Lagoa Dos Patos, Sul do Brasil. Geociências, 33(2):79-86.

Torrence, C. and Compo, G. P. 1998. A Practical guide of wavelet analyses. Bulletin of the American Meteorological Society. Vol. 79. nº1. 61-79.

Vaz, A.C., Parada, C.E., Palma, E.D., Muelbert, J.H. and Campos, E. J.D. 2007. Modeling transport and retention of Engraulis anchoita Hubbs & Marini, 1935 (Clupeiformes, Engraulidae) early life stages along the Central Southwestern Atlantic Continental Shelf. PanAmerican Journal of Aquatic Sciences, 2(2): 179-190.

Vaz, A.C., Möller, O.O. and Almeida, T.L. 2006. Análise quantitativa da descarga dos rios afluentes da Lagoa dos Patos. Atlântica, vol. 28, nº 1, pp 13-23.

Vaz, Ana Carolina. 2005. Modelagem do transporte e retenção larval da anchoita Engraulis anchoita na plataforma continental do Atlântico Sudoeste. IO – Universidade de Sao Paulo. Dissertação de Mestrado.

Vieira, João P., Garcia, Alexandre e Moraes, Leonardo. 2010. A assembleia de peixes. O estuário da Lagoa dos Patos: Um século de Transformação. Edição: U. Seeliger e C. Odebrecht. FURG. Pp. 79-88.

Vieira, J. P., and Castello, J. P. 1997. Environment and biota of the Patos Lagoon Estuary. Fish fauna. In 'Subtropical Convergence Environments. The Coast and Sea in the Southwestern Atlantic'. Eds U. Seeliger, C. Odebrecht, and J. P. Castello. pp. 56-61. Springer: Heidelberg.

Walstra, L., Van Rijn, L., Blogg, H., and Van Ormondt, M. 2001. Evaluation of a hydrodynamic area model based on the coast3d data at Teignmouth 1999. p. D4.1–D4.4.

Weiss, G. 1981. Ictioplancton del Estuario de Lagoa dos Patos, Brasil. Unversidade Nacional de La Plata. Tese de Doutorado. 164p.

Whitfield, Alan K. 2016. The role of seagrass meadows, mangrove forests, salt marshes and reed beds as nursery areas and food sources for fishes in estuaries. Rev. Fish Biol. Fisheries, Spriner. Doi: 10.1007/s11160-016-9454-x.

Wong, L., Chen, J., Xeu, H., Dong, L., Su, J., and Heinke G. 2003ª. A model study of the circulation in the Pearl River Estuart (PRE0 and its adjacent coastal water: 1: Simulations and comparison with observations. J. Geophys. Res,. 108, C3156. Doi: 10.1029/2002JC001451.

Yuk, J. H. and Aoki, S. 2007. Impact of Jetty construction on the current and Ecological Systems in the Estuary with a Narrow Inlet. Journal of coastal research, 784-788.

Zhao, J., Guo, L., He, Q., Wang, Z. B., Maren, D. S. V. and Wang, X. 2018. An analysis on half centurry morphological changes in the Changjiang Estuary: Saptial variability under natural processes and human intervention. Journal of Marine Systems, 181. Pp. 25-36. Doi: 10.1016/j.jmarsys.2018.01.007

TELEMAC-3D model information www.opentelemac.org

Discharge data. National Water Agency http://www.ana.gov.br

Salinity and Temperature data. Hybrid Model Coordinate Oceanic, https://hycom.org/

Wind data. European Center for Medium-Range Weather Forecasts, http://www.ecmwf.int